HYDROGEN PEROXIDE ELECTROSYNTHESIS IN SOLID POLYMER ELECTROLYTE (SPE) REACTORS WITH AND WITHOUT POWER CO-GENERATION

by

Winton Li

B.A.Sc., The University of British Columbia, 2005
M.A.Sc., The University of British Columbia, 2010

A THESIS SUBMITTED IN PARTIAL FULFILLMENT OF THE REQUIREMENTS FOR THE DEGREE OF

DOCTOR OF PHILOSOPHY

in

THE FACULTY OF GRADUATE AND POSTDOCTORAL STUDIES
(Chemical and Biological Engineering)

THE UNIVERSITY OF BRITISH COLUMBIA
(Vancouver)

June 2017

© Winton Li, 2017

Abstract

For applications that require small amounts of H_2O_2 or have economically difficult transportation means, an alternate, on-site H_2O_2 production method to the current industrial anthraquinone auto-oxidation process is needed. Thus far neutral production of H_2O_2 has been limited to bench-top laboratory scaled research with low yield of H_2O_2 [1]. To produce neutral H_2O_2 on-site and on-demand for drinking water purification, the electroreduction of oxygen at the cathode of a solid polymer electrolyte (SPE) cell could be a possible solution. The work presented here has utilized a SPE cell operating in either fuel cell mode (power generating) or electrolysis mode (power consuming) to produce H_2O_2. The SPE cell reactor is operated with a continuous flow of cathode carrier water flowing through the cathode to remove the product H_2O_2. Two catalysts were chosen for further study in this work, one is the inorganic cobalt-carbon composite catalyst, to be used in both fuel cell mode and electrolysis mode operation. The other is the riboflavin-anthraquinone-carbon composite catalyst, to be used in only the electrolysis mode operation.

Through parametric experiments in both modes of operation, the Co-C catalyst was able to achieve peroxide production rate of ~200 μmol hr^{-1} cm^{-2} and 4 mW cm^{-2} operating at a cell temperature of 60°C with a current density of 30 mA cm^{-2} and 30% current efficiency in fuel cell mode operation. Long term recycle experiments over a period of 72 hours showed an accumulated H_2O_2 concentration of over 1400 ppm. Investigation of both catalysts in electrolysis mode operation showed that the AQ-C catalyst achieved maximum H_2O_2 production of 580 μmol hr^{-1} cm^{-2} operating at 40°C and a current density of 240 mA cm^{-2} with an 8% current efficiency; while the Co-C catalyst had a maximum H_2O_2 production rate of 360 μmol hr^{-}

^{1} cm^{-2} operated at 240 mA cm^{-2} with 8% current efficiency. Long term recycle study of both catalysts in electrolysis mode generated maximum H_2O_2 concentrations of over 3000 ppm in 72 hours. Water sample analysis showed no degradation of the catalysts in either mode of operation.

Preface

All of the work presented in this dissertation was based on experiments performed by Mr. Winton Li at the Clean Energy Research Center at the University of British Columbia at the Point Grey Campus. Where the intellectual property is co-developed by Winton Li, Arman Bonakdarpour, David P. Wilkinson and Elod L. Gyenge.

A version of Chapter 5 has been published in

- W. Li, A. Bonakdarpour, E. Gyenge, D.P. Wilkinson, Drinking Water Purification by Electrosynthesis of Hydrogen Peroxide in a Power-Producing PEM Fuel Cell, CHEMSUSCHEM 6(11) (2013): 2137-2143.

A version of Chapter 6 is being prepared for journal submission:

- W. Li, A. Bonakdarpour, E. Gyenge, D.P. Wilkinson, Bifunctional Electrodes for Co-Generation of Electrical Power and Hydrogen Peroxide, In preparation, 2017.

And a version of Chapter 7 is being prepared for journal submission:

- W. Li, A. Bonakdarpour, E. Gyenge, D.P. Wilkinson, Electrolytic generation of Hydrogen Peroxide in a Solid polymer electrolyzer using organic and inorganic catalysts, In preparation, 2017.

For all of the work in these three manuscripts as well as this dissertation, I was the lead investigator, responsible for all collaborations in areas of concept formation, data collection and analysis, as well as manuscript composition and edits.

Table of Contents

List of Tables

List of Figures

List of Abbreviations

AC	activated carbon
AEM-FC	anion exchange membrane fuel cell
AHQ	2-alkyl 9,10-dihydroanthraquinone
AOP	advanced oxidation process
AQ	alkylanthraquinone
AQAO	anthraquinone auto-oxidation
BDD	boron-doped diamond
CAQ	anthraquinone-2-carboxylic acid
CCM	catalyst coated membrane
CE	counter electrode
CE	current efficiency
CEM	cation exchange membrane
CNT	carbon nano-tubes
DBP	disinfection by-product precursors
DI	de-ionized
DMFC	direct methanol fuel cell
DSA	dimensionally stable anode
EC	electrochemical
GC	glassy carbon
GDE	gas diffusion electrode
GDL	gas diffusion layer
GEP	gross economic potential

HER	hydrogen evolution reaction
HOPG	highly oriented pyrolytic graphite
ICP-MS	inductively-coupled plasma mass spectrometry
KHP	potassium hydrogen phthalate
KI	potassium iodide
MEA	membrane electrode assembly
MCFC	molten carbonate fuel cell
NaOH	sodium hydroxide
N/A	not available
NEP	net economic potential
OER	oxygen evolution reaction
OPG	ordinary pyrolytic graphite
ORR	oxygen reduction reaction
PAFC	phosphoric acid fuel cell
PEM-FC	proton exchange membrane fuel cell
PPy	polypyrrole
RE	reference electrode
RF-AQ	riboflavin-anthraquinone-2-carboxylate ester
ROI	return on investment
RRDE	rotating ring-disk electrode
RVC	reticulated vitreous carbon
SOFC	solid oxide fuel cell
SPE	solid polymer electrolyte
S.S.	stainless steel

TMPP	tetramethoxyphenyl porphyrin
TPP	5,10,15,20-tetrakis(phenyl)-21H,23H-porphyrin
UV	ultraviolet
UV-VIS	ultraviolet-visible
VGCF	vapor grown carbon fiber
WE	working electrode

List of Symbols

Â	pre-exponential factor	
Abs_{sample}	absorbance reading of sample	
Abs_{blank}	absorbance reading of blank solution	
A_c	cell active area	cm^2
A_{geom}	geometric active area per cell	cm^2
C	H_2O_2 concentration	mol L^{-1}
C_{ac}	cost of ac energy	\$ hr^{-1}
C_{el}	cost of dc electrical energy per electrochemical reactor unit	\$ hr^{-1}
$C_{E,ML}$	maintenance and labor cost for H2O2 process	\$
C_{IA}	installed capital cost of the auxiliary equipments	\$
C_{IC}	total installed cost	\$
$C_{I,E}$	total installed capital cost	\$
C_{IEC}	installed capital cost of the cells	\$
$C_{p,c}$	heat capacity of liquid in cathode stream	kJ kg^{-1} K^{-1}
C_{PS}	installed capital cost of the power supply system	\$
$C_{p,w}$	heat capacity of liquid in cooling water	kJ kg^{-1} K^{-1}
D	design diameter of separator	m
ΔP	pressure differential	kPa
ΔT_m	logarithmic temperature difference	K
E_a	activation energy	J mol^{-1}
$E^{\circ}_{25\,℃}$	standard potential at 25°C	V
E°_{cell}	standard cell potential	V

ε_c	compressor efficiency	
ε_p	pump effciency	
F	faraday's constant	C mol^{-1}
$F_{m,c}$	flow rate of cathode stream	m^3 s^{-1}
$F_{m,w}$	flow rate of cooling water	m^3 s^{-1}
f_{Nafion}	nafion loading	
F_v	volumetric flow rate	m^3 s^{-1}
G_c	cost constant	\$ m^{-2}
I	current	A
I	current density	mA cm^{-2}
M	scale component (0.8 – 0.9)	
m/m	mass / mass	
m_{Naf_sol}	mass of nafion solution	g
$m_{Pt+VuulcanXC}$	mass of Pt catalyst on Vulcan XC-72 powder	g
m_v	molar oxygen flow rate	mol s^{-1}
N_c	number of cells	
Φ_{Pt}	catalyst loading	mg_{geom} cm^{-2}
P_{out}/P_{in}	ratio of outlet to inlet pressure for the compressor	
P_r	H_2O_2 production rate	kmol s^{-1}
P_w	total power consumption	kW
Q	carrier water flow rate	L s^{-1}
Q_G	volumetric gas flow rate in the separator	m^3 hr^{-1}
Q_{HEX}	heat transferred from process stream to cooling water	W
R	universal gas constant (8.314)	J mol^{-1} K^{-1}

r	ratio of specific heats (C_p/C_v)	
RE	rectifier efficiency (0.96)	
ρ_G	gas density	kg m^{-3}
ρ_L	liquid density	kg m^{-3}
σ_{Pt}	percent of Pt catalyst in Vulcan XC-72 powder	%
T_{in}	inlet oxygen temperature to the compressor	K
U	overall heat transfer coefficient (1.6)	kW m^{-2} K^{-1}
U_{ave}	gas velocity in the separator	m s^{-1}
V_c	voltage per cell	V
V_t	total voltage	V
W_s	required shaft power	W
$W_{s,c}$	calculated shaft power	W
Z	number of electrons (2)	

Acknowledgements

Upon completion of this thesis project, I see myself having completed a major milestone in my academic career. Along the way a number of people have provided strong support which helped to encourage me to complete this goal.

A sincere and heartfelt thank you to both of my supervisors, Drs. David Wilkinson and Elöd Gyenge. Their endless unconditional support, advice and positive criticism over the last five years provided me with the necessary support to tackle issues big and small for both this research project as well as other areas of my academic and personal life. For that I am deeply grateful.

I would also like to thank my committee members, Dr. Madjid Mohseni and Dr. Pierre Berube for their support and assistance on certain sections of this project, as well as for taking the time to provide feedback on this thesis.

I would like to extend a special gratitude and appreciation to everyone in my research group at UBC. A special thanks goes to Dr. Arman Bonakdarpour for always being their when I needed some advice, and for reviewing my thesis. I would like to thank Andrew Wang, Saad Dara, Jeanette Leeuwner, Greg Afonso, Amin Aziznia, and countless other peers for just being the great friends that they are.

A special thank you to all the staff at the Department of Chemical and Biological Engineering, to members of the machine shop and the office for putting up with my odd requests these years.

A special heartfelt thank you to my family, especially my mom and dad for their unconditional support during my life. No matter the situation or issues, they were always steadfast in their support of whatever decisions that I have made. For that I am truly grateful.

Lastly I would like to give a special thank you to the love of my life, Selina. You are my guiding light, my sweetheart, thank you for believing in me and providing balance in my life.

To my loved ones

Chapter 1 Introduction

1.1 Hydrogen Peroxide

Hydrogen peroxide (H_2O_2) was first discovered by the French chemist Louis-Jaques Thenard in 1818 [2]. It is an environmentally friendly oxidizing agent that is widely used in the pulp and paper industry, mining, cosmetic and pharmaceutical industries, as well as common household cleaners such as disinfectants and antiseptics [3]. Breakdown of the industrial use of H_2O_2 is shown in Figure 1.1. The most important factor of this green chemical is that it produces only water and oxygen through the oxidation process [4]. In 2012 the world annual H_2O_2 production was about 4 million tonnes with the shipping cost at about ten times that of the production cost [5]. The significant transportation cost arises from the hazardous nature of this compound, namely corrosiveness, explosive vapors, and health hazards [6].

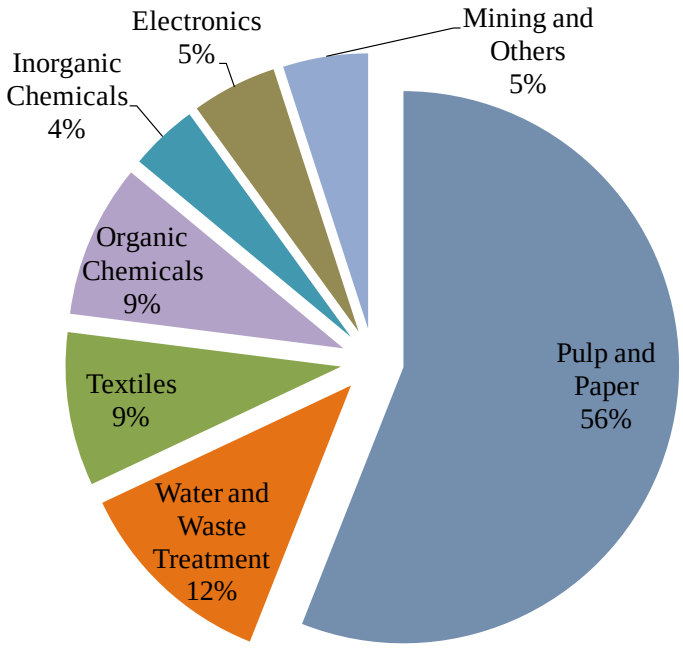

Figure 1.1 Industrial uses of hydrogen peroxide[6].

Hydrogen peroxide was produced by the Thenard process until the middle of the twentieth century [7]. In this process, barium oxide is reacted with nitric acid to form hydrogen peroxide and barium nitrate [2, 7]. The concentration of the H_2O_2 product by this process is quite low; however, it can be increased if hydrochloric acid is used (Eqn 1.1). At its time a peak H_2O_2 production of 2000 metric tonnes of H_2O_2 per year was achieved using this method[7]. Two major disadvantages was faced by the Thenard process: 1) low yield and 2) stability. The maximum yield of the Thenard process was only 3 % *m/m*, which lead to high production costs. The product H_2O_2 also had a high decomposition rate as a result of the high impurity levels in the product H_2O_2[7].

$$BaO_{2(aq)} + 2HCl_{(aq)} \rightarrow BaCl_{2(aq)} + H_2O_{2(aq)} \quad \text{(Eqn 1.1)}$$

$$BaCl_{2(aq)} + H_2SO_{4(aq)} \rightarrow BaSO_{4(S)} + 2HCl_{(aq)} \quad \text{(Eqn 1.2)}$$

$$BaO_{2(aq)} + H_2SO_{4(aq)} \rightarrow BaSO_{4(S)} + H_2O_{2(aq)} \quad \text{(Eqn 1.3)}$$

Currently, H_2O_2 can be produced either chemically or electrochemically. Examples of chemical processes include: i) oxidation of isopropanol to ketone and peroxide, ii) anthraquinone auto-oxidation by cyclic reduction/oxidation, and iii) oxidation of alkali metals to peroxides. Electrochemical processes include: i) the electrolysis of ammonium sulfate followed by the hydrolysis of persulfate to peroxide, ii) cathodic reduction of oxygen to alkaline peroxide solution, and iii) electrochemical reduction of a quinone to continuously regenerate hydroquinone in aqueous medium [8]. Industrial production of H_2O_2 is mainly based on one of two processes: the anthraquinone auto- oxidation (AQAO) process (thermal-chemical process) and the DOW-Huron process (electrochemical process) [3, 8-9].

1.2 Anthraquinone Auto-Oxidation (AQAO) Process

The anthraquinone process is a cyclic auto-oxidation process, which involves indirect oxidation of hydrogen to H_2O_2. A diagram of this cyclic process is shown in Figure 1.2. It is a two step process [3, 8] where an alkylanthraquinone (AQ) is chemically reduced with hydrogen under pressure in the presence of a hydrogenation catalyst (e.g., Pt or Pd) to 2-alkyl 9,10-dihydroanthraquinone (AHQ). The AHQ is then oxidized in the presence of oxygen or air back to the originating alkylanthraquinone (AQ) plus hydrogen peroxide. The resulting alkylanthraquinone is available to enter the cyclic process for further hydrogen peroxide production. This auto-oxidation process is carried out in non-aqueous media [10]. In order to achieve high yields of peroxide, solubility of the working compound – anthraquinone – needs to be maximized. This is accomplished by using a mixture of organic solvents, such as esters/hydrocarbons or octanol/methyl-naphthalene [3]. The resulting H_2O_2 concentration is usually 30% by weight, which can be increased through distillation under reduced pressure to eliminate impurities [3].

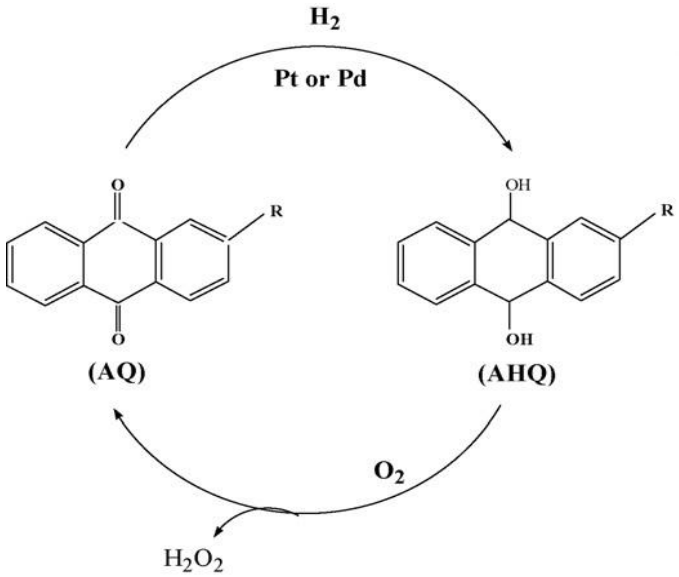

Figure 1.2 Cyclic anthraquinone auto-oxidation process for hydrogen peroxide production.

The AQAO process produces most of the world's supply of H_2O_2. However, it is not without significant drawbacks. The same complex organic solvent mixture used to maximize peroxide yield can contaminate the peroxide formed, generate undesirable side products such as acetone, and result in safety concerns from potentially explosive reactions [8]. The removal of organic impurities can require energy intensive process steps, thus increasing operating costs. Capital costs are also high as the hydrogenation step is non-selective, and the H_2O_2 product can lead to deactivation of the hydrogenation catalyst, leading to periodic replacement of costly quinone derivatives [11]. These high capital and operating costs means that H_2O_2 produced by the AQAO process must be in large quantities, thus is only suitable for large scale operations.

1.3 Trickle Bed Electrochemical Reactor

Electroreduction of oxygen to H_2O_2 in sodium hydroxide was first discovered over 100 years ago by M. Traube[12]. This original cell design, along with all other cells afterwards, all have one thing in common. They all use carbon for their cathode electrode [9]. In the 1970s Colin Oloman experimented with monopolar and bipolar geometry of the cell design [13-14] as part of his research work with Dr. Paul Watkinson. They studied cathodes packed with carbon particles and also carbon graphite felt. Their cell design, shown in Figure 1.3, utilized a simple one compartment that housed both the cathode and the anode, separated by a porous diaphragm separator [14].

1.3.1 Tickle Bed Electrochemical Cell

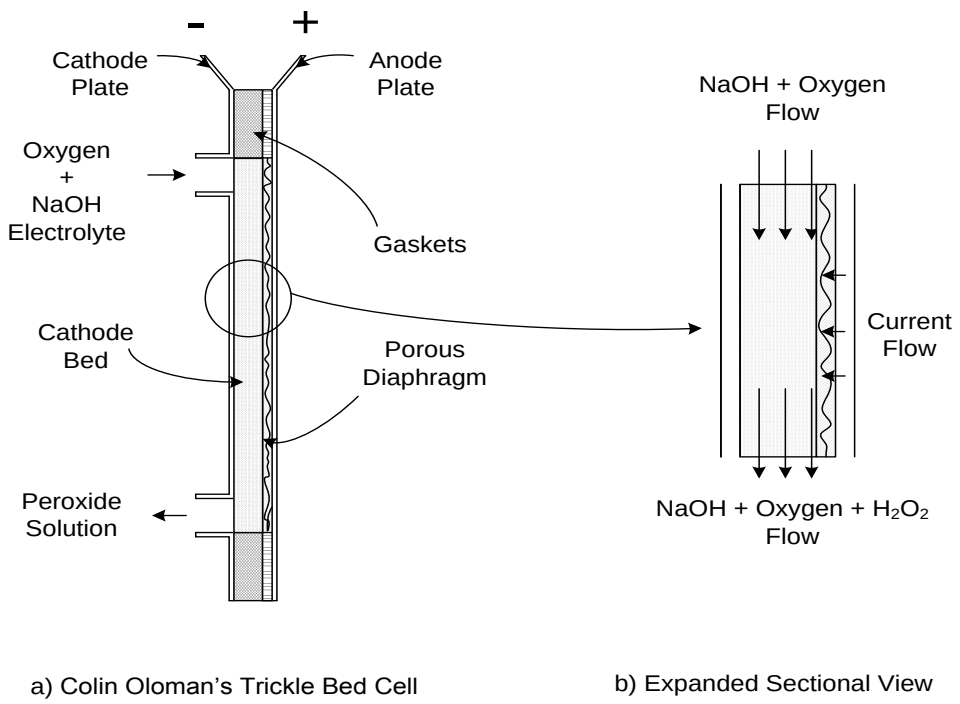

Figure 1.3 Colin Oloman's trickle bed electrochemical cell [14].

Oloman's cell design (Figure 1.3) flows sodium hydroxide (NaOH) electrolyte co-currently downward with oxygen through the graphite bed. External current is applied to the attached metal electrode plates and flows perpendicular to the liquid and gas flow direction [14]. Alkaline hydrogen peroxide was produced at a current efficiency of 60% with the trickle bed reactor operating at 1.8 V and 1200 A m^{-2}. Oloman's work showed that carbon graphite felt had better overall H_2O_2 production rates than a packed carbon particle bed [14]. Foller *et al.*[9] also reported this improvement, which was primarily due to the carbon felt's smaller resistive losses [9].

1.3.2 Dow-Huron Process

The most commercially successful application of the trickle bed system has been the DOW-Huron process. This commercial application of the cathodic electroreduction of oxygen to alkaline H_2O_2 has some similarities to the one first introduced by Oloman and Watkinson in 1979 [14]. The Dow process followed the same basic principle of Oloman's design, i.e., reduction of oxygen to H_2O_2 on the cathode (made with either a thin bed of graphite particles or graphite felt) of a trickle bed cell with alkaline solution as the electrolyte [9, 14-15]. However, Oloman was faced with mass transfer limitations as a result of low oxygen solubility. He overcame the issue by applying 800 kPa pressure to the cathode side. DOW improved this basic design with the use of Teflon coated graphite chips as packed bed material (Figure 1.4), which enhanced the mass transfer of oxygen without pressurizing the system [16]. This improvement has led to successful commercial application of the process in the pulp and paper industry.

Unlike the original Oloman design, DOW's design operated under counter current flow, where gas and liquid flowed in opposite directions (Figure 1.4a). The Teflon coated graphite chips (Figure 1.4b) led to a partially wetted electrode, creating a thin film of NaOH coated on the graphite chips, which in turn improved oxygen transfer at atmospheric conditions, thus improving the H_2O_2 production.

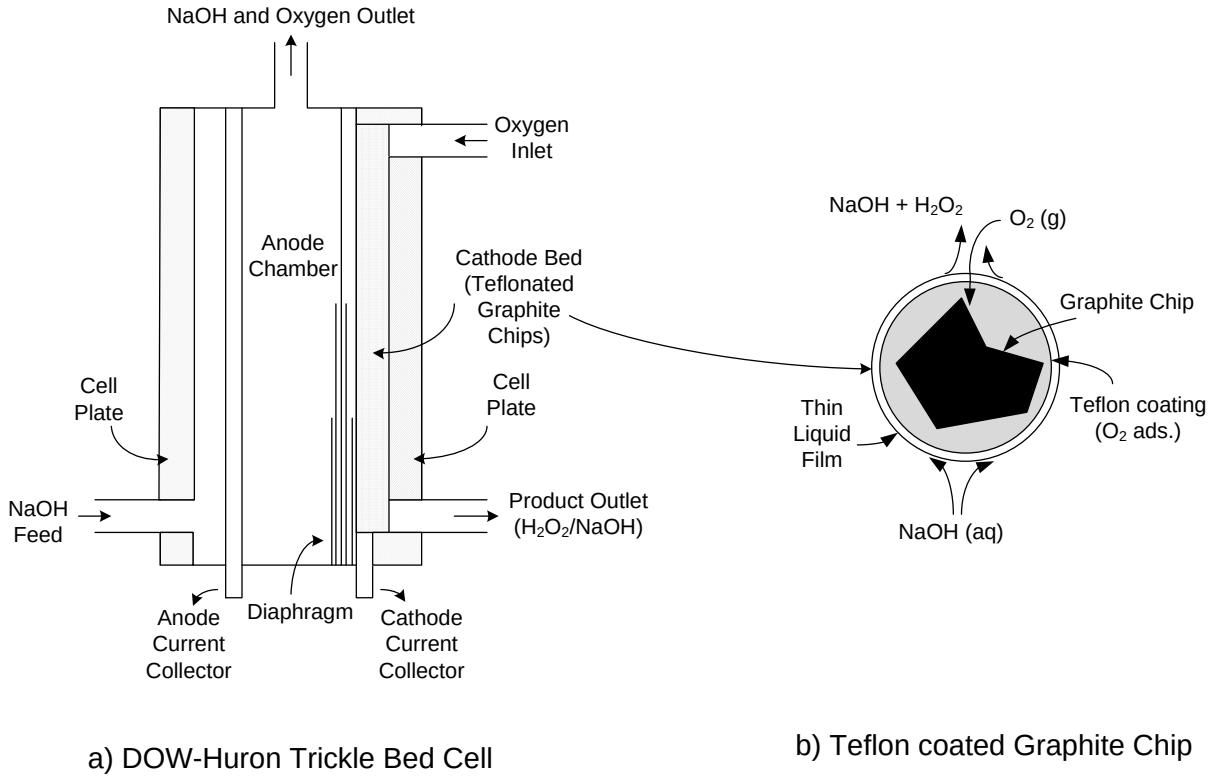

a) DOW-Huron Trickle Bed Cell

b) Teflon coated Graphite Chip

Figure 1.4 Dow-Huron Trickle Bed Electrolyzer cell [9].

Compared to the AQAO process, the DOW-Huron process is much more portable and thus suitable for on-site and in-situ H_2O_2 generation. However, as the product H_2O_2 is alkaline, long term stability of the H_2O_2 is affected. Additional steps are required to reduce the alkalinity before applications to neutral or acidic processes. The stability of the alkaline H_2O_2 could also lead to potential problems in transportation and long term storage [8].

1.4 Electro-Reduction of Oxygen

The oxygen reduction reaction process is a complex multi-reaction process that reduces oxygen via either the 4 electron pathway or the 2 electron pathway[17]. The two overall pathways for this process are shown below.

$O_2 + 4H^+ + 4e^- \rightarrow 2H_2O$ $E^{\circ}_{25\,^{\circ}C} = +1.23$ V (vs. SHE) Eqn. 1-4

$O_2 + 2H^+ + 2e^- \rightarrow H_2O_2$ $E^{\circ}_{25\,^{\circ}C} = +0.68$ V (vs. SHE) Eqn. 1-5

$O_2 + H_2O + 2e^- \rightarrow HO_2^- + OH^-$ $E^{\circ}_{25^{\circ}C} = +0.076$V (vs. SHE) Eqn. 1-6

The direct 4 electron reduction pathway of oxygen to water (Eqn. 1-4) breaks the strong O=O double bond early, thereby maximizing the electrical efficiency of the PEM fuel cell where this pathway is favored [18]. The 2 electron pathway, where H_2O_2 is produced in solution, is favored when oxide-covered metals (e.g., Ni & Co), transition metal oxides (e.g., NiO) and graphite are used as cathode electrode materials [17].

Electro-synthesis of hydrogen peroxide from electro-reduction of oxygen can be carried out in two different modes: 1) electrolyzer mode or 2) fuel cell mode. In either mode the reactions can take place either with an aqueous electrolyte or with a solid electrolyte membrane. In electrolyzer cells, H_2O_2 generation from electro-reduction of oxygen requires an external DC power source. This mode is also referred to as a power sink and it follows the 2-electron pathway:

- 1. Alkaline Electrolyte or Membrane (pH = 13): $E^{\circ}_{cell} = -0.48$ V
  - Anode (-): $2OH^- \rightarrow \frac{1}{2}O_2 + H_2O + 2e^-$ $E^{\circ} = -0.40$V Eqn. 1-7
  - Cathode (+): $O_2 + H_2O + 2e^- \rightarrow HO_2^- + OH^-$ $E^{\circ} = 0.076$V Eqn. 1-8
- 2. Acidic Electrolyte or Membrane (pH < 7): $E^{\circ}_{cell} = -1.93$ V
  - Anode (-): $H_2O \rightarrow \frac{1}{2}O_2 + 2H^+ + 2e^-$ $E^{\circ} = -1.23$ V Eqn. 1-9
  - Cathode (+): $O_2 + 2H^+ + 2e^- \rightarrow H_2O_2$ $E^{\circ} = +0.70$ V Eqn. 1-10

For applications where external power sources are not available, electro-reduction of oxygen to H_2O_2 can also be achieved in fuel cell mode powered by hydrogen (or other electrochemical fuels) and oxygen/air using either a proton exchange membrane or an anion exchange membrane. This mode is also referred to as a power supply and also follows the 2-electron pathway:

- 1. Acidic Electrolyte or Proton exchange membrane (PEM-FC) $E^{o}_{cell} = 0.70$ V
  - Anode (-): $H_2 \rightarrow 2H^+ + 2e^-$ $E° = +0.0$ V Eqn. 1-11
  - Cathode (+): $O_2 + 2H^+ + 2e^- \rightarrow H_2O_2$ $E° = +0.70$ V Eqn. 1-12
- 2. Alkaline Electrolyte or Anion exchange membrane (AEM-FC) $E^{o}_{cell} = 0.75$ V
  - Anode (-): $H_2 + 2OH^- \rightarrow 2H_2O + 2e^-$ $E° = +0.83$ V Eqn. 1-13
  - Cathode (+): $O_2 + 2H_2O + 4e^- \rightarrow 4\ OH^-$ $E° = +0.076$ V Eqn. 1-14

1.4.1 Inorganic Electrocatalyst

In alkaline solutions carbon based electrodes have very good reaction kinetics for reduction of oxygen to hydrogen peroxide [17]. Kolyagin *et al*. (2007) experimented with three different carbon black mixtures in a thin catalyst layer gas diffusion electrode setup operating in electrolyzer mode [19-20]. Kolyagin chose three types of carbon black for his study: A 473-E (hydrophobic acetylene black, particle size 30 – 39 nm), P 702 (particle size 60 – 100 nm) and P 268-E (particle size 19 – 35 nm) brands (hydrophilic furnace black) [20]. Their experiments produced a maximum H_2O_2 concentration of 1.1 M at 70% current efficiency with a 5 cm^2 active area electrode and a A473-E carbon catalyst in 0.5 M NaOH at 0.52 V and 50 mA cm^{-2} for 5 – 7 hrs [19].

However, in acidic solutions, these carbon electrodes have much slower reaction kinetics as indicated by their high oxygen reduction overpotentials. Tatapudi and Fenton (1993) experimented with powders of activated carbon, gold and graphite as cathode materials for their studies of H_2O_2 electrosynthesis in a proton exchange membrane electrochemical reactor [21-22]. They found that using a graphite powder at a catalyst loading of 10 mg cm^{-2} with 20% TFE binder, gave a maximum H_2O_2 concentration of 0.74 mM at 2.5 V with a 10% current efficiency [21].

In the last few decades, various researchers have looked into the addition of transition metals (e.g. Co and Fe) and nitrogen in order to form complex catalytic sites and enhance the kinetics of the oxygen reduction reaction to peroxide [23-27]. Cobalt activated carbon has also been shown to enhance reaction kinetics for reducing O_2 to H_2O_2. Bonakdarpour *et al.* provided a short review of these papers [28]. Table 1-1 outlines some key points from some of these papers.

Table 1-1 List of publications on Cobalt activated carbon for O_2 reduction to H_2O_2.

Author/Year	**Catalyst Complex**	**Medium**	**H_2O_2 Production**
Marcotte et al. 2004 [29]	CoN_4/C	Acidic	N/A
Olson et al. 2010 [30]	Co-Nx/C	Acidic	N/A
Yang et al. 2007 [31]	Co-C-N	Acidic	N/A
Guillet et al. 2006 [15]	CoTMPP	Acidic	300 μmol cm^{-2} hr^{-1}
Zhang et al. 2009 [32]	Co/CNT	Acidic	N/A
Olson et al. 2010 [33]	CoPPy/C	Alkaline	N/A
Yamanaka et al. 2008 [34]	CoTPP	Acidic	139 μmol cm^{-2} hr^{-1}

N/A ≡ not available

Perhaps the most comprehensive study to date using a H_2/O_2 fuel cell for H_2O_2 production comes from Yamanaka and his co-workers [1, 34-38]. In their work, a three phase system is used where the thin solid electrodes separated by a Nafion membrane are immersed in a liquid electrolyte solution and O_2 gas is passed through the cathode electrode while H_2 gas is passed through the anode. This was a stationary system where the H_2O_2 concentration was allowed to increase with time. In 2008 Yamanaka reported a maximum H_2O_2 concentration of 1.2 M with Mn-porphyrin in an H_2SO_4 electrolyte and 2.4 M with a vapor grown carbon fiber (VGCF) electrode in NaOH electrolyte. Yamanaka also reported H_2O_2 production in neutral electrolyte solutions of up to 3.4 M from O_2 and water using activated carbon (AC) and a VGCF cathode in 2008 (Figure 1.5). In 2010, Yamanaka reported a H_2O_2 concentration of 1.69 M with a 31.5% current efficiency using a heat treated (at 1000°C) cathode catalyst composed of $CoCl_2$ and N-bidentate complex supported on XC-72 carbon black.

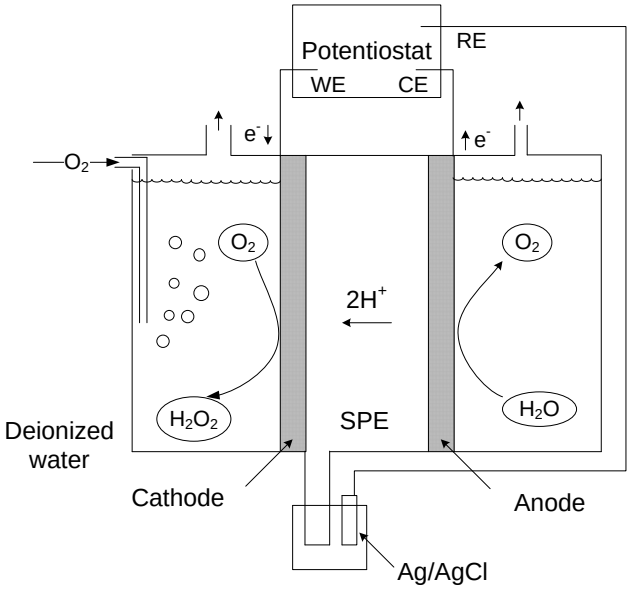

Figure 1.5 Diagram of Yamanaka's SPE electrolysis cell [38].

WE = working electrode, CE = counter electrode, RE = reference electrode, SPE = solid polymer electrolyte.

Around the same time, Bonakdarpour *et al.* at UBC also worked on a cobalt-carbon catalyst mixture as an oxygen reduction reaction (ORR) catalyst for H_2O_2 production[28]. They experimented with a catalyst composition of $Co(NO_3)_2$ supported on Vulcan XC-72 carbon black after heat treatment at 900 ℃ on a Toray graphite substrate support. Testing in an electrolysis cell gave a maximum H_2O_2 concentration of 0.03 M after 25 hours of electrolysis using O_2 dissolved in 0.5 M H_2SO_4 with 85% current efficiency operating at 0.24 V (vs RHE).

1.4.2 Power Co-Generation

This cathodic reduction of oxygen, can be coupled with either the anodic oxidation of a fuel (e.g., hydrogen) or the anodic oxidation of water. The former approach produces electrical power and is referred to as the *fuel cell mode* and the latter requires a power input and is referred to as the *electrolysis mode*, herein after. Co-generation of power and hydrogen peroxide can be achieved in the *fuel cell mode*. Details of these two approaches were discussed earlier.

With the right configuration, fuel cells can produce electrical power and value-added chemicals simultaneously [39-44]. In particular, co-generation of power and hydrogen peroxide has been reported [34-35, 45-48]. Brillas *et al.* focused their research on an alkaline fuel cell producing HO_2^-, the base form of H_2O_2 [48]. At varying electrolyte flow rates (between 2.1 and 20.0 mL min^{-1}), HO_2^- productivity was between 1.24 to 7.82 mmol cm^{-2} over an hour of reaction time. The current efficiency reached 96% with a corresponding power density of 33.2 mW cm^{-2} at these production rates. In 2010, Agladze *et al.* presented a direct methanol fuel cell concept, with 1 M CH_3OH / 7 M KOH in the anolyte and 30 g L^{-1} NaCl in the catholyte, which produced H_2O_2 and electricity, at a rate of 277 μmol hr^{-1} cm^{-2} and the corresponding power density was 2.5 mW cm^{-2}. The current efficiency for hydrogen peroxide generation reached 95%. [45]. Agladze also reported

an aluminum-air semi fuel cell that produced H_2O_2 at a rate of 1,715 μmol hr^{-1} cm^{-2} (current efficiency: 85%) with 8 mW cm^{-2} of power density operating at 100 mA cm^{-2} with a 6 M KOH electrolyte solution and anion-exchange membrane [46]. The research group of Yamanaka has published a number of papers on production of H_2O_2 in a batch-mode PEMFC set-up [1, 34-36, 49]. In their work, the thin electrodes separated by a Nafion membrane, are immersed in a batch solution, either 1.2 M HCl [35-36] or deionized water [1, 34] and O_2 and H_2 gas are purged in the cathode and anode compartments, respectively. The authors also experimented with several cathode catalysts such as: activated carbon/vapor grown carbon fibre, Mn-porphyrin, and $CoCl_2$/N-bidentate complex [1, 34-36]. In 2010, Yamanaka *et al.* reported a H_2O_2 concentration of 1.69 M in deionized water and a rate of H_2O_2 production of 470 μmol cm^{-2} hr^{-1}, when operating at a current density of 80 mA cm^{-2} corresponding to a 32% current efficiency.

1.4.3 Organic Electrocatalyst

The present commercial dependence of H_2O_2 supply on the AQAO chemical process has led to several studies using anthraquinone as an electrocatalyst in solid polymer electrolyte (SPE) cells. These researches focused on various methods of attaching the quinone group onto the carbon back support, alternately named quinone modified electrodes.

The oxygen reduction process on these quinone modified electrodes, first introduced by Hossain *et al*. [50], is an electrochemical-chemical (EC) approach. This approach suggests that the surface attached quinone group is reduced electrochemically and forms the quinone radical anion on the carbon surface. The quinone radical then reduces oxygen into the superoxide radical anion, which is further reduced to form hydrogen peroxide.

$$Q + e^- \rightarrow Q^{\bullet -} \qquad \text{Eqn 1-17}$$

$$Q^{\bullet -} + O_2 \rightarrow Q + O_2^{\bullet -} \qquad \text{Eqn 1-18}$$

$$2O_2^{\bullet -} + H_2O \rightarrow O_2 + HO_2^- + OH^- \qquad \text{Eqn 1-19}$$

or

$$O_2^{\bullet -} + H_2O + e^- \rightarrow HO_2^- + OH^- \qquad \text{Eqn 1-20}$$

Where the second reaction step (Eqn 1-18) is the rate determining step.

In recent years, other researchers have published work on the proposed mechanism [51-59]. These research efforts utilized various different carbon support structures with surface adsorbed quinone groups, and studied the effects these modified electrodes have on the kinetics and the pH dependence of oxygen reduction. Table 1-2 lists some of the findings from these publications.

Table 1-2 Surface modified carbon electrodes with quinone groups for O_2 reduction.

Author/year	Carbon Structure	Quinone Type	Modification Type
Hossain et al. / 1989 [50]	HOPG	9,10-phenanthrenequinone	Surface Adsorption
	OPG	2-aminoanthraquinone	Chemical attachment
Tammeveski et al. / 2001 [57]	GC/RRDE	anthraquinone	Electrochemical grafting
Sarapuu et al. / 2005 [54]	BDD HOPG	9,10-anthraquinone 9,10-phenanthraquinone	Electrochemical grafting
Jürmann et al. / 2007 [53]	GC	Anthraquinone Phenanthrenequinone	Electrochemical grafting
Vaik et al. / 2004 [60]	GC/RRDE	Phenanthrenequinone	Covelant attachment
Manisankar et al. / 2004 [61-62]	GC/riboflavin	1,4-naphthoquinone 9,10-anthraquinone	Organic media
Wang et al. / 2012 [63]	GC/RRDE GDE	9,10-anthraquinone riboflavin	Surface adsorption

An alternate reaction mechanism, proposed by Tissot and Huissoud [64], showed a 2 proton and 2 electron process on surface confined anthraquinones [56]:

$$Q(ads) + 2H^+(aq) + 2e^- \rightarrow H_2Q(ads) \quad \text{Eqn 1-21}$$

$$H_2Q(ads) + O_2\,(aq) \rightarrow Q(ads) + H_2O_2(aq) \quad \text{Eqn 1-22}$$

Almost all of the research focused on carbon electrode modifications with a variation of the quinone group, with the aim to increase O_2 reduction kinetics, especially in neutral pH mediums. One exception is the use of riboflavin modified carbon electrodes described by Berchmans and Vijayavali [65]. Manisankar *et al*. [61] used these modified carbon electrodes, with the riboflavin acting as an electron transfer mediator, together with naphthoquinone and anthraquinone as organic media, increased O_2 reduction kinetics by lowering the overpotential 500 – 750 mV. In his Master's project, Andrew Wang [63] at UBC used this unique characteristic of riboflavin, grafted a riboflavin-anthraquinone-2-carboxylate ester (RF-AQ) and showed an increase in O_2 reduction kinetics.

1.5 Fuel Cell System

A solid polymer electrolyte (SPE) cell is a type of electrochemical cell that uses an ion conducting membrane as the electrolyte between the cathode and anode electrodes. It is commonly known as polymer electrolyte membrane or a proton exchange membrane (PEM) in an acidic fuel cell. A diagram of the PEM fuel cell is shown in Figure 1.6. PEM fuel cells typically operate around 80 ℃ and use an electrochemical fuel such as hydrogen and oxygen or air as the oxidant.

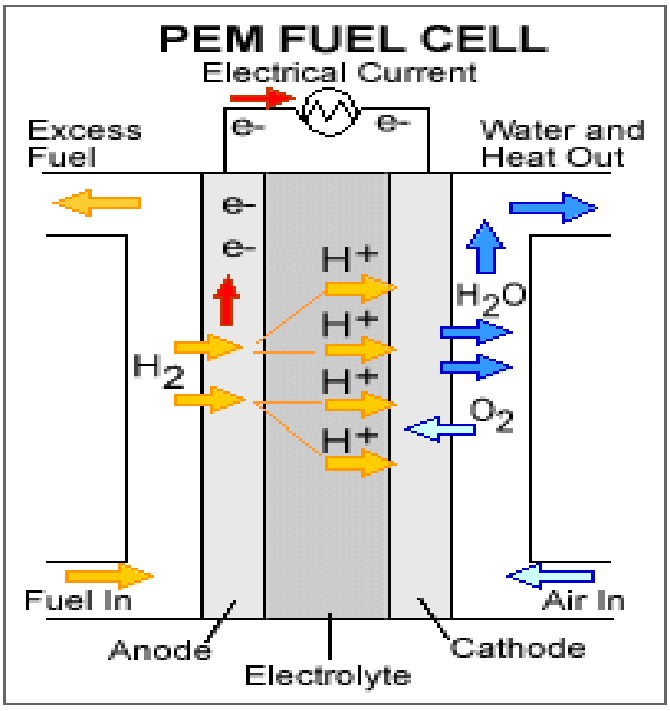

Figure 1.6 Diagram of a PEM fuel cell[66].

The solid polymer electrolyte (typically made from a fluorinated sulfonic acid polymer or other similar polymers) carries out the main operating principle of the PEM fuel cell. The solid polymer is an excellent proton conductor as well as an excellent electron inhibitor, and separates the reactant gases. A hydrogen molecule is dissociated into electrons and protons at the anode with the help of a catalyst (typically platinum). The polymer electrolyte allows the protons to pass through to the cathode side. At the cathode electrode (typically platinum), protons and electrons (from the external load) will reduce oxygen molecules to water. At the same time, electro-osmotic drag passes liquid water from the anode to the cathode via the porous membrane (solid electrolyte) and is released at the cathode outlet.

1.5.1 Fuel Cell Mode Operation

Electrochemical synthesis of H_2O_2 in fuel cell mode operation uses hydrogen as the fuel on one electrode and oxygen or air as the oxidant on the other electrode. In this mode of operation, the reduction of oxygen happens on the cathode (+) and the oxidation of hydrogen occurs at the anode (-) (Figure 1.7).

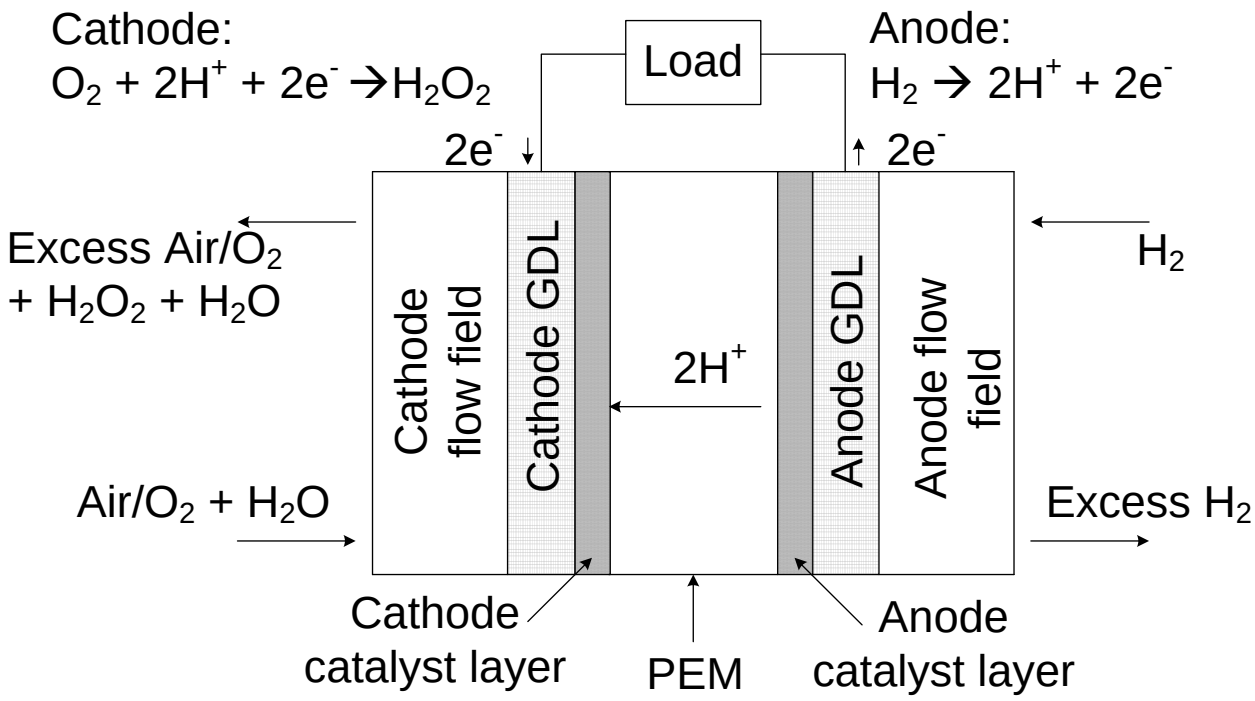

Figure 1.7 Schematic of a PEM fuel cell.

1.5.1.1 Standard Reduction Potential Scale – Fuel Cell Mode Operation

The fuel cell mode of operation is usually operated galvanostatically. Hence at a given applied load, the corresponding potential must be at or below the reduction potential for O_2/H_2O_2 in order to sustain prolonged production. Figure 1.8 depicts various standard reduction potentials and their corresponding reactions relating to H_2O_2 production.

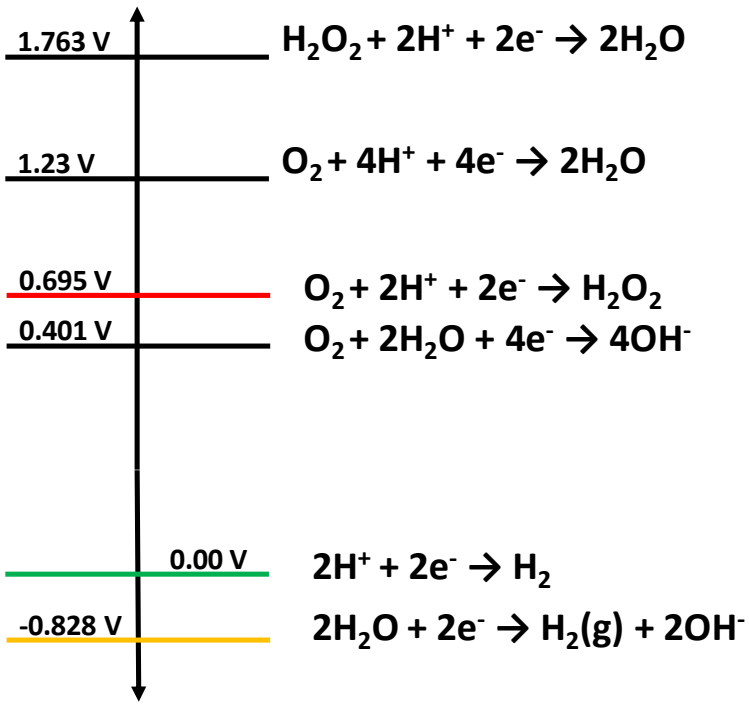

Figure 1.8 Standard reduction potential scale for half-cell reactions involving H_2, O_2, H_2O, and H_2O_2.

1.5.1.2 Fuels Available

Different fuels are available for the anode of the SPE cell. Although a number of different fuels are available for fuel cells [67], the most common fuel is hydrogen.

Table 1-3 Primary and alternate fuels for different types of fuel cells [67].

Gas Species	PAFC	MCFC	SOFC	SPE-C
H_2	Fuel	Fuel	Fuel	Fuel
CO	Poison	Fuel	Fuel	Poison
CH_4	Diluent	Diluent	Fuel	Diluent
CH_4OH	--	--	--	Fuel for DMFC

Other fuels such as methane, ethanol, biomass, or even landfill gas can be used as fuels for fuel cells as well; however, they will require the use of steam reforming or partial oxidation in order

to extract the hydrogen first. A particular challenge with extraction of hydrogen from hydrocarbon sources is the potential for the presence of impurities such as CO which will poison the catalyst (platinum) used in the SPE cells.

Another possible option is the direct methanol fuel cell (DMFC). The anode reaction ($CH_3OH + H_2O \rightarrow CO_2 + 6H^+ + 6e^-$) converts methanol directly into electrical energy, without the use of a reformer. The problem that DMFCs face is extended efficiency loss due to methanol crossover, and also more sluggish kinetics for the oxidation of methanol [68-69].

From a contamination point of view, hydrogen is the best fuel for production of hydrogen peroxide in SPE cells. There are no harmful side products or costly side processes. Most importantly it will not contaminate the drinking water (which a DMFC would as a result of the methanol crossover).

1.5.2 Electrolysis Mode Operation

In a typical PEM water electrolysis cell, the anodic reaction (Eqn. 1-23) splits liquid water into gaseous oxygen and protons with the use of external electric current [70-71]. The cathodic reaction (Eqn. 1-24) reduces the protons that diffuse across the solid electrolyte to form molecular hydrogen.

- Anode (-): $2H_2O \rightarrow O_2 + 4H^+ + 4e^-$ $E°_{25°C} = -1.23$ V Eqn. 1-23
- Cathode (+): $4H^+ + 4e^- \rightarrow 2H_2$ $E°_{25°C} = +0.0$ V Eqn. 1-24

Similar to a PEM fuel cell, a PEM electrolysis cell consists of a SPE membrane, sandwiched between two layers of electrocatalysts, the anode and the cathode. On the anode electrode, the oxygen evolution reaction (OER) takes place. On the cathode electrode, the hydrogen evolution reaction (HER) releases hydrogen gas. The two reactions are closely related to each other. The amount of protons available for the HER depends on the reaction kinetics of the OER on the anode electrode. The complex oxide-metal interactions in the OER reaction mechanism means the electrode surface needs to be highly active, while being able to withstand the highly oxidative conditions. The slow reaction kinetics lead to a much higher overvoltage on the anode electrode than on the cathode electrode. Hence the operating potential needs to be higher than the thermodynamic water splitting potential of 1.23 V in order to provide the extra power needed to carry the reaction forward at a reasonable rate [70].

Electrosynthesis of H_2O_2 in a PEM cell operated in electrolysis mode (Figure 1.9) uses an external power supply to break water down to hydrogen protons and oxygen on the anode (+) electrode. This mode of operation is similar to water electrolysis; however the cathode reaction is different. On the cathode electrode, hydrogen evolution reaction is replaced by oxygen reduction to H_2O_2, which occurs with the aid of an appropriate catalyst.

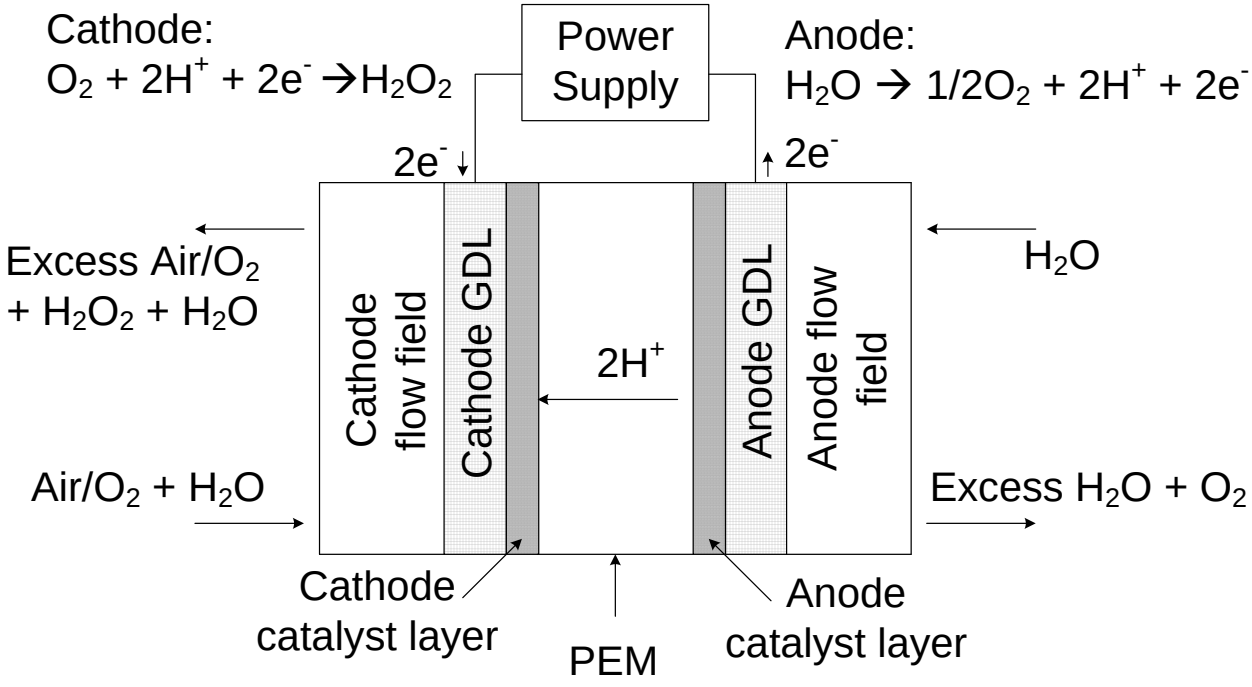

Figure 1.9 A PEM fuel cell operating in electrolysis mode.

Electrolytic production of alkaline H_2O_2 utilizing the Oloman/DOW-Huron Process [14, 16] had been commercialized at some point with good success in the pulp and paper industry, although it is no longer in operation. Davison *et al.*[72] and Yamada *et al.*[16] have also reported similar H_2O_2 production in an alkaline medium. Table 1-4 summarizes findings from these three publications.

Table 1-4 Important findings of electrolytic alkaline H_2O_2 production in various media.

Author/Year	Davison 1983 [72]	Yamada 1999 [16]	Oloman 1979 [14]
Cell area	0.025 m^2	0.8 m^2	0.2 m^2
Cathode (thickness)	RVC foam (0.3 cm)	Carbon felt (0.2cm)	Graphite chips (0.1cm)
Anode	S.S. mesh	S.S. mesh	S.S. plate
Membrane	Nafion 425	Nafion 117	porous diaphragm
electrolyte	2 M NaOH	2 M NaOH	2M NaOH
Voltage	1.3 V	2.1 V	1.8 V
Current Density	876 A m^{-2}	1500 A m^{-2}	1200 A m^{-2}
Current Efficiency	46%	97.4%	60%
[H_2O_2]	0.45 M	0.90 M	0.8 M

Other researchers have reported success in H_2O_2 production in their bench-top electrochemical reactors utilizing either acidic or neutral medium [8, 19-22, 38, 73-77]. In 2000, Drogui *et al*. used a cylindrical electrolysis cell with a diaphragm separator that oxidized water into oxygen and protons at the anode, and hydrogen peroxide was produced at the cathode through oxygen reduction [74]. Ando and Tanaka proposed a polymer electrolyte cell setup that generates hydrogen gas at the anode and alkaline hydrogen peroxide at the cathode [77]. Table 1-5 lists examples of this research, as well as some of their important findings.

Table 1-5 Important finding of electrolytic H_2O_2 production in acidic or neutral media.

Author/Year	Wakita 2000 [73]	Kolyagin 2003 [19]	Tatapudi & Fenton 1993 [21]	Gopal 2004 [8]	Drogui 2001 [74]	Gyenge 2001 [76]
Cell area	20 cm^2	5 cm^2	13 cm^2	6.4 cm^2	177 cm^2	267 cm^2
Cathode	Gold on Carbon	A 473-E carbon	10 mg cm-2 graphite powder (CCM)	Quinone/ Nonionic Surfactant	RVC (0.4cm)	Graphite felt (0.45cm)
Anode	Pt on Carbon	Pt plate	Pt black/Teflon	Same as cathode	DSA	DSA
Membrane	Nafion 117	MF-4SK-100 CEM	Nafion 117	Nafion 115	Diaphragm	Nafion 350
electrolyte	NaCl	1 M H_2SO_4	Humid O_2/water	1 N H_2SO_4	Tap Water	1 M Na_2SO_4
Voltage	2 V	0.52 V	2.5 V	2.5 V	25 V	5.6 – 6.5 V
Current Density	50mA cm^{-2}	50 mA cm^{-2}	50 mA cm^{-2}	25 mA cm^{-2}	11.3 mA cm^{-2}	100 mA cm^{-2}
Current Efficiency	80 %	70 %	10 %	25 %	21%	55 – 90 %
[H_2O_2]	17.6 mM	1.1 M	0.74 mM	0.2 M	0.5 mM	0.24 M

Wakita *et al.* [73] claimed a 17.6 mM H_2O_2 and 80% current efficiency at 2 V and 1 A using pure water with carbon supported gold catalyst as cathode and Nafion 117 as the SPEM. Gopal (2004) reported the successful production of 0.92 M H_2O_2 with 90% current efficiency in a small 6.4 cm^2 cell using 1N H_2SO_4 electrolyte solution and a quinone redox catalyst/nonionic surfactant mixture [8]. Gyenge *et al.* (2001) used anthraquinone as a mediator in a trickle bed type electrochemical cell with a Nafion 350 membrane separator [76]. Through experiments with 3D graphite felt and RVC, they produced 40 mM H_2O_2 at 70% current efficiency in acidic solution (pH=3). By recycling the catholyte back to the cell, they increased H_2O_2 concentration to 240 mM, but the current efficiency dropped to 55% after just 3 hours.

1.5.2.1 Quinones as Oxygen Reduction Catalysts for H_2O_2 Production

As discussed previously in Section 1.2, successful commercialization of hydrogen peroxide production through the cyclic chemical AQAO process has become the dominant process for the world's supply of H_2O_2. One major drawback of this process is the anthraquinone degradation in the chemical reduction step. The cost of this drawback can be reduced for large scale H_2O_2 production. For small scale or on site H_2O_2 productions, however, a more economical alternative is needed. Several researchers have focused on electrochemical reduction of anthraquinone to replace the chemical reduction process [78-81].

Although the various research efforts on quinone modified carbon electrodes have seen success as an electrocatalyst for O_2 reduction, a few have reported successful production of H_2O_2 in their results (Table 1-6). In 2004 Gopal reported the successful production of 0.92 M H_2O_2 with 90% current efficiency in a small 6.4 cm^2 cell using 1N H_2SO_4 electrolyte solution and a quinone redox catalyst/nonionic surfactant mixture [8]. In 2003 Gyenge *et al.* used anthraquinone as a mediator in a trickle bed type electrochemical cell with a Nafion 350 membrane separator [79]. Through experiments with 3D graphite felt and reticulated vitreous carbon (RVC), they produced 40 mM H_2O_2 at 70% current efficiency in acidic solution (pH = 3). By recycling the catholyte back to the cell, they increased H_2O_2 concentration to 240 mM, but the current efficiency dropped to 55% after just 3 hours.

Wang *et al.*[63] was able to synthesize a novel riboflavinyl-anthraquinone (RF-AQ) composite catalyst and surface adsorb onto Vulcan XC-72 carbon support which led to an increase in the onset of O_2 reduction and also an increase in H_2O_2 selectivity. Through bench top

chronoamperommetry in electrolysis mode, they were able to generate H_2O_2 at a rate of 21 μmol hr^{-1} cm^{-2} at a current density of 1.3 mA cm^{-1} with a current efficiency of 70% operating at 0.1 V [63].

Table 1-6 List of quinone modified carbon electrode studies for O_2 reduction to H_2O_2.

Author/Year	**Catalyst Complex**	**Modification Type**	**H_2O_2 Production**
Gopal 2004 [8]	Quinone/surfactant	Surface Attachment	0.90 M @ 90% CE
Gao *et al.* 2007 [82-83]	Poly(1,5-diaminoanthraquinone)	Surface Polymerization	N/A
Lobyntseva *et al.* 2007 [84]	Glassy carbon/Carbon-anthraquinone	Surface Attachment	1% CE
Forti *et al.* 2007 [85]	2-ethylanthraquinone	Surface Adsorption	22 mmol L^{-1} hr^{-1}
Wilson *et al.* 2006 [86]	Anthraquinone-2-carboxylic-allyl Ester	Surface Adsorption	3.8 mM @ 74% CE
Gyenge 2003 [78]	anthraquinone	Three phase emulsion	240 mM @ 55% CE
Wang 2012 [63]	RF-AQ	Surface Adsorption	21 μmol hr^{-1} cm^{-2}

N/A ≡ not available

One important advantage of the quinone modified carbon electrodes is their slow rate of reduction for H_2O_2 [56]. Most other electrocatalyst used in H_2O_2 electrosynthesis tend to further reduce H_2O_2 into H_2O and O_2, including the inorganic catalyst described previously, i.e., the Co-C composite catalyst. Hence the advantage the quinone modified electrodes has can be very useful.

1.5.2.2 Standard Reduction Potential Scale – Electrolysis Mode Operation

In a typical electrolysis operation, water decomposition occurs at an external applied potential of about -2 V, and hydrogen evolution occurs at the cathode. In electrolysis mode operation for H_2O_2 production, there is an additional reduction potential of H_2O_2 to be considered at the

cathode. Figure 1.10 shows the various different reduction potentials related to electrolytic H_2O_2 production.

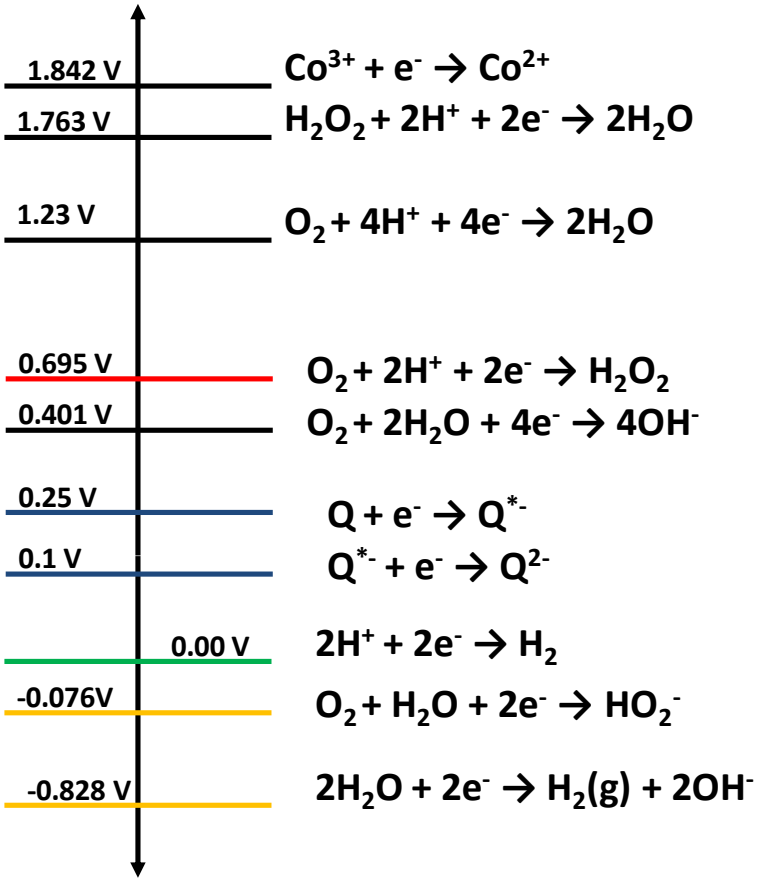

Figure 1.10 Standard Potential Scale Diagram for H_2O_2 production in electrolysis mode of operation.

1.6 Advanced Oxidation Processes for Water Treatment

Increasing environmental concerns in the last decade has led to a concentrated effort on the application of advanced oxidation processes (AOPs) in the areas of water treatment and water purification [87-88]. Andreozzi *et al.* [88] list nine AOPs: H_2O_2/Fe^{2+}, H_2O_2/Fe^{3+}, $H_2O_2/Fe^{2+}(Fe^{3+})$/UV, H_2O_2/Fe^{3+}-Oxalate, Mn^{2+}/Oxalic acid/Ozone, $TiO_2/h\upsilon/O_2$, O_3/H_2O_2, O_3/UV,

H_2O_2/UV[88]. Six of these involve hydrogen peroxide. The following three are commonly used today.

O_3/H_2O_2: $2O_3 + H_2O_2 \rightarrow 2OH^{\bullet} + 3O_2$ Eqn 1-25

O_3/UV: $O_3 + h\upsilon + 2H_2O \rightarrow H_2O_2 \rightarrow 2OH^{\bullet}$ Eqn 1-26

H_2O_2/UV: $H_2O_2 + h\upsilon \rightarrow 2OH^{\bullet}$ Eqn 1-27

These processes use very strong oxidants such as hydrogen peroxide (H_2O_2) and ozone (O_3) along with ultraviolet (UV) radiation to produce hydroxyl ($OH^{\bullet}$) radicals at or near ambient temperature and pressure to attack and destroy most organic compounds in water [89]. Other AOP processes include the well known Fenton process, where the $OH^{\bullet}$ radical is formed through a simple chemical reaction between H_2O_2 and Fe^{2+} cations. The hydrogen peroxide itself is also a very reactive oxidant, as evidenced in Table 1-7 [90], but hydroxyl radicals are almost twice as reactive as hydrogen peroxide.

Table 1-7 Relative oxidation power of some oxidizing species [90]

Oxidizing species	**Relative oxidation power**
Chlorine	1.00
Hypochlorous acid	1.10
Permanganate	1.24
Hydrogen peroxide	1.31
Ozone	1.52
Atomic oxygen	1.78
Hydroxyl radical	2.05
Positively charged hole on TiO_2^{+}	2.35

1.6.1 Ozone/UV Process

At a wavelength of 254 nm, Ozone (O_3) decomposes to the hydroxyl radical ($OH^{\bullet}$) with the following reaction mechanism [89, 91]:

$$O_3 + h\nu \rightarrow O^1(D) + O_2 \qquad \text{Eqn 1-28}$$

$$O^1(D) + H_2O \rightarrow H_2O_2 \qquad \text{Eqn 1-29}$$

$$H_2O_2 + h\nu \rightarrow 2OH^\bullet \qquad \text{Eqn 1-30}$$

Ozone itself has a very high extinction coefficient (3600 M^{-1} cm^{-1}) at this wavelength. However, since the reaction mechanism involves several pathways as well as two different phases, the use of stirred tank photochemical reactors has been recommended to achieve better mass transfer between the reacting species [89]

1.6.2 H_2O_2/UV Process

At wavelengths lower than 280 nm, hydrogen peroxide (H_2O_2) undergoes hemolytic cleavage, forming the hydroxyl radical:

$$H_2O_2 + h\nu \rightarrow 2OH^\bullet \qquad \text{Eqn 1-31}$$

The extinction coefficient of H_2O_2 is much lower (18.6 M^{-1} cm^{-1} at 254 nm), thus the hydroxyl radicals can attack the unreacted H_2O_2:

$$H_2O_2 + OH^\bullet \rightarrow HO_2^\bullet + H_2O \qquad \text{Eqn 1-32}$$

$$H_2O_2 + HO_2^\bullet \rightarrow OH^\bullet + H_2O + O_2 \qquad \text{Eqn 1-33}$$

$$2HO_2^\bullet \rightarrow H_2O_2 + O_2 \qquad \text{Eqn 1-34}$$

The H_2O_2/UV process is more favored than the O_3/UV process, even though ozone has a higher oxidative potential than H_2O_2. The H_2O_2/UV process is simpler, involving just one reaction;

whereas the O_3/UV process produces H_2O_2 as an intermediate. From a reaction medium point of view, H_2O_2 is a liquid and is completely miscible with water and stable in most neutral aqueous solutions, whereas ozone requires a two phase reaction contactor and it has a low solubility of just 1.05 g cm^{-3} [92].

1.7 System Implementation

Water treatment systems and their associated processes, including AOP processes, are designed and built in different sizes depending on the size of the end user community. A H_2O_2 generating reactor can be integrated with an AOP H_2O_2 /UV reactor in different ways in order to meet the requirements of an efficient water treatment system. Two different approaches will be discussed briefly.

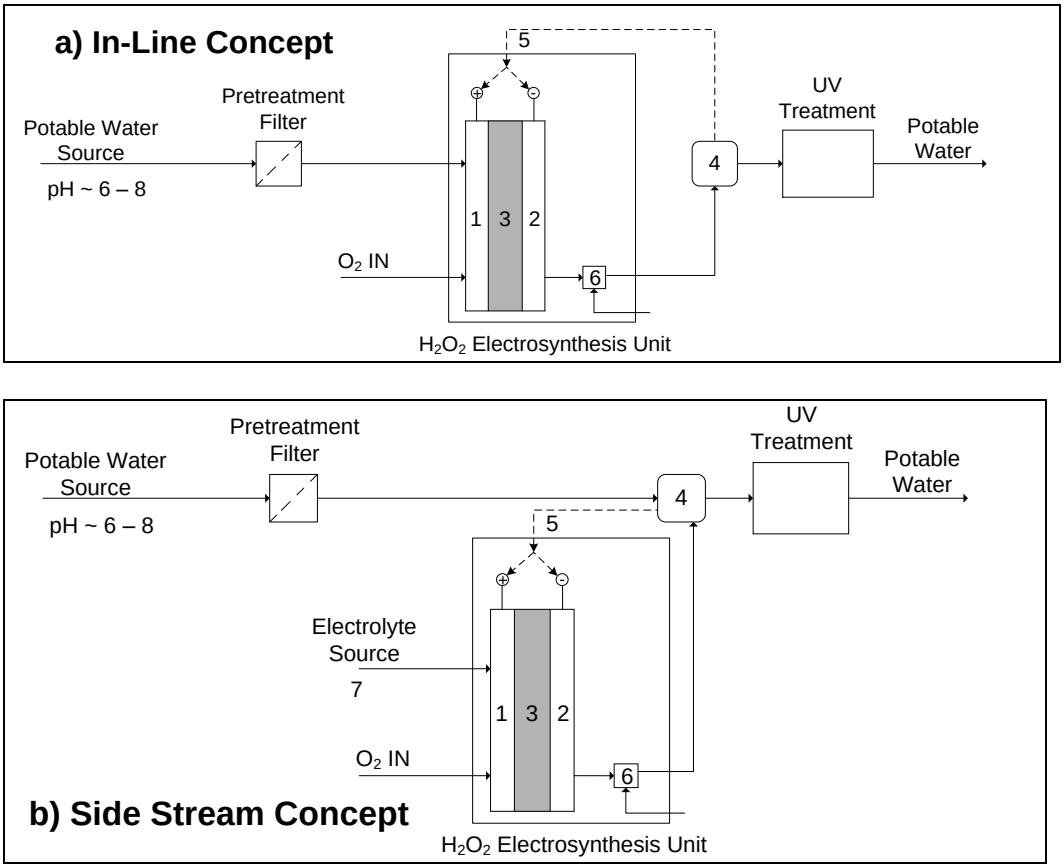

Figure 1.11 Block diagram of an AOP H_2O_2 /UV water treatment process with in-situ generation of hydrogen peroxide. a) In-Line H_2O_2 electrosynthesizer and b) Side Stream H_2O_2 electrosynthesizer. The numbered components are: 1. Anode, 2. Cathode, 3. Polymer electrolyte; 4. H_2O_2 analyzer and process control system; 5. Control loop to monitor H_2O_2 output; 6. pH adjustment unit; 7. One of three possible electrolyte sources: NaOH (pH > 13), buffer electrolyte (pH 6-8), or pure H_2O from potable water source (note: this is for option b only).

The In-Line production and integration concept (Figure 1.11a) is a compact on-stream design. This concept implies that the H_2O_2 unit can be designed as a modular unit that can easily be exchanged if failures occur. Possible problems include low conductivity, fouling of electrodes and/or porous separator/membranes by the organic matter in the source water. If this option is used, the entire treatment process will need to stop when the H_2O_2 generating unit needs replacement. One other factor to consider is the volumetric flow of the water to be treated.

Companies like Bi Pure Water Inc. can provide complete small water treatment plants that deliver treated potable water at a minimum rate of 75 L min^{-1} [93]. To date the most successful commercial application of the H_2O_2 electro-synthesis design, the DOW-Huron process, was able to handle a maximum water flowrate of 11.6 L min^{-1} with a 7.5 m^2 active area [94]. For typical laboratory scaled H_2O_2 electrosynthesis reactors like the UBC Trickle Bed Reactor with a 0.04 m^2 active area is only capable of handle source water flowrates of just 50 mL min^{-1}! Water flowrates require proper management in a H_2O_2 electrosynthesis reactor. If the water flowrate is too high the reactor will become flooded, thus interrupting the electrochemical reaction necessary for the production of H_2O_2.

The Side Stream production and integration concept (Figure 1.11b) allows for more flexible electrochemical cell design and operation. Maintenance to the H_2O_2 electrosynthesizer unit would not require total treatment shutdown. In addition, water flowrates would not be an issue as the liquid flow through the electrosynthesizer unit is separate from the water treatment system's high flowrates. This could potentially be a more simpler design. Another advantage of the side stream concept is that H_2O_2 can be produced in concentrated form, stored and fed to the H_2O_2/UV treatment system as necessary. This means that the H_2O_2 electrosynthesizer unit would only operate when H_2O_2 levels are low in the supply tank. Therefore, the flexibility of this side stream electrosynthesizer design and operation suggests that this is the preferred choice for our project.

1.8 Water Management

Achieving high performance and efficiency in fuel cells requires proper water management. In order to achieve this two conflicting needs are considered: 1) adequate membrane hydration and 2) prevention of water flooding in the catalyst layers. Both the fuel (hydrogen) and oxidant (air) streams are humidified before entering the fuel cell. However, lower operating temperatures, combined with high humidification levels and high current densities can cause condensation of the water vapor in the gas streams, leading to flooding in the catalyst layers and a decrease in cell performance.

In a PEM fuel cell, water is generated at the cathode catalyst-membrane interface as a result of the ORR. Thus the two phase mixture that leaves the cathode is a mixture of the water generated from various sources, as shown in the following equation and depicted in Figure 1.12:

$$W_{total,\ cathode\ exit} = W_{H2/O2\ reaction} + W_H + W_{E\text{-}O} - W_{B\text{-}D} \qquad \text{Eqn 1-35}$$

Where $W_{total,\ cathode\ exit}$ is the total H_2O at cathode exit, $W_{H2/O2\ reaction}$ is the water from the H_2/O_2 reaction, W_H is the water from the humidified air that enters the cathode, $W_{E\text{-}O}$ is the water from electro-osmotic drag transport from the anode, and $W_{B\text{-}D}$ is the water from back diffusion transport to the anode.

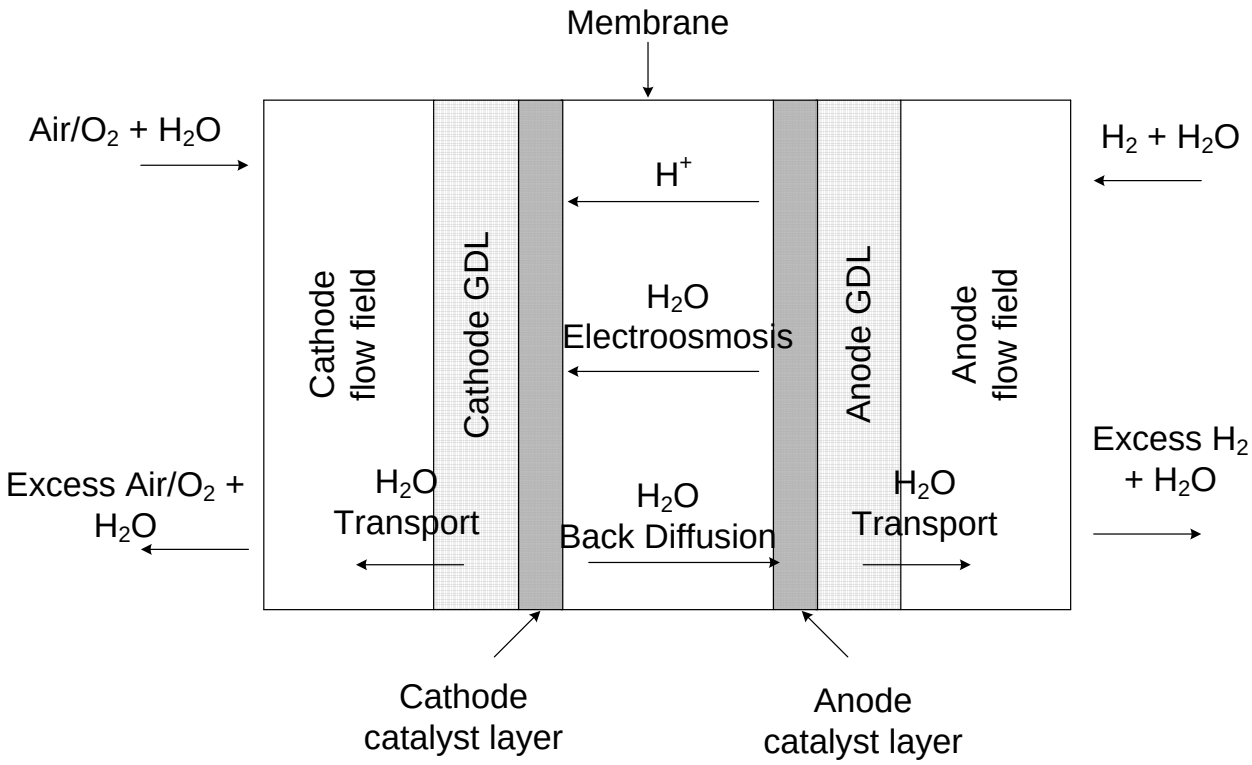

Figure 1.12 Water movements inside a PEM fuel cell.

For our system, as the oxygen reduction reaction that occurs on the cathode primarily produces hydrogen peroxide, thus the water generated as a result of the reaction will be from H_2O_2 reduction to water rather than O_2 reduction to water. Hence the new water balance equation will be as follows:

$$W_{total,\ cathode\ exit} = W_{H2O2\ reduction} + W_H + W_{E\text{-}O} - W_{B\text{-}D} \qquad \text{Eqn 1-36}$$

Where $W_{total,\ cathode\ exit}$ is the total H_2O at cathode exit, $W_{H2O2\ reduction}$ is the water from the H_2O_2 reduction, W_H is the water from the humidified air that enters the cathode, $W_{E\text{-}O}$ is the water from electro-osmotic drag transport from the anode, and $W_{B\text{-}D}$ is the water from back diffusion transport to the anode.

Therefore, it is essential that the cathode and the electrolyte membrane be properly hydrated.

Chapter 2 Research Objectives and Methodology

The primary objective of this project is to develop, optimize, and apply a novel in-situ hydrogen peroxide electrosynthesis reactor for coupling with AOPs in a side-stream concept (Figure 2.1) to eliminate pathogens, disinfection by-product precursors (DBPs) and harmful micro-pollutants in drinking water for small and remote communities.

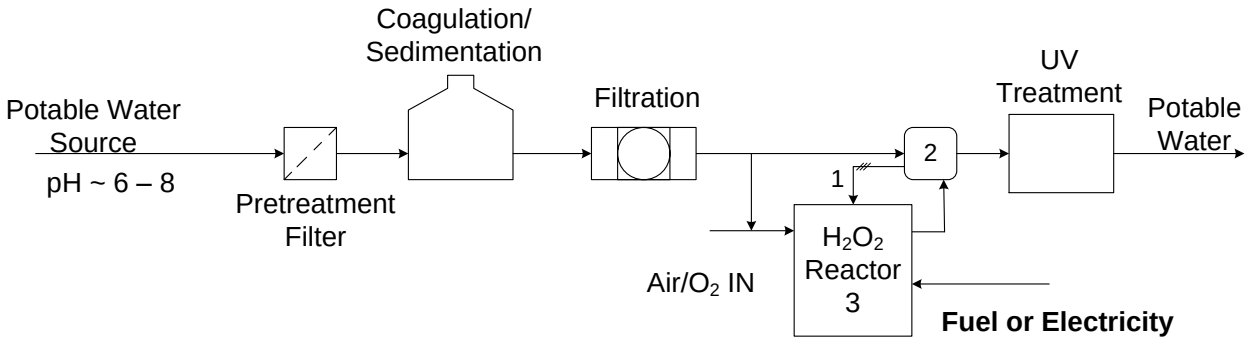

Figure 2.1 Integrating an H_2O_2 reactor in a small water treatment plant The side-stream components are: (1) Control loop to maintain the correct H_2O_2 output, (2) H_2O_2 analyzer and process control system, and (3) the H_2O_2 reactor.

This project was part of a larger research initiative, the RES'EAU WaterNet Program, which is a federally funded research program aimed at studying the drinking water issues currently affecting small rural communities across Canada[95]. The intent of this program is to introduce a cost effective portable water treatment to these communities. This portable H_2O_2/UV water treatment unit is intended to treat enough water supplies for a small community of 500 residents. Based on 500 liters per day of water required for each resident in the community, the H_2O_2/UV treatment unit would require 10 ppm (or 0.3mM) of H_2O_2 in order to provide sufficient treatment to the amount of water (250,000 liters supplied at 100 – 300 L/min) needed [96]. A H_2O_2 electrosynthesizer utilizing solid polymer electrolyte membrane (SPEM) can be integrated with

an AOP H_2O_2 /UV reactor in different ways in order to meet the requirements of the RES'EAU WaterNet research program.

Further examination of the project focused the scope of this thesis to a feasibility study of the use of SPEs in continuous flow mode for the reduction of oxygen to peroxide. This is a new approach since currently no other continuous flow SPE reactor for peroxide generation at neutral pH has been reported. In order to effectively develop this process in a systematic approach, the focus of the proposed research was geared towards:

1. Evaluation of the inorganic catalyst (cobalt-carbon complex) in a 50 cm^2 PEM fuel cell in a two stage parametric study (uni-variate experiment and factorial design experiment) utilizing thin catalyst layer membrane electrode assembly approaches and different operating conditions to determine maximum H_2O_2 production and power output.

2. Evaluation of both the inorganic catalyst (cobalt-carbon complex) and the organic catalyst (anthraquinone-riboflavinyl complex) with a 50 cm^2 SPE cell operated in electrolysis mode in a parametric study utilizing membrane electrode assembly and different operating conditions for H_2O_2 production.

3. Evaluation of the SPE reactor for the above cases to produce sufficient H_2O_2 in a continuous flow mode to meet small water treatment facility requirements.

The methodology of this work is based on the following aspects:

1. The evaluation of Fuel cell mode operation – based on an Inorganic catalyst study which consists of:
    - Cathode catalyst layer design (inorganic catalyst)
    - Baseline study with pure carbon catalyst
    - Thin catalyst layer test in 50 cm^2 SPE cell
        - Inorganic catalyst polarization experiments to study the impact of:
            - Temperature
            - Cathode catalyst loading
            - Cathode liquid flow rate
            - Cathode catalyst layer Teflon loading
        - Inorganic catalyst long term test
        - H_2O_2 stability test
    - Energy and material balance.

2. The evaluation of the Power Co-generation in fuel cell mode operation – which consists of:
    - Cathode catalyst layer design.
    - Baseline study with pure carbon catalyst.
    - Electrode preparation technique (with and without additional catalyst).
    - Baseline polarization study of the different catalyst layer designs.
    - Feasibility study

3. The evaluation of the Electrolysis mode operation – based on an Inorganic and organic catalyst study which consists of:
    - Cathode catalyst layer design (organic catalyst)
    - Anode electrode redesign – electrode preparation technique
    - Thin catalyst layer test in 50 cm^2 SPE cell
        - Organic catalyst polarization test
        - Organic catalyst long term test
        - Inorganic catalyst polarization test
        - Inorganic catalyst long term test
        - H_2O_2 stability test
    - Energy and material balance.

Chapter 3 Thesis Layout

There are a total of nine chapters in this thesis. Chapter 1 presents a brief introduction to hydrogen peroxide and its methods of production. In particular the electrochemical approaches for the synthesis of H_2O_2 are discussed. Chapter 2 provides an overview of the research objectives for this project, as well as an outline of the different tasks needed in order to accomplish the objectives. These tasks include experiments in both the fuel cell mode and the electrolysis mode, as well as long term recycle studies. Chapter 4 gives the experimental procedure and detailed instructions for both the fuel cell mode of operation and the electrolysis mode of operation, along with fuel cell materials and equipment used throughout the research project.

Chapter 5 focuses on the fuel cell mode of operation for the project. The catalyst studied in this mode of operation was the cobalt-carbon composite catalyst. A three variable factorial analysis was performed with the composite catalyst. These variables included catalyst loading, electrode Teflon content, and carrier water flow rate. In addition, the effect of cell temperature on H_2O_2 production was also studied. Parts of the material in this chapter have already been published:

- W. Li, A. Bonakdarpour, E. Gyenge, D.P. Wilkinson, Drinking Water Purification by Electrosynthesis of Hydrogen Peroxide in a Power-Producing PEM Fuel Cell, CHEMSUSCHEM 6(11) (2013): 2137-2143.

In Chapter 6, the power co-generation aspect of the project was studied. The cobalt-carbon composite catalyst was mixed with Platinum in a variety of configurations on the cathode electrode to test the feasibility of producing power as well as H_2O_2 in fuel cell mode operation. Parts of the materials presented in this chapter are currently in preparation for publication:

- W. Li, A. Bonakdarpour, E. Gyenge, D.P. Wilkinson, Multi-Functional Electrodes for Co-Generation of Electrical Power and Hydrogen Peroxide, In preparation, 2017.

- Chapter 7 discusses the main findings from the electrolysis mode of operation for the project. Both the cobalt-carbon composite catalyst and the Riboflavinyl-anthraquinone composite catalyst were studied. As well, a novel half-CCM approach on the anode electrode was utilized to study its effects on MEA durability on long term recycle tests. Parts of the materials presented in this chapter are currently being prepared for journal submission:

- W. Li, A. Bonakdarpour, E. Gyenge, D.P. Wilkinson, Electrolytic generation of Hydrogen Peroxide in a Solid polymer electrolyzer using organic and inorganic catalysts, In preparation, 2017.

Chapter 8 discusses the economic analysis for the design and processes for H_2O_2 generations.

Chapter 9 provides final conclusion and recommendations for the thesis work.

Chapter 4 Experimental Procedures

The primary focus of this thesis project centered around two different operation modes, fuel cell mode and electrolysis mode. Both operation modes utilized a solid polymer electrolyte cell to study several different parameters including cell temperature, cathode DI water flow rate, cathode gas diffusion layer (GDL) catalyst loading, cathode GDL Teflon loading, and catalyst implementation in different membrane electrode assemblies (MEAs). All tests were done in a Greenlight 2 kW Fuel Cell Test Station using a Tandem Cell Configuration.

4.1 PEM Fuel Cell Materials

4.1.1 Cathode Electrode Catalysts for Peroxide Generation

To further test the capability of down selected peroxide catalysts, MEAs were prepared and tested with a Tandem Cell using a Greenlight 2 kW Fuel Cell Test Station. The inorganic cobalt composite catalyst was tested in both the fuel cell mode and electrolysis mode of operation, while the organic RF-AQ catalyst was only tested in electrolysis mode operation. For the inorganic cobalt composite catalyst, the procedures outlined in Appendix A-1 were followed in order to generate the inorganic cathode catalyst. The organic RF-AQ catalyst was prepared following the steps outlined in Appendix A-2. To prepare the cathode electrode, an ink mixture of either the inorganic or organic cathode catalyst was prepared following the protocol given in Appendix A-3.1. Then the cathode electrode was prepared using the procedure outlined in Appendix A-4.

4.1.2 Anode Electrode

For the fuel cell mode operation, methods similar to preparing conventional gas diffusion electrodes with platinum black catalyst were used. Following the standard protocol for preparing ink mixture with platinum catalyst (outlined in Appendix A-3.2), the ink slurry was sprayed (Mastercraft HVLP air spray gun) onto a piece of non-wet-proofed carbon paper (Toray® TGP-H-060) heated to 80 ℃. The new anode gas diffusion electrode was allowed to dry overnight in the fume hood before final weighing in order to determine the platinum catalyst loading.

For electrolysis mode operation, the same Pt-black catalyst ink outlined in Appendix A-3.2 was used. However, due to carbon corrosion issues with electrolysis, two different catalyst support approaches were considered. The first approach was a commercially available titanium mesh with Pt-black catalyst (no carbon support) sprayed directly on the mesh. The titanium mesh was from Unique Wire LTD and had 99.99% commercial grade purity with 27% porosity. The titanium mesh was cut to 8 cm x 8 cm, cleaned in isopropanol for 4 hours under sonication. Then the Pt-black catalyst ink mixture was sprayed on the heated mesh following the same protocol used for Toray paper spraying. After spraying, the titanium mesh was annealed in an oven at 350 ℃ for 30 minutes. The annealed titanium mesh was then weighed and the platinum catalyst loading was determined. The second approach was the use of Pt-black catalyst coated on only one side of the Nafion membrane (also known as a half-CCM). The procedure for preparing the Pt-black catalyst half-CCMs is outlined in Appendix A-5. For this approach the titanium mesh used at the anode served only as the current collector.

4.1.3 Membrane Electrode Assembly

For both fuel cell mode and electrolysis mode operation, the membrane electrode assemblies were prepared following procedures outlined in Appendix A-6. However, for fuel cell mode operation, the MEA was hot-pressed (DAKE 44-426 Press) following the protocol listed in Appendix A-6. For electrolysis mode operation, the same hot press was used to prepare MEAs with Ti-Mesh as a support for the Pt-black catalyst layer. However MEAs with half-CCMs did not use the hot press to prepare MEAs (Please see Appendix A-6).

4.1.4 Fuel Cell Hardware

Commercially available research fuel cell hardware from Tandem Technologies Ltd was used throughout the project. This Tandem research fuel cell has an active area of 49 cm^2. The inlets and outlets for the anode and cathode, as well as the cooling water loop are all located in the manifold placed below the bottom current collector plate (Figure 4.3). Six thermocouples were inserted into the cell hardware through the bottom endplate to the test station, and monitored the temperature of the cooling water loop, the anode and cathode gas stream (both inlet and outlet), and the cell temperature.

Table 4-1 Flow field plate channel dimensions for anode and cathode in Fuel Cell Mode and Electrolysis Mode operation.

		Channel Width	Channel Depth	Channel Shape	Flow Field Type	Material
Fuel Cell Mode	**Anode**	1.00 mm Top 1.27 mm Bot.	0.51 mm	Trapezoidal	Serpentine	Graphite
	Cathode	0.89 mm Top 1.57 mm Bot.	1.27 mm	Trapezoidal	Serpentine	Graphite
Electrolysis Mode	**Anode**	1.00 mm	1.00 mm	Square	Serpentine	Gold plated Brass
	Cathode	0.89 mm Top 1.57 mm Bot.	1.27 mm	Trapezoidal	Serpentine	Graphite
Water Flow Field Plate		3.00 mm*	2.00 mm*	Rectangle	Serpentine	Graphite

Note: Data taken from [97], * indicates measured values.

A standard single pass serpentine flow field was used for both the anode and the cathode flow field plates. For fuel cell mode operation, these plates were made with graphite, as received from Tandem Technologies (Figure 4.1). For electrolysis mode operation, the cathode plate remained the same, while the anode plate was made of brass coated with nickel and gold for corrosion resistance (Figure 4.2). These plates were used to sandwich the MEA inside the cell hardware (Figure 4.3).

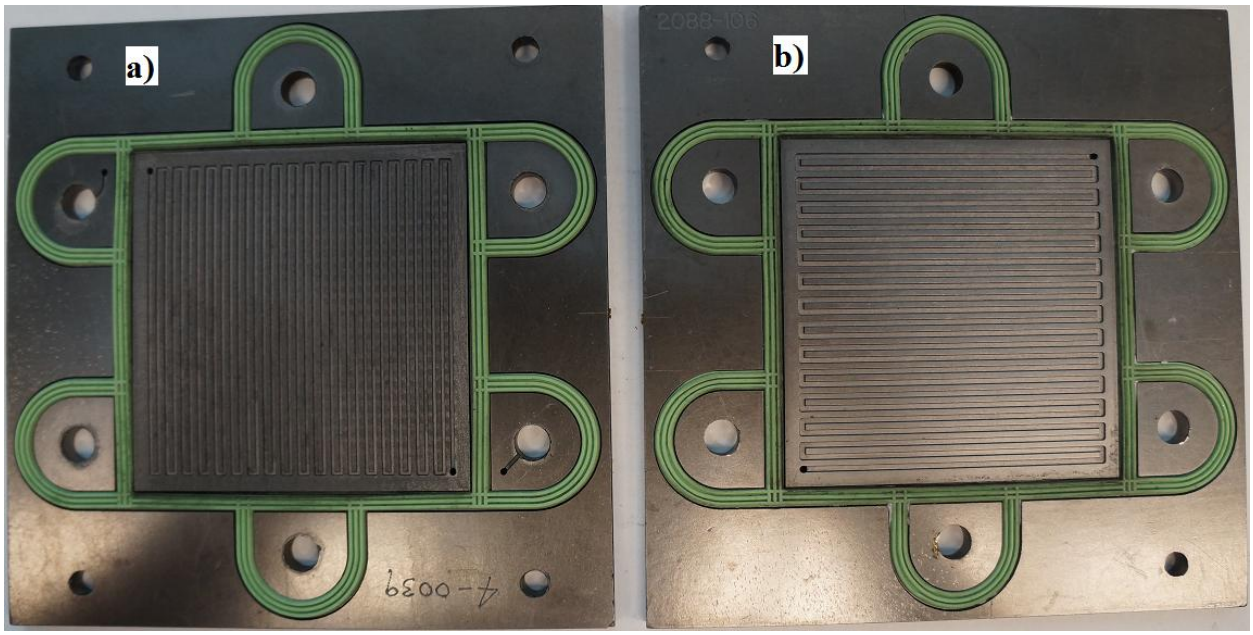

Figure 4.1 Anode and cathode flow field plates for fuel cell mode operation a)Anode flow field plate; b) Cathode flow field plate. Note the cross flow direction.

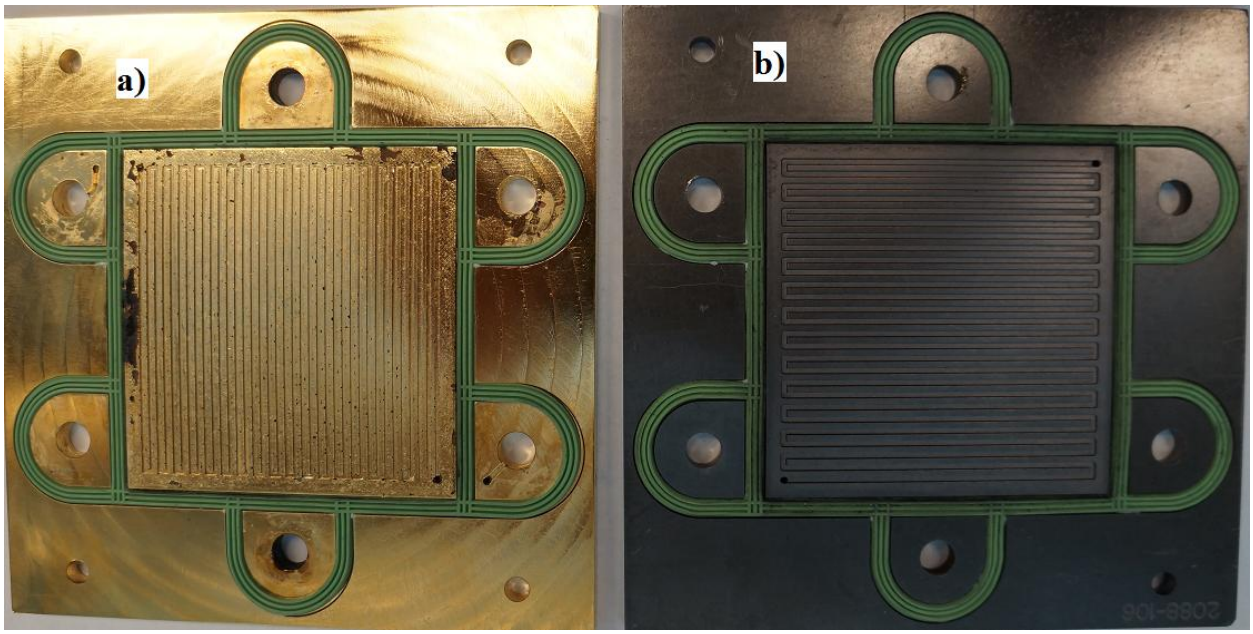

Figure 4.2 Anode and cathode flow field plates for electrolysis mode operation a) Anode flow field plate made from brass plated with nickel and gold; b) Cathode flow field plate. Note the cross flow direction. Note: Figure 4.2a showed result of anode corrosion on thinly plated brass. Possible alternative include titanium.

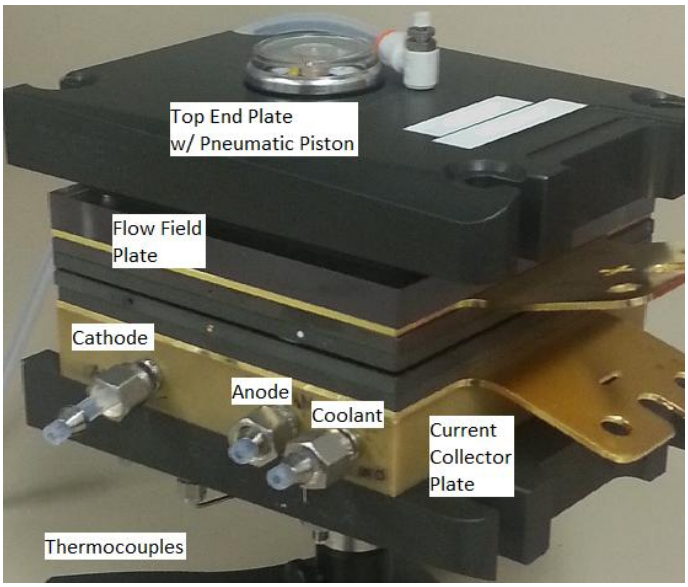

Figure 4.3 Picture of Tandem 50 cm^2 Research Cell hardware.

The completed cell was pressurized with nitrogen gas using a pneumatic piston in the top end plate that provided even pressure distribution across the cell (Figure 4.3). Sealing of the MEA between the flow field plates was achieved with Silicone JRTV gasket from Dow Corning (Figure 4.1 and 4.2).

4.1.5 Greenlight 2 kW Fuel Cell Test Station

Experiments for both fuel cell mode operation and electrolysis mode operation were conducted on a 2 kW Greenlight fuel cell test station (model G100, Figure 4.4). This test station is capable of providing humidified reactant gases for both the anode and cathode, DI water for the cooling water loop through the SPE cell, as well as an integrated load bank to provide an electric load to the SPE cell. Furthermore, the station can record data via its internal software (HYWARE II) from all the inlet and outlet lines, temperature readings from the thermocouples, as well as the loadbank values.

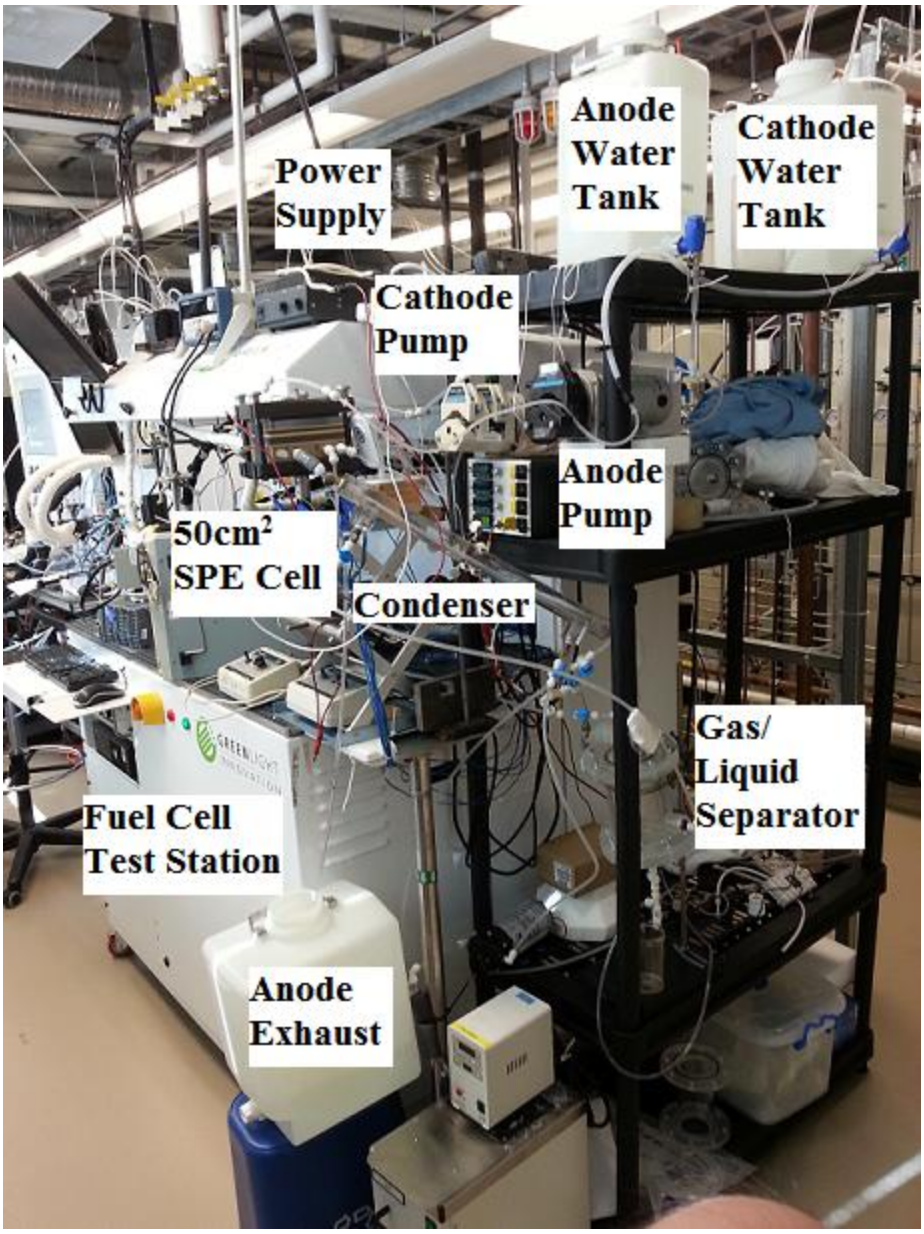

Figure 4.4 Picture of Greenlight 2 kW Fuel Cell Test Station with electrolysis mode operation setup.

4.2 External Water collection System

Hydrogen peroxide is generated on the cathode side as a result of the electrochemical reaction described by Eqn 1-5 for either the fuel cell or electrolysis mode operation. Only a small amount of water is produced due to low current efficiencies and peroxide reduction within the cell. This small amount of water, together with the water from humidification will be insufficient as a peroxide carrier on the cathode exhaust. Thus it is essential that the oxidant supply be properly humidified before entering the SPE cell. Once the H_2O_2 product mixture leaves the cathode exhaust of the SPE cell, it will go through the external water collection system, shown in Figure 4.5, in order to collect as much of the H_2O_2 as possible.

Decomposition of hydrogen peroxide increases with increasing temperature. The pre-primary water collection system minimizes this issue, even if the SPE cell operating temperature is high. Also, the peroxide collection system is constructed from acrylic and other plastic materials, so as to minimize the possibility of peroxide decomposition from metals.

As stated earlier in the literature review section on PEM fuel cells, the proper hydration of the MEA in the fuel cell is crucial for the successful operation of the PEM fuel cell. In this project, where most of the oxygen reduction at the cathode generates hydrogen peroxide, gas line humidification is even more important than a standard PEM fuel cell. The Greenlight fuel cell test station is equipped with a "primary water collection system" to remove the excess water leaving the fuel cell. However, published work from Atiyeh *et al*. showed that this primary system does not close the water balance equation of the PEM fuel cell (Eqn 1-35) [98]. Hence, a secondary water collection system was designed and built to determine the amount of water that

could be collected from both humidification and generation as a result of the H_2/O_2 reaction on the cathode side. This secondary collection system was only used to quantify the collection of water leaving the SPE cell, and differs from the system described by Atiyeh *et al.* Shown in Figure 4.5, this secondary, or external water collection system, passes the exhaust air from the cathode through a heat exchanger and collects the condensed water in a container before sending the dehumidified air back to the fuel cell test station.

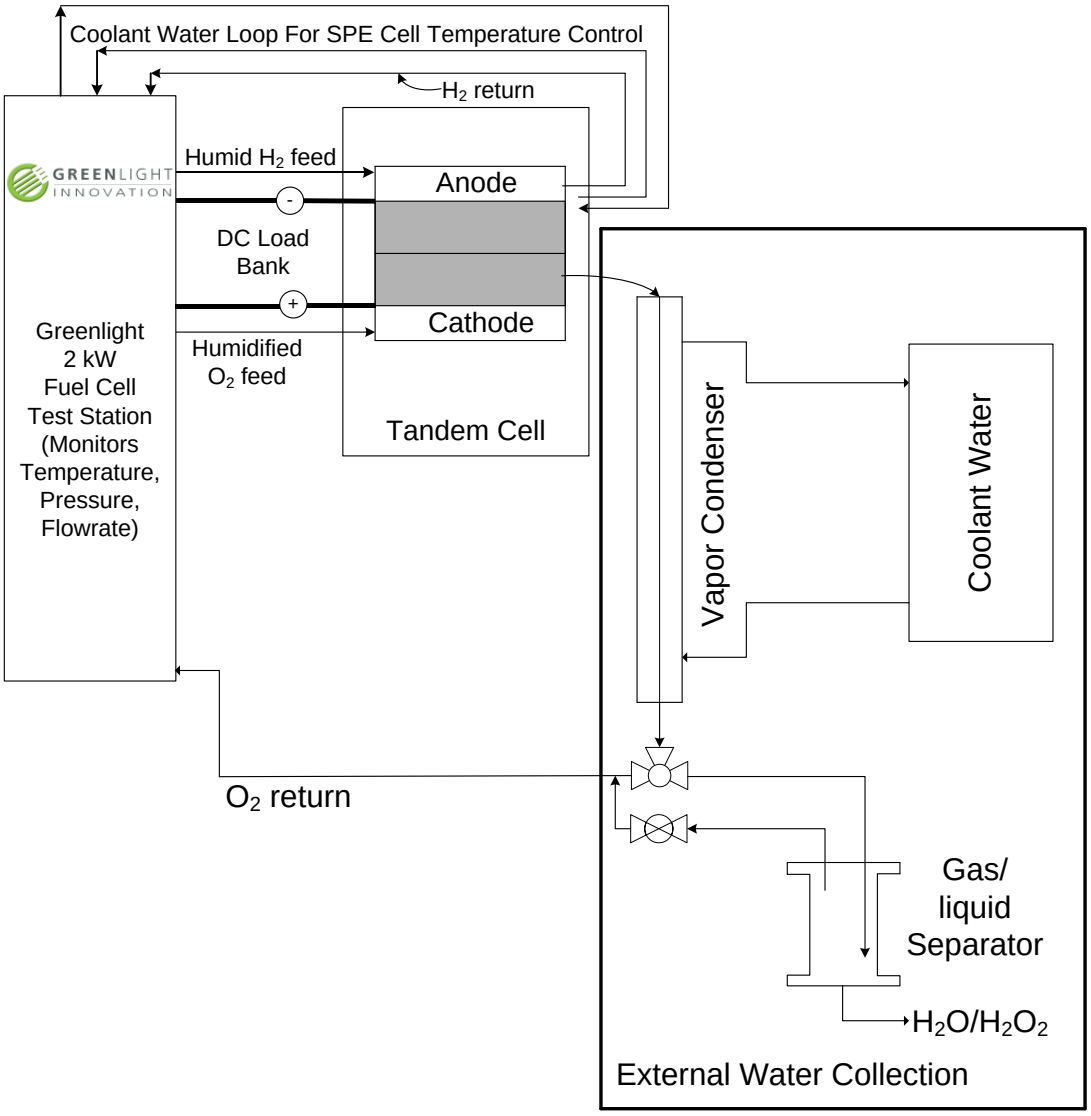

Figure 4.5 Greenlight test station with Tandem Cell and external water collection.

However, early results with the external water collection system showed that a 100% humidified cathode gas produced only small amounts of water. Therefore an alternative method is required in order to remove the product H_2O_2.

4.3 Fuel Cell Mode Operation

During fuel cell mode operation, the Greenlight 2 kW fuel cell test station controlled the gas flow rate, humidity, temperature and pressure to the anode, the cathode, as well as the coolant loop of the fuel cell. At the same time the test station also monitored the flow rate, temperature and pressure at the outlet of the anode and cathode. The gas flow rate was not maintained in stoichimetric ratios, but rather at a constant flow rate.

As the hydrogen peroxide is produced on the cathode electrode, a method of removing the product H_2O_2 is needed. To achieve this, DI water is added to the humidified cathode gas stream just before entering the fuel cell (Figure 4.6). The cathode gas stream was kept at 100% humidification to allow for better comparison with standard PEM fuel cell results. This DI water stream is pumped with a peristaltic pump with variable speed setting. On the outlet of the cathode electrode, the $H_2O_2/H_2O/O_2$ mixture goes through a vapor condenser in order to cool the mixture and minimize further H_2O_2 decomposition. The cooled mixture then goes through a gas liquid separator to separate the oxygen gas and the liquid H_2O_2/H_2O mixture. The O_2 gas is returned to the test station, while the liquid mixture is sampled for analysis of the H_2O_2 concentration.

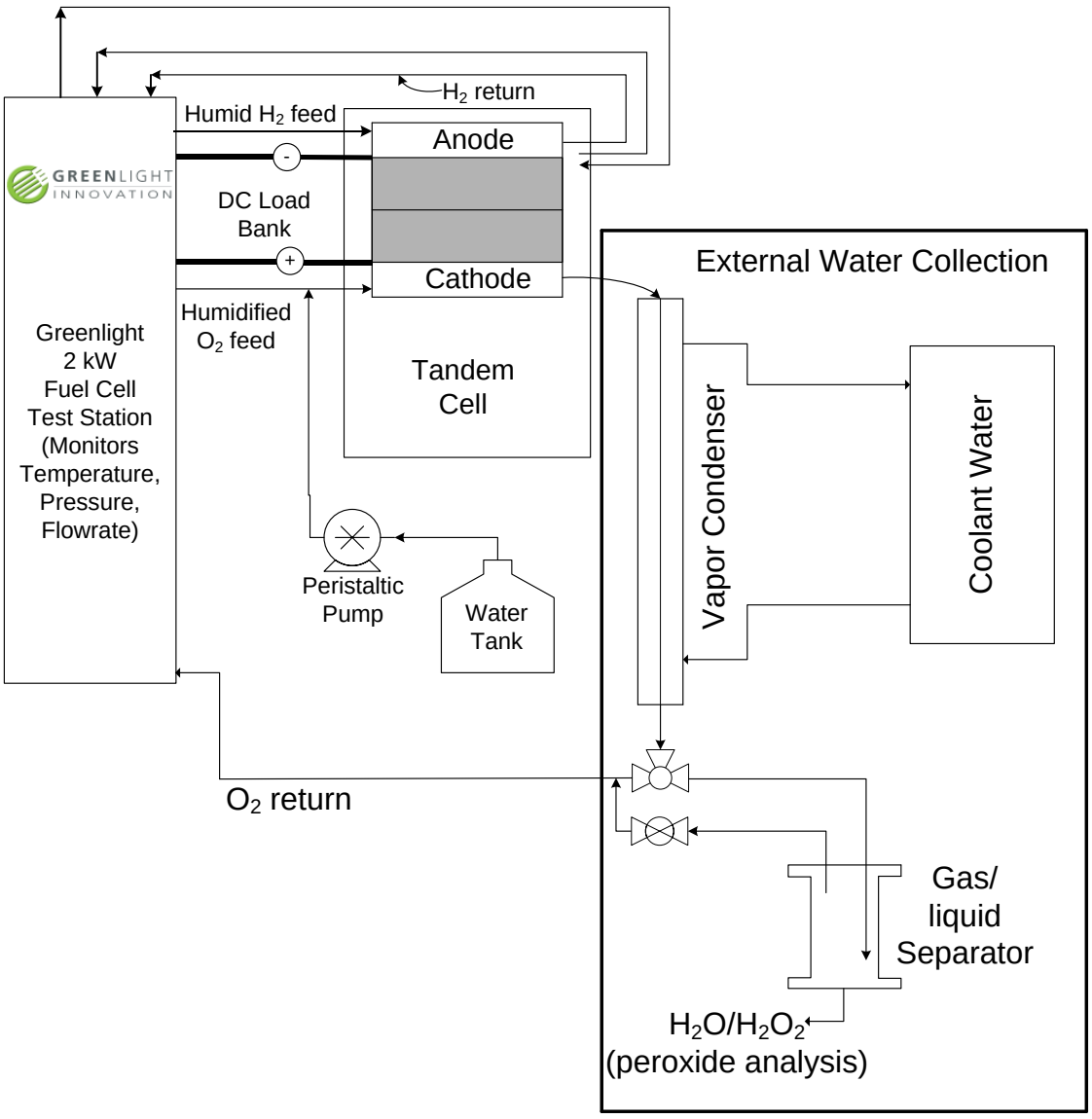

Figure 4.6 Process diagram of fuel cell mode operation.

Table 4-2 lists the standard operating conditions for the fuel cell mode operation. Note the addition of DI water to the cathode. This added water flow allowed the removal of the corrosive product H_2O_2 from the electrode surface and structure.

Table 4-2 Standard operating conditions for the fuel cell mode operation.

Operating Variable	Baseline Value
Cell Temperature [°C]	60
Fuel Cell Compression [kPa(g)]	827
Anode Relative Humidity [%]	100
Anode Gas Flow [mL min^{-1} H_2]	500 Eq. Stoic: 14.6 @ 100 mA cm^{-2}
Anode Pressure [kPa]	150
Cathode Relative Humidity [%]	100
Cathode Gas Flow [mL min^{-1} O_2]	1000 Eqv. Stoic: 58.6 @ 100 mA cm^{-2}
Cathode Pressure [kPa]	150
Cathode DI Water Flow [mL min^{-1}]	15

4.3.1 MEA Conditioning and Polarization Measurements

The H_2O_2 producing MEA with the Co-C cathode complex was conditioned for one hour before polarization measurements were taken. The MEA was inserted into the Tandem Cell hardware and pressurized to 827 kPa(g) with N_2 gas. The Greenlight test station was turned on. On the main HYWAREII screen, the operating conditions for anode and cathode inlets as well as the coolant water was set according to Table 4-2. When the operating condition was reached, the cathode DI water stream was turned on to allow for water flow through the cathode. A small current density (~1 mA cm^{-2}) was applied through the external load bank. The current density is slowly increased every 10-15 minutes up to ~20 mA cm^{-2}, while maintaining the cell potential at or above 0.3 V. The MEA was conditioned at this higher current density for one hour.

All polarization measurements for the fuel cell mode operation were carried out using the current density values listed in Table 4-3. The gas flow rates for both the anode and cathode were set at

the values listed in Table 4-2. Each polarization current density point was held for 2 minutes, during which time the voltage was approximately constant throughout, and the value at the end of the 2 minute period was recorded. The current densities used are shown in Table 4-3. At the beginning of the polarization measurements, the water accumulated in the gas liquid separator was emptied. As the polarization progressed, the liquid was emptied at the end of each polarization pointed and collected for later analyses. During fuel cell mode polarization, the voltage for each of the polarization points was surprisingly stable throughout most of the current density range, and these steady-state representations were shown on polarization results for all the MEAs tested.

Table 4-3 Polarization current densities for the Co-C complex MEA in fuel cell operation mode.

Point #	**Current Density [mA cm^{-2}]**
1	0.4
2	1
3	2
4	4
5	6
6	10
7	14
8	18
9	22
10	26
11	28
12	30
13	34
14	36
15	38

The peak current density chosen (30 mA cm^{-2}) for these polarization tests was within the mass transport region, given that the initial H_2O_2 production began at 0.695 V. At the same time, almost all of the protons that passed through the membrane were involved in the H_2O_2

production by the Co-C composite catalyst, hence minimal water was produced, which leads to lower power generated.

4.3.2 Long Term Recycle Tests

The long term recycle tests for the Co-C complex MEA is essentially an extended conditioning period for the MEA. The difference is the liquid in the gas liquid separator was recycled through the cathode inlet in order to allow for accumulation of the H_2O_2 concentration over time, i.e., the recycle period.

The long term recycle tests started the same way as the MEA conditioning. The current density selected for the long term recycle tests was 8.2 mA cm^{-2} (current setting = 0.4 A). Peak H_2O_2 production occurs at a much higher current density, however, for these bench top long term testing it is best to keep the current density for H_2O_2 production at a much lower value in order to test the feasibility of the catalyst and not have mass transport issues. The operating conditions are the same as those listed in Table 4-2. Before the start of the recycle test, the cell was held at 8.2 mA cm^{-2} for about 30 minutes in order to accumulate enough liquid for the recycle test. The long term recycle test was conducted for a period of 72 hours. Samples were taken from the sample port following the schedule in Table 4-4, and collected for later analysis.

Table 4-4 Long Term Recycle Test Sampling schedule

Point #	Sampling Time [hr]
1	0
2	1
3	2
4	4
5	8
6	24
7	48
8	72

4.4 Electrolysis Mode Operation

The Greenlight 2 kW fuel cell test station was also used to do testing operating in electrolysis mode. However, in this mode the test station only controls the cathode gas flow and coolant loop flow to the cell. DI water to the anode and the cathode were both manually controlled via the peristaltic pumps (Figure 4.7). An external power supply (Xantrex XHR 20-50) provides the power to the cell.

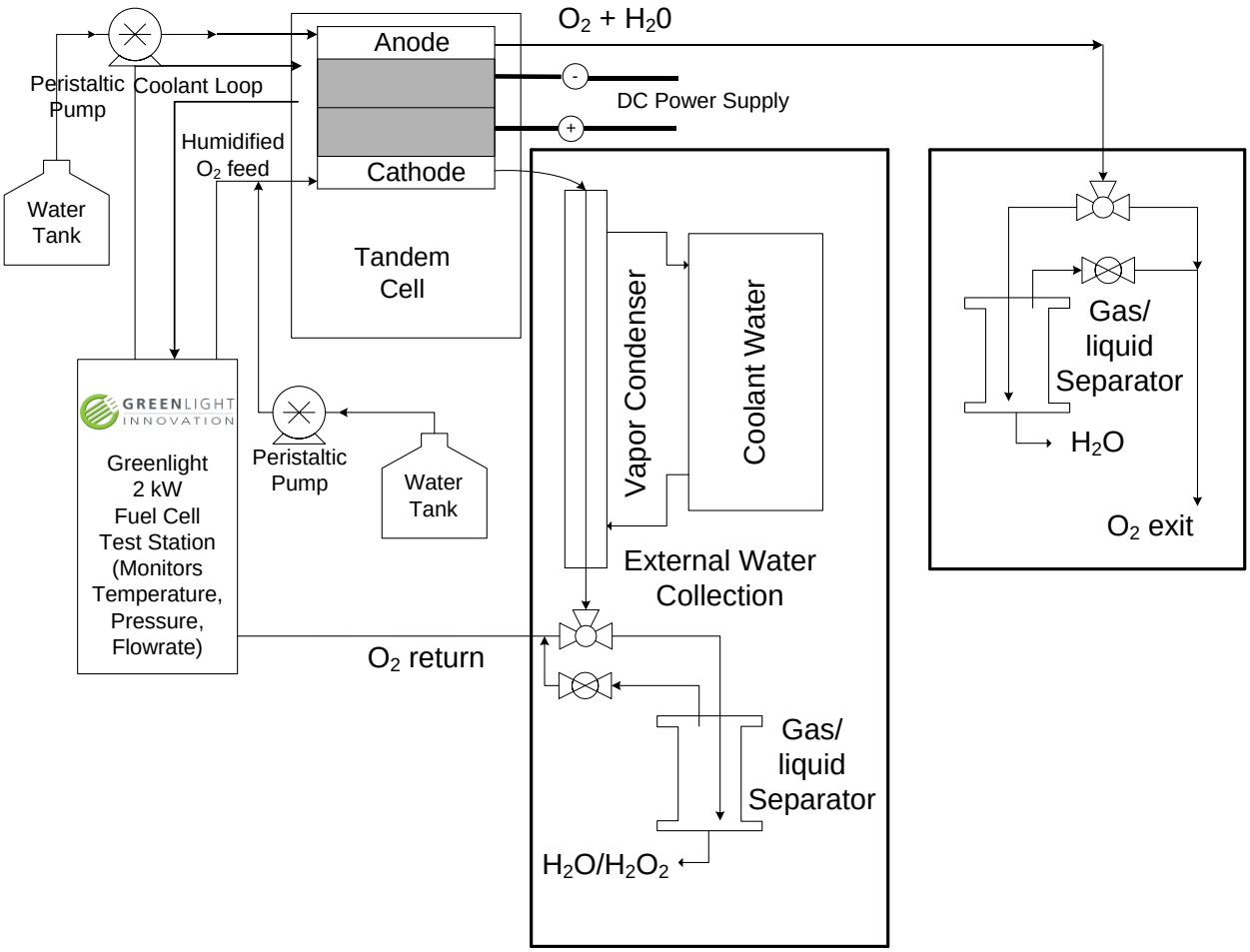

Figure 4.7 Process Diagram for Electrolysis Mode Operation.

Table 4-5 Standard operating condition for Electrolysis Mode Operation.

Operating Variable	**Baseline Value**
Cell Temperature [°C]	60
Fuel Cell Compression [kPa(g)]	827
Anode DI Water Flow [mL min^{-1}]	15
Cathode Relative Humidity [%]	100
Cathode Gas Flow [mL min^{-1} O_2]	1000 Eqv. Stoic: 58.6 @ 100 mA cm^{-2}
Cathode Pressure [kPa]	150
Cathode DI Water Flow [mL min^{-1}]	15

4.4.1 MEA Conditioning and Polarization Measurements

Both the inorganic Co-C composite catalyst and the organic RF-AQ composite catalyst were tested for polarization performance in electrolysis mode operation. Two operating parameters were studied in the electrolysis mode polarization tests. These parameters and their respective values are listed in Table 4-6.

Table 4-6 Experimental variables investigated for the generation of H_2O_2 in electrolysis mode.

Variable	**Range**			
Operating Temperature (℃)	20	40	60	80
Cathode water flow rate (mL min^{-1})	5		15	

The parameters studied were the same for both cathode catalysts. The MEA was inserted into the Tandem Cell hardware and pressurized to 827 kPa(g) with N_2 gas. The anode water pump was turned on and a flow of 15 mL min^{-1} was applied. The Greenlight test station was turned on. On the main HYWAREII screen, only the cathode conditions were controlled and monitored by the test station, as outlined in Table 4-5. All other variables including anode water flow and power supplied from the external power supply were manually controlled. When the operating condition was reached, the cathode DI water stream was turned on to allow for water flow through the cathode. The external power supply was turned on, and an initial current density (~28.6 mA cm^{-2}) was applied. The current density was slowly increased every 10-15 minutes up to ~142.8 mA cm^{-2}, while monitoring the cell potential. The MEA was conditioned at this higher current density for one hour.

All polarization measurements for the electrolysis mode operation were carried out galvanostatically using the current density values listed in Table 4-7. The gas flow rate for the

cathode was set at the values listed in Table 4-5. As it was the case in fuel cell mode operation testing, each polarization current density point was held for 2 minutes, during which time the voltage was approximately constant throughout, and the value at the end of the 2 minute period was recorded. At the beginning of the polarization measurements, the water accumulated in the gas liquid separator was emptied. As the polarization progressed, the liquid was emptied at the end of each polarization point and collected for later analysis. The same stable voltage reading observed during fuel cell mode operation was also observed in electrolysis mode operation. For both the inorganic and the organic cathode catalysts tested, the same steady-state potential readings were observed throughout the current density region for all MEAs tested during the electrolysis mode polarization tests.

Table 4-7 Polarization current densities for Electrolysis Mode Operation.

Point #	**Current Density [mA cm^{-2}]**
1	30.61
2	32.65
3	34.69
4	38.77
5	40.82
6	42.86
7	46.94
8	53.06
9	61.22
10	71.43
11	91.84
12	102.1
13	112.2
14	122.4
15	142.9
16	183.7
17	244.9
18	306.1

4.4.2 Long Term Recycle Tests

Just like the long term recycle tests performed in fuel cell mode operation, the long term recycle tests in electrolysis mode operation is an extension of the MEA conditioning period. Also, the product liquid is recycled back to the cathode inlet to allow for accumulation of the H_2O_2 concentration over time, i.e., the recycle period.

The operating conditions for the long term recycle tests were the same as those listed in Table 4-5. Once the MEA had finished conditioning, the current density was set to 62 mA cm^{-2} (current setting = 3 A) and allowed to run for 30 minutes in order to accumulate sufficient liquid for the recycle run. Just as in the case with the fuel cell mode long term tests, peak H_2O_2 production in electrolysis mode operation occurs at a much higher current density. However, a lower current density near the kinetic region was chosen here in order to study the feasibility of the catalysts being studied. The long term recycle tests were also run for 72 hours. Samples were taken following the same schedule listed in Table 4-4, and collected for later analysis.

4.5 Water Analysis for Fuel Cell and Electrolysis Mode Operation

For fuel cell mode operation, water collected from the cathode outlet stream was analyzed for H_2O_2 concentration, and trace metal and ion analysis for possible cathode electrode leaching. For electrolysis mode operation, both the anode and the cathode outlet stream were sampled. For the anode, sample water was tested for trace metal and ions from possible anode corrosion. For the cathode, samples were analyzed for H_2O_2 concentration, as well as trace metals and ion analysis.

4.5.1 Hydrogen Peroxide Analysis

The cathode outlet stream samples were analyzed for H_2O_2 concentration for both the fuel cell mode operation as well as the electrolysis mode operation. For quick qualitative measurements peroxide test strips from Indigo Instruments provided initial H_2O_2 concentration assessments in the range between 0 and 400 ppm (~ 0 – 0.012 M). Two additional quantitative analysis methods were used depending on the outlet H_2O_2 concentrations: redox titration and spectrophotometric analysis. The redox titration method uses 0.1 N $KMnO_4$ in 0.2 N H_2SO_4 to titrate against undiluted samples with H_2O_2 concentrations greater than 0.01 M (340 ppm) [99-100], based on the following reaction:

$$2MnO_4^- + 5H_2O_2 + 6H^+ \rightarrow 2Mn^{2+} + 5O_2 + 8H_2O \qquad \text{Eqn 4-1}$$

Five milliliters of concentrated sulfuric acid were added to 100 mL of H_2O_2 solution. Then the $KMnO_4$ titrant was slowly added via a burette while maintaining constant stirring of the mixture. The reaction end point occurs when the solution mixture turns a light pink color for more than one minute. The redox titration method is carried out in acidic conditions in order to avoid manganese dioxide formation and is best suited for H_2O_2 concentrations greater than 340 ppm.

The spectrophotometric method, a modified iodate/UV-vis spectroscopy method, measures diluted H_2O_2 concentrations below 0.01 M (340 ppm) [100], and follows the reaction scheme:

$$H_2O_2 + 2I^- + 2H^+ \xrightarrow{catalyst} I_2 + 2H_2O \qquad \text{Eqn 4-2}$$

$$I_2 + I^- \Leftrightarrow I_3^- \qquad \text{Eqn 4-3}$$

Procedures for this method are outlined in Appendix B-1. The H_2O_2 sample is added to equal volumes of solutions A and B and allowed to mix for 2 minutes before absorbance in a UV-VIS spectrophotometer at 351 nm. The catalyst used here is ammonium molybdate tetrahydrate. This method is carried out under neutral conditions and is best suited for H_2O_2 concentrations between 0 – 10 ppm. For higher concentrations, the samples needed to be diluted with dH_2O before adding to the solution mixture (A+B).

As the titration method requires large volumes (> 100 mL) of H_2O_2 samples for analysis, it is best suited for bulk testing of samples from long term recycle tests as well as samples with higher H_2O_2 concentrations. While the spectrophotometric method requires ~0.5 mL of H_2O_2 sample and has a suitable concentration range of 0 – 10 ppm, it is best suited for smaller volume samples and low concentration samples.

Chapter 5 In-Situ Hydrogen Peroxide Production in a Power Producing PEM Cell – Fuel Cell Mode Operation

5.1 Introduction

As presented in Section 1.3.1, in-situ electrochemical synthesis of H_2O_2 in fuel cell mode operation requires the use of hydrogen as fuel and oxygen as oxidant. Research in this mode of operation has been limited primarily due to the strong oxidizing characteristic of H_2O_2 itself, as the product H_2O_2 can severely degrade the Nafion membrane if not removed promptly, leading to a decrease in fuel cell performance. Thus far all electrochemical synthesis of H_2O_2 via PEM fuel cell research has been conducted in a bench top electrochemical cell behaving as a batch reactor, with the product H_2O_2 remaining in the reactor vessel. As mentioned in Section 1.2.1, work performed by Yamanaka *et al.* best resembled H_2O_2 production in a PEM fuel cell [1, 34, 36].

In order to improve H_2O_2 production in the PEM fuel cell, a novel concept was extended onto the PEM fuel cell where a water stream was pumped into the cathode compartment, thus carrying out the H_2O_2 produced at the cathode electrode. This allows the PEM fuel cell to maintain its performance throughout the operating current density range, and reduces the exposure of membrane to H_2O_2.

With the introduction of carrier water into the cathode compartment, water management becomes an even more important factor that must be addressed as it affects the oxygen mass transport within the cathode compartment [101-105]. The basis of this novel concept of two-phase flow entering the cathode compartment is to pump the carrier water flow at a much lower rate

than the cathode gas flow rate (minimum ratio of 1:30). At this ratio, the carrier water enters and leaves the cathode compartment as a continuous stream of droplets, which if managed properly, can prevent cathode flooding and maintain a steady state PEM fuel cell performance.

In this section, several operating variables will be considered in order to determine the optimum operating parameters in order to achieve the best H_2O_2 production rate. These variables include: a) operating temperature, b) cathode catalyst loading, c) cathode GDL Teflon loading, as well as d) cathode carrier water flow rate. Then long term operation of the cell will be presented and discussed.

5.2 Experimental Procedure

For most of the experiments conducted in the fuel cell mode operation, the fuel cell hardware used was the 49 cm^2 Tandem Research Cell described in Section 4.1.4. However, initially the tests were conducted on a 5 cm^2 Tandem Research Cell. This small fuel cell hardware was used to conduct a baseline polarization curve using the Pt catalyst, as well as initial tests with the Co-C composite catalyst operating at 40°C. Figure 5.1 shows a picture of the 5 cm^2 Tandem Research Cell hardware as well as the flow field plates and one of the membrane electrode assemblies used for this part of the project.

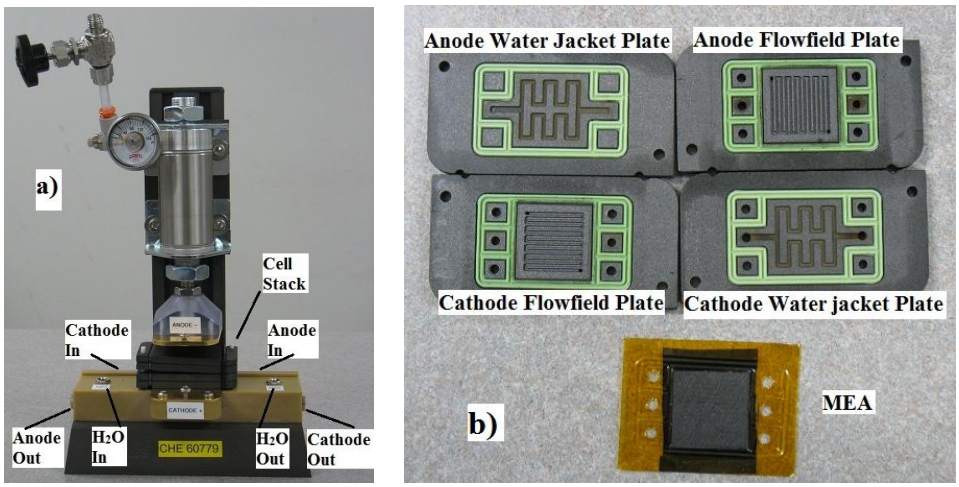

Figure 5.1 a) 5 cm^2 Tandem Research Cell and compression assembly; b) 5 cm^2 flow field plates and membrane electrode assembly.

Table 5-1 Anode and cathode flow field plate channel dimensions for the 5 cm^2 Tandem cell.

	Channel Width	Channel Depth	Channel Shape	Flow Field Type	Material
Anode	0.91 mm Top 0.51 mm Bot.	0.76 mm	Trapezoidal	Serpentine	Graphite
Cathode	0.84 mm Top 0.51 mm Bot.	0.64 mm	Trapezoidal	Serpentine	Graphite

Note: please see Appendix A-10 for Tandem Specification Sheet.

This 5 cm^2 Tandem cell was connected to the Greenlight 2 kW Fuel Cell Test Station for testing using the same operating parameters as the 49 cm^2 Tandem cell, described in Section 4.3.1. The MEAs were prepared following the steps outlined in Appendix A-7. For the baseline Pt-MEA tests, both GDE electrodes (prepared in the lab following protocol outlined in Appendix A-3.2 and A-4) and Gore CCMs (commercially available product from Fuel Cell Earth) were used to assemble the Pt-MEA. The Pt-MEA made with GDE had a catalyst loading of 0.68 mg_{Pt} cm^{-2} on both sides; while the Pt-MEA made with CCMs had a catalyst loading of 0.4 mg_{Pt} cm^{-2} on both

sides. For the Co-C MEAs tested in the 5 cm^2 Tandem cell, the anode GDE had a catalyst loading of 0.65 mg_{Pt} cm^{-2}, and the cathode GDE had a catalyst loading of 5.97 $mg_{Co\text{-}C}$ cm^{-2}.

For experiments using the 49 cm^2 Tandem cell, the test equipment used, as well as the fuel cell hardware used to test the inorganic cathode catalyst are described in detail in Section 4.1. Both the anode and cathode electrodes were prepared in house. Procedures for preparing the anode and cathode electrodes, as well as the membrane electrode assembly can be found in Appendices A-4 and A-6, respectively. The catalyst used for the anode was a 40 wt% Pt/C powder from Johnson Matthey (HiSPEC 4000) and had a catalyst loading of 0.7 mg_{Pt} cm^{-2}. The inorganic cathode catalyst used in this chapter was a 4 wt% Co-C composite catalyst (Appendix A-1) and had a catalyst loading ranging from 1.5 to 6.6 mg 4 wt% Co-C cm^{-2}. Section 4.3 outlined the operating conditions for both the polarization tests as well as the long term recycle tests.

Current efficiencies (*CE*) for H_2O_2 production based on the two-electron pathway (Eqn. 1-5) were calculated using the following equation:

$$\mathrm{CE} = \frac{2\mathrm{FQC}}{\mathrm{I}} \times 100\% \qquad \text{(Eqn 5-1)}$$

where *F* is the Faraday constant (96,485 C mol^{-1}), *Q* is the carrier water flow rate (L s^{-1}), *C* is the H_2O_2 concentration (mol L^{-1}), and *I* is the current (A).

5.3 Results and Discussion

5.3.1 Baseline Polarization Performance Comparison between Pt and Co-C Composite Catalyst – 5 cm^2 Tandem Research Cell

Initially the Tandem TP5 Research Cell was selected as the testing hardware as it had a small active area of 5 cm^2, which would be beneficial for any catalyst study as it would save time in catalyst preparation and cost. Baseline polarizations (on air and H_2) with two different Pt-MEAs were conducted (Figure 5.2).

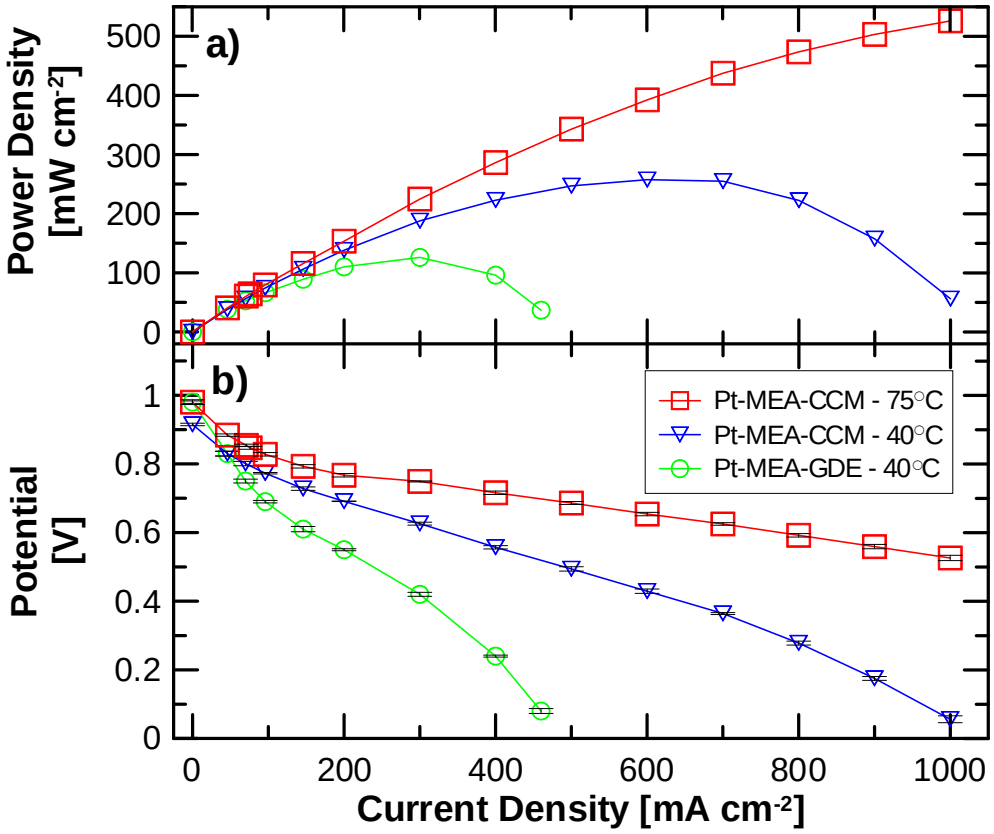

Figure 5.2 Tandem TP5 Polarization comparisons between a Pt-MEA made with GDE and a Pt-MEA made with CCM. Note: the Pt-MEA-CCM was operated at 75°C and 330 kPa in order to obtain a baseline polarization curve. Please refer to Tables 5-2 and 5-3 for MEA properties and operating conditions.

Properties for the two Pt-MEAs tested in Figure 5.2 are given in Table 5-2. The operating conditions for the Greenlight fuel cell test station for these tests are listed in Table 5-3. Each polarization was conducted twice and errors associated with the polarization are shown in the figure.

Table 5-2 5 cm^2 Pt-MEA Properties.

	Pt-MEA-GDE	**Pt-MEA-CCM**
Anode	0.68 mg Pt cm^{-2} on Toray 60 No PTFE	Fuel Cell Earth 25DC GDL w/ 20% PTFE and MPL
Cathode	0.68 mg Pt cm^{-2} on Toray 60 No PTFE	Fuel Cell Earth 25BC GDL w/ 5% PTFE and MPL
Membrane	Nafion 112	GORE 55-10 CCM w/ 0.4 mg_{Pt} cm^{-2} both sides

Table 5-3 GreenLight Fuel Cell Test Station parameters for 5 cm^2 Pt-MEA tests.

Parameter	**Pt-MEA-GDE**	**Pt-MEA-CCM**	**Pt-MEA-CCM**
Cell Temperature	40°C	75°C	40°C
Anode Pressure	150 kPa	330 kPa	150 kPa
Anode Gas Flow	60 nmL H_2 min^{-2}	55.66 nmL H_2 min^{-2}	60 nmL H_2 min^{-2}
Anode Humidity	100% RH	100% RH	100% RH
Cathode Pressure	150 kPa	330 kPa	150 kPa
Cathode Gas Flow	200 nmL Air min^{-2}	178.4 nmL Air min^{-2}	200 nmL Air min^{-2}
Cathode Humidity	100% RH	100% RH	100% RH

The Pt-MEA with CCM had the better performance, as expected given the lower contact resistance between the catalyst layer and the membrane, leading to better mass transport, and ohmic resistance. The Pt-MEA with GDE on the other hand, did not perform as well. The GDE (prepared in-house) likely did not bond to the membrane as well as the CCM, thus having a higher contact resistance between the catalyst layer and the membrane, which lead to lower performance.

As with all Pt-MEA testing, these two Pt-MEAs were conditioned for a minimum of eight hours before the polarizations were done. During conditioning the gas flow were run under stoichiometric control. However the cell performance kept fluctuating and would frequently drop below 0.1 V. To counteract this, the gas flow was changed to constant flow rate above the maximum flow rate required at the maximum current density under stoic control (for example at current density = 1 A cm^{-2}, an air stoic of 2 requires 0.17 SLPM of compressed air, and a fuel stoic of 1.5 requires minimum 0.52 SLPM of compressed hydrogen gas). This would provide sufficient reactant gases to both the anode side as well as the cathode side. With this constant reactant gas flow rate, the MEA was able to stabilize during the conditioning period.

Typical Pt-MEAs operated at 75-80°C and 330 kPa for the anode and cathode. For baseline comparisons the two Pt-MEAs were operated at 75°C and 330 kPa as well as 40°C and 150 kPa (Figure 5.2). When operated at the higher temperature and pressure the same MEA had much better performance, as expected.

A 5 cm^2 Co-C composite catalyst MEA was prepared according to protocol outlined in Appendix A-7 and tested. These Co-MEAs were operated at 40°C and 150 kPa, and the additional Greenlight Test Station operating parameters are listed in Table 5-3. Initial polarization tests included operating the cell with and without the addition of liquid DI water to the cathode side (see Figure 5.3). For the "No Water" run, the cathode was fed with 100% humidified air; while for the "Add Water" run, the cathode was fed with 100% humidified air, with an added liquid DI water stream at a flow rate of 2 mL min^{-1}.

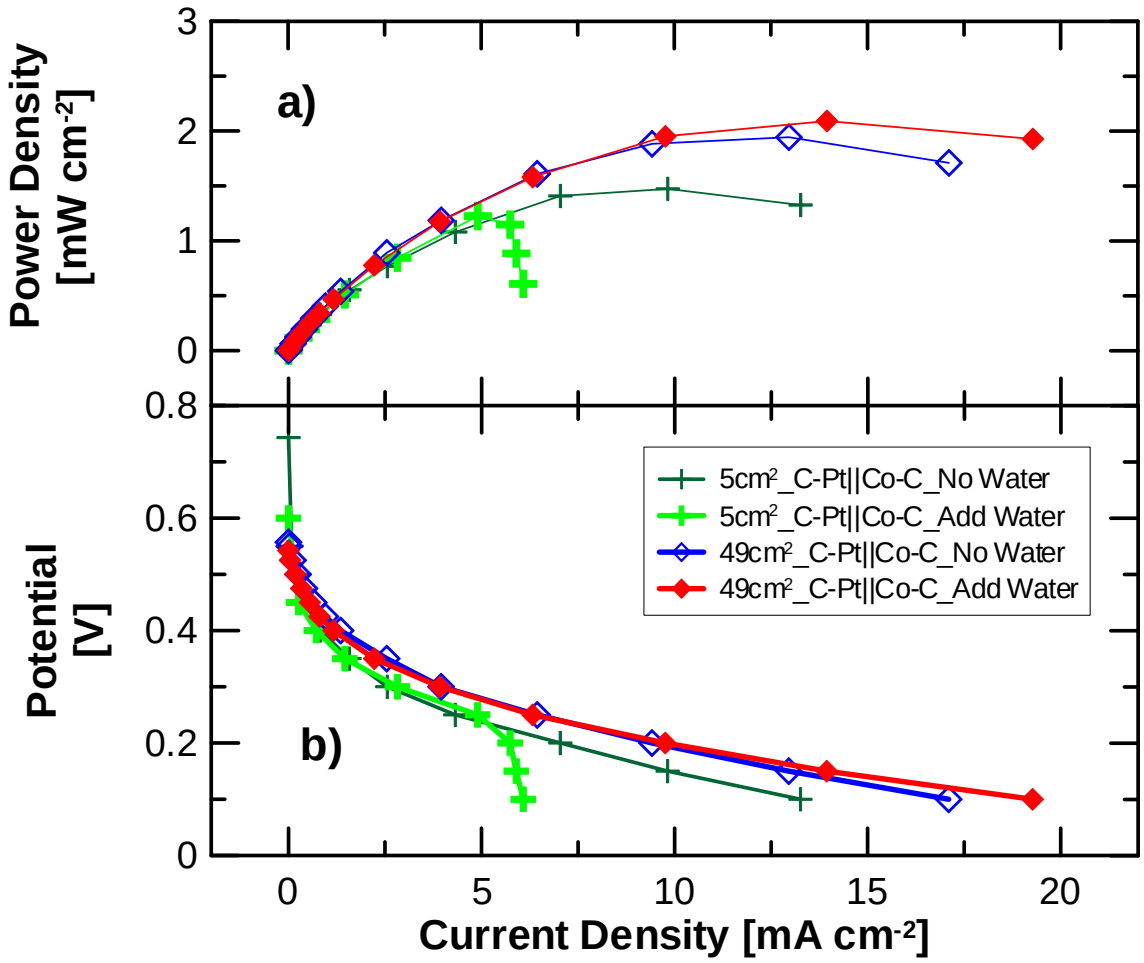

Figure 5.3 Initial polarization results of H_2O_2 producing MEA made with cobalt-carbon composite cathode catalyst with and without added water stream. Active area: 5 cm^2 (+) and 49 cm^2 (◇). Please see Table 5-3 for operating conditions.

Table 5-3 Greenlight fuel cell test station parameters for initial 5 cm^2 Co-MEA tests.

Parameter	**5 cm^2**	**49 cm^2**
Cell Temperature	40°C	40°C
Anode Pressure	150 kPa	150 kPa
Anode Gas Flow	300 nmL H_2 min^{-2}	300 nmL H_2 min^{-2}
Anode Humidity	100% RH	100% RH
Cathode Pressure	150 kPa	150 kPa
Cathode Gas Flow	400 nmL O_2 min^{-2}	400 nmL O_2 min^{-2}
Cathode Humidity	100% RH	100% RH

The polarization test without liquid DI water to the cathode side ("No Water" run) showed higher limiting operating current density than the test run with liquid DI water to the cathode (wet condition). Both the dry condition and the wet condition runs showed similar performance at lower current densities. As the current densities increased, the wet condition run had a sharp drop in performance and flooding was observed in the cell hardware. In addition, the liquid DI water flow in the flow field channels over the active area on the cathode side was not uniform as the small flow channels within the cell plates caused water plugging which lead to mal-distribution and a drop in performance. This was more noticeable as the cathode water flow rate increased above 2 mL min^{-1}.

The small 5 cm^2 Co-MEA was able to produce H_2O_2 during the polarization test. However, the water samples collected for H_2O_2 sampling was over the entire polarization time, not for individual polarization points during the test. Initial Co-C polarization tests involved water sampling for individual polarization points. However, the pressure drop as a result of the water sampling caused major drops in cell performance from which the cell could not recover. As a result after 2-3 polarization points the performance dropped to below 0.05 V, leading to termination of the polarization test.

For a given cathode DI water flow rate (15 mL min^{-1}), the larger 49 cm^2 cell was able to handle ten times as much H_2O on a per unit area basis versus the smaller 5 cm^2 cell (0.31 mL min^{-1} cm^{-2} vs. 3 mL min^{-1} cm^{-2}). In addition, upon comparison between the cell hardware dimensions of the 5 cm^2 cell (Table 5-1) and the 49 cm^2 cell (Table 4-1), the 49 cm^2 cell's channel cross sectional area for the cathode flow field was 3 times larger than that of the 5 cm^2 cell (1.56 mm^2 vs. 0.43

mm^2). Hence it was decided that moving to cell hardware with a larger active area could alleviate this pressure drop issue. As shown in Figure 5.3 and Figure 5.4, a Co-MEA with a 49 cm^2 active area had consistent performance between the dry condition test and the wet condition test (Figure 5.3), as well as H_2O_2 sampling for production rate and current efficiency calculations at individual polarization points (Figure 5.4). Furthermore, as it will be shown later in this chapter, the 49 cm^2 Tandem cell was able to provide consistent test data over a range of operating temperatures, catalyst loading, and cathode water flow rates.

It is important to note the type of gas used for the cathode reactant during the Co-C experiments. Initially compressed air was used as the cathode reactant gas for the small 5 cm^2 cell. However, open circuit voltage with compressed air was inconsistent, ranging from 0.323 V to 0.821V for the twelve Co-MEAs tested. Sources of this problem comes from impurities in the air supply (such as CO, CO_2), as well as the lower partial pressure of oxygen in the air supply versus the partial pressure of oxygen when pure oxygen is used. When laboratory grade oxygen (99.9% pure, Praxair) was used as the cathode reactant for the same twelve Co-MEAs, the OCV range had a relatively narrower range: 0.533 V to 0.677 V. Although no polarization tests were conducted using the compressed air as cathode reactant, based on the OCV measurements, it was decided that oxygen was the most optimal cathode reactant gas to study H_2O_2 production using the Co-C and AQ-C catalysts.

Additionally, the open circuit cell impedance for the twelve 5 cm^2 Co-MEAs ranged from 0.05 – 0.1 Ω, measured with both an LCR meter as well as a Fluke voltmeter. These values are within the acceptable values for typical PEM fuel cell MEAs of this size. However, the cell voltage

dropped 200 – 300 mV as soon as the LCR meter or the voltmeter was attached to the cell. This lead to an OCV of only ~ 0.3 V, which would be insufficient to sustain a polarization test. Hence it was decided that the impedance test would be conducted before and after polarization tests.

5.3.2 49 cm^2 Tandem Research Cell – Uni-Variate Experiments and Factorial Tests

For this part of the thesis project, the inorganic Co-C composite catalyst was tested to determine the effects of different operating variables on the generation of H_2O_2 through a set of uni-variate experiments. These operating variables and their respective range of values are listed in Table 5-5. All other variables of the experiment, including the Fuel Cell Test Station operating parameters, can be found in Section 4.3.

Table 5-5 Uni-Variate experimental variables investigated for the generation of H_2O_2.

Variable	**Range**		
Operating Temperature (°C)	40	60	80
Catalyst loading (mg $_{Co\text{-}C}$ cm^{-2})	1.5	3.6	6.6
Cathode GDL (Toray carbon paper) Teflon content (wt%)	0	10	20
Cathode water flow rate (mL min^{-1})	5	15	25

5.3.2.1 Effect of Temperature on H_2O_2 Production

In theory, H_2O_2 production rate should increase with an increase in operating temperature. However, temperature increase can have an adverse effect on the degradation of H_2O_2: H_2O_2 decomposition increases as temperature increases. Hence three different temperatures were selected to study these competing characteristics of H_2O_2 between production and degradation:

40°C, 60°C and 80°C. The anode and cathode catalyst materials were the same as those described in Section 5.2. The Fuel Cell Test Station operating parameters were the same as those described in Section 4.3. Figure 5.4 shows the polarization curves, the production rates, and the current efficiencies for these three operating temperatures.

As expected, the I-V performance curve showed a direct relationship between temperature and fuel cell performance: performance increased as temperature increased. However this relationship did not correlate to H_2O_2 production over the entire operating current density range. At current densities below 18 mA cm^{-2}, H_2O_2 production increased as operating temperature increased. However, once the operating current density reached above 18 mA cm^{-2}, a reverse trend started to appear between the 60°C and 80°C runs. Between these two runs, the H_2O_2 production was less for the 80°C run when compared to the H_2O_2 production for the 60°C run at the same current density point. Hence it appears that operation at 80°C leads to a more enhanced H_2O_2 degradation resulting in a smaller net H_2O_2 production.

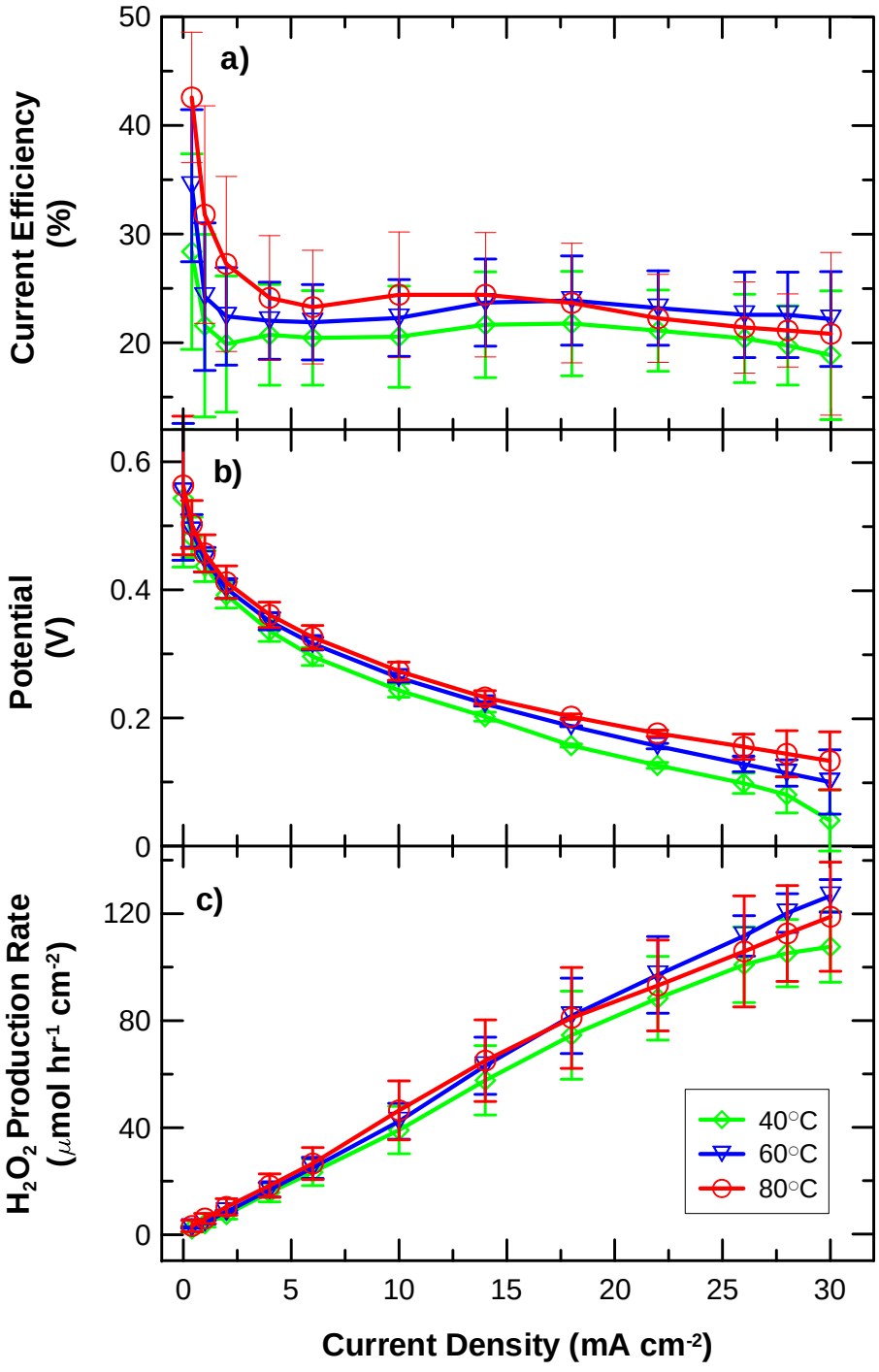

Figure 5.4 Effect of cell operating temperature on: a) the current efficiency for H_2O_2 production, b) fuel cell polarization performance, and c) H_2O_2 production rate. Anode conditions: H_2 flow rate 500 mL min^{-1} pressure at 150 kPa(g) and 100% RH, anode catalyst loading 0.7 mg $_{Pt}$ cm^{-2}. Cathode conditions: O_2 flow rate 1000 mL min^{-1} O_2, pressure 150 kPa(g), water flow rate 5 mL min^{-1}, Co-C loading 3.6 $mg_{Co\text{-}C}$ cm^{-2}.

The 10 wt% Teflonated cathode GDL was used for the temperature testing and was considered to be the reason for the stable I-V performance and stable current efficiency throughout the current density range. Please see Section 5.3.2.3 for further discussions on the effect of teflonation on H_2O_2 production. The 40°C run had the lowest current efficiency, while the 60°C run had the best overall stable current efficiency. As a result 60°C was chosen as the operating temperature for the other three variables tested.

The stability of the product H_2O_2 was further examined at these three different temperatures to evaluate their degradation within the cell hardware environment. Discussions of this study can be found in Section 5.4.

5.3.2.2 Effect of Cathode (Co-C) Catalyst Loading on H_2O_2 Production

The effect of the Co-C catalyst loading on the H_2O_2 production and the fuel cell polarization behavior are presented in Figure 5.5. The carrier water flow rate was held constant at 5 mL min^{-1} throughout the polarization test and the unteflonated GDL was used. Increasing the Co-C catalyst loading generally increases the rate of H_2O_2 production, as seen in Figure 5.5c. At the same time, a maximum current efficiency of 40% was obtained with 6.6 $mg_{Co\text{-}C}$ cm^{-2} at a superficial current density of 1 mA cm^{-2} (Figure 5.5a). As the current density increases, the cell became increasingly flooded. As a result, insufficient oxygen reaches the catalyst layer, leading to a decrease in current efficiency (Figure 5.5a).

From Figure 5.5a it is clear that 3.6 $mg_{Co\text{-}C}$ cm^{-2} had the best overall current efficiency in terms of magnitude and consistency over a larger current density range.

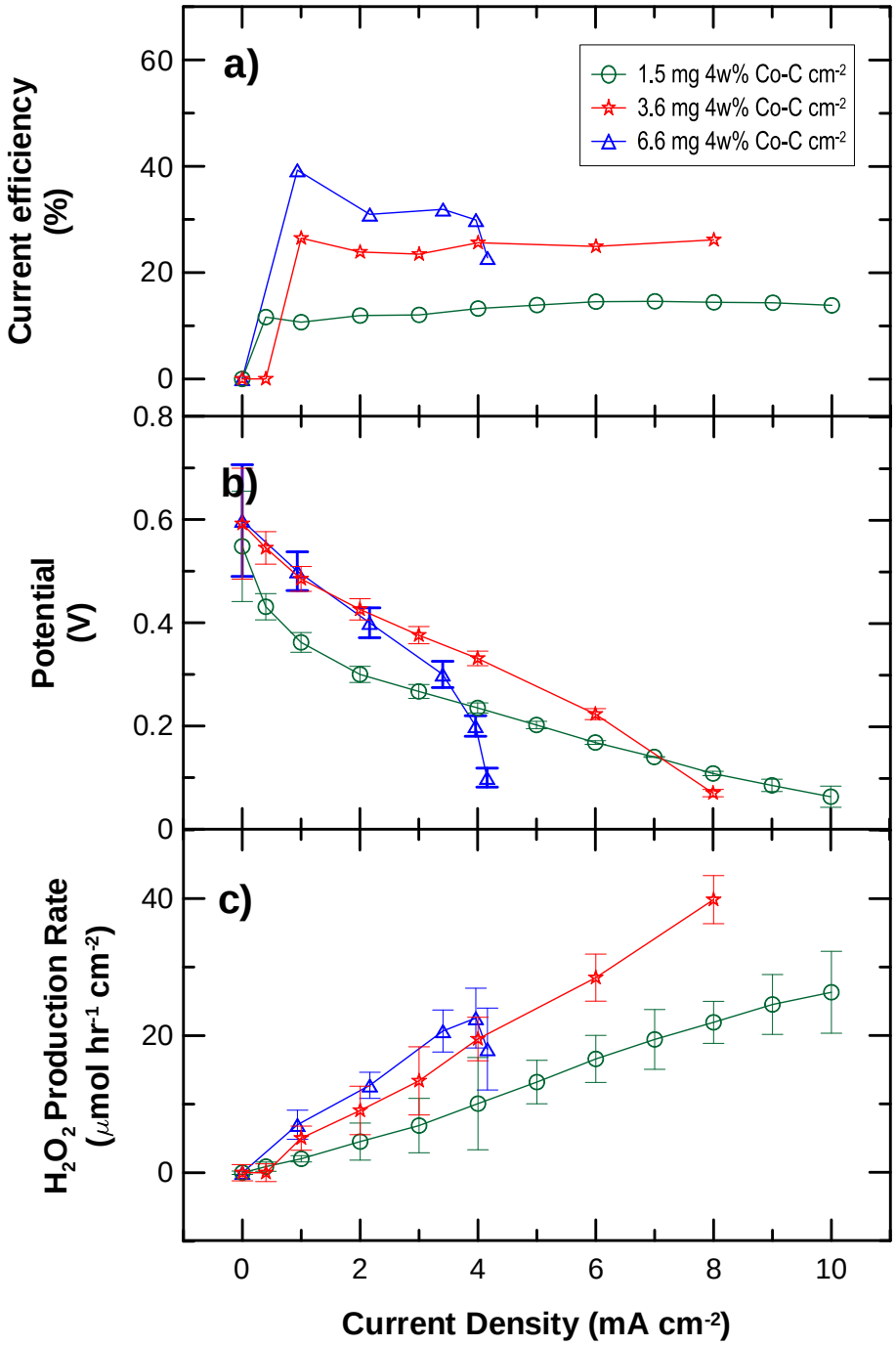

Figure 5.5 Effect of cathode catalyst loading on: a) the current efficiency for H_2O_2 production, b) fuel cell polarization performance, and c) H_2O_2 production rate. Cell temperature: 60 ℃. Anode conditions: H_2 flow rate 500 mL min^{-1}, pressure: at 150 kPa(g), anode catalyst loading 0.7 mg $_{Pt}$ cm^{-2}. Cathode conditions: O_2 flow rate 1000 mL min^{-1} O_2, pressure 150 kPa(g), GDL Teflon content: 0 wt%, water flow rate 5 mL min^{-1}.

Furthermore, the fuel cell polarization curve in Figure 5.5b shows marked improvements in the kinetic region when the Co-C loading was increased from 1.5 $mg_{Co\text{-}C}$ cm^{-2} to either 3.6 or 6.6 $mg_{Co\text{-}C}$ cm^{-2}. For the 6.6 $mg_{Co\text{-}C}$ cm^{-2} loading, at current densities higher than 2 mA cm^{-2} the polarization curve drops off sharply, an indication of significant O_2 gas mass transport limitation, i.e., a clear limiting current. Several factors contributed to this limitation. First, the high catalyst loading of 6.6 $mg_{Co\text{-}C}$ cm^{-2} implied a much thicker catalyst layer (thickness = 0.674 mm). The cathode electrodes were prepared following the procedures outlined in Appendix A-4, where the catalyst layer is essentially formed by spraying one thin layer on top of another. It is very likely that only a small fraction of the catalyst layer was involved in the reaction, while the rest of the thick catalyst layer serves only as an extended GDL zone. Furthermore, the cathode reactant gas was already at 100% RH, while an additional water stream was injected into the cathode in order to remove the product H_2O_2, increasing the occurrence of water flooding in the cathode electrode due to the excess of water in the cathode compartment. Lastly, the cathode GDL used here was not teflonated. This meant that any water created or injected into the cathode could fill the GDL pores, causing excessive cathode flooding. This is most likely the reason for the poor performance. The combination of these three factors impeded O_2 gas mass transport to the reaction sites. There exists a need to improve the O_2 mass transport at the cathode catalyst layer while allowing sufficient carrier water flow rate to remove the product H_2O_2. Therefore, it was important to study the effect of cathode GDL teflon content on the production of H_2O_2.

5.3.2.3 Effect of Cathode GDL Teflon Content on H_2O_2 Production

It is well documented that the addition of teflon to the GDL improves water management by preventing serious drying and flooding conditions within the electrode [106]. This would result in an improved, more stable polarization performance as the current density increased. Toray TGPH-060 carbon GDL with 0, 10 and 20 wt% teflon content were used as cathode back support for the Co-C complex catalyst in this testing. The fuel cell polarization and H_2O_2 production results are shown in Figure 5.6. A quick glance at the figure shows significant improvements for MEAs with teflon in the cathode GDL in terms of improved stability of polarization curve and increased current efficiencies at higher current densities. For example, for the MEA with 20 wt% teflon loading, with the fuel cell operating in the higher end current density range (25 to 235 mA cm^{-2}), the I-V performance was stable with a peak power of 4.5 mW cm^{-2}, while producing H_2O_2 at a rate of 120 μmol hr^{-1} cm^{-2} and maintaining a current efficiency of about 18% (Figure 5.6).

In the lower current density range, i.e., less than 8 mA cm^{-2} (Figure 5.6a), the un-teflonated cathode had higher current efficiencies for H_2O_2 generation than for the teflonated ones. However, as the current density increased, the un-teflonated cathodes became unstable due to cathode flooding; while the teflonated cathodes maintained a stable current efficiency throughout the current density range. This finding revealed two different opposing trends for the Teflon content as a function of the operating current density. The un-teflonted cathode had a small operating current density range. At ~5 mA cm^{-2} it was operating at 25% current efficiency since it was not limited by O_2 mass transfer. However, the carrier water flow stream quickly limited the O_2 mass transfer in the hydrophilic un-teflonated cathode, resulting in a sharp drop in I-V performance (Figure 5.6b). The two teflonated cathodes, at 10 wt% and 20 wt%, had a much

higher range of operating current density. The stable current efficiencies for both teflonated cathodes meant sufficient hydrophobicity (due to teflonation) had overcame the O_2 mass transfer limitation, especially in the higher current density domain above 18 mA cm^{-2} (Figure 5.6). This higher operating current density domain also resulted in higher H_2O_2 production rates, reaching a maximum of 128 μmol hr^{-1} cm^{-2} for the 20 wt% teflonated cathode. This result coincides with other published work indicating 20 wt% as the optimal PTFE loading for the best fuel cell performance [106-107]. To further investigate these two opposing trends, the combined effects of carrier water flow rate and Teflon content are looked at in the next section. The Teflon content chosen for further study was 10 wt%, as it showed a more stable current efficiency and H_2O_2 production rate over a larger operating current density range.

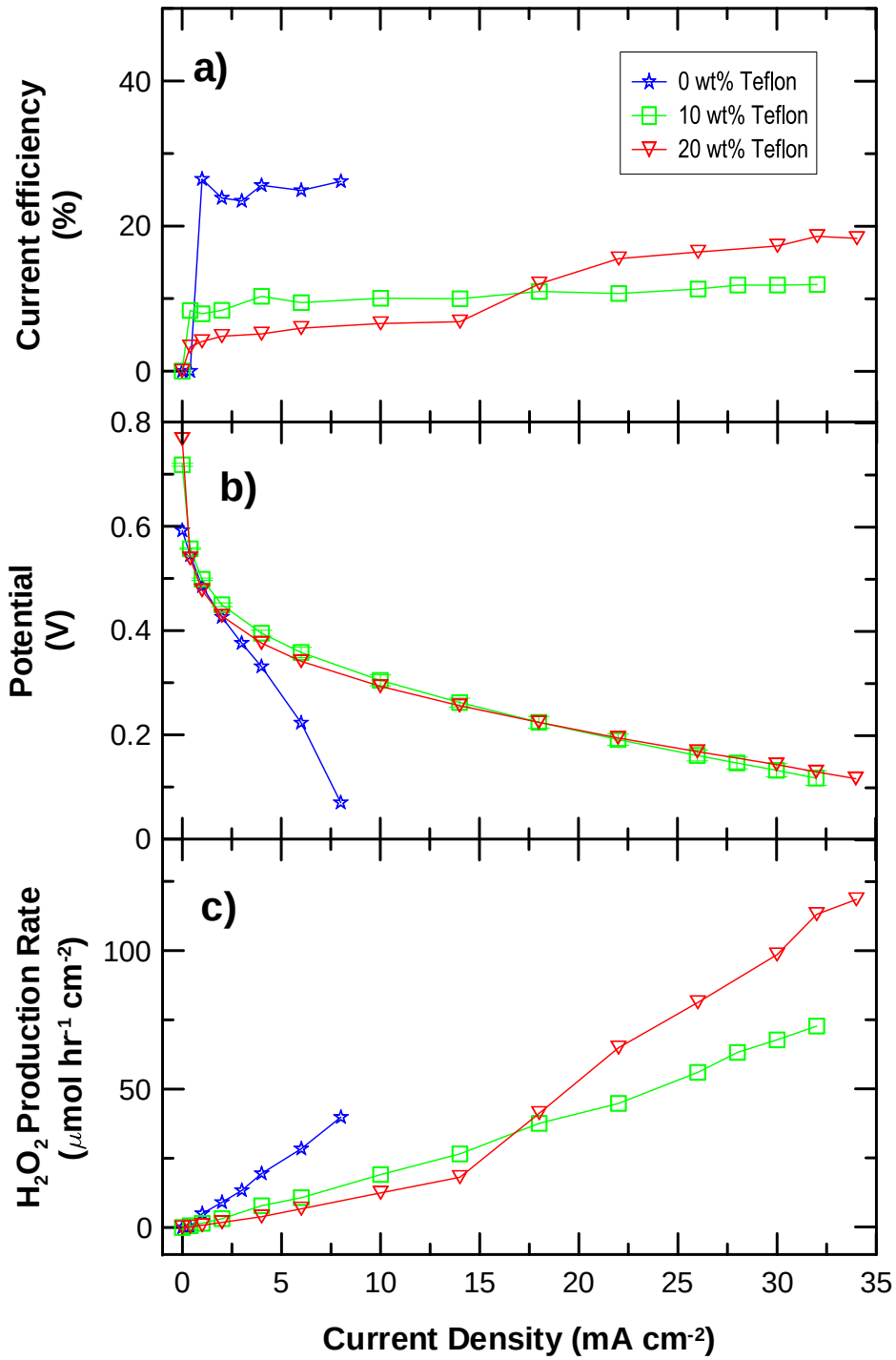

Figure 5.6 Effect of cathode GDL Teflon content on: a) the current efficiency for H_2O_2 production, b) fuel cell polarization performance, and c) H_2O_2 production rate. Cell temperature: 60 ℃. Anode conditions: H_2 flow rate 500 mL min^{-1} pressure at 150 kPa(g), anode catalyst loading 0.7 mg $_{Pt}$ cm^{-2}. Cathode conditions: O_2 flow rate 1000 mL min^{-1} O_2, pressure 150 kPa(g), water flow rate 5 mL min^{-1}, Co-C loading 3.6 mg_{Co-C} cm^{-2}.

5.3.2.4 Effect of Cathode Carrier Water Flow Rate on H_2O_2 Production

To help facilitate the removal of the product H_2O_2 in this two-phase gas-liquid system, a carrier water flow stream was added to the cathode inlet. Several cathode carrier water flow rate were tested to investigate its effect on cell performance and H_2O_2 production: 0, 5, 15 and 25 mL min^{-1} (Figure 5.7). The I-V performance for the 10 wt% teflonated cathode GDL was almost identical at all four flow rates. Figure 5.8b showed a well defined kinetic (up to 5 mA cm^{-2}) and ohmic (up to 30 mA cm^{-2}) regions of the polarization curves. This suggested that the Teflon in the cathode GDL was sufficient in preventing water flooding as well as mass transfer related issues in the cathode catalyst layer. Both the current efficiency and the H_2O_2 production rate showed a direct relationship to the cathode carrier water flow rate. As the carrier water flow rate increased, the current efficiency increased (Figure 5.7a) and the H_2O_2 production rate increased (Figure 5.7c) accordingly. As the water flow rate increased, the product H_2O_2 was removed at a faster rate, which lead to a lower residence time for the product H_2O_2 in the cathode electrode, thus reducing the chances of the secondary electroreduction of H_2O_2 to H_2O, as well as minimizing the thermochemical decomposition of H_2O_2 to H_2O. Figure 5.7 showed that with the cathode carrier water flow rate at 25 mL min^{-1}, a maximum H_2O_2 production rate of 203 μmol hr^{-1} cm^{-2} with a current efficiency of 31% operating at a current density of 34 mA cm^{-2}.

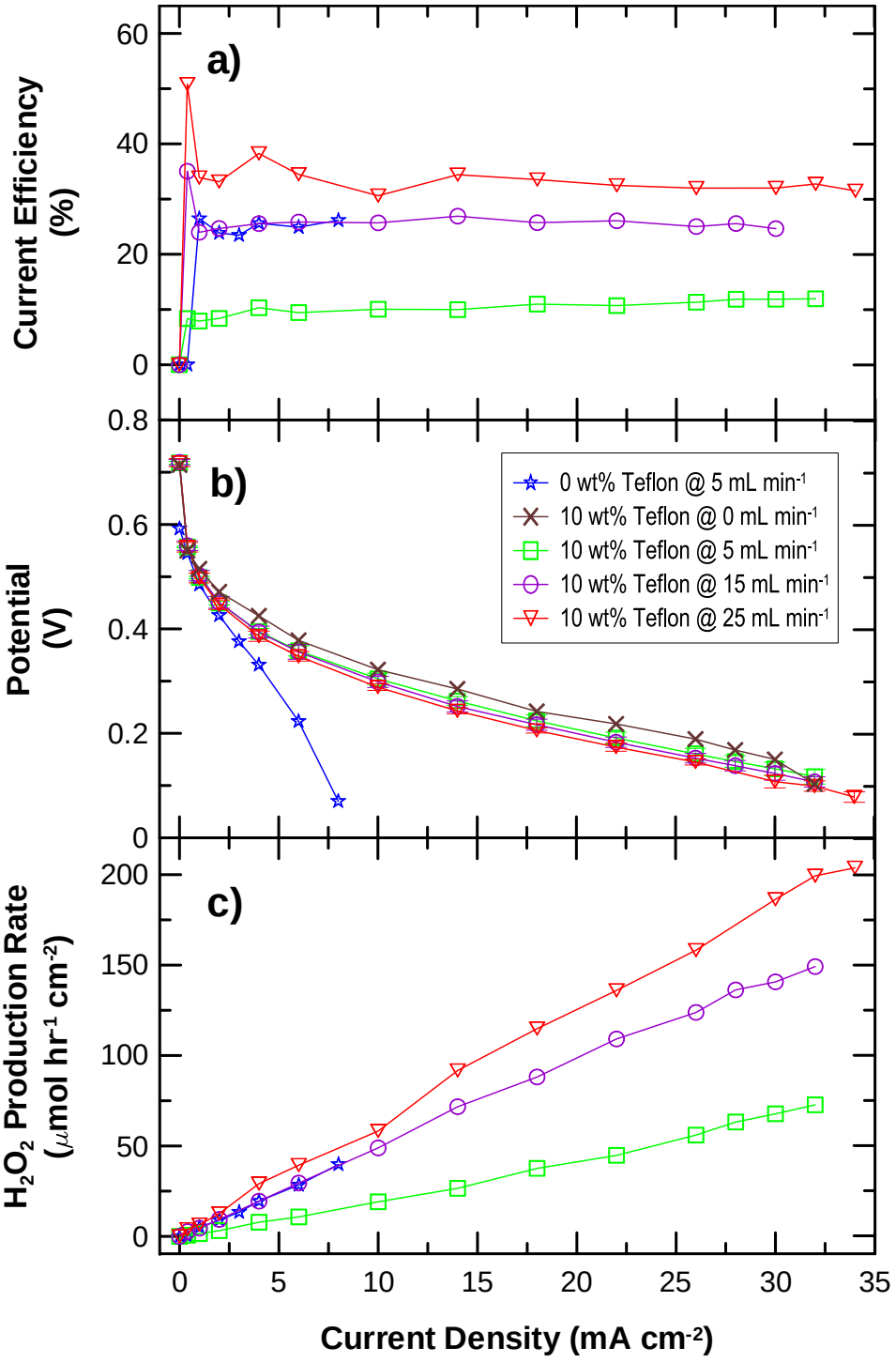

Figure 5.7 Effect of cathode carrier water flow rate on: a) the current efficiency for H_2O_2 production, b) fuel cell polarization performance, and c) H_2O_2 production rate. Cell temperature: 60 ℃. Anode conditions: H_2 flow rate 500 mL min^{-1} pressure at 150 kPa(g), anode catalyst loading 0.7 mg_{Pt} cm^{-2}. Cathode conditions: O_2 flow rate 1000 mL min^{-1} O_2, pressure 150 kPa(g), Co-C loading 3.6 $mg_{Co\text{-}C}$ cm^{-2}.

To further test this direct relationship, the cathode carrier water flow rate was increased up to 47 mL min^{-1}. At such high carrier water flow rates, significant flooding in the cell became a serious issue, as the operating current density only reached 8 mA cm^{-2} before the cell performance deteriorated. Figure 5.8 showed the results of the higher carrier water flow rates for this operating current density range. For each of the current density point that was sampled, H_2O_2 production actually decreased as the carrier water flow rate increased (Figure 5.8a), a clear indication that the Teflon content in the cathode GDL could not prevent flooding at such high water flow rates. Another explanation is that at these higher water flow rates, most of the water simply flows over the cathode electrode, thus not carrying a sufficient amount of the product H_2O_2 away from the cathode, leading to a lower measured H_2O_2 production rate (Figure 5.8b).

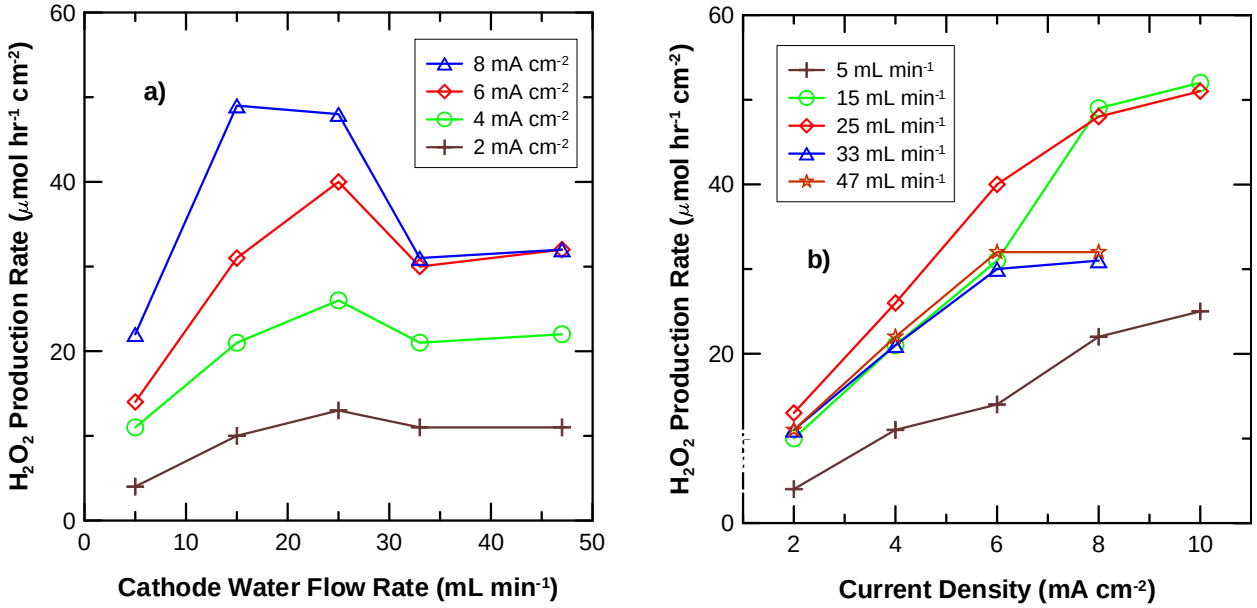

Figure 5.8 Optimization of the cathode carrier water flow rate for the production of H_2O_2 Cell temperature: 60 ℃. Anode conditions: H_2 flow rate 500 mL min^{-1} pressure at 150 kPa(g), anode catalyst loading 0.7 mg_{Pt} cm^{-2}. Cathode conditions: O_2 flow rate 1000 mL min^{-1} O_2, pressure 150 kPa(g), Co-C loading 3.6 $mg_{Co\text{-}C}$ cm^{-2}.

From Figures 5.7 and 5.8 it is clear that there is an optimum cathode carrier water flow rate of about 25 mL min^{-1} or 0.5 mL min^{-1} cm^{-2}. When operating at or below this optimum flow rate, product H_2O_2 can be efficiently removed without any flooding or mass transfer issues. However, once the carrier water flow rate goes above this optimum flow rate, significant water flooding occurs in the cathode electrode (even with teflonated electrodes) limiting O_2 mass transfer into the catalyst layer is limited, causing an overall decrease in H_2O_2 production rate.

5.3.4 Continuous Recycle Operation Mode

In the previous sections it was determined that the best H_2O_2 production occurred with the cathode carrier water flow rate at 25 mL min^{-1}, with a 20 wt% cathode GDL and a 3.6 $mg_{Co\text{-}C}$ cm^{-2} cathode catalyst loading. However, as it is the case with typical PEM fuel cells, real world operations requires the H_2O_2 producing fuel cell run under constant loading for prolonged periods (days to weeks). Hence longer-term continuous two-phase recycle operation was conducted to evaluate the potential degradation of the fuel cell performance and H_2O_2 production and to determine if recycling would increase the H_2O_2 concentration. The recycle operation began with the fuel cell operating in a single pass operation for 25 minutes with the cathode carrier water flow at 15 mL min^{-1} at a load of 8.2 mA cm^{-2}. By keeping the water flow rate at 60% optimum level, the MEA life can be prolonged due to less flooding effects in the cell, while still maintaining 80% optimum H_2O_2 production rate (Figure 5.7c). After 25 minutes of single pass mode, sufficient product solution was accumulated in the collection reservoir to allow for subsequent water sampling throughout the recycle operation. The recycle pump was then turned on, with the recycle cathode carrier flow rate fixed at 15 mL min^{-1}. The current density was constant throughout at 8.2 mA cm^{-2}. The current density chosen for the recycle test was near the

beginning of the ohmic region, with stable H_2O_2 production and current efficiency. Even though the H_2O_2 concentration (~100 ppm) was low at this current density, the load was sufficiently low that thermal decomposition would not significantly affect the final H_2O_2 concentration.

The recycle experiment run lasted 72 hours (Figure 5.9), with the cell load potential dropping ~60 mV (includes ~50 mV drop in first 24 hours and only ~10 mV drop in the last 48 hours). During this test run, the total accumulated H_2O_2 concentration increased to 1400 ppm (0.14 wt%). The H_2O_2 production rate decreased over the 72 hr recycle test run. Coincidentally, the H_2O_2 production rate also showed a large drop in the first 24 hours (from 33% to 1.5%), while for the last 48 hours the H_2O_2 production rate remained almost constant at ~1.5%, until the end of the recycle test, when the production rate dropped to 0.2%. The likely explanation could still be due to thermalchemical decomposition of H_2O_2 in the recycle stream, as well as the H_2O_2 saturation in the catalyst layer. With the exception of the Tandem cell itself (which is maintained at the operating temperature of 60°C), the entire recycle stream is cooled to 3°C with the aid of a chiller water bath. Hence, as the recycle stream enters the fuel cell, the sudden increase in temperature would increase the potential of thermo-chemical decomposition of H_2O_2 in the recycle stream. Additionally, as the H_2O_2 concentration in the recycle stream increases, more cathode catalyst participates in the electrochemical decomposition of H_2O_2 rather than the electrochemical production of H_2O_2, thus leading to a large decrease in H_2O_2 production rate.

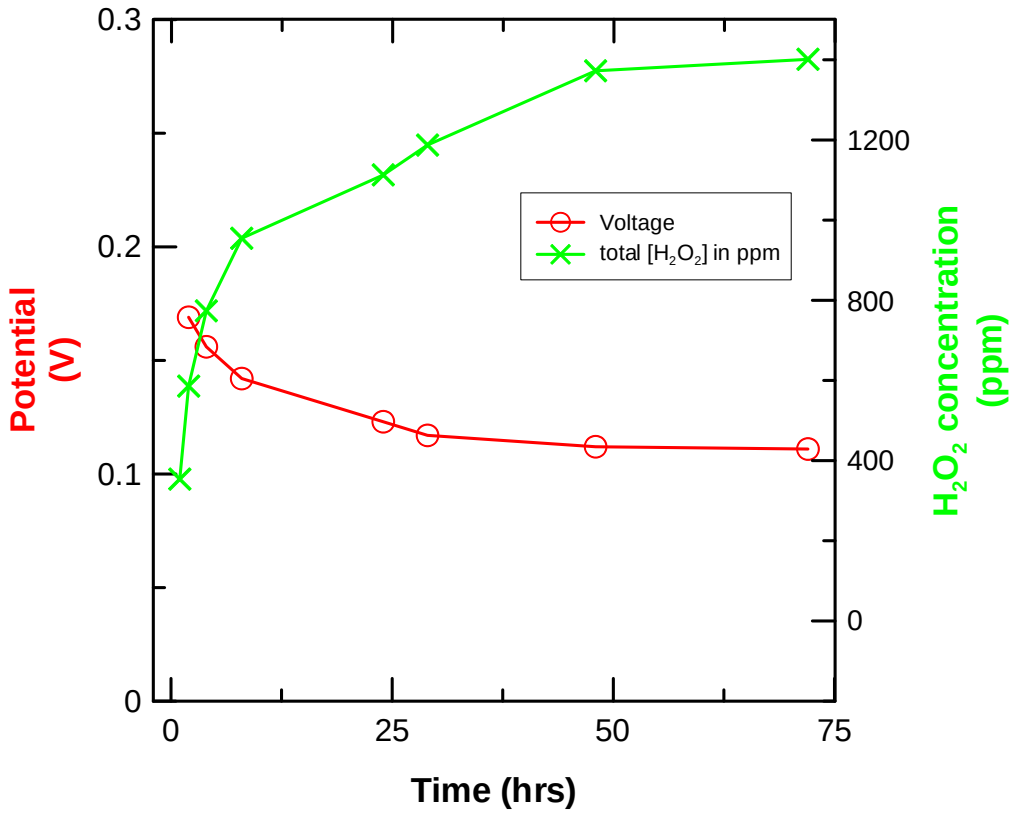

Figure 5.9 Long term (72 hours) continuous recycle operation of the SPE cell in fuel cell mode at a constant current density of 8.2 mA cm^{-2}. Cell temperature: 60 ℃. Anode conditions: H_2 flow rate 500 mL min^{-1} pressure: at 150 kPa(g), anode catalyst loading 0.7 mg_{Pt} cm^{-2}. Cathode conditions: O_2 flow rate 1000 mL min^{-1} O_2, pressure 150 kPa (g), water flow rate 15 mL min^{-1}, Teflon content: 10 wt%, Co-C loading 3.6 $mg_{Co\text{-}C}$ cm^{-2}.

The capability to produce more concentrated H_2O_2 solutions is essential for improving the economic prospects of the overall system and to enhance the capability to treat large amounts of drinking water. For example, a typical AOP water treatment system capable of treating 250 m^3 of water per day in a rural community of 500 people would require 2.5 kg of H_2O_2. The latter H_2O_2 concentration exceeds the H_2O_2 concentration (0.5 g) presented in Figure 5.10. However, data presented here are preliminary and further experiments will need to be carried out to improve H_2O_2 production rate and optimize the fuel cell performance. Furthermore, the single cells can be stacked where many cells could be connected in series and operated in recycle mode to reach

the target H_2O_2 concentration to assure the daily purification requirements for a typical rural remote community.

5.4 Effect of Temperature on Degradation of Product H_2O_2

As discussed earlier in this chapter, temperature has a significant effect on the stability of H_2O_2. Typical fuel cells operated at 75 – 80°C. Through the temperature effect test on H_2O_2 production in Section 5.3.2.1, it was determined that the optimal operating temperature for H_2O_2 production in fuel cell mode operation is 60°C. While the external water collection system was designed to collect water samples for analysis, it also included a condenser unit (Figure 4.8) where the product liquid stream is cooled to room temperature in order to minimize the chances of rapid H_2O_2 decomposition due to higher operating temperatures.

However, during recycle mode, or multi-pass mode operation, where the product liquid stream is pumped back into the SPE cell in order to increase H_2O_2 concentration, the product H_2O_2 in the liquid stream could undergo thermal decomposition as a result of re-entering an elevated temperature environment. Thus a peroxide stability test was conducted to determine the stability and lifetime of the product H_2O_2 exposed to the cell components at different temperatures. Two sets of recycle tests were conducted. The first set were done with no load applied to the SPE cell, while maintaining the cell pressure at 150 kPa as well as gas feed to both the anode and the cathode, and varying the cell temperature between 40 and 80°C (Figure 5.10). The second set of recycle tests were done with no load applied, no gas feed to both electrodes, only maintaining the cell pressure at 150 kPa, while varying the cell temperature between 40 and 80°c (Figure 5.11).

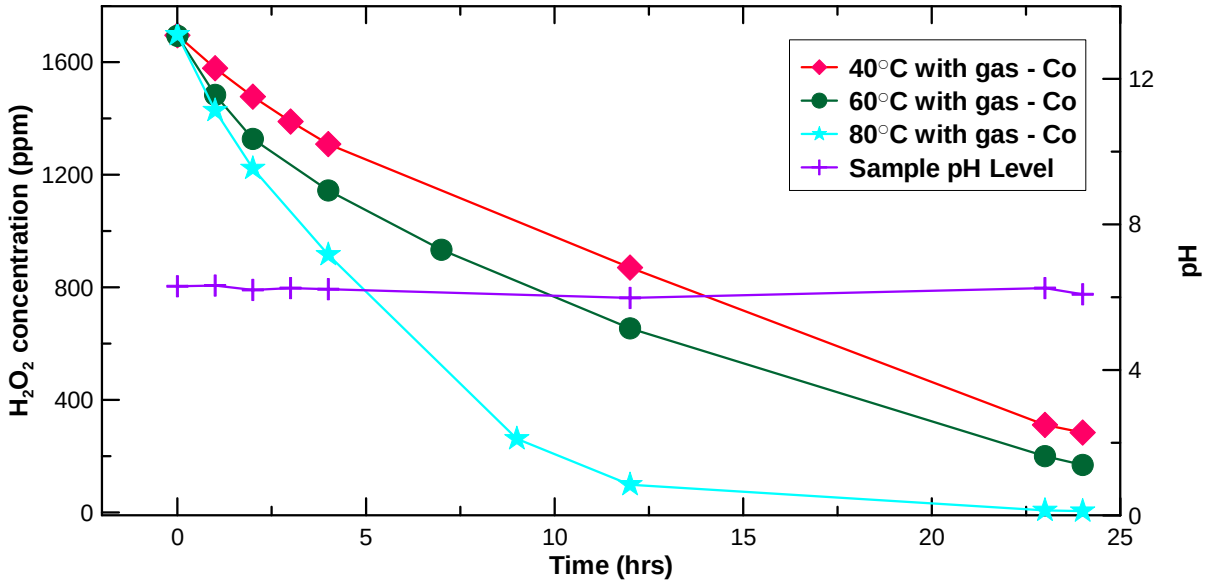

Figure 5.10 Longer-term H_2O_2 stability in the fuel cell set-up without load as a function of temperature and gas flows with continuous recycle of the cathode water carrier flow. Anode conditions: H_2 flow rate 500 mL min^{-1} pressure: at 150 kPa (g), anode catalyst loading 0.7 mg $_{Pt}$ cm^{-2}. Cathode conditions: O_2 flow rate 1000 mL min^{-1} O_2, pressure 150 kPa (g), water flow rate 15 mL min^{-1}, Teflon content: 10 wt%, Co-C loading 3.6 $mg_{Co\text{-}C}$ cm^{-2}.

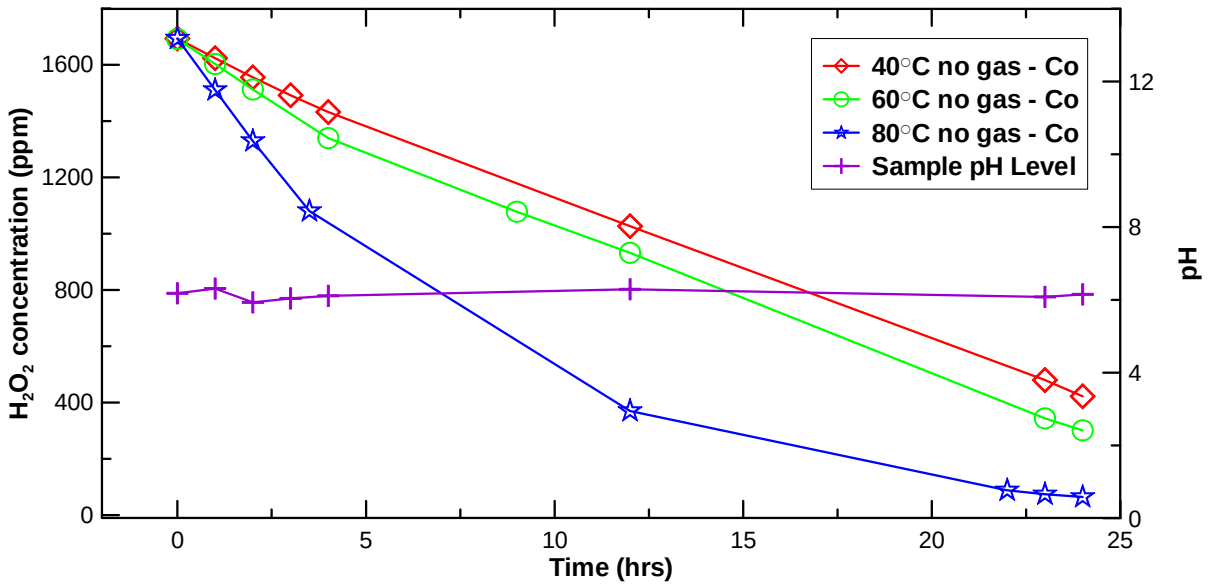

Figure 5.11 Longer-term H_2O_2 stability in the fuel cell set-up without load and gas flow as a function of temperature with continuous recycle of the cathode water carrier flow. Anode conditions: pressure at 150 kPa (g), anode catalyst loading 0.7 mg_{Pt} cm^{-2}. Cathode conditions: pressure 150 kPa (g), water flow rate 15 mL min^{-1}, Teflon content: 10 wt%, Co-C loading 3.6 $mg_{Co\text{-}C}$ cm^{-2}.

Both stability tests lasted approximately 24 hours. For the stability test with gas feeds to the electrodes, the H_2O_2 degradation was approximately linear over the test period at the lower testing temperature of 40°C. At higher temperatures (80°C), the H_2O_2 degradation exhibited exponential decay, and almost all of the H_2O_2 had decomposed at the end of the test period. The H_2O_2 thermochemical decomposition here is mainly caused by the cobalt oxide formed as a result of the oxygen flowing through the cathode. The cobalt oxide oxidizes the H_2O_2 into HO_2 radicals, which reacts rapidly with other H_2O_2 in the liquid, forming H_2O in the process [108]. On the other hand, the stability test without gas flow did not exhibit this rapid thermochemical decomposition from the cobalt catalyst, even at higher temperatures. For all three temperatures tested, the degradation was fairly linear, with the highest degradation rate coming in during the first five hours of the stability test.

5.4.1 H_2O_2 Decomposition Kinetics

With the concentration profile in Figures 5.10 and 5.11, the rate constant for peroxide decomposition for the three temperatures tested can be determined. First the natural log of peroxide concentration is plotted against time (Figures 5.12 and 5.13).

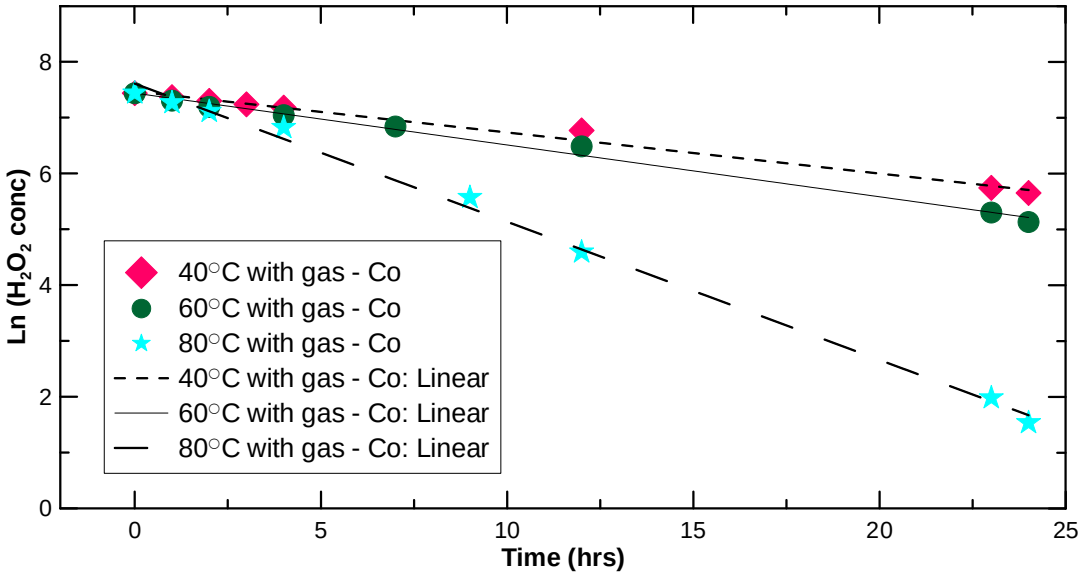

Figure 5.12 Rate constant determination for peroxide decomposition in the fuel cell set-up without load as a function of temperature and gas flows with continuous recycle of the cathode water carrier flow. Anode conditions: H_2 flow rate 500 mL min^{-1} pressure: at 150 kPa(g), anode catalyst loading 0.7 mg_{Pt} cm^{-2}. Cathode conditions: O_2 flow rate 1000 mL min^{-1} O_2, pressure 150 kPa(g), water flow rate 15 mL min^{-1}, Teflon content: 10 wt%, Co-C loading 3.6 $mg_{Co\text{-}C}$ cm^{-2}.

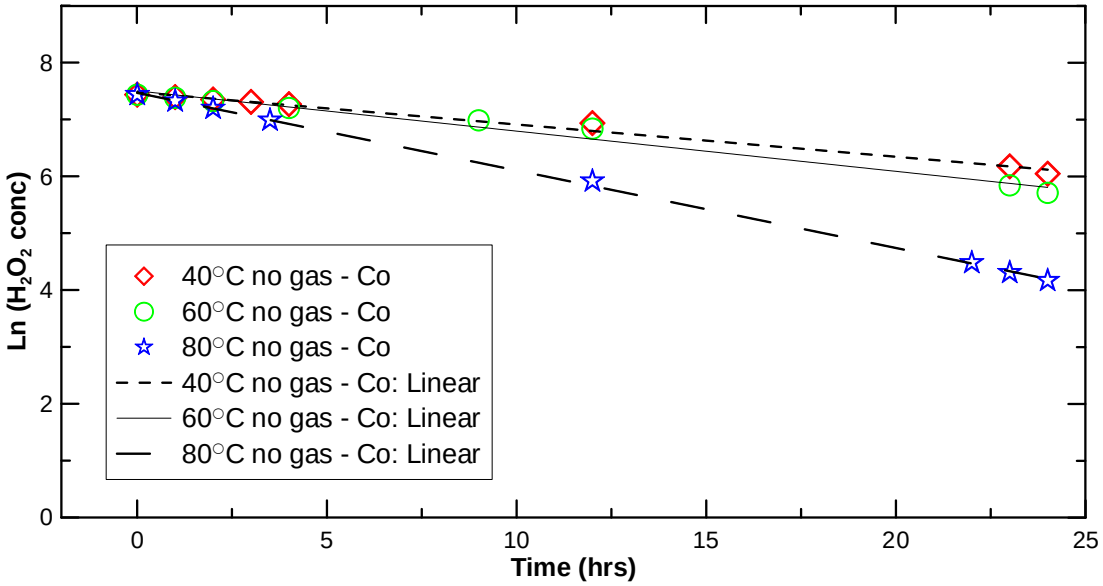

Figure 5.13 Rate constant determination for peroxide decomposition in the fuel cell set-up without load as a function of temperature and gas flows with continuous recycle of the cathode water carrier flow. Anode conditions: H_2 flow rate 500 mL min^{-1} pressure: at 150 kPa(g), anode catalyst loading 0.7 mg_{Pt} cm^{-2}. Cathode conditions: O_2 flow rate 1000 mL min^{-1} O_2, pressure 150 kPa(g), water flow rate 15 mL min^{-1}, Teflon content: 10 wt%, Co-C loading 3.6 $mg_{Co\text{-}C}$ cm^{-2}.

Table 5-6 Decomposition rate constant values for the fuel cell set-up.

Temperature	With gas	Without gas
40°C	0.07358	0.05673
60°C	0.09281	0.07072
80°C	0.24744	0.13632
Â (s^{-1})	2489.91	109.95
E_a (J mol^{-1})	27474.9	19909.3

Note: Â = pre-exponential factor, E_a = activation energy.

These rate constants are then plotted against the inverse of temperature° to determine the activation energy for peroxide decomposition (Figure 5.14). The activation energy for peroxide decomposition was calculated to be 2.74 x 10^4 J mol^{-1} with gas flow, and 2 x 10^4 J mol^{-1} without gas flow. For further discussion on kinetic parameters please see Appendix D.

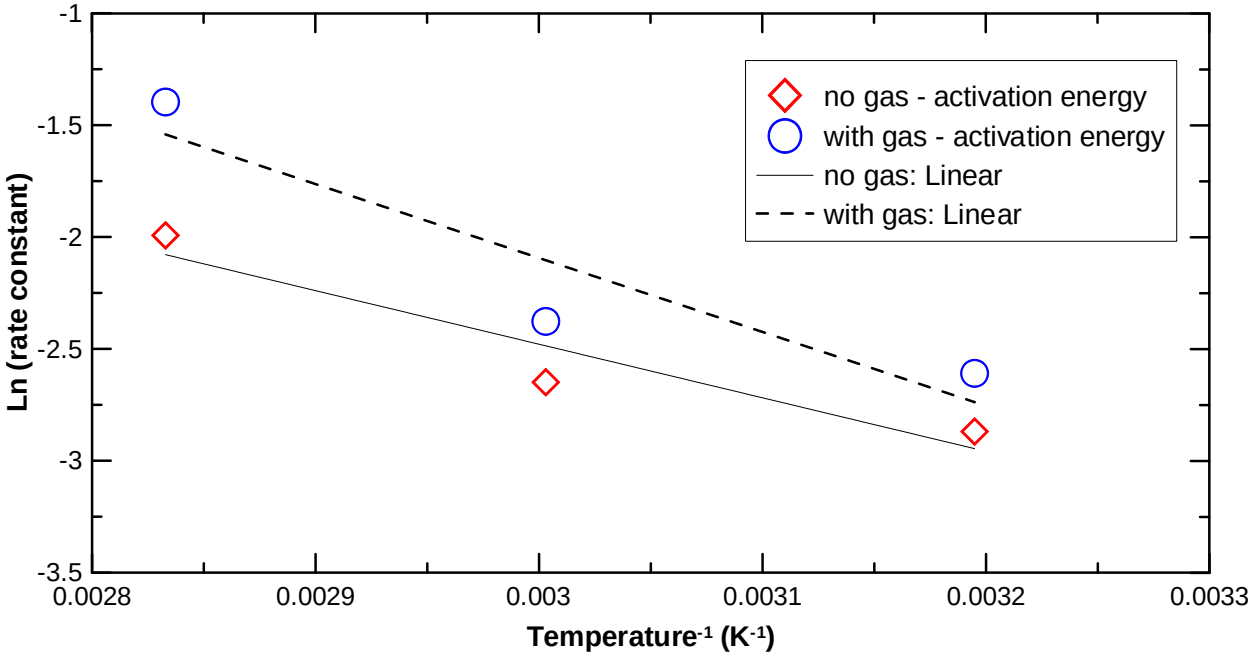

Figure 5.14 Determination of activation energy for peroxide decomposition.

5.5 Effluent Water Analysis

As the product H_2O_2 solution will be entering the final phase of the drinking water treatment facility, it is crucial that the solution would meet the drinking water guidelines for dissolved trace metals and ions in the solution. For this research, these dissolved metals and ions can include inorganics such as cobalt and fluoride ions in fuel cell mode operation.

For both cobalt and fluoride ions, the best method of analysis was inductively-coupled plasma mass spectrometry (ICP-MS). The analytical procedure for cobalt and fluoride ions can be found in Appendix B-2 and B-3. For both cobalt and fluoride ions, samples from polarization runs as well as long term recycling tests were analyzed.

5.5.1 Cobalt Analysis

For experiments in fuel cell mode operation, the cathode carrier water can remove trace amounts of cobalt ions as it passes through the cathode catalyst layer. Cathode water samples of various polarization runs at different temperatures were tested for cobalt concentration using ICPMS. The concentrations are normalized and plotted in Figure 5.15. Samples from the long term recycling runs were also tested for cobalt concentration, and the normalized cobalt leaching rate are plotted in Figure 5.16.

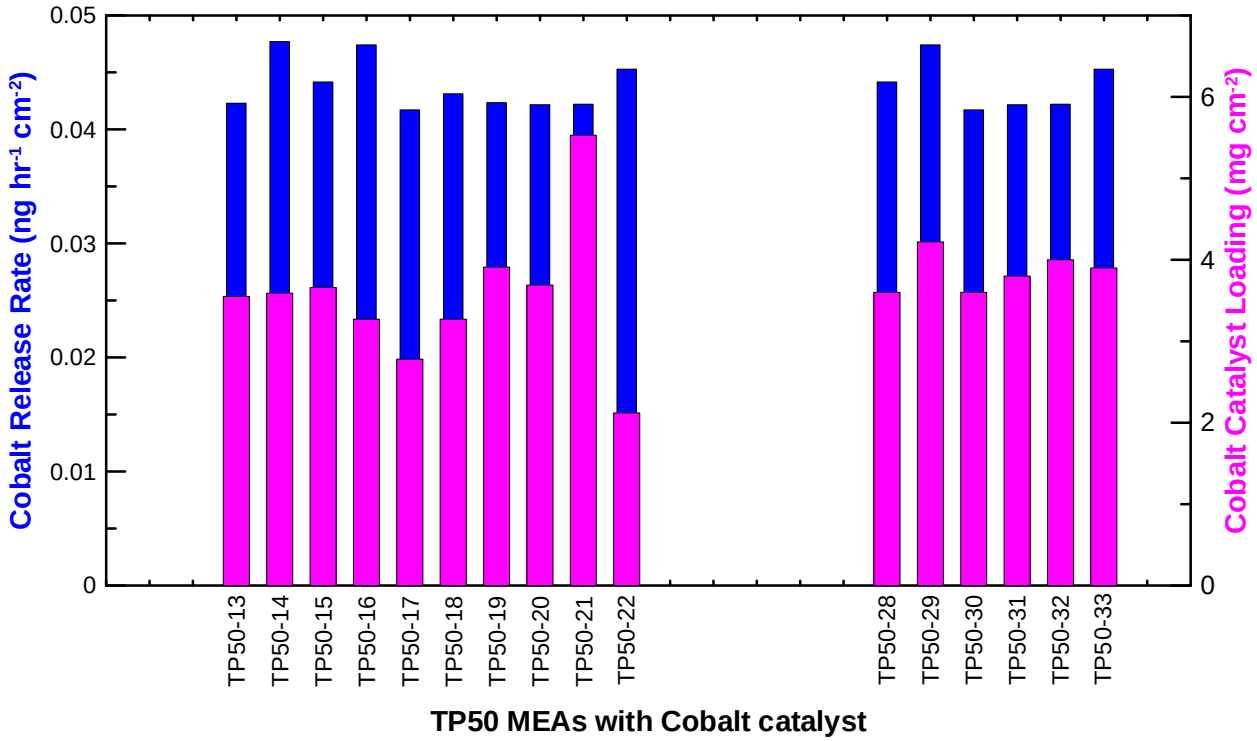

Figure 5.15 Normalized cobalt release rates for various different TP50 MEAs.

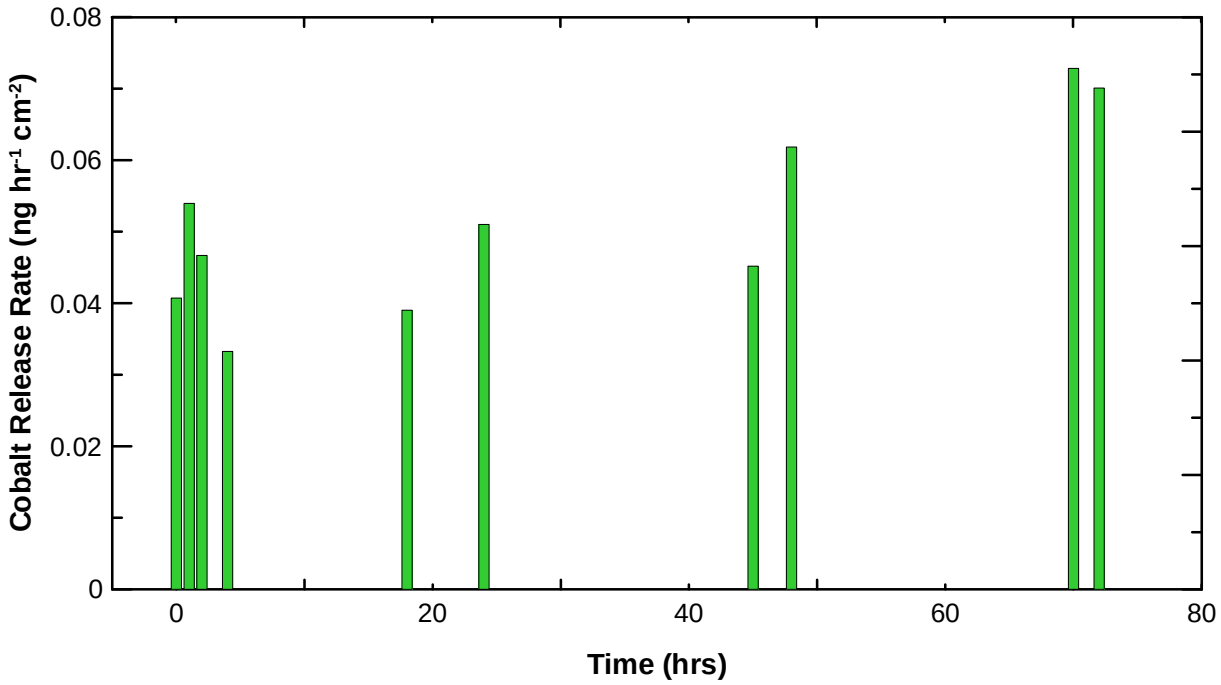

Figure 5.16 Normalized cobalt release rate for long term recycling runs.

Of the samples analyzed for cobalt content, the median cobalt release rate was 0.045 ng hr^{-1} cm^{-2} (2.46 μg L^{-1}). Published reports from different governing bodies showed a typical cobalt limit of 2 – 5 μg L^{-1} [109-110]. Results from the long term recycle experiments showed that the cumulative cobalt concentrations after three days of continuous operation (< 6 μg L^{-1}) is still within the limit set out by the guidelines.

5.5.2 Fluoride Ion Analysis

For experiments in fuel cell mode operation, the presence of hydroxyl radicals in the cathode carrier water puts additional strain on the membrane, which can lead to an increase in membrane decomposition. Fluoride ions can form as a result of this membrane decomposition. Hence the cathode water samples of various polarization runs at different temperatures was tested for fluoride ion concentration using ICPMS. The concentrations are normalized and plotted in Figure 5.17. Samples from the long term recycling runs were also tested for fluoride ion concentration, and the normalized fluoride leaching rate are plotted in Figure 5.18.

The median fluoride release rate was ~ 0.03 ng hr^{-1} cm^{-2} (~ 1.59 μg L^{-1}) for the sixteen samples analyzed. Drinking water guidelines from the Government of B.C., as well as the World Health Organization indicated a fluoride limit of 1.0 – 1.5 mg L^{-1} [111-112]. The long term recycle experiments showed the cumulative fluoride concentration over the three day run was well below the limit set out by the guidelines, at about 2.2 μg L^{-1}.

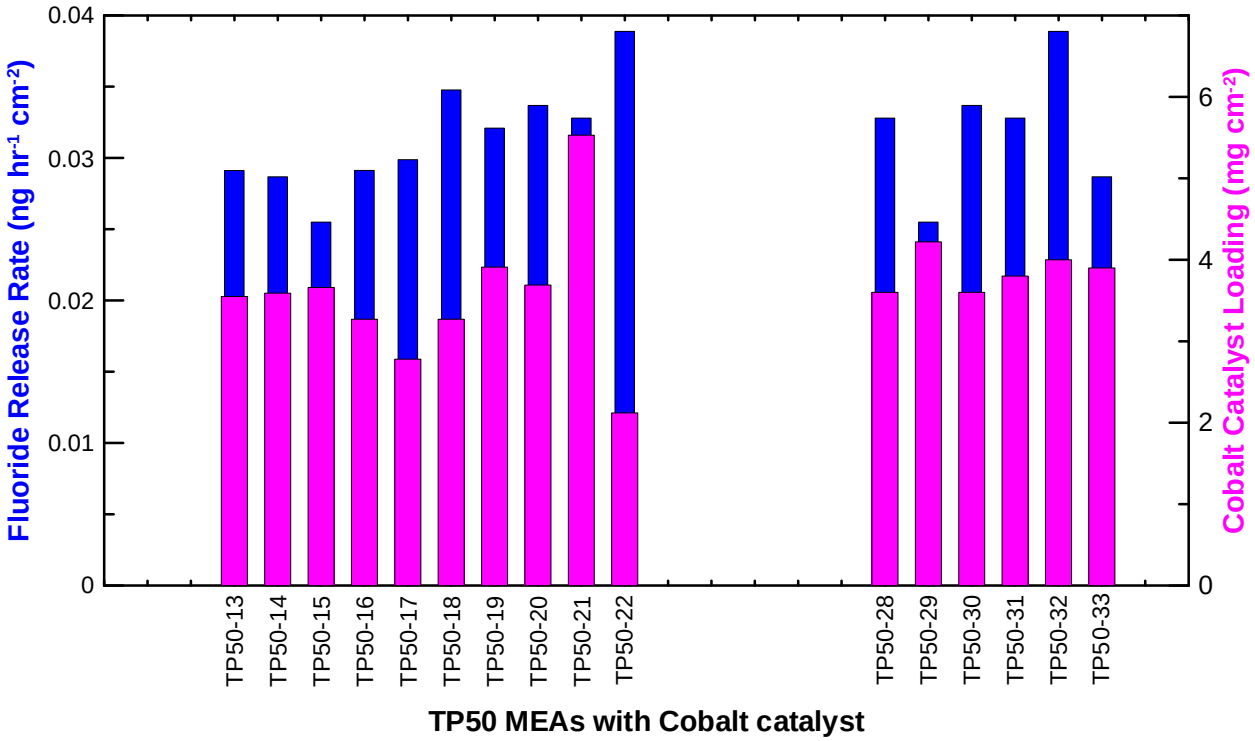

Figure 5.17 Normalized fluoride ion release rates for various different TP50 MEAs.

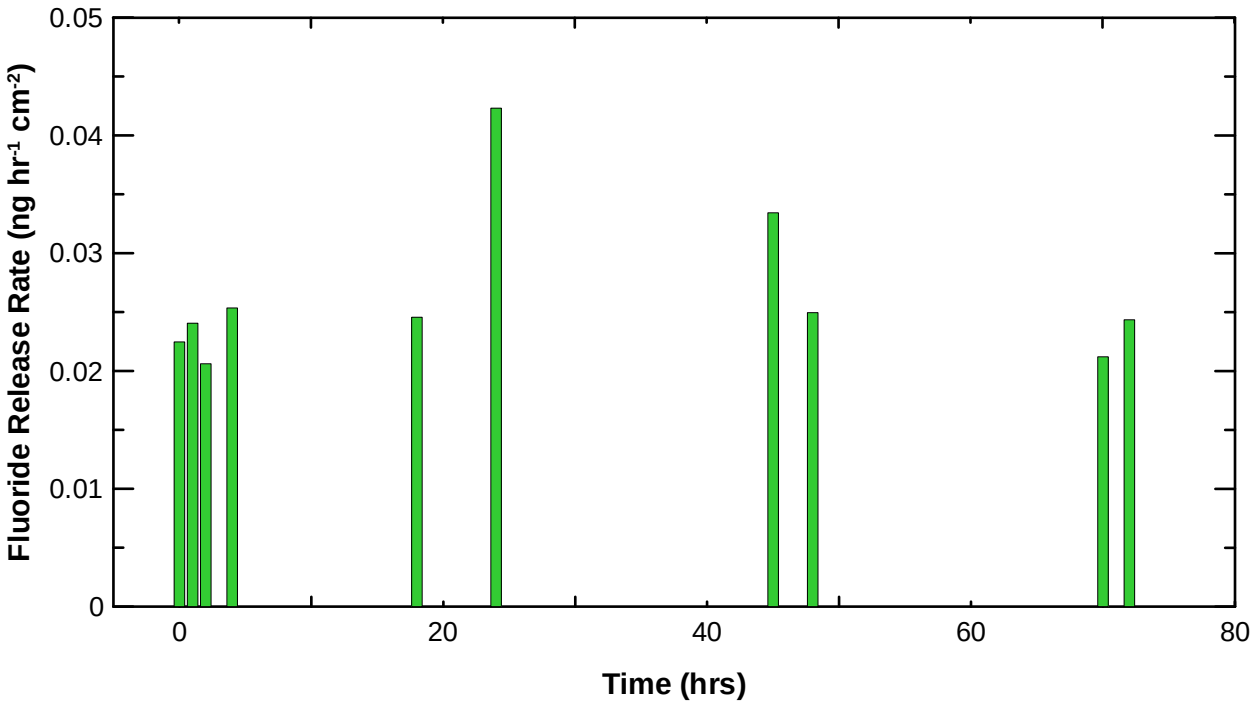

Figure 5.18 Normalized fluoride ion release rate for long term recycling runs.

5.5 Conclusion

The Co-C composite catalyst was previously introduced by Bonakdarpour *et al.*[28] as a suitable cathode catalyst for electroreduction of oxygen to hydrogen peroxide. In this section, parametric experiments with this Co-C composite catalyst in a 49 cm^2 H_2/O_2 PEM fuel cell were conducted to determine the optimal operating conditions in order to achieve maximum H_2O_2 production. The cathode was fueled with pure oxygen as well as a carrier DI water flow which help to efficiently remove the product H_2O_2 from the cathode compartment. This two phase flow regime requires careful management in order to minimize cathode flooding (which can impede O_2 mass transfer) while maximizing H_2O_2 production and removal. The best fuel cell polarization performance and H_2O_2 production rate was achieved with a cathode catalyst loading of 3.6 mg_{Co-C} cm^{-2} using 10 wt% Teflon content Toray carbon paper GDL and a carrier water flow rate of 25 mL min^{-1}. A maximum H_2O_2 production rate of 203 μmol hr^{-1} cm^{-2} was obtained at 60 ^{0}C with the fuel cell operated at 30 mA cm^{-2} with 30% current efficiency. The corresponding cell voltage was 0.1 V. The current efficiency is the net results of H_2O_2 generation and consumption processes such as electrochemical reduction and thermochemical decomposition.

Longer-term (72 hrs) experiments conducted with complete recycle of the carrier water containing the generated H_2O_2 showed that H_2O_2 concentrations up to 1400 ppm can be obtained, without significant degradation of the Co catalyst. The capability to produce high concentrations of H_2O_2 in a fuel cell stack (i.e., multiple single cells connected in series) is very important to improve the economic outlet of the water treatment system and to address efficiently the peroxide needs of the purification system. Engineering scale-up studies are required on stack

level with geometric electrode areas per cell up to 1000 cm^2, to further advance this promising technology of co-generation of H_2O_2 and electric power.

As the continuous generation of H_2O_2 in a PEM fuel cell is a novel concept, and the work presented in this section is a first demonstration of such a concept. At this stage of research, the voltage generated by the peroxide producing fuel cell is low between 0.6 V and 0.1 V per cell (depending on the current density). For the drinking water treatment application, our goal for future research is for the peroxide producing fuel cell stack to supply the electric power needs of the advanced oxidation water treatment unit (e.g., pumps, UV-reactor, control equipment). This would be especially important in situations without easy access to the electric power grid. It is expected that further improvements in the cathode electrocatalyst could improve the power output. One possible improvement is in the cathode catalyst configuration, which will be discussed in the next section.

Chapter 6 Co-Generation of Power and Hydrogen Peroxide in a PEM Fuel Cell

6.1 Introduction

The previous chapter discussed findings of H_2O_2 production in a continuous flow reactor using a 49 cm^2 electrode area PEMFC. Parts of the chapter have been published in ChemSUSChem [113]. With a cathode catalyst loading of 3.6 $mg_{Co\text{-}C}$ cm^{-2}, a maximum H_2O_2 production rate of 200 μmol cm^{-2} hr^{-1} and 3 mW cm^{-2} at 30% current efficiency operating at 30 mA cm^{-2} and 25 mL min^{-1} cathode carrier water flow rate was achieved. As with all PEMFCs, power generation is one key benefit. Although the principle goal of the thesis research project was to test different SPE assemblies and operating conditions for H_2O_2 production, the production of a small amount of power, albeit small compared to the typical power output of a PEMFC of similar size in active area, provided an intriguing area of interest for power cogeneration. Hence a number of different cathode catalyst mixtures and catalyst layer configurations have been investigated here in order to increase power generation of the continuous flow reactor, while maintaining H_2O_2 production.

6.2 Experimental Procedure

Details regarding the fuel cell hardware and testing equipment used were described in Chapter 4. The preparation methodologies of the anode and cathode catalyst layers can be found in the appendices. For the anode, electrodes were either prepared following the protocol listed in Appendix A-3 or a commercially available catalyst coated membrane (GORE) was used. In both cases the anode catalyst consisted of only platinum. The anode catalyst layer type and concentration are listed in Table 6-1. For the cathode, a total of nine catalyst configurations were

tested and compared. Table 6-1 lists these configuration types, as well as the concentration of each catalyst used in the specific configuration.

Table 6-1 Anode/cathode catalyst composition of the different catalyst configuration used.

Cathode GDL Configuration (Geometry Type)	**Anode/Cathode Catalyst Composition**
No MPL:	
A: Pt / GDL (Single Layer)	Anode: 0.7 mg Pt cm^{-2} (40% wt.Pt on C) Cathode: 0.7 mg Pt cm^{-2} (40% wt.Pt on C) GDL: TGPH-060 Toray paper no PTFE (for both sides)
B: Co-C / GDL (Single Layer)	Anode: 0.7 mg Pt cm^{-2} (40% wt.Pt on C) Cathode: 3.6 mg Co-C cm^{-2} (4% wt.Co on C) GDL: anode TGPH-060 Toray paper no PTFE GDL: cathode TGPH-060 Toray paper 10wt.% PTFE
C: Pt CCM and Co-C / GDL	Membrane: CCM (0.4 mg_{Pt} cm^{-2} both side) Cathode: 3.6 mg Co-C cm^{-2} (4% wt Co on C) GDL: anode TGPH-060 Toray paper no PTFE GDL: cathode TGPH-060 Toray paper 10wt.% PTFE
D: Pt on Co-C / GDL	Anode: 0.4 mg Pt cm^{-2} (40% wt Pt on C) GDL: anode TGPH-060 Toray paper no PTFE Cathode: 0.2 mg Pt cm^{-2} (40% wt Pt on C) on 3.6 mg Co-C cm^{-2} GDL: cathode TGPH-060 Toray paper 10wt.% PTFE
E: Pt + Co-C / GDL (Mixed Single Layer)	Anode: same as above Cathode: 0.1 mg Pt cm^{-2} (40 %wt. Pt on C) mixed with 3.6 mg Co-C cm^{-2} GDL: anode – same as above GDL: cathode – same as above
F: Pt/Co-C 50/50 GDL (Side-by-Side Single Layers)	Anode: same as above Cathode: 3.6 mg Co-C cm^{-2} and 0.2 mg Pt cm^{-2} (40 %wt. Pt on C) GDL: anode – same as above GDL: cathode – same as above
With MPL:	
G: Pt on MPL GDL	Anode: 0.4 mg Pt cm^{-2} (40% wt Pt on C) GDL: anode TGPH-060 Toray paper no PTFE Cathode: 0.4 mg Pt cm^{-2} (40% wt Pt on C) on 0.9 mg cm^{-2} MPL on TGPH-060 Toray paper 10wt.% PTFE
H: Co-C on MPL GDL	Anode: same as above Cathode: 3.6 mg Co-C cm^{-2} (4% wt Co on C) on 0.9 mg cm^{-2} MPL on TGPH-060 Toray paper 10wt.%

	PTFE
I: Pt/Co-C 50/50 on MPL (Side-by-side Single Layers)	Anode: same as above Cathode: 3.6 mg Co-C cm^{-2} with 0.2 mg 40% Pt cm^{-2} on 0.9 mg cm^{-2} MPL on TGPH-060 Toray paper 10wt.% PTFE

Note: GDL: Gas Diffusion Layer; CCM: Catalyst Coated Membrane; MPL: Micro Porous Layer; PTFE: Polytetrafluoroethylene.

For a better understanding of the different configuration types, MEA cut-out views of each of the nine configurations types are shown in Figures 6.1 (w/o MPL) and 6.2 (with MPL).

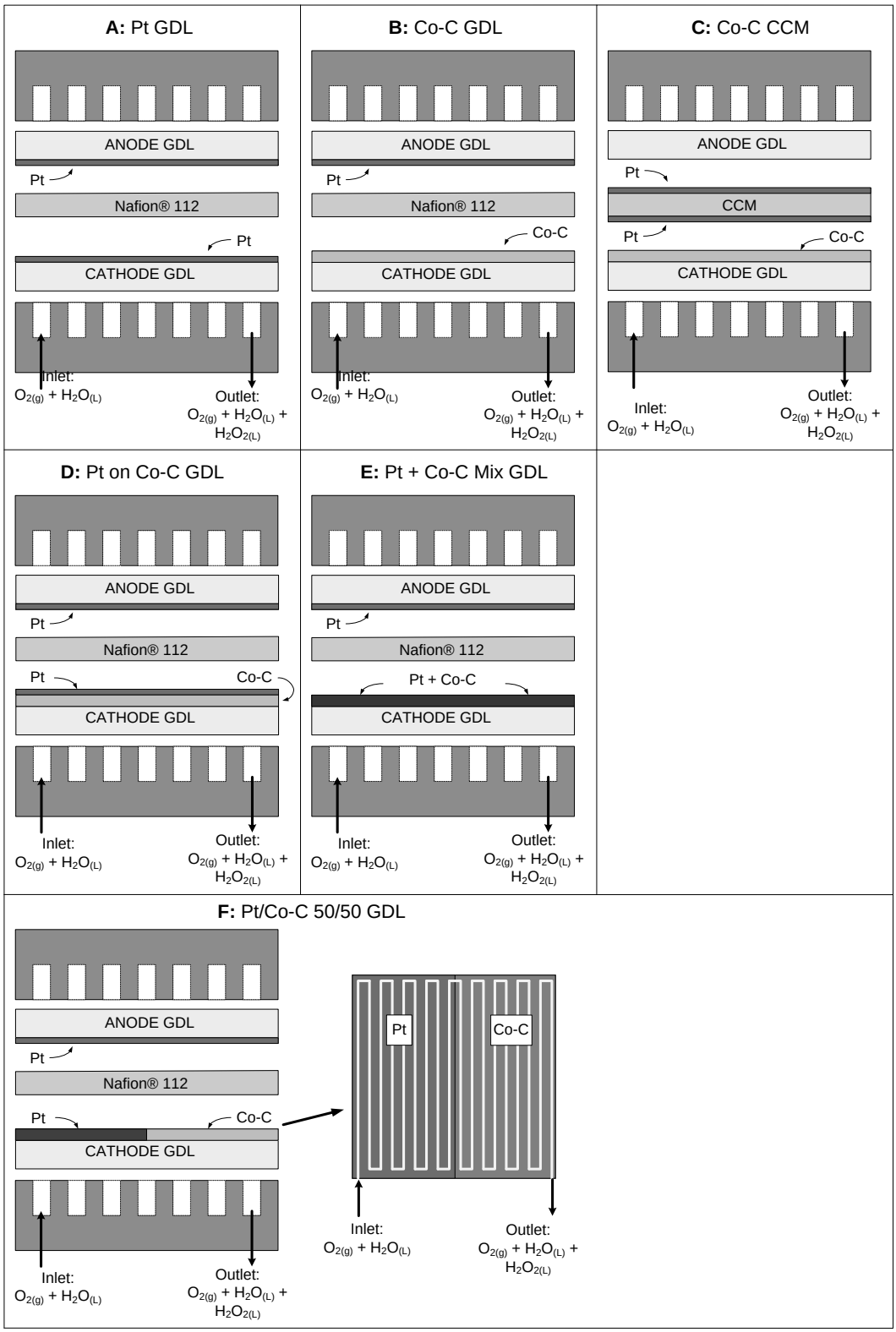

Figure 6.1 The layout and catalyst composition of six catalyst layer configurations tested without micro-porous layer.

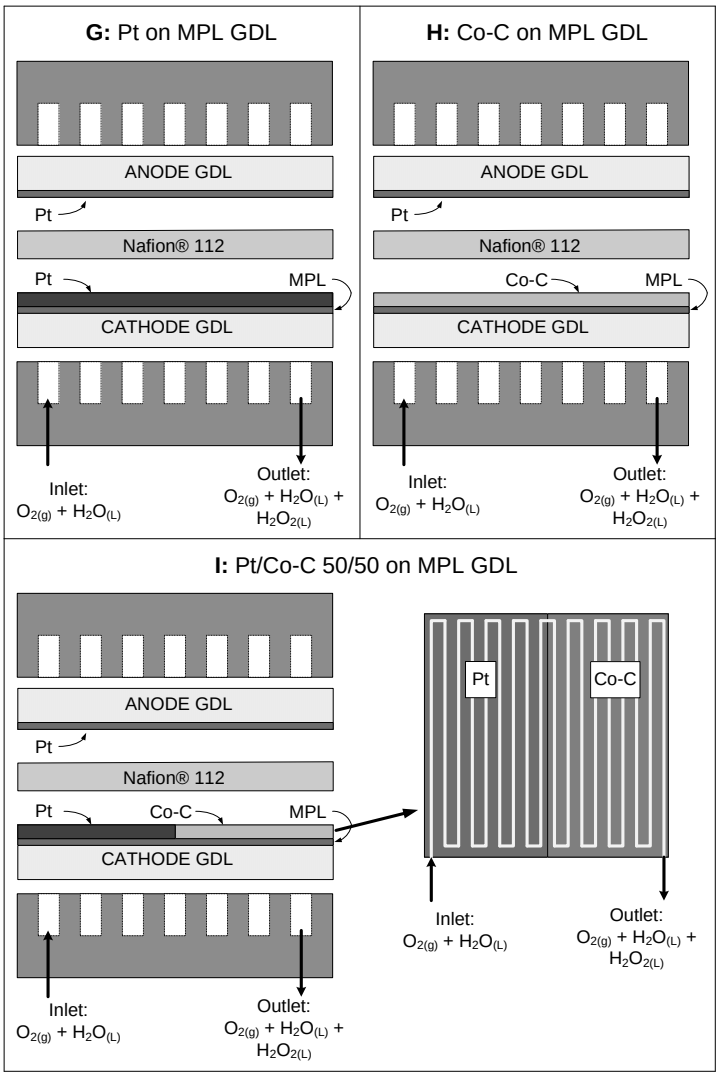

Figure 6.2 Geometric layout and catalyst composition of three configurations with micro-porous layer.

The first configuration (Figure 6.1A) consisted of a Pt-catalyst layer on top of a GDL for both the anode and the cathode, with a Nafion 112 membrane sandwiched in-between. This is the typical configuration for a standard Pt-catalyst based PEMFC. Figure 6.1B has a Pt catalyst layer on top of the anode GDL and a cobalt-carbon (Co-C) composite catalyst layer on the cathode GDL, with a Nafion 112 membrane sandwiched between them. This was the configuration used to test the cathode catalyst in the previous chapter. Figure 6.1C utilized a

commercially available catalyst coated membrane (CCM) from GORE, sandwiched between a plain anode GDL, and a cathode GDL with the Co-C composite catalyst layer on top. Figure 6.1D has the Pt catalyst layer on top of the anode GDL, the Co-C composite catalyst layer on the cathode GDL, and an additional Pt catalyst layer on top of the Co-C composite catalyst layer, with a Nafion 112 membrane sandwiched in-between. Figures 6.1C and 6.1D have essentially the same configuration. However, they have some differences during operation in relation to mass transport. The CCM in Figure 6.1C has better mass transport due to lower interface resistance between the catalyst layer and the membrane [114]. However, the same Pt catalyst layer is next to the membrane on the cathode side, most of the protons that crosses the membrane will undergo the 4 electron pathway. While for the GDE in Figure 6.1D, the thin Pt catalyst layer could have small holes in the CL, hence it is possible some protons pass through these holes un-reacted and partake in the 2 electron pathway. Figure 6.1E has Pt catalyst layer on the anode GDL, and a mixed cathode catalyst layer consisting of an admixture of Pt catalyst and the Co-C composite catalyst on the cathode GDL, with a Nafion 112 membrane in-between. The close proximity of the Pt and Co-C catalysts will likely interfere with H_2O_2 production, as Pt is known to decompose H_2O_2 into water and oxygen [7]. Figure 6.1F has a Pt catalyst layer on the anode GDL, and the Pt catalyst and Co-C composite catalyst mix are configured in a side-by-side configuration on the cathode GDL, with a Nafion 112 membrane in-between. In this configuration, the Pt catalyst layer covers the first half of the active area, with the Co-C composite catalyst layer covering the second half of the active area. The intent of this configuration is that the 2 reaction pathways do not interfere with one another.

The next three configurations, shown in Figure 6.2, all includes a micro porous layer (MPL) between the cathode catalyst layer and the cathode GDL. The purpose of the MPL is to improve fuel cell performance by improving cathode water management [104, 106, 115-118]. A recent study by Blanco and Wilkinson [119] shows he effect and mechanism of anode and cathode MPLs on water management in a PEMFC. Figure 6.2G is the same as Figure 6.1A, but with a MPL in-between the cathode Pt catalyst layer and the cathode GDL. Figure 6.2H is the same as Figure 6.1B, with an additional MPL in-between the cathode Co-C composite catalyst layer and the cathode GDL. Figure 6.2I is the same as Figure 6.1F, but with a MPL in-between the cathode catalyst layer and the cathode GDL.

6.3 Results and Discussions

6.3.1 Co-Generation of Power and H_2O_2 with Different Cathode Catalyst Layer Configurations without a Micro-Porous Layer (MPL)

Figure 6.3 shows the performance comparison among the cathode catalyst layer configurations A) to F) from Table 2 and Fig. 2, respectively. The power density obtained from the Co-C cathode catalyst (~ 4 mW cm^{-2}) is about two orders of magnitude smaller than that of the Pt cathode catalyst MEA without MPL (> 250 mW cm^{-2}). For the Pt cathode catalyst the 4-electron oxygen reduction pathway dominates without production of hydrogen peroxide.

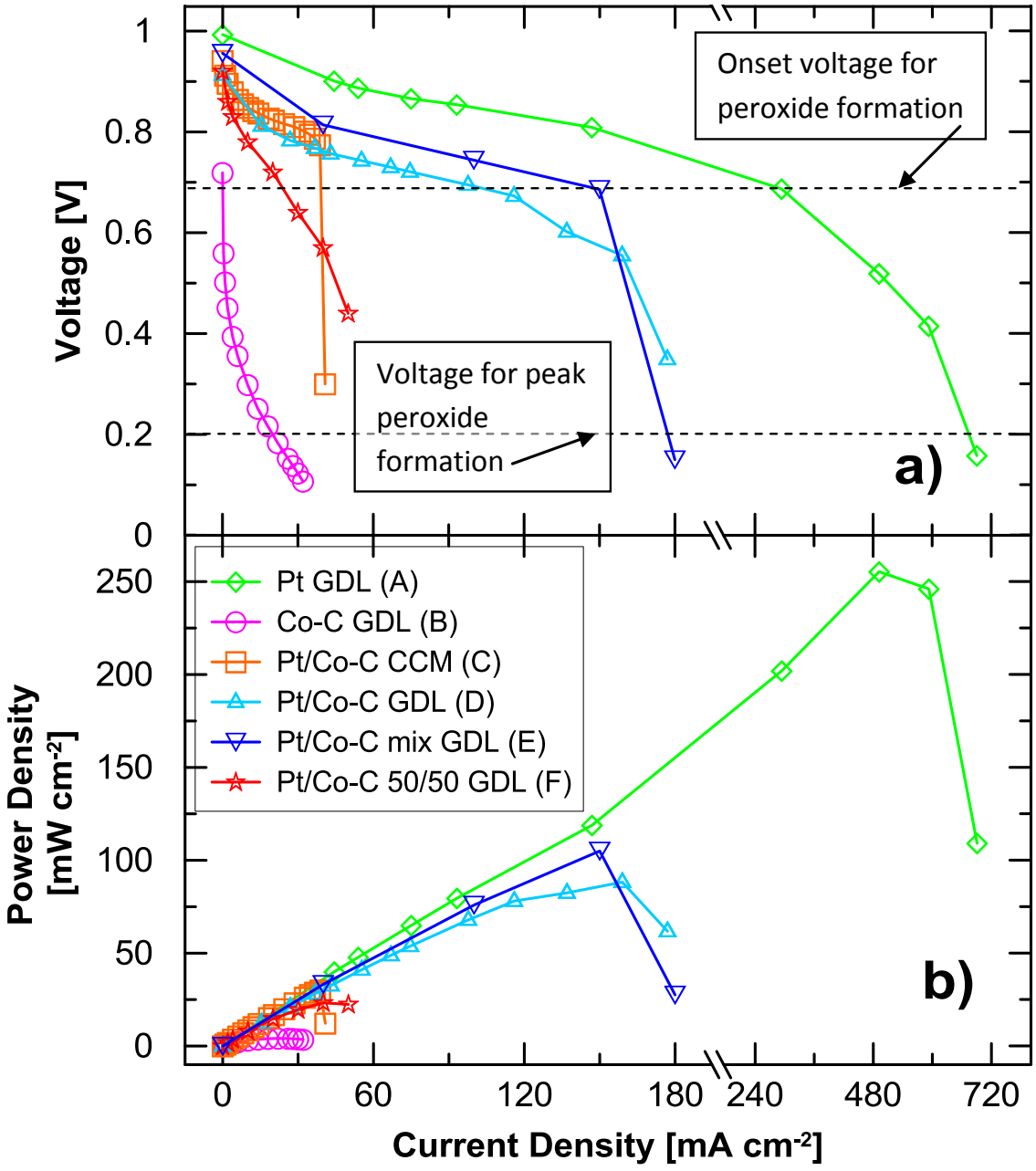

Figure 6.3 Polarization results for four cathode Co-C/Pt configurations versus the reference Co-C GDL MEA (config. A) and Pt GDL MEA (config. B). Note: Cathode water flow rate = 15 mL min^{-1} for all runs; letter in brackets corresponds to configuration listed in Table 2; the entire current density spectrum is shown with breaks in the axis line to better show relationships between the MEA configurations; only Co-C GDL (○) and Pt/Co-C 50/50 GDL (★) resulted in peroxide production (**Figure 6.4**). Please refer to Table 1 for operating conditions.

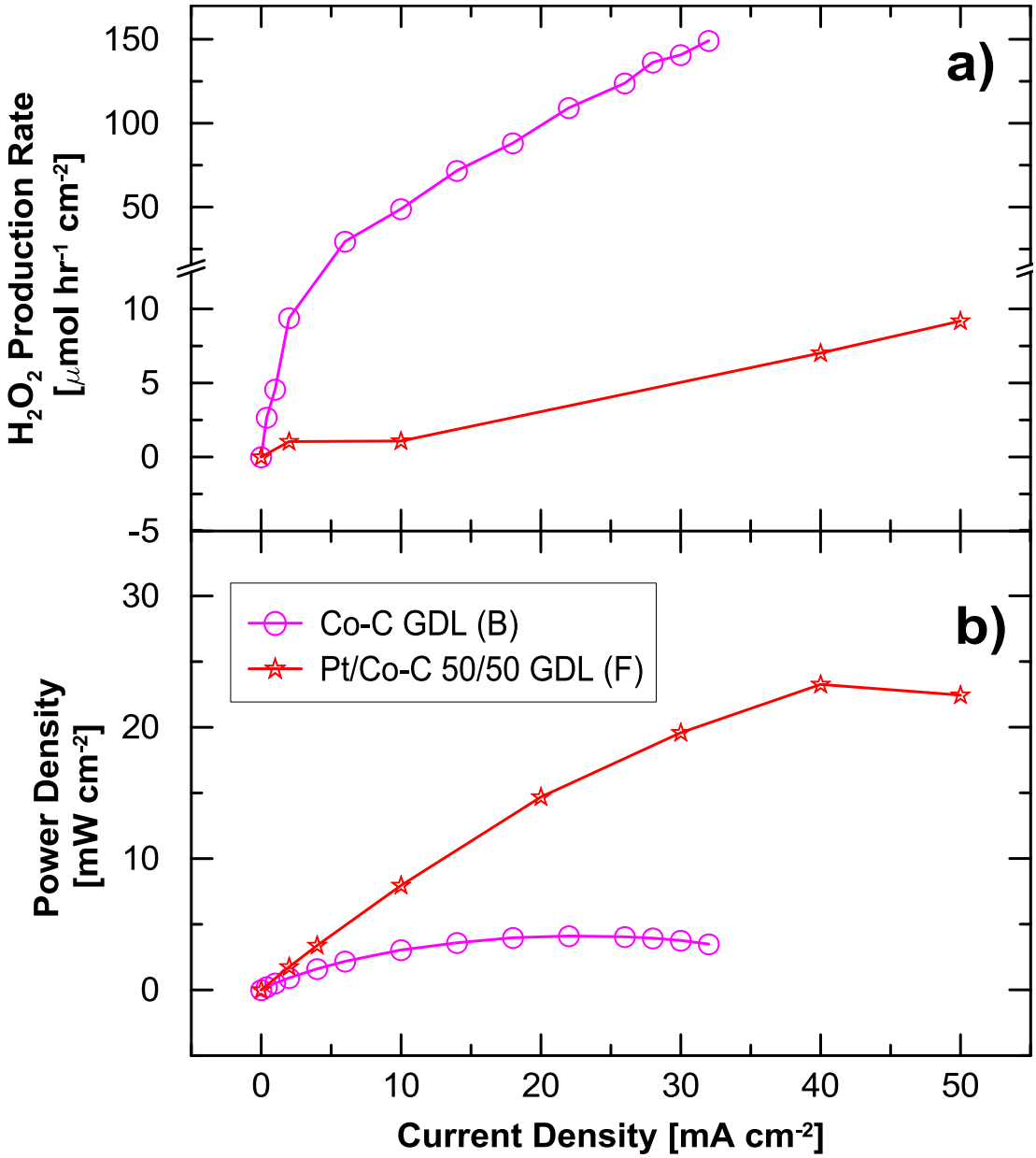

Figure 6.4 Power density and H_2O_2 production results for two cathode configurations that produced peroxide. Note: Cathode water flow rate = 15 mL min^{-1} for all runs; letter in brackets in figure legend corresponds to configuration listed in Figure 6.1; the H_2O_2 production rate spectrum is shown with breaks in the axis line to better show the relationships between the MEA configurations. Please refer to Table 4-2 for operating conditions.

For hydrogen peroxide electrosynthesis the cathode potential (vs. SHE) must be lower than 0.695 V. Hence, as shown by Figures 6.3 a and c, only the catalyst layers B and F produced any measurable amount of H_2O_2. With the composite Co-C catalyst layer, a H_2O_2 production flux of almost 160 μmol hr^{-1} cm^{-2} has been achieved (Figure 6.3 a) with a peak power at around 0.2 V. In most cases adequate peroxide production does not coincide with the peak in power. For example, configuration B with the Co-C catalyst layer had a peak power at just under 0.2 V, while all configurations with Pt in the catalyst layer had peak powers between 0.6 – 0.8 V. Furthermore, as a water carrier is needed to remove the product H_2O_2, especially at higher current densities required to get to the low voltage where H_2O_2 forms, flooding becomes a serious issue. In addition, the peak power current density of the Co-C catalyst was below 40 mA cm^{-2}, while the peak power current density for the Pt catalyst was at 500 mA cm^{-2}. Clearly, there is a trade-off between peroxide synthesis and power output.

In case of the ad-mixture of Pt and Co-C catalyst (configuration E), a small amount of Pt catalyst (0.1 mg_{Pt} cm^{-2}) was mixed with Co-C catalyst prior to application on the GDL. The polarization results are shown in Figure 6.3. In the current density region below 150 mA cm^{-2} the polarization performance of the ad-mixture is the closest to that of Pt GDL configuration A). At high current densities, (i.e., > 150 mA cm^{-2}) the performance of the ad-mixture configuration falls off precipitously due to H_2O flooding at the much lower Pt loading. In the case with configurations C and D, since the cell operation potential was primarily above 0.6 V no H_2O_2 was detected in the water samples collected, and once current densities were high enough for lower voltages significant flooding occurred.

The competing nature of the two reactions (i.e., two and four-electron ORR) led to configuration F, a single layer side-by-side catalyst layer where Pt is located in the first half of the catalyst layer (0.2 mg_{Pt} cm^{-2}) and Co-C (3.6 mg_{Co-C} cm^{-2}) is located in the last half of the catalyst layer (Figure 6.1F) matching the cathode flow field from inlet to outlet. The fuel cell polarization measurements of configuration F showed an improved performance in the power generated with respect to the Co-C GDL reference (configuration B), albeit at a much lower H_2O_2 production rate. A H_2O_2 production rate of 9 μmol hr^{-1} cm^{-2} at a peak power of 22 mW cm^{-2} shows promise that the two competing reactions can co-exist in a co-generation mode in the fuel cell.

6.3.2 Effect of Micro-Porous Layer on Co-Generation of H_2O_2 and Power of Side-by-Side Catalyst Configuration

An MEA with the side-by-side cathode configuration of Pt and Co-C was constructed with a micro-porous layer (Figure 6.2I). Figure 6.4 shows polarization results for this MEA, the side-by-side configuration without micro-porous layer (Figure 6.1F) and the Co-C GDL reference configuration with and without micro-porous layer (Figures 6.2H and 6.1B, respectively). The micro-porous layer showed much better performance for the side-by-side configuration, but only minor performance gains for the Co-C GDL reference configuration. Figure 6.4 (a and b) showed that power density increased to 130 mW cm^{-2} for the side-by-side configuration with the micro-porous layer, while still maintaining a similar H_2O_2 production flux of 8 μmol hr^{-1} cm^{-2} at the peak power output. This "shifting" of peak H_2O_2 production to a higher current density with increased power output is a good indication that co-generation of H_2O_2 and power can be modified and improved with appropriate catalyst and electrode design.

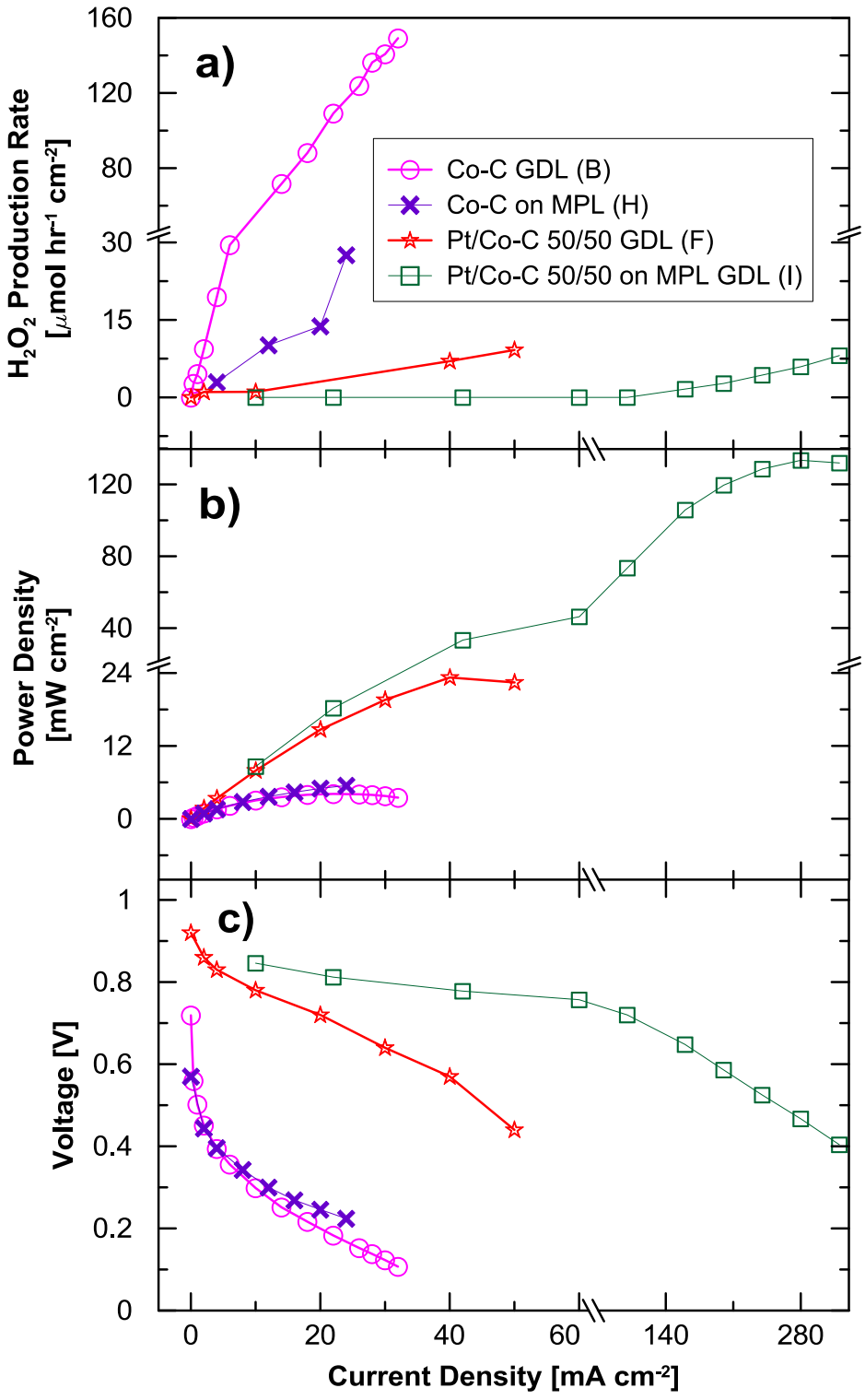

Figure 6.4 H_2O_2 production in side by side configuration, with and without MPL. Note: breaks in the axis to better show performance at the limiting operating ranges.

6.4 Conclusion

Nine different configurations of Pt and Co-C cathode catalysts were studied for co-generation of power and H_2O_2. Only the Co-C reference MEA and the side-by-side cathode configuration of Pt and Co-C catalyst in a single layer approach showed co-generation of power. The side-by-side cathode configuration without an MPL resulted in a power density of 22 mW cm^{-2} and a H_2O_2 production of 9 μmol hr^{-1} cm^{-2}. Addition of a micro-porous layer to the side-by-side configuration assisted with the management of water produced and introduced to the cell, and led to an improved co-generation of power (130 mW cm^{-2}) and H_2O_2 (8 μmol hr^{-1} cm^{-2}). In comparison, the Co-C MEA produced H_2O_2 at a rate of 120 μmol hr^{-1} cm^{-2} with a power density of 4 mW cm^{-2}, and the Co-C on MPL GDL produced H_2O_2 at 27 μmol hr^{-1} cm^{-2} with power density of 5.5 mW cm^{-2}. Further improvements of the catalyst layer composition and configuration should improve the cell performance and increase power output while maintaining H_2O_2 production at a reasonable and useable rate.

Chapter 7 Hydrogen Peroxide Production in a Solid Polymer Electrolyzer Cell with Organic and Inorganic Cathode Catalysts

7.1 Introduction

The previous two chapters discussed alternative methods of producing hydrogen peroxide through electrochemical oxygen reduction utilizing a solid polymer electrolyte (SPE) cell operating in fuel cell mode. The inorganic Co-C cathode electrocatalyst used for this method was tested under various conditions in order to maximize H_2O_2 production. A method of altering the cathode catalyst configuration was also studied in order to test the feasibility of producing power along with H_2O_2 production.

Whereas the previous two chapters discussed H_2O_2 production in fuel cell mode, H_2O_2 can also be produced in a SPE cell operating in electrolysis mode. In electrolysis mode operation, the same hardware with some modifications is used with the MEA made with the same catalysts. Principles of electrolysis mode operation were discussed in Section 1.5.2. Electrolytic H_2O_2 production has been thoroughly studied [8, 14, 16, 19, 21, 72-74, 76], with solid porous electrolytes as well as liquid electrolytes in both acidic and alkaline medium.

7.2 Experimental Procedure

Fuel cell hardware used for this section of the work was the same 49 cm^2 Tandem Research Cell used in the previous two sections, details of which are described in Section 4.1.4. However some modifications to the hardware, specifically the anode electrode, were performed in order to

accommodate the electrolysis experiments. These modifications were outlined in Section 4.1.2 and electrolysis mode operation conditions were outlined in section 4.4.

Two different cathode catalysts were tested for electrolytic H_2O_2 production, the inorganic Co-C composite catalyst and the organic anthraquinone-riboflavin on carbon (AQ-C) composite catalyst [28, 63]. Details on preparing the two catalysts can be found in Appendix A-1 (Co-C) and Appendix A-2 (AQ-C). Methods for preparing the anode and cathode electrodes as well as assembling the membrane electrode assemblies (the same between the two catalysts) can be found in Appendices A-3 to A-6. For the anode electrode, a Pt-Black catalyst from Johnson Matthey (Pt-STD) was used to prepare three different types of anodes. The first was a Pt-Black catalyst on Toray carbon paper support (identified as C-Pt) with a catalyst loading of 0.2 $mg_{Pt\text{-}black}$ cm^{-2} sprayed on TGP-H060 Toray carbon paper with no Teflon loading. The second was a Pt-Black catalyst on Ti-mesh support (identified as Ti-Pt) with a catalyst loading of 1 $mg_{Pt\text{-}black}$ cm^{-2} sprayed on 8 cm x 8 cm pre-cleaned titanium mesh. The third was a Pt-Black catalyst on a Nafion membrane (identified as a Half-CCM) with 0.4 $mg_{Pt\text{-}black}$ cm^{-2} sprayed on one side of a Nafion 112 membrane. The inorganic cathode catalyst was a 4 wt% Co-C composite catalyst and had a catalyst loading of 3.6 $mg_{Co\text{-}C}$ cm^{-2} on TGP-H060 Toray carbon paper with 10 wt% Teflon loading. The organic cathode catalyst was a 10 wt% RF-AQ-C composite catalyst and had a catalyst loading of 3.6 $mg_{AQ\text{-}C}$ cm^{-2} on TGP-H060 Toray carbon paper with 10 wt% teflon loading. The same catalyst loadings were chosen for better comparison between the inorganic and organic catalysts.

7.3 Results and Discussion

While several operating variables were tested in fuel cell mode operation to study their effect on H_2O_2 generation with the inorganic Co-C composite catalyst, only two operating variables were studied in electrolysis mode operation (Table 4-5). The two operating variables that were not studied in the electrolysis mode were the catalyst loading and cathode GDL Teflon content. As these two variables were only associated with the cathode side, they had identical properties compared to those tested in the fuel cell mode operation. These two cathode variables should provide the same results whether in electrolysis or fuel cell mode operation.

Both the inorganic Co-C and the organic AQ-C composite catalysts were studied in electrolysis mode operation for the cathode. For the two variables investigated, the Pt-Black on Toray carbon paper (C-Pt) was used as the anode in order to provide a more suitable comparison to the performance results in fuel cell mode operation.

7.3.1 Effect of Temperature on H_2O_2 Production

The effect of cell operating temperature for the Co-C catalyst is shown in Figure 7.1, and for the AQ-C catalyst is shown in Figure 7.2.

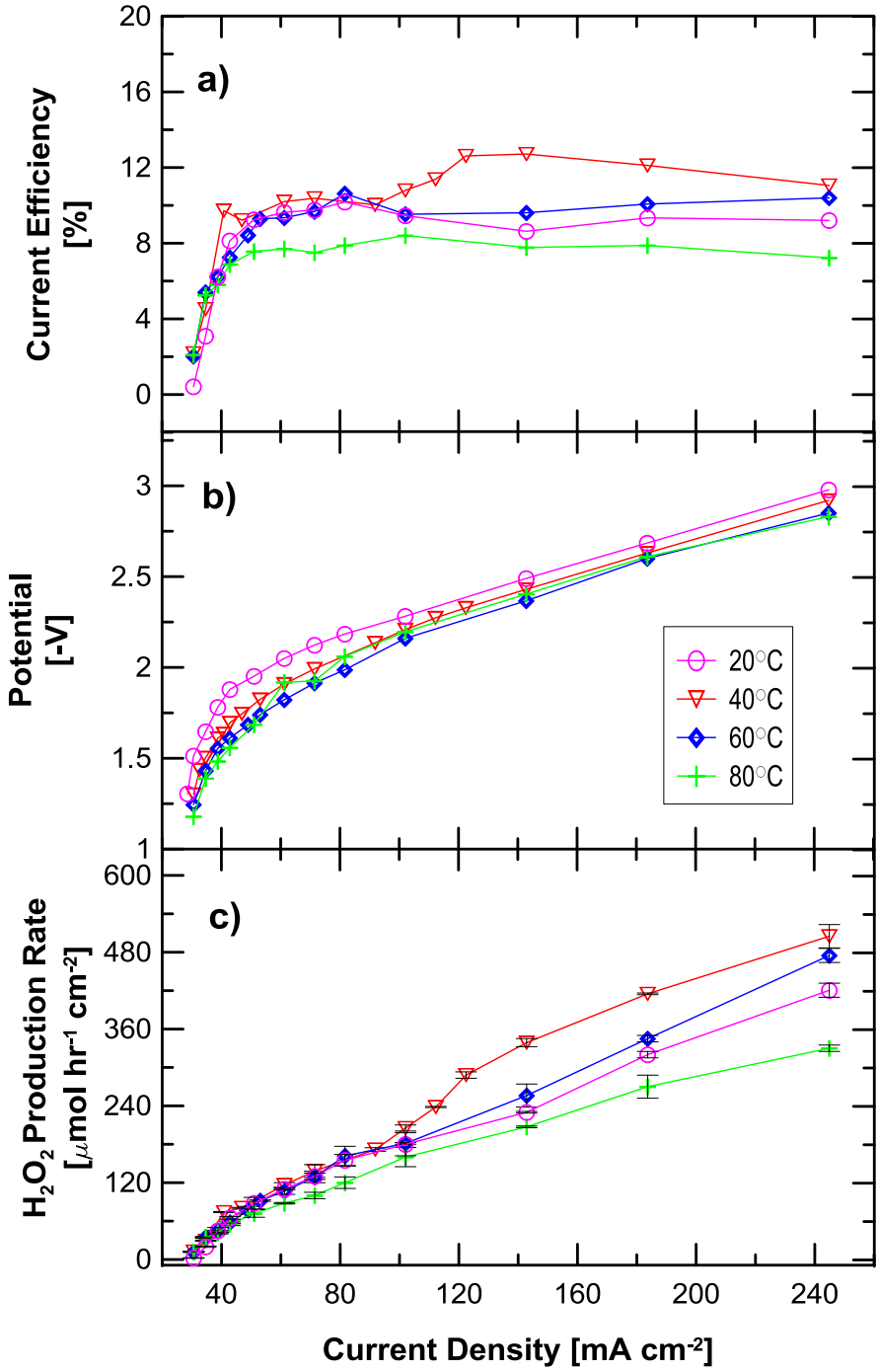

Figure 7.1 Effect of cell operating temperature with C-Pt||Co-C MEA in electrolysis mode operation on: a) the current efficiency for H_2O_2 production, b) fuel cell polarization performance, and c) H_2O_2 production rate. Anode conditions: **15 mL min^{-1}** DI water flow, anode catalyst loading 0.2 $mg_{Pt\text{-}black}$ cm^{-2} on TGP-H060 0 wt% WP Toray paper. Cathode conditions: O_2 flow rate 1000 mL min^{-1} O_2, pressure 150 kPa(g), water flow rate **15 mL min^{-1}**, Co-C catalyst loading 3.6 $mg_{Co\text{-}C}$ cm^{-2} on TGP-H060 10 wt% WP Toray paper.

As temperature increases, the increased reaction kinetics result in an increase in electrolysis cell performance; i.e., the cell overpotential decreases, leading to a lower power requirement at a given operating current density. As Figure 7.1b showed, at a temperature of 20°C, the C-Pt||Co-C MEA had the lowest performance, while the higher temperatures had almost identical performances throughout the entire polarization current density range. When it came to H_2O_2 production, the electrolysis mode operation of the C-Pt||Co-C MEA followed a similar trend to the same MEA when operated in fuel cell mode, at lower current densities. At current densities below 80 mA cm^{-2}, the H_2O_2 production rate was almost identical between all temperatures tested. As the current densities increased, a more distinct and different trend began to emerge (Figure 7.1c). As the temperature increased from 20°C to 40°C, there is a noticeable increase in H_2O_2 production, as well as the corresponding increase in current efficiency (Figure 7.1a); however, as the temperature increased to 60°C and 80°C, both the H_2O_2 production and the current efficiency were much less compared to those at 40°C. This clearly indicates that at elevated operating temperatures, the H_2O_2 decomposition rate increases more significantly with increasing current densities.

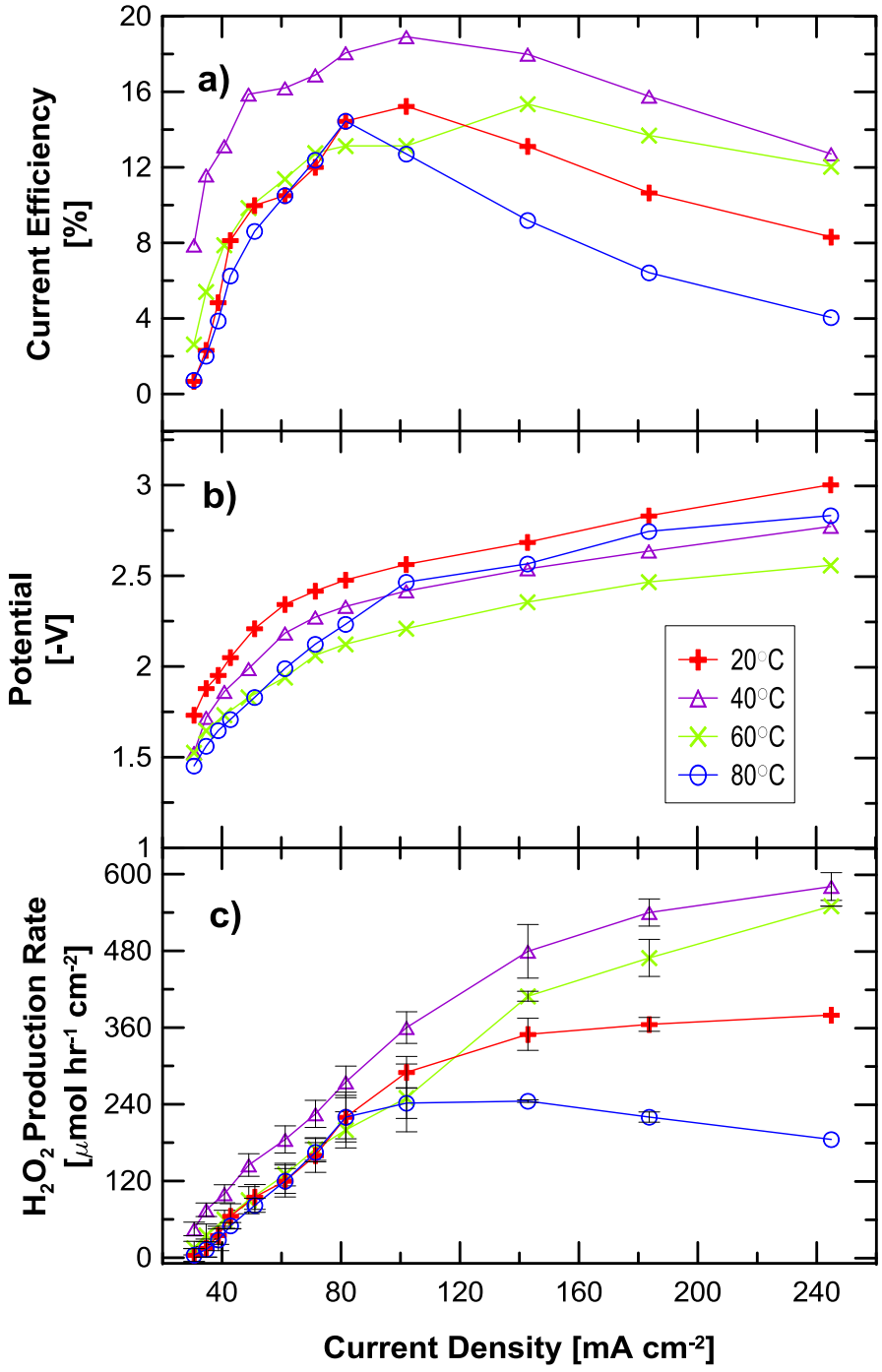

Figure 7.2 Effect of cell operating temperature with C-Pt||AQ-C MEA in electrolysis mode operation on: a) the current efficiency for H_2O_2 production, b) fuel cell polarization performance, and c) H_2O_2 production rate. Anode conditions: **15 mL min^{-1}** DI water flow, anode catalyst loading 0.2 mg$_{Pt\text{-}black}$ cm^{-2} on TGP-H060 (0 wt% WP) Toray paper. Cathode conditions: O_2 flow rate 1000 mL min^{-1} O_2, pressure 150 kPa(g), water flow rate **15 mL min^{-1}**, AQ-C catalyst loading 3.6 mg$_{AQ\text{-}C}$ cm^{-2} on TGP-H060 (10 wt% WP) Toray paper.

Testing of the C-Pt||AQ-C MEA (Figure 7.2) with the same operating parameters listed in Table 4-5 showed a similar trend when compared to the C-Pt||Co-C MEA. At lower current densities below 80 mA cm^{-2}, the AQ-C cathode performed similarly to the inorganic Co-C catalyst, in terms of production rates and current efficiencies. One exception is the 40°C, where the H_2O_2 production rate and the current efficiency for the AQ-C catalyst were much higher throughout the entire operating current density range. As the current density increased beyond 80 mA cm^{-2}, the current efficiencies for all temperatures began to decrease (Figure 7.2a). Typically as current density increases, overpotential increases, which leads to an increase in heat generated and lost to the surrounding environment. This excess heat helped to facilitate H_2O_2 decomposition, leading to lower current efficiencies. Increase in cell temperature also has a negative effect on H_2O_2 production and current efficiency. This is evident from experiments at higher temperatures and higher current densities (Figure 7.2 a and c), note the 80°C run at current densities above 140 mA cm^{-2}, had much lower current efficiencies and H_2O_2 production rates.

By comparing the results from Figures 7.1 and 7.2, the C-Pt||AQ-C MEA performs better than the C-Pt||Co-C MEA, up to its peak value at about 110 mA cm^{-2}. Overall the AQ-C catalyst had better maximum current efficiencies at all temperatures. For H_2O_2 production at 40°C, which is the optimal operating temperature for electrolysis mode operation, the AQ-C catalyst had a maximum H_2O_2 production rate of 580 μmol hr^{-1} cm^{-2} while the Co-C catalyst had a maximum H_2O_2 production rate of 505 μmol hr^{-1} cm^{-2}.

7.3.2 Effect of Cathode Carrier Water Flow Rate on H_2O_2 Production

The two different cathode catalysts were further tested at lower cathode carrier flow rates for temperature effects on H_2O_2 production. The water flow rate was 5 mL min^{-1} and the temperatures tested were 40°C and 60°C. Results of the test are shown in Figure 7.3. The cell performance of both the Co-C and the AQ-C catalysts are very close to their respective cell performances at a 15 mL min^{-1} water flow rate and at 40°C and 60°C in Figures 7.1b and 7.2b, respectively. At the same time both the current efficiencies and the H_2O_2 production rates of both catalyst followed a similar trend to their counterpart at the higher water flow rate. The current efficiency for the Co-C catalyst became very stable as the current densities increased, while the current efficiencies for the AQ-C catalyst decreased at higher current densities. As for H_2O_2 production, both the AQ-C and the Co-C catalysts had lower production rates at the lower water flow rate compared to their counterpart at the higher water flow rate. This is expected as the lower water flow rate results in a longer residence time in the cell compartment, causing higher H_2O_2 decomposition, resulting in lower overall H_2O_2 production.

The production rates for both the Co-C and the AQ-C catalyst showed the same correlation to carrier water flow rate for both the electrolysis mode and fuel cell mode operation. Figure 7.4 shows this correlation for the electrolysis mode operation. The Co-C catalyst showed the same trend as in fuel cell mode, both the production rate and the current efficiencies increased as the carrier water flow rate increased. While this same trend also occurred for the AQ-C catalyst, the difference is much smaller when compared to the Co-C catalyst.

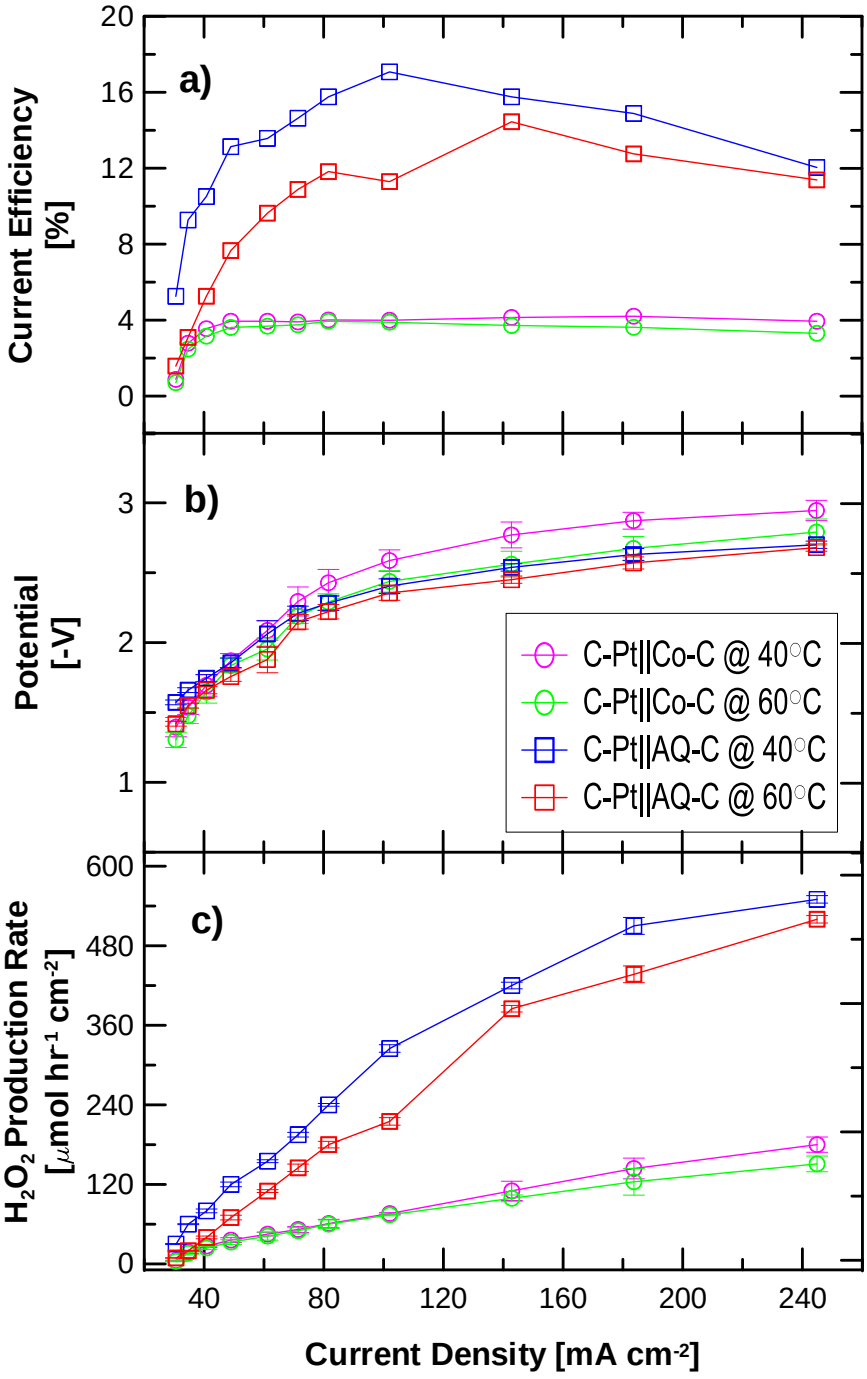

Figure 7.3 Comparison between C-Pt||Co-C MEA and C-Pt||AQ-C MEA in electrolysis mode operation operated at T=40°C and T=60°C, with a cathode carrier water flow rate of **5 mL min^{-1}**. Anode conditions: **15 mL min^{-1}** DI water flow, anode catalyst loading 0.2 $mg_{Pt\text{-}black}$ cm^{-2} on TGP-H060 (0 wt% WP) Toray paper. Cathode conditions: O_2 flow rate 1000 mL min^{-1} O_2, pressure 150 kPa(g), AQ-C catalyst loading 3.6 $mg_{AQ\text{-}C}$ cm^{-2} on TGP-H060 (10 wt% WP) Toray paper; Co-C catalyst loading 3.6 $mg_{Co\text{-}C}$ cm^{-2} on TGP-H060 (10 wt% WP) Toray paper.

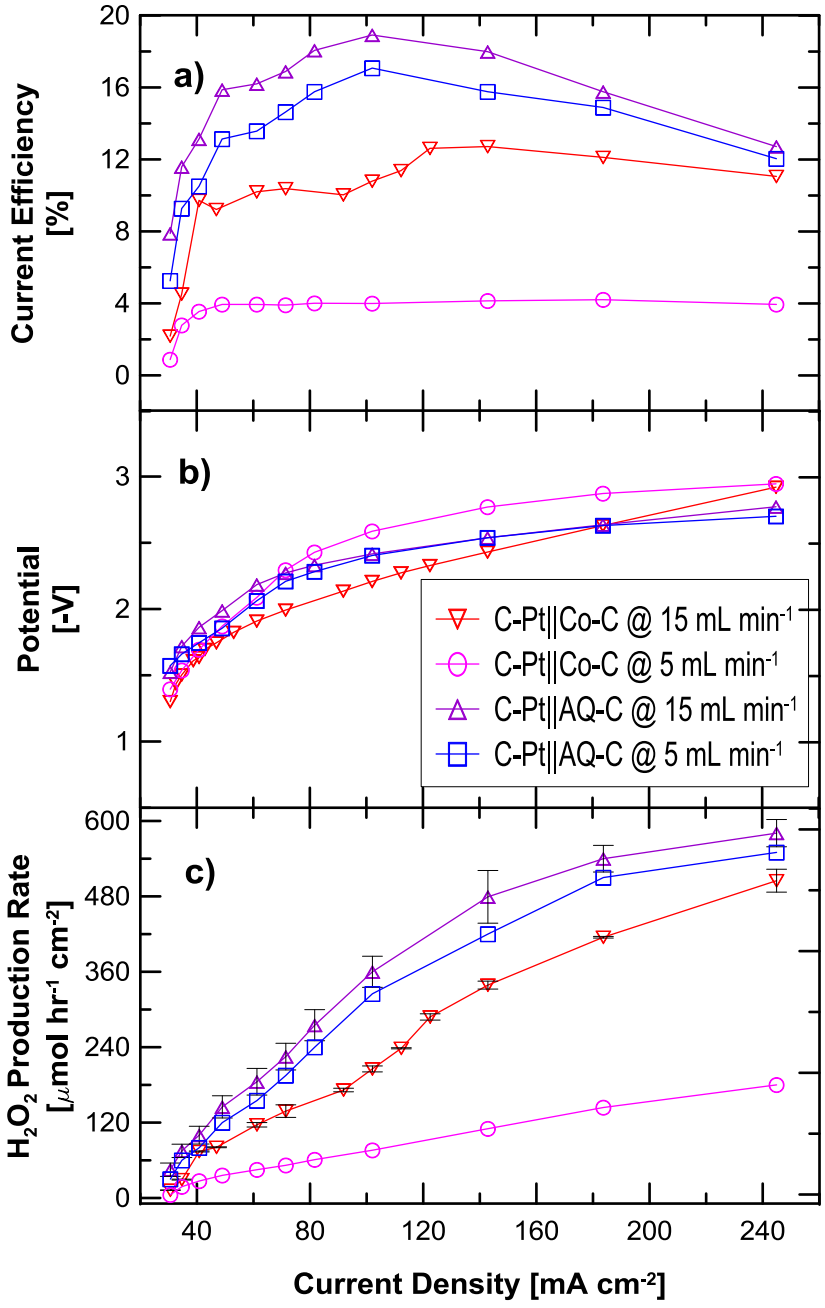

Figure 7.4 Comparison between C-Pt||Co-C MEA and C-Pt||AQ-C MEA in electrolysis mode operation operated at T=40°C, with a cathode carrier water flow rate of **5 mL min^{-1}** and **15 mL min^{-1}** Anode conditions: 15 mL min^{-1} DI water flow, anode catalyst loading 0.2 mg$_{Pt\text{-}black}$ cm^{-2} on TGP-H060 (0 wt% WP) Toray paper. Cathode conditions: O_2 flow rate 1000 mL min^{-1} O_2, pressure 150 kPa(g), AQ-C catalyst loading 3.6 mg$_{AQ\text{-}C}$ cm^{-2} on TGP-H060 (10 wt% WP) Toray paper; Co-C catalyst loading 3.6 mg$_{Co\text{-}C}$ cm^{-2} on TGP-H060 (10 wt% WP) Toray paper.

7.3.3 Anode Backing Layer Support

So far all experiments utilized the Toray TGP-H060 (0 wt% WP) carbon paper as the anode back substrate support. In the electrolysis mode operation, the DI water stream that was pumped through the anode caused an irreversible physical damage to the carbon fibre paper support (Figure 7.4) during electrolysis. To overcome this, an alternative, corrosion-resistant anode support was required. This support needed to have similar porous transport and conductivity properties to those of the carbon paper back support but be corrosion-resistant. Two different anode catalyst supports were considered for the remainder of the electrolysis mode operation experiments: a 99.99% commercial grade purity titanium mesh with Pt catalyst sprayed on one side of the mesh (1 mg cm^{-2} Pt-black) and a half-CCM with Pt catalyst sprayed on one side of the Nafion membrane (0.4 mg cm^{-2} Pt-black), with the CCM side laying next to a clean Ti mesh. The properties of these two supports are described in Section 4.1.2. The Ti-Pt anode was tested with both the Co-C and the AQ-C cathode catalysts at two different temperatures, 40°C and 60°C (Figure 7.5).

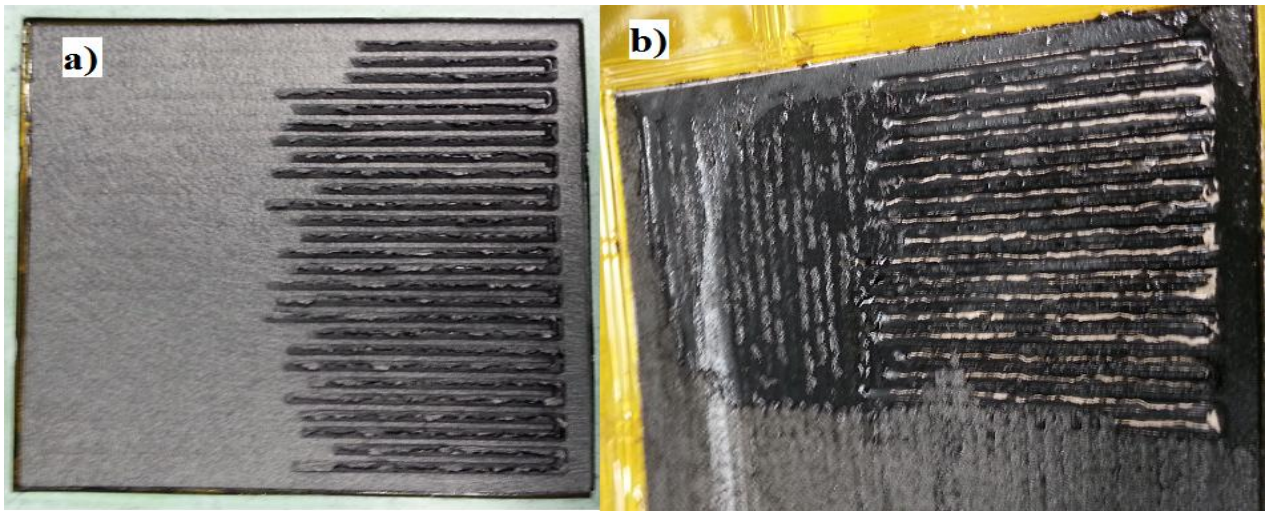

Figure 7.4 Physical damage to AQ-MEA with carbon back support on both sides after polarization tests in electrolysis mode operation. a) cathode, b) anode.

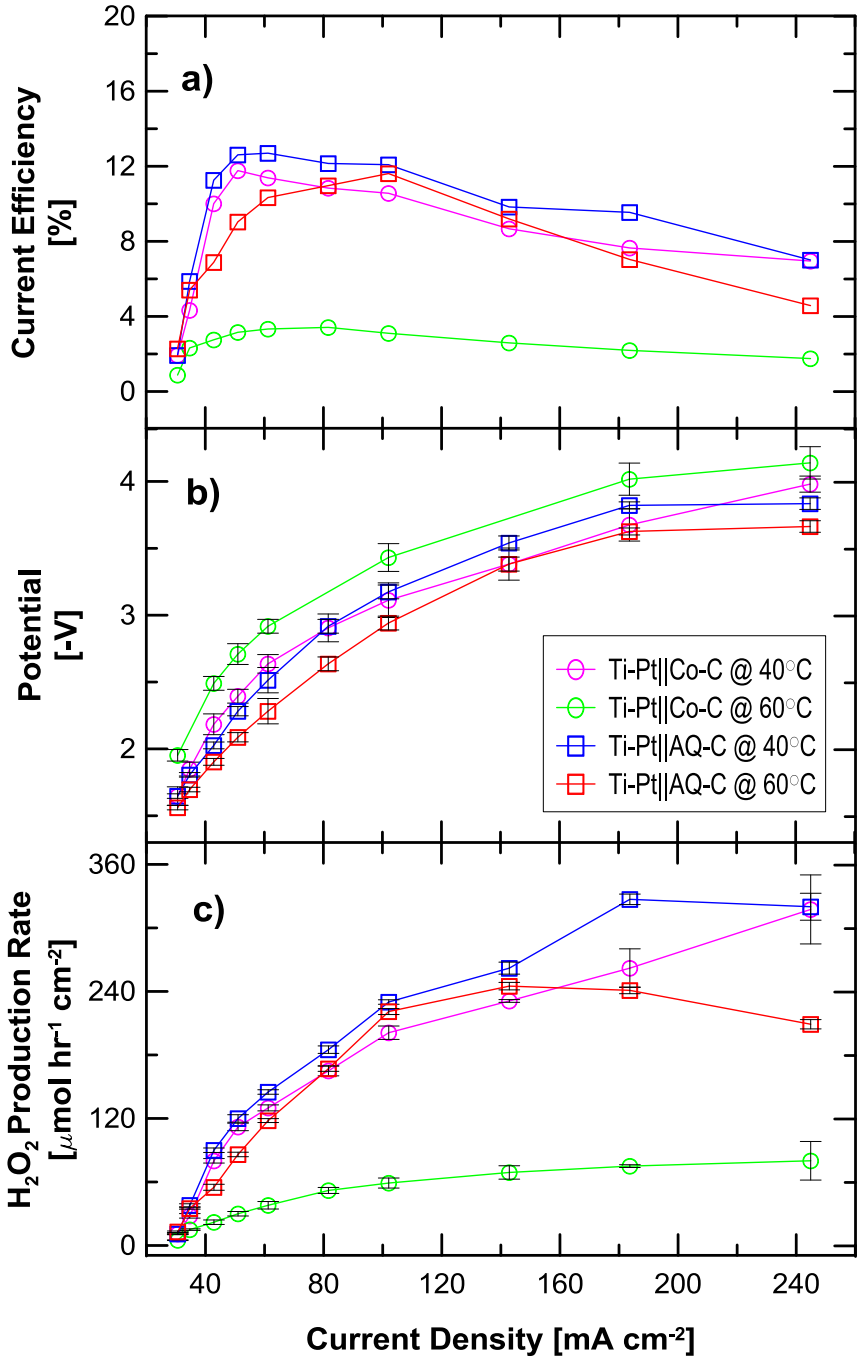

Figure 7.5 Comparison between Ti-Pt||Co-C MEA and Ti-Pt||AQ-C MEA in electrolysis mode operation operated at T=40C and T=60C, with a cathode carrier water flow rate of **15 mL min^{-1}**. Anode conditions: **15 mL min^{-1}** DI water flow, anode catalyst loading 1.0 mg$_{Pt\text{-}black}$ cm^{-2} on 99.99% Commercial grade purity Titanium mesh. Cathode conditions: O_2 flow rate 1000 mL min^{-1} O_2, pressure 150 kPa(g), AQ-C catalyst loading 3.6 mg$_{AQ\text{-}C}$ cm^{-2} on TGP-H060 10 wt% WP Toray paper; Co-C catalyst loading 3.6 mg$_{Co\text{-}C}$ cm^{-2} on TGP-H060 10 wt% WP Toray paper.

Figure 7.5 shows that with the titanium mesh as an anode back support, both the Co-C and the AQ-C cathode catalysts had similar performances which was also observed with the carbon paper anode back support. A major difference for the two different supports was that the V-I curves for both the Co-C and the AQ-C catalysts (Figure 7.5b) showed much higher potential compared to the respective V-I curves in Figure 7.3b, which used the carbon paper anode back support. Even though the Ti-Pt anode had higher Pt catalyst loading (1 $mg_{Pt\text{-}black}$ cm^{-2}) compared to the C-Pt anode used in Figure 7.3 (0.2 $mg_{Pt\text{-}black}$ cm^{-2}), the larger opening (27% open area) of the titanium mesh meant that only a small percentage of the Pt catalyst layer was in contact with the membrane, thus resulting in a lower current efficiency (Figure 7.5a), leading to a lower H_2O_2 production rate on the cathode side (Figure 7.5c).

The increased overpotential as a result of limited contact between the catalyst layer and membrane meant that an alternative anode with better catalyst utilization was needed. A corrosion resistant back support such as the Titanium mesh is important for the high potentials used. An alternative chosen for further study was the half-catalyst coated membrane (half-CCM) with catalyst coated only on one side of the treated Nafion membrane which should increase catalyst utilization. The anode consisted of a titanium mesh as back support with a half-CCM having 0.4 $mg_{Pt\text{-}black}$ cm^{-2} on the anode side of the membrane. The cathode remained the same, Pt coated carbon fiber paper. Due to time restrictions, this anode was only tested with the AQ-C cathode catalyst at 40°C (Figure 7.6).

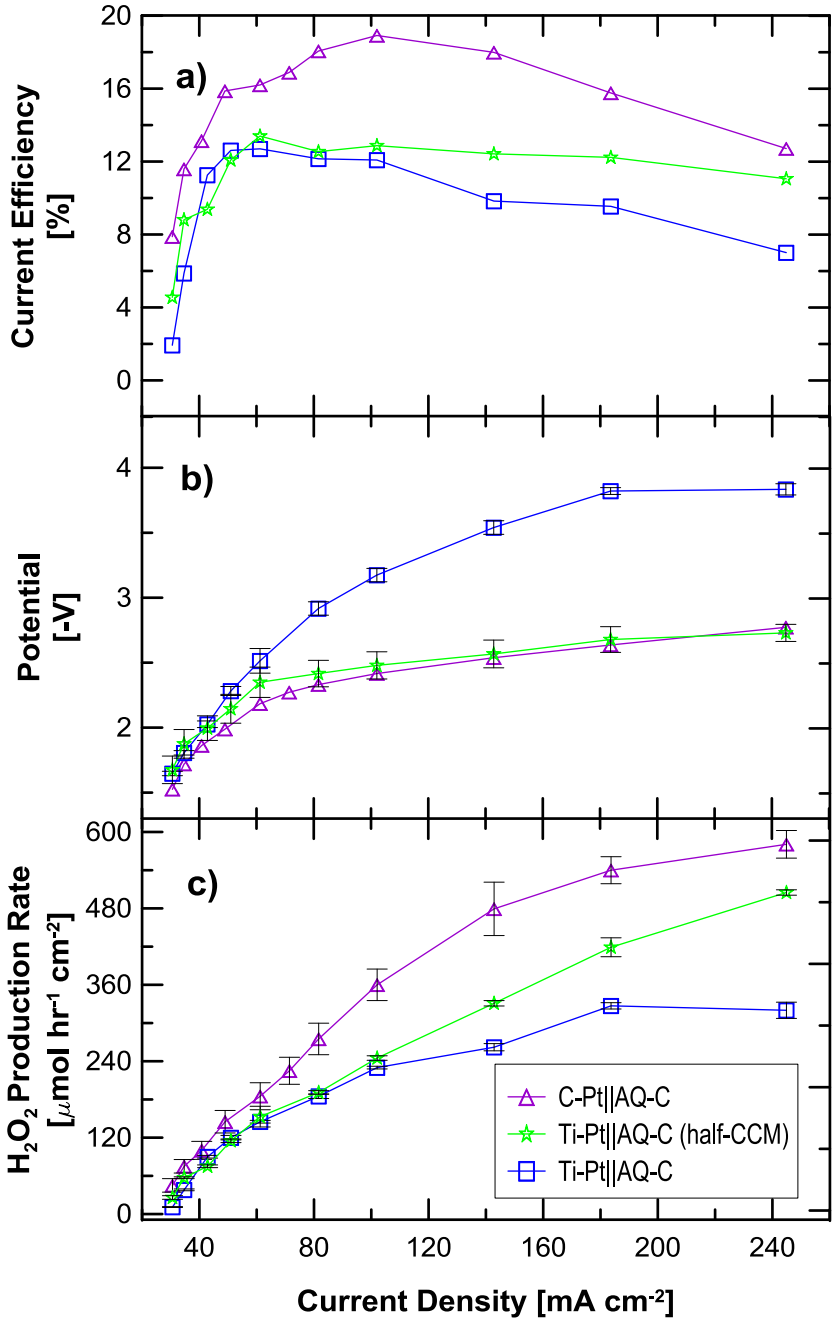

Figure 7.6 Comparison between Ti-Pt||AQ-C with half-CCM MEA, Ti-Pt||AQ-C MEA and C-Pt||AQ-C MEA in electrolysis mode operation operated at T=40°C, with a cathode carrier water flow rate of **15 mL min^{-1}**. Anode conditions: **15 mL min^{-1}** DI water flow, anode catalyst loading 0.4 $mg_{Pt\text{-}black}$ cm^{-2} on pre-treated Nafion 112 membrane, with 99.99% Commercial grade purity titanium mesh as back support. Cathode conditions: O_2 flow rate 1000 mL min^{-1} O_2, pressure 150 kPa(g), AQ-C catalyst loading 3.6 $mg_{AQ\text{-}C}$ cm^{-2} on TGP-H060 (10 wt% WP) Toray paper.

The V-I performance of the half-CCM MEA showed that it is similar to that of the AQ-C MEA with the carbon supported Pt anode. As a result, the half-CCM MEA had better current efficiency vs. the AQ-C MEA with the Ti-Pt anode (Figure 7.6a), as well as better H_2O_2 production (Figure 7.6c). However, the half-CCM AQ-C MEA still produced less H_2O_2 when compared to the AQ-C MEA with the carbon back support anode. The reason for this decreased performance can be attributed to the preparation of the MEAs. The AQ-C MEA with the carbon paper back support was prepared with the hot press method for MEA preparation (Appendix A-6), while the AQ-C MEA with half CCM was not prepared with the hot press method. The hot press method was not used here mainly due to the half CCM. The membrane in the half-CCM were already dry, the high pressure and temperature of the hot press would have caused the membrane to deform and split apart, destroying the membrane in the process. The AQ-C MEA with the half-CCM did have lower current efficiencies and lower H_2O_2 production, when compared to the C-Pt||AQ-C MEA; however its current efficiency at higher current densities were much more stable than the C-Pt||AQ-C MEA, and did not exhibit the sharp decrease trend that the C-Pt||AQ-C MEA had.

7.3.4 Continuous Recycle Operation Mode

As is the case with the fuel cell mode operation testing, the ability to produce H_2O_2 at a constant rate over a long period of time is crucial for applying this technology in real world operations. Both the Co-C MEA and the AQ-C MEA were tested in a long term continuous electrolysis mode using two-phase recycle operation to evaluate cell performance and H_2O_2 production. In the same manner as in fuel cell mode operation experiments, the electrolysis mode operation

with recycling was started with the cell operating in a single pass mode for 25 minutes with the cathode carrier water flow at 15 mL min^{-1} at a current density of 61.2 mA cm^{-2}. Once sufficient product solution was accumulated in the collection reservoir in order to allow for subsequent water sampling during the recycle operation, the recycle pump was turned on, with the recycle cathode carrier flow rate fixed at 15 mL min^{-1}. The anode water was not recycled during the recycle test and was operated in a single pass mode with a fixed flow rate of 15 mL min^{-1} throughout the test. This was chosen in order to minimize any loose particles in the anode recycle stream from affecting the water electrolysis reaction if the DI water was recycled back to the anode water reservoir.

All recycle operations were run for 72 hours. The Ti mesh with Pt catalyst anode was tested with both the Co-C and the AQ-C cathode electrodes (Figure 7.7). By comparison, the Co-C MEA with the Ti-Pt anode had similar H_2O_2 total production to the Co-C MEA with C-Pt anode operated in fuel cell mode recycle test (Figure 5.9). At the end of the 72 hour run, the Co-C MEA with Ti-Pt anode had accumulated 1300 ppm (0.13 wt %) H_2O_2, while the AQ-C MEA with Ti-Pt anode had accumulated about 3000 ppm (0.3 wt %) H_2O_2. As well, the H_2O_2 production rate also decreased during the 72 hour recycle test run. The H_2O_2 production trend for the Co-C catalyst in electrolysis mode operation with recycling was almost identical to that of fuel cell mode operation. The hourly H_2O_2 production rate were the highest in the first 24 hours (from 25 μmol hr^{-1} cm^{-2} to 3 μmol hr^{-1} cm^{-2} after 24 hours), then the production rate leveled off and remained steady until the end of the recycle test run.

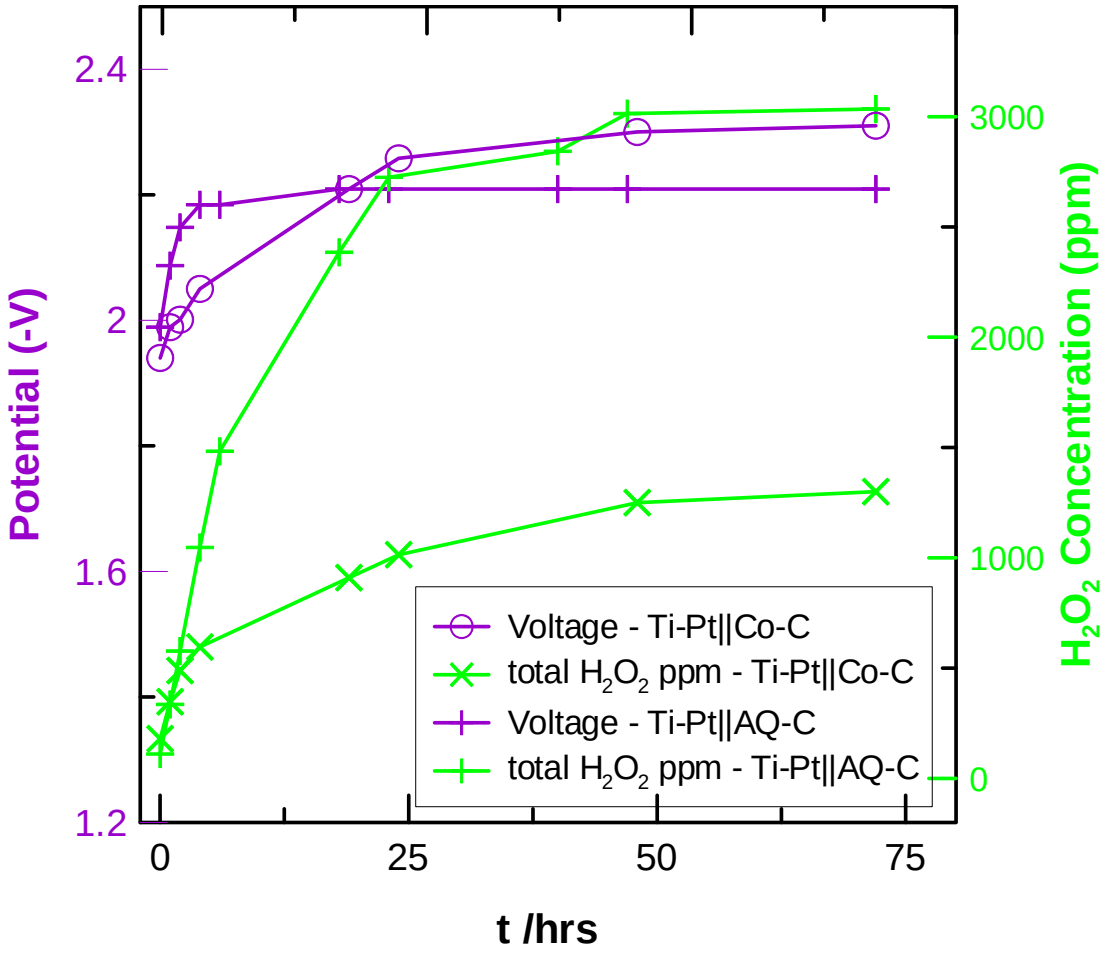

Figure 7.7 Long term (72 hours) continuous recycle operation testing of the H_2O_2 producing Co-C and AQ-C cathode catalyst in electrolysis mode with a Ti-Pt anode. Cell conditions: current density: 61.2 mA cm^{-2}. Cell temperature: 40 ℃. Anode conditions: **15 mL min^{-1}** DI water flow, anode catalyst loading 1.0 $mg_{Pt\text{-}black}$ cm^{-2} on 99.99% Commercial grade purity titanium mesh. Cathode conditions: O_2 flow rate 1000 mL min^{-1} O_2, pressure 150 kPa(g), water flow rate: **15 mL min^{-1}**, AQ-C catalyst loading 3.6 $mg_{AQ\text{-}C}$ cm^{-2} on TGP-H060 (10 wt% WP) Toray paper. Co-C catalyst loading 3.6 $mg_{Co\text{-}C}$ cm^{-2} on TGP-H060 (10 wt% WP) Toray paper.

All the recycle tests conducted in the electrolysis mode had a cell temperature of 40°C, which is lower than the recycle tests conducted in the fuel cell mode, at 60°C. Yet the H_2O_2 production rates were similar between the electrolysis mode recycle test and the fuel cell mode recycle test, throughout the 72 hour recycle run. The lower temperature was chosen for the electrolysis mode operation tests as polarization results showed higher H_2O_2 production at 40°C versus 60°C.

The recycle test for the AQ-C MEA with Ti-Pt anode showed a better overall performance improvement over the Co-C MEA with Ti-Pt anode. The AQ-C MEA also showed a similar trend compared to the Co-C MEA in terms of decrease in H_2O_2 production rate with time. The AQ-C MEA had the highest increase in H_2O_2 production rate in the first 6 hours of operation (hourly H_2O_2 production of over 30 μmol hr^{-1} cm^{-2}) and had accumulated almost 1500 ppm of H_2O_2. The production rate began to stabilize for the next 18 hours, dropping to about 10 μmol hr^{-1} cm^{-2}, before finally settling to about 2 μmol hr^{-1} cm^{-2} for the last 48 hours. The total accumulated concentration was over 3000 ppm at the end of the 72 hour recycle run. The H_2O_2 production rate trend described here confirms the findings described previously in Section 5.3.4 on the effect of thermal-chemical decomposition of H_2O_2 in the recycle stream.

The AQ-C MEA with half-CCM was also tested in the 72 hour recycle test, and compared to the results from the AQ-C MEA with Ti-Pt anode (Figure 7.8). The AQ-C MEA with half-CCM had a much lower cell potential, indicating better contact and catalyst utilization between the anode catalyst layer and the membrane.

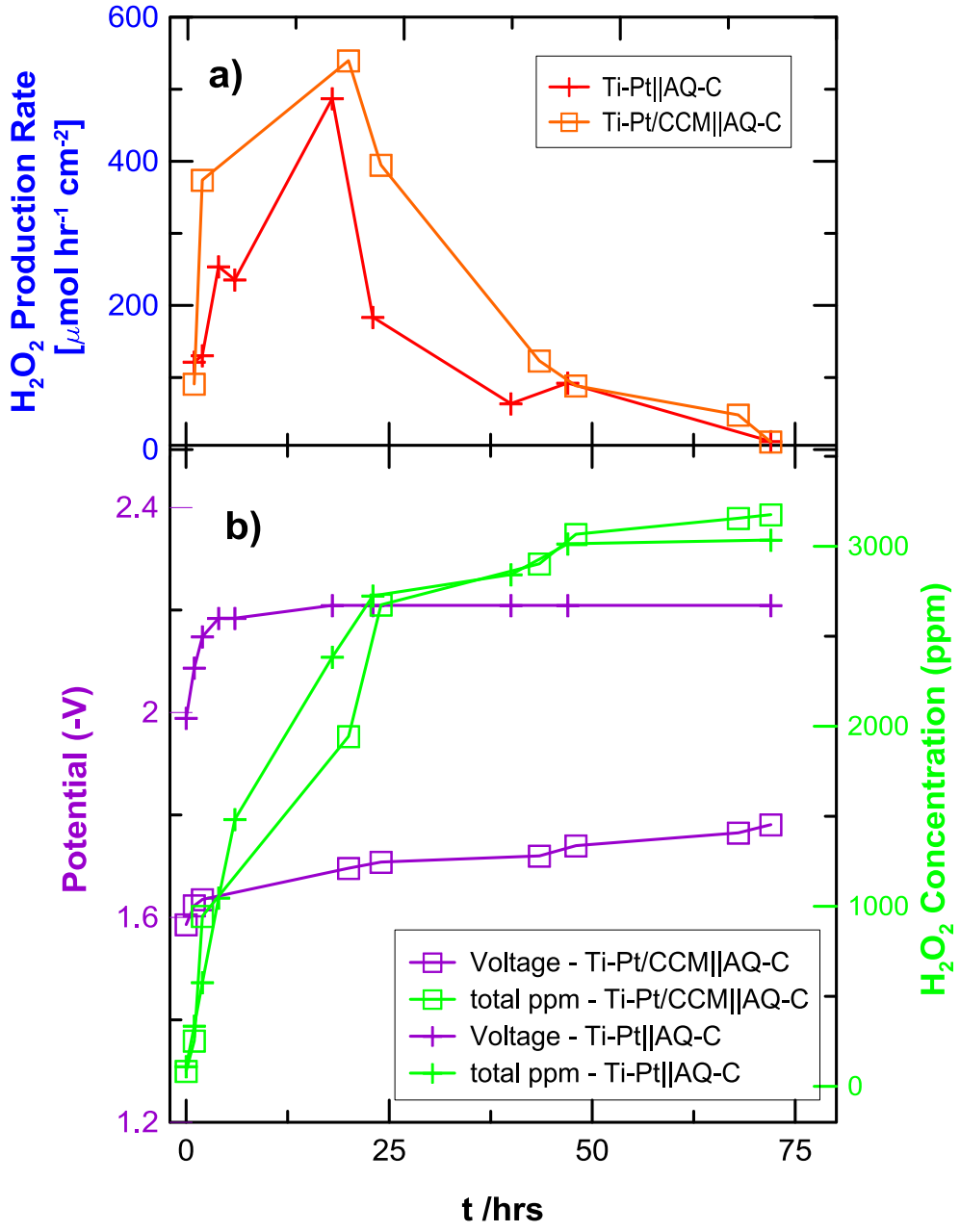

Figure 7.8 Long term (72 hours) continuous recycle operation testing of the H_2O_2 producing AQ-C cathode catalyst in electrolysis mode with Ti-Pt anode and half-CCM. a) H_2O_2 production rate, b) voltage performance with time, and total accumulated H_2O_2 concentration. Cell conditions: current density: 61.2 mA cm^{-2}. Cell temperature: 40 ℃. Anode conditions: **15 mL min^{-1}** DI water flow, Ti-Pt anode: 1.0 $mg_{Pt\text{-}black}$ cm^{-2} on 99.99% Commercial grade purity titanium mesh; half-CCM: 0.4 $mg_{Pt\text{-}black}$ cm^{-2} on pre-treated Nafion 112 membrane, with 99.99% Commercial grade purity titanium mesh as back support.. Cathode conditions: O_2 flow rate 1000 mL min^{-1} O_2, pressure 150 kPa(g), water flow rate: **15 mL min^{-1}**, AQ-C catalyst loading 3.6 $mg_{AQ\text{-}C}$ cm^{-2} on TGP-H060 (10 wt% WP) Toray paper.

Most of the V-I performance gain for the half-CCM AQ-C MEA came as a result of better catalyst utilization from the half-CCM anode. A graphical representation of this performance gain is shown in Figure 7.8. The MEA with the Ti-Pt anode had the catalyst layer sprayed on the wires of the Ti-mesh (Figure 7.9a), which had much smaller area of contact with the membrane when compared with the catalyst layer in the half-CCM (Figure 7.9b). Since the cathode remained the same for both the half-CCM AQ-C MEA and the Ti-Pt||AQ-C MEA, the total accumulated H_2O_2 concentration for both MEAs were similar after the 72 hour recycle test, at about 3000 ppm (0.3 wt%). Further breakdown of the trends for the recycle test showed that the AQ-C MEA with the Ti-Pt anode had better H_2O_2 production rate in the first 25 hours of the recycle test. This initial difference is likely the result of the method used to assemble each of the two MEAs. The AQ-C MEA with the Ti-Pt anode utilized the hot press method, while the AQ-C MEA with the half-CCM did not. This implied that the AQ-C MEA with the Ti-Pt anode had better bonding on cathode side due to heat bonding from the hot press method during the initial stages of the recycle test. With time the AQ-C MEA with the half-CCM probably improves the cathode bonding due to cell compression, thus increasing the H_2O_2 production rate.

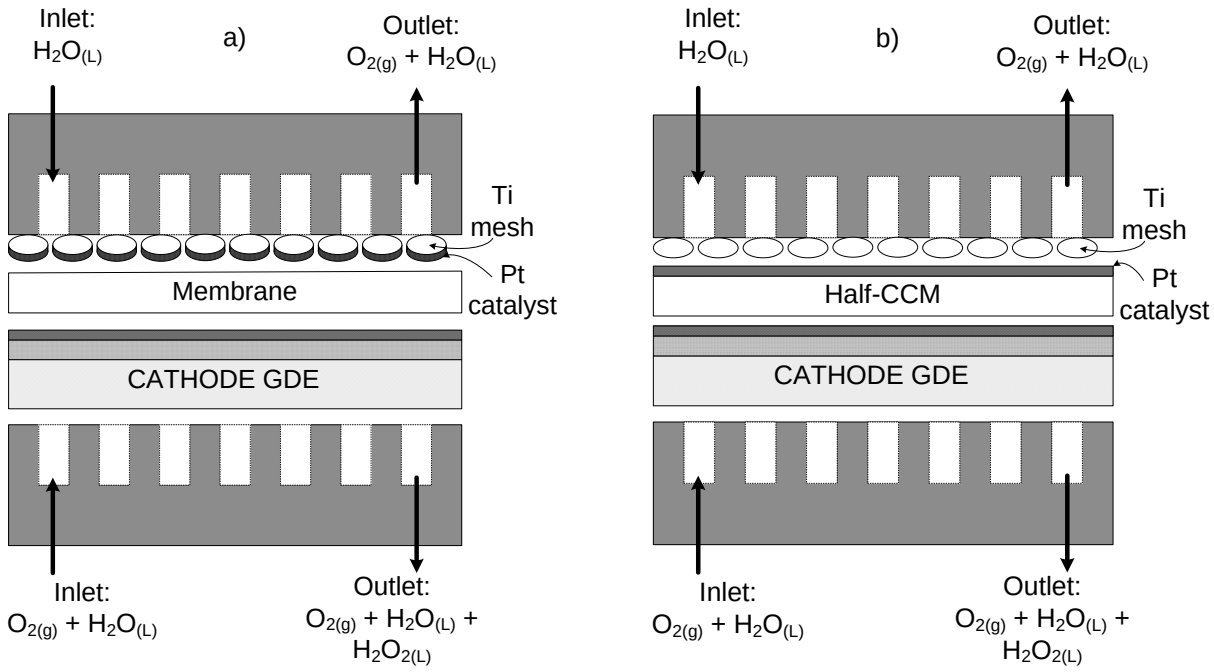

Figure 7.9 Comparison of MEA configuration with differently prepared anodes , a) MEA with Pt catalyst layer sprayed directly on Ti-mesh, and b) MEA with Pt catalyst layer sprayed on membrane (half-CCM).

7.4 Effect of Temperature on Degradation of Product H_2O_2

Just as in fuel cell mode operation, in electrolysis mode operation changes in temperature can have a significant effect on the product H_2O_2 concentration. Therefore, a similar temperature experiment to the one carried out in fuel cell mode operation was also conducted for electrolysis mode operation. It was determined previously in this chapter that the optimum operating temperature for maximum H_2O_2 production was 40°C. The peroxide stability test conducted here also tested the stability and lifetime of the product H_2O_2 exposed to the cell components at three different temperatures. The same external water collection system with the condenser unit to cool the product liquid stream is used here as well.

Similar to the tests conducted in fuel cell mode operation, two sets of recycle tests were conducted. The first set were done with no load applied to the SPE cell, while maintaining the cell pressure at 150 kPa as well as gas feed to both the anode and the cathode, and varying the cell temperature between 40 and 80°C (Figure 7.10). The second set of recycle tests were done with no load applied, no gas feed to both electrodes, only maintaining the cell pressure at 150 kPa, while varying the cell temperature between 40 and 80°C (Figure 7.11).

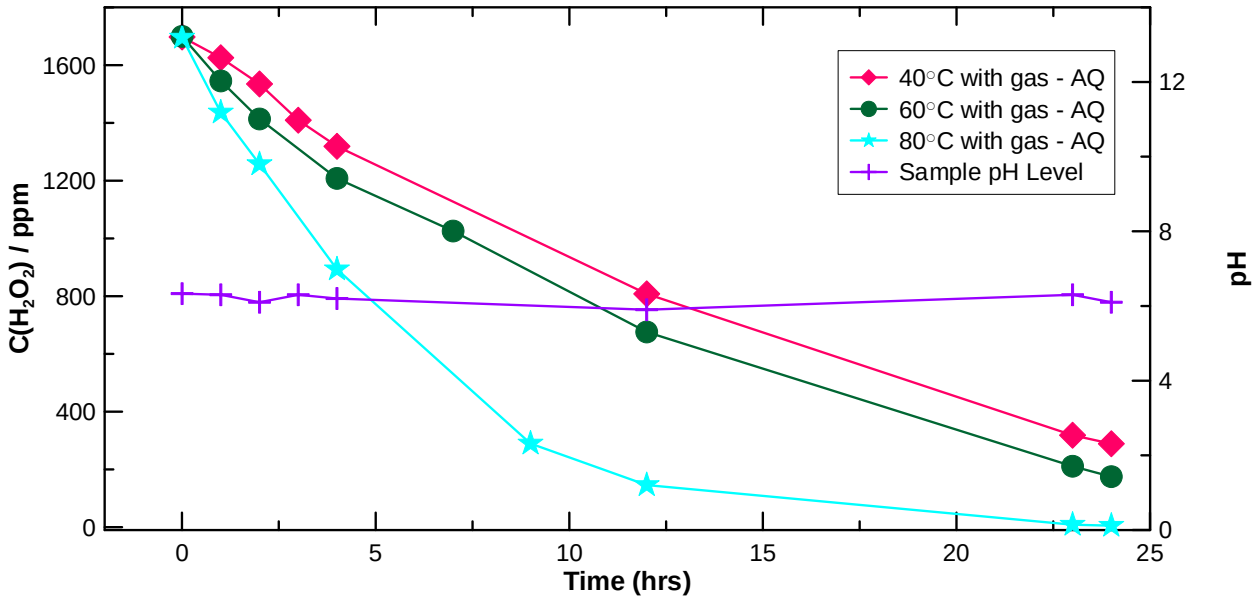

Figure 7.10 Longer-term H_2O_2 stability in the electrolysis mode set-up without load as a function of temperature and gas flows with continuous recycle of the cathode water carrier flow. Anode conditions: **15 mL min^{-1}** DI water flow, Ti-Pt anode: 1.0 mg$_{Pt\text{-}black}$ cm^{-2} on 99.99% Commercial grade purity titanium mesh; half-CCM: 0.4 mg$_{Pt\text{-}black}$ cm^{-2} on pre-treated Nafion 112 membrane, with 99.99% Commercial grade purity titanium mesh as back support.. Cathode conditions: O_2 flow rate 1000 mL min^{-1} O_2, pressure 150 kPa(g), water flow rate: **15 mL min^{-1}**, AQ-C catalyst loading 3.6 mg$_{AQ\text{-}C}$ cm^{-2} on TGP-H060 (10 wt% WP) Toray paper.

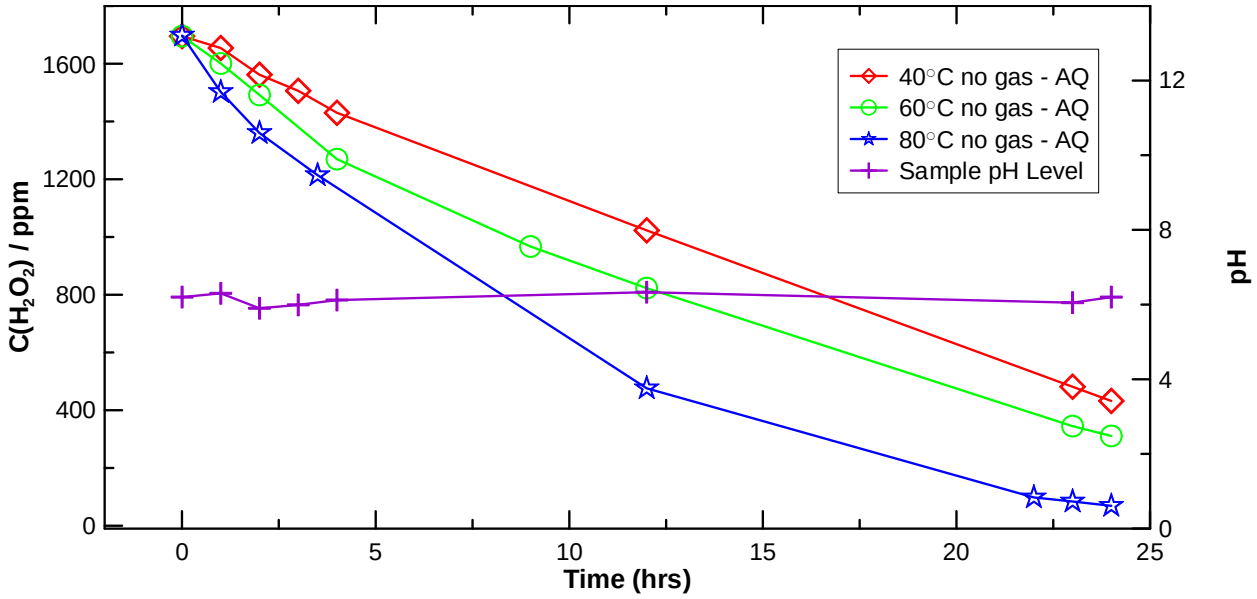

Figure 7.11 Longer-term H_2O_2 stability in the electrolysis mode set-up without load and gas flow as a function of temperature with continuous recycle of the cathode water carrier flow. Anode conditions: **15 mL min^{-1}** DI water flow, Ti-Pt anode: 1.0 $mg_{Pt\text{-}black}$ cm^{-2} on 99.99% Commercial grade purity titanium mesh; half-CCM: 0.4 $mg_{Pt\text{-}black}$ cm^{-2} on pre-treated Nafion 112 membrane, with 99.99% Commercial grade purity titanium mesh as back support.. Cathode conditions: pressure 150 kPa(g), water flow rate: **15 mL min^{-1}**, AQ-C catalyst loading 3.6 $mg_{AQ\text{-}C}$ cm^{-2} on TGP-H060 (10 wt% WP) Toray paper.

Both stability tests lasted approximately 24 hours. Both tests showed a linear H_2O_2 degradation over the test period for all three temperatures tested. This linear degradation across all three temperatures tested indicated that the RF-AQ catalyst did not play a role in further H_2O_2 degradations, which supported findings from literature [56]. There is evidence of thermal decomposition of H_2O_2, as shown in both Figures 7.10 and 7.11: as temperature increased H_2O_2 decomposition also increased. One trend which is similar to the tests carried out in fuel cell mode operation, the highest degradation rate also came in the first five hours of the stability test.

7.4.1 H_2O_2 Decomposition Kinetics

With the concentration profile in Figures 7.10 and 7.11, the rate constant for peroxide decomposition for the three temperatures tested can be determined. First the natural log of peroxide concentration is plotted against time (Figures 7.12 and 7.13).

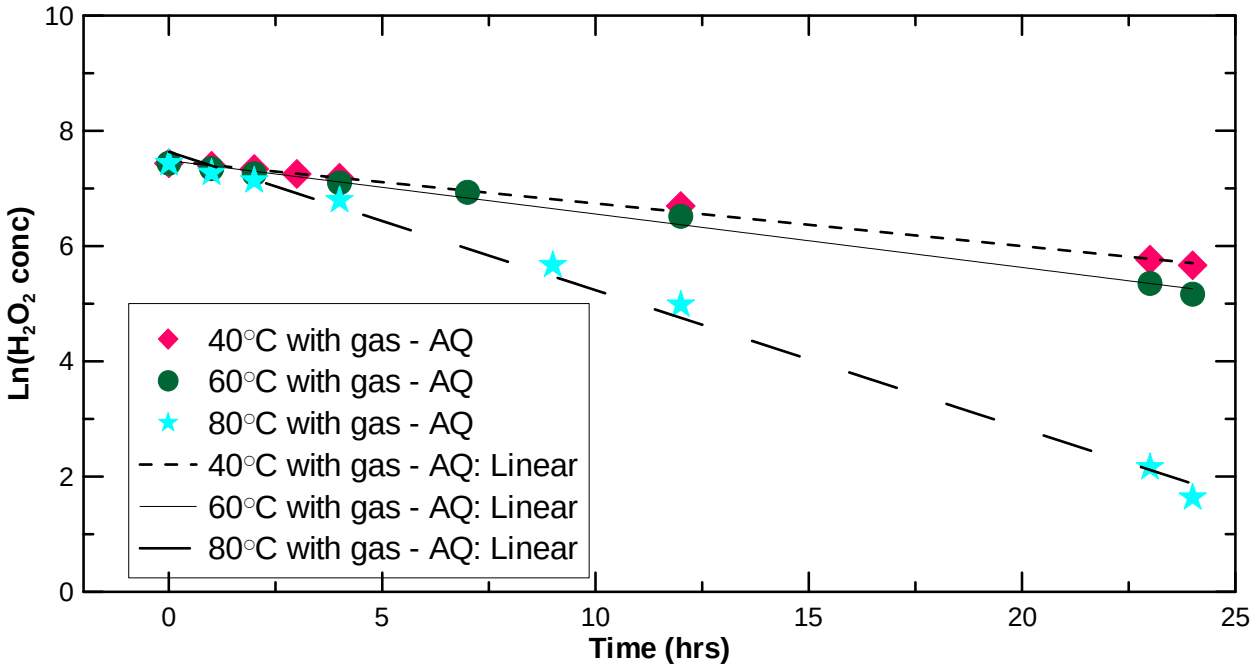

Figure 7.12 Rate constant determination for peroxide decomposition in the electrolysis mode set-up without load as a function of temperature and gas flows with continuous recycle of the cathode water carrier flow.Anode conditions: **15 mL min^{-1}** DI water flow, Ti-Pt anode: 1.0 $mg_{Pt\text{-}black}$ cm^{-2} on 99.99% Commercial grade purity titanium mesh; half-CCM: 0.4 $mg_{Pt\text{-}black}$ cm^{-2} on pre-treated Nafion 112 membrane, with 99.99% Commercial grade purity titanium mesh as back support.. Cathode conditions: O_2 flow rate 1000 mL min^{-1} O_2, pressure 150 kPa(g), water flow rate: **15 mL min^{-1}**, AQ-C catalyst loading 3.6 $mg_{AQ\text{-}C}$ cm^{-2} on TGP-H060 (10 wt% WP) Toray paper.

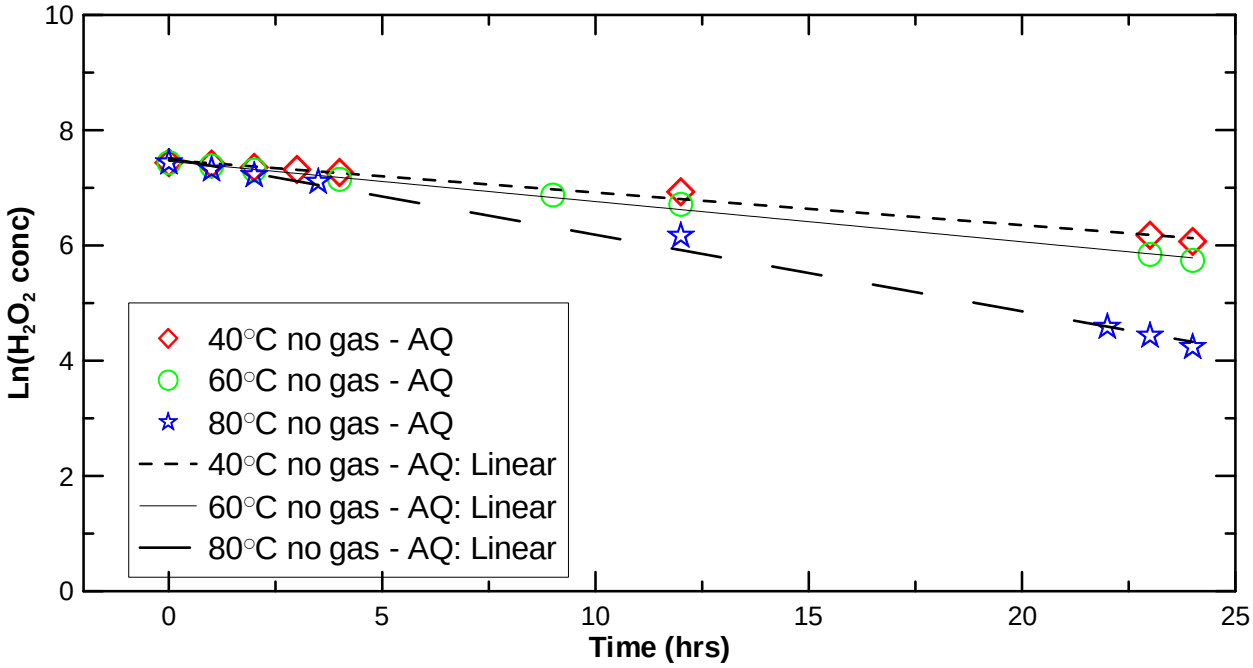

Figure 7.13 Rate constant determination for peroxide decomposition in the electrolysis mode set-up without load as a function of temperature and gas flows with continuous recycle of the cathode water carrier flow. Anode conditions: **15 mL min^{-1}** DI water flow, Ti-Pt anode: 1.0 $mg_{Pt\text{-}black}$ cm^{-2} on 99.99% Commercial grade purity titanium mesh; half-CCM: 0.4 $mg_{Pt\text{-}black}$ cm^{-2} on pre-treated Nafion 112 membrane, with 99.99% Commercial grade purity titanium mesh as back support.. Cathode conditions: pressure 150 kPa(g), water flow rate: **15 mL min^{-1}**, AQ-C catalyst loading 3.6 $mg_{AQ\text{-}C}$ cm^{-2} on TGP-H060 (10 wt% WP) Toray paper.

Table 7-1 Decomposition rate constant values for the electrolysis mode set-up.

Temperature	With gas	Without gas
40C	0.074	0.0565
60C	0.0927	0.0698
80C	0.2399	0.1328
Â (s^{-1})	1828.04	90.92
E_a (J mol^{-1})	26644.71	19404.04

Note: Â = pre-exponential factor, E_a = activation energy.

These rate constants are then plotted against the inverse of temperature to determine the activation energy for peroxide decomposition (Figure 7.14). The activation energy for peroxide decomposition was calculated to be 2.66 x 10^4 J mol^{-1} with gas flow, and 2 x 10^4 J mol^{-1} without gas flow. For further discussion on kinetic parameters please see Appendix D.

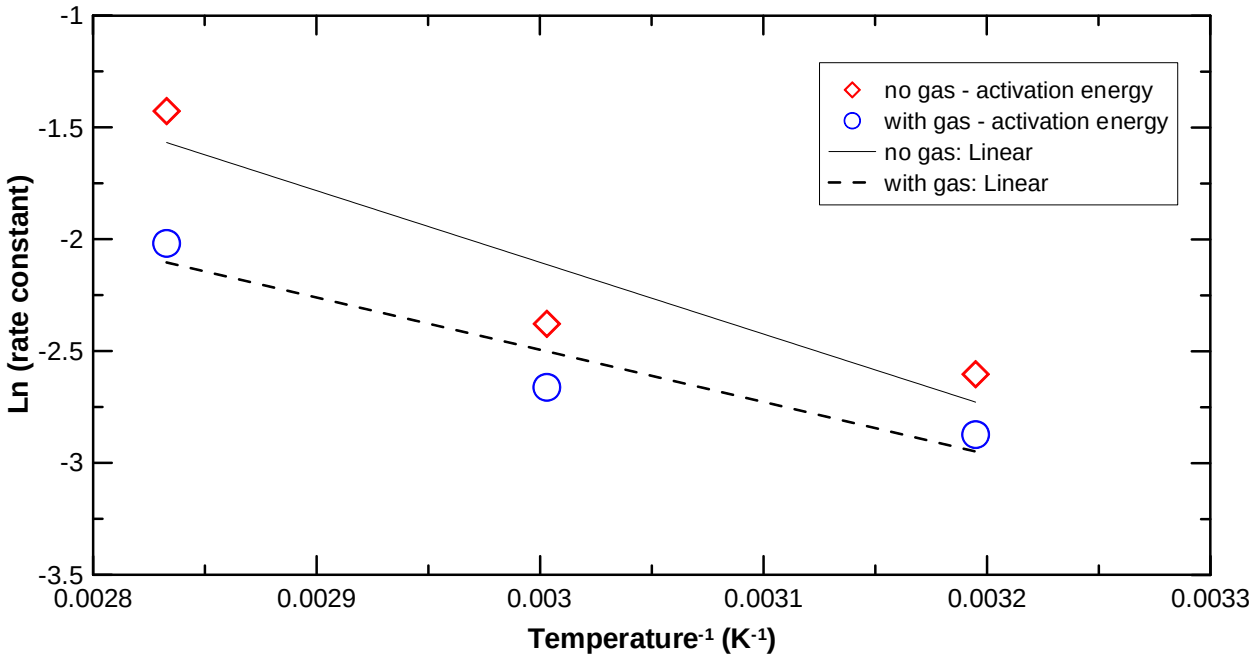

Figure 7.14 Determination of activation energy for peroxide decomposition.

7.4 Effluent Water Analysis

For the product H_2O_2 solution in electrolysis mode operation that will be entering the final phase of the drinking water treatment facility, it must also meet the same criterion that was explained in the fuel cell mode operation: the solution would meet the drinking water guidelines for dissolved trace metals and ions in the solution. For the electrolysis mode operation, these dissolved metals and ions can include inorganics such as cobalt and fluoride ions.

For both cobalt and fluoride ions, the best method of analysis was inductively-coupled plasma mass spectrometry (ICP-MS). The analytical procedure for cobalt and fluoride ions can be found in Appendix B-2 and B-3. For both cobalt and fluoride ions, samples from polarization runs as well as long term recycling tests were analyzed.

7.4.1 Cobalt Analysis

For experiments in electrolysis mode operation, the cathode carrier water can remove trace amounts of cobalt ions as it passes through the cathode catalyst layer. Cathode water samples of various polarization runs at different temperatures was tested for cobalt concentration using ICP-MS. The concentrations are normalized and plotted in Figure 7.15. Samples from the long term recycling runs were also tested for cobalt concentration, and the normalized cobalt leaching rate are plotted in Figure 7.16.

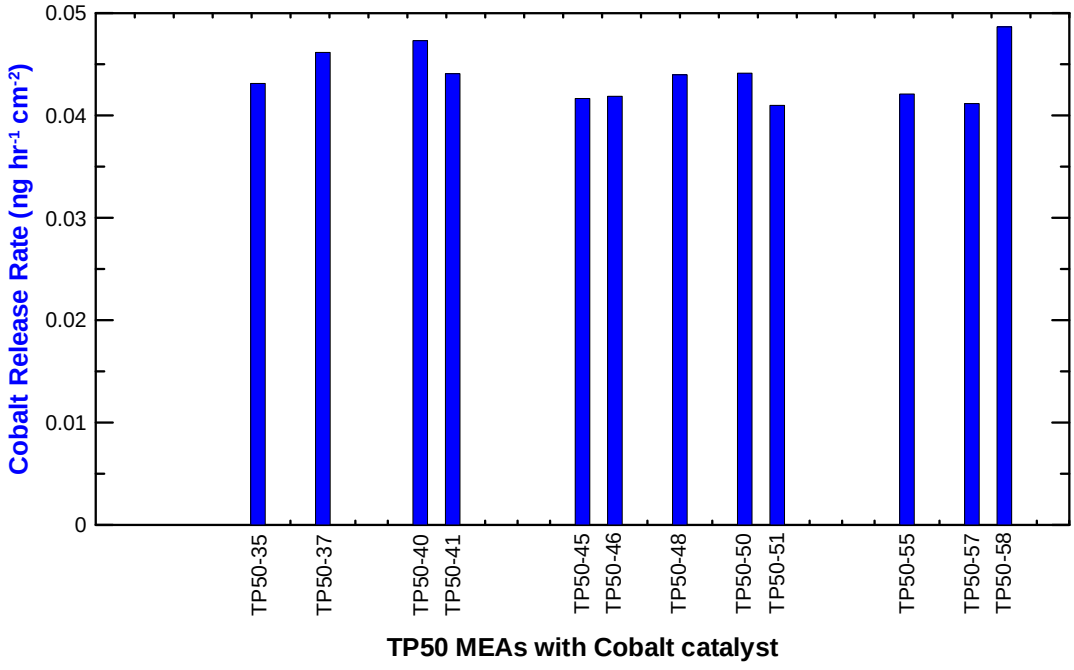

Figure 7.15 Normalized cobalt release rates for various different TP50 MEAs.

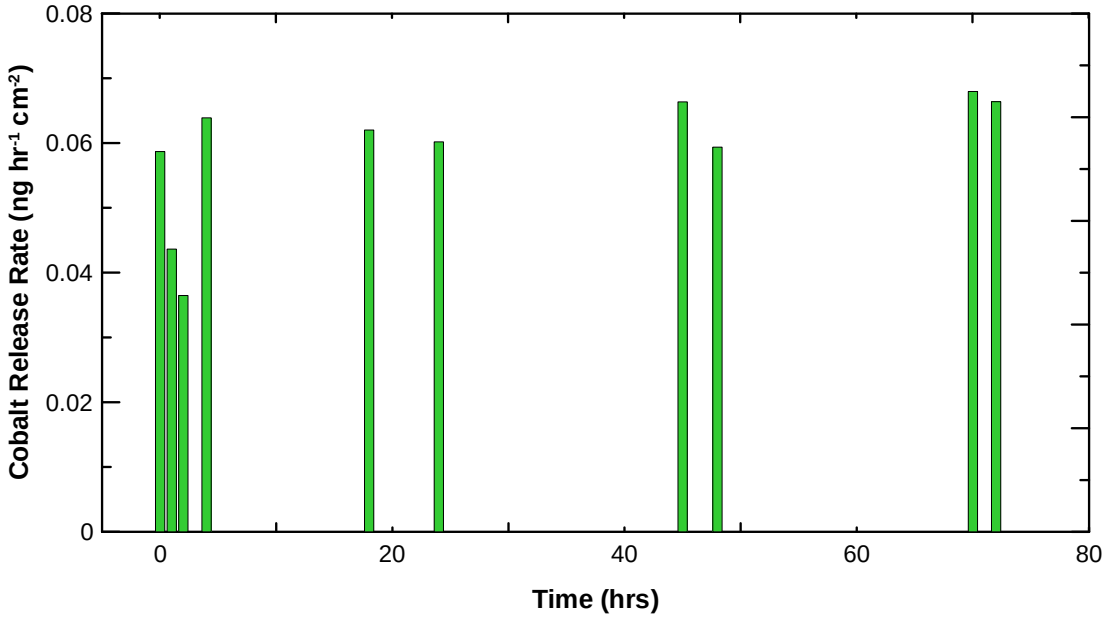

Figure 7.16 Normalized cobalt release rate for long term recycling runs.

7.4.2 Fluoride Ion Analysis

For experiments in electrolysis mode operation, the presence of hydroxyl radicals in the cathode carrier water puts additional strain on the membrane, which can lead to an increase in membrane decomposition. Fluoride ions can form as a result of this membrane decomposition. Hence the cathode water samples of various polarization runs at different temperatures was tested for fluoride ion concentration using ICP-MS. The concentrations are normalized and plotted in Figure 7.17. Samples from the long term recycling runs were also tested for fluoride ion concentration, and the normalized fluoride leaching rate are plotted in Figure 7.18.

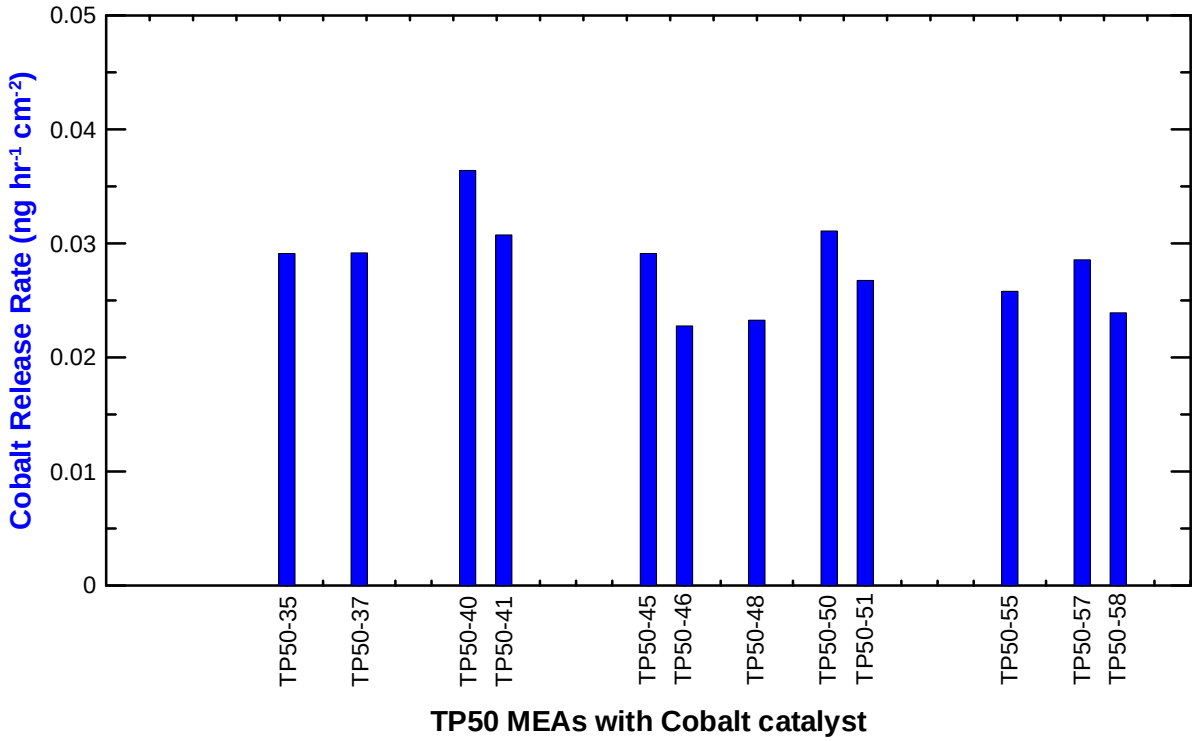

Figure 7.17 Normalized fluoride ion release rates for various different TP50 MEAs.

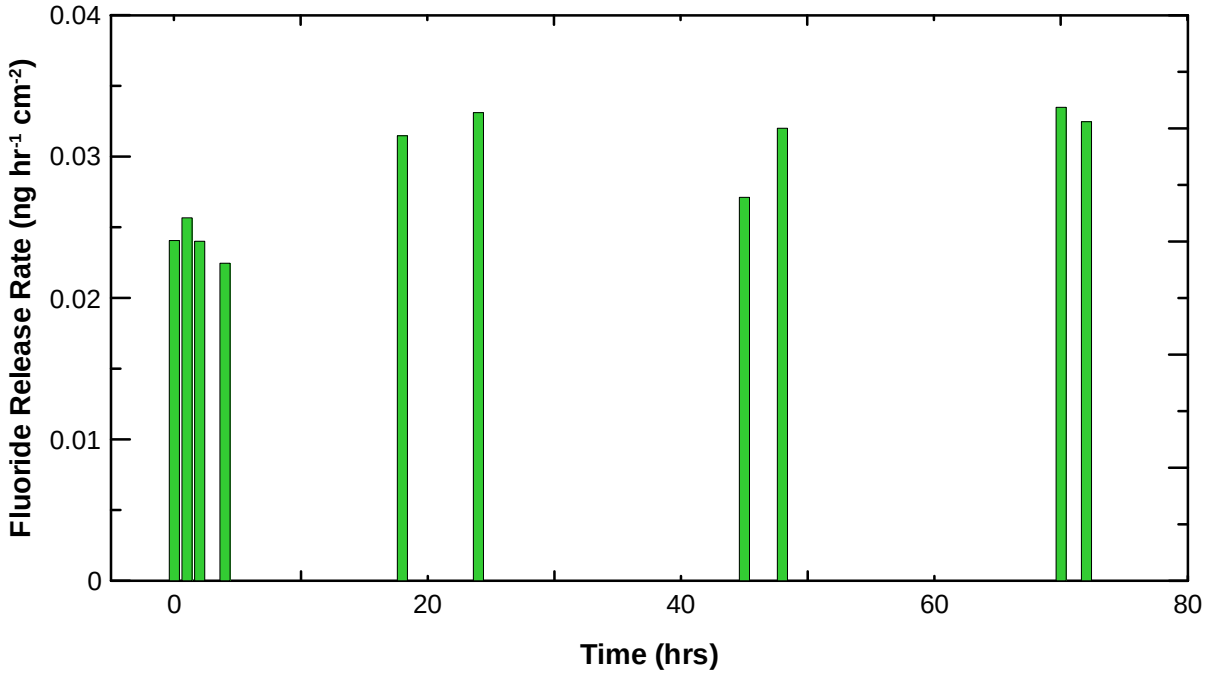

Figure 7.18 Normalized fluoride ion release rate for long term recycling runs.

7.5 Conclusion

The inorganic Co-C composite catalyst previously tested in fuel cell mode operation as well as the organic AQ-RF composite catalyst were both tested as a suitable cathode catalyst for electrolytic H_2O_2 production using a SPE cell. In this section, only 2 operating parameters were tested with the two catalysts, operating temperature and cathode carrier water flow rate. Due to time constraints, more emphasis was focused on testing the AQ-RF composite catalyst. For the electrolysis mode operation, the anode consisted of a thin layer of Pt-black catalyst on a commercially clean Ti-Mesh (as a corrosion resistant back support), or a thin layer of Pt-Black catalyst on one side of a Nafion membrane (Half-CCM), and fed with DI water pumped at 15 mL min^{-1}. The cathode consisted of either the Co-C catalyst on Toray paper or the AQ-RF catalyst on Toray paper. Electrolysis experiments showed that the Co-C catalyst had a similar H_2O_2 production rate to the fuel cell operation mode, at about 360 μmol hr^{-1} cm^{-2} operated at 240 mA cm^{-2} with 8% current efficiency. The AQ-RF catalyst resulted in better H_2O_2 production, at about 580 μmol hr^{-1} cm^{-2} operated at 240 mA cm^{-2} with a 8% current efficiency. The electrolysis mode operation had an optimum operating temperature of 40°C versus 60°C for the fuel cell mode operation.

Longer term (72 hours) experiments conducted with complete recycle of the cathode carrier water containing the generated H_2O_2 show a maximum steady-state H_2O_2 concentration of 1400 ppm for the Co-C composite catalyst, and 3000 ppm for the AQ-RF composite catalyst. Even though these results show great reproducibility (all runs were duplicated at least once), the work presented in this section represents only the first demonstration of such a novel concept. The high overpotential of the anode polarization results means there is significant room for improvement. The electrolytic production of H_2O_2 using either the Co-C composite catalyst or the AQ-RF composite catalyst can provide an adequate supply of H_2O_2 for drinking water treatment applications in remote communities. Electrolysis provides a suitable alternative to electrosynthesis of H_2O_2 using a H_2/O_2 fuel cell.

Chapter 8 Economic Analysis

8.1 Introduction

Thus far discussions in previous chapters have focused on the effect of an inorganic and an organic cathode electrocatalyst for hydrogen peroxide production via different operating parameters, including, catalyst loading, operating temperatures, Teflon loading, as well as cathode carrier water flow rate. This design process is meant for an on-site, in-situ operation to offset transportation and storage costs normally associated with hydrogen peroxide. Hence an economic analysis (one that includes manufacturing as well as operating costs) on this design process is conducted here.

The economic analysis is performed for both the fuel cell mode and electrolysis mode operations producing 0.4 kmol hr^{-1} and 0.72 kmol hr^{-1} H_2O_2, respectively, using 200 cells each with an active area of 1 m^2.

8.2 Operating Conditions

The following operational conditions are used in the economic evaluation of the neutral H_2O_2 processes in either fuel cell mode or electrolysis mode operation. Values given are for individual cells each with 1 m^2 active area.

8.2.1 Fuel Cell Mode Operation

Anode: Toray carbon paper

Anode catalyst: platinum on carbon

H_2 flow rate: 500 mL min^{-1} (Eq. Stoic: 14.6 @ 100 mA cm^{-2})

Membrane: Nafion 112

Cathode: Toray carbon paper

Cathode catalyst: Cobalt on Carbon

O_2 flow rate: 1000 mL min^{-1} (Eqv. Stoic: 58.6 @ 100 mA cm^{-2})

Cathode carrier water flow rate: 15 mL min^{-1}

Current Density: 100 – 340 A m^{-2} (10 – 34 mA cm^{-2})

Current Efficiency: 30%

Cell Voltage: 0.1 – 0.5 V

Operating temperature: 40 – 60°C

Pressure: 150 kPa(g)

Maximum H_2O_2 Production Rate: 200 μmol hr^{-1} cm^{-2}

8.2.2 Electrolysis Mode Operation

Anode flow field plate: Gold plated nickel plate

Anode: titanium mesh

Anode catalyst: platinum black

Anode water flow rate: 15 mL min^{-1}

Membrane: Nafion 112

Cathode: Toray carbon paper

Cathode catalyst: cobalt on carbon, AQ-RF on carbon

Cathode flow field plate: graphite plate

O_2 flow rate: 1000 mL min^{-1} (Eqv. Stoic: 58.6 @ 100 mA cm^{-2})

Cathode carrier water flow rate: 15 mL min^{-1}

Current Density: 600 – 2450 A m^{-2} (60 – 245 mA cm^{-2})

Current Efficiency: 10%

Cell Voltage: 2 – 3 V

Operating temperature: 40 – 60°C

Cathode Pressure: 150 kPa(g)

H_2O_2 Production Rate: 360 μmol hr^{-1} cm^{-2}

8.3 Gross Economic Potential (GEP)

In fuel cell mode operation, the net stoichiometry for the H_2O_2 generation is:

$$H_2 + O_2 \rightarrow H_2O_2 \qquad \text{Eqn 8.1}$$

While in electrolysis mode operation, the net stoichiometry for the H_2O_2 generation is:

$$H_2O + 0.5O_2 \rightarrow H_2O_2 \qquad \text{Eqn 8.2}$$

Table 8-1 Single cell flow rates and costs of chemicals used for GEP in fuel cell mode operation [5]

	H_2	O_2	H_2O_2
Molar mass (kg $kmol^{-1}$)	2	32	34
Price (\$ kg^{-1})	0.176	0.0108	0.70
Inlet (kmol hr^{-1})	1.38×10^{-2}	9.16×10^{-3}	0
Outlet (kmol hr^{-1})	1.18×10^{-2}	7.16×10^{-3}	2.0×10^{-3}

Table 8-2 Single cell flow rates and costs of chemicals used for GEP in electrolysis mode operation [5]

	H_2O	O_2	H_2O_2
Molar mass (kg $kmol^{-1}$)	18	32	34
Price (\$ kg^{-1})	0.010	0.0108	0.70
Inlet (kmol hr^{-1})	9.718	1.83×10^{-2}	0
Outlet (kmol hr^{-1})	9.714	1.47×10^{-2}	3.6×10^{-3}

Based on Eqns 8.1 and 8.2, as well as values given on Tables 8-1 and 8-2, the gross economic potential associated with the production of 4.0 x 10^{-1} kmol hr^{-1} neutral H_2O_2 (fuel cell mode operation with 200 cells each with 1 m^2 active area) and 7.2 x 10^{-1} kmol hr^{-1} neutral H_2O_2 (electrolysis mode operation with 200 cells each with 1 m^2 active area) are:

Fuel cell mode operation:

GEP = [Value of Products] – [Value of Feeds] (Eqn 8-3)

GEP = ($4.0x10^{-1}$ x 34 x 0.7) – ($4.00x10^{-1}$ x 1 x 0.176 + $4.00x10^{-1}$ x 32 x 0.0108)

GEP = \$ 9.31 hr^{-1}

Electrolysis mode operation:

GEP = [Value of Products] – [Value of Feeds] (Eqn 8-4)

GEP = ($7.20x10^{-1}$ x 34 x 0.7) – ($7.20x10^{-1}$ x 18 x 0.100 + $3.60x10^{-1}$ x 32 x 0.0108)

GEP = \$ 16.94 hr^{-1}

The targeted H_2O_2 price of 0.70 US \$ kg^{-1} is the current market price of commercial hydrogen peroxide based on current production costs which includes associated transportation and storage costs (h2o2.com, 2015).

For any process to be economically viable the gross economic potential must be positive, otherwise the process will need to be discarded from an economic standpoint. The processes presented here both have positive GEP (though they may be small considering the small size of the processes), hence both processes can be further evaluated.

8.4 Net Economic Potential (NEP) and Return on Investment (ROI)

For a more realistic analysis of the processes, a net economic potential analysis and a return on investment assessment is carried out. This expansion includes different types of equipment used for the various operations as well as the recycled streams. Based on the preliminary design and sizing of the process equipment involved, the capital and operational costs can be estimated.

Conceptual flowsheets for both the fuel cell mode process and the electrolysis mode process are shown in Figures 8.1 and 8.2, respectively.

Table 8-3 H_2O_2 production process fuel cell mode operation component list

Component ID	Description
C1, C2	Gas compressor
E1, E2	Heat exchanger
GL1, GL2	Gas/Liquid separator
P1, P2	pump
T1	Hydrogen gas tank
T2, T3	Water supply tank
T4	Oxygen gas tank
T5	Product H_2O_2 storage tank

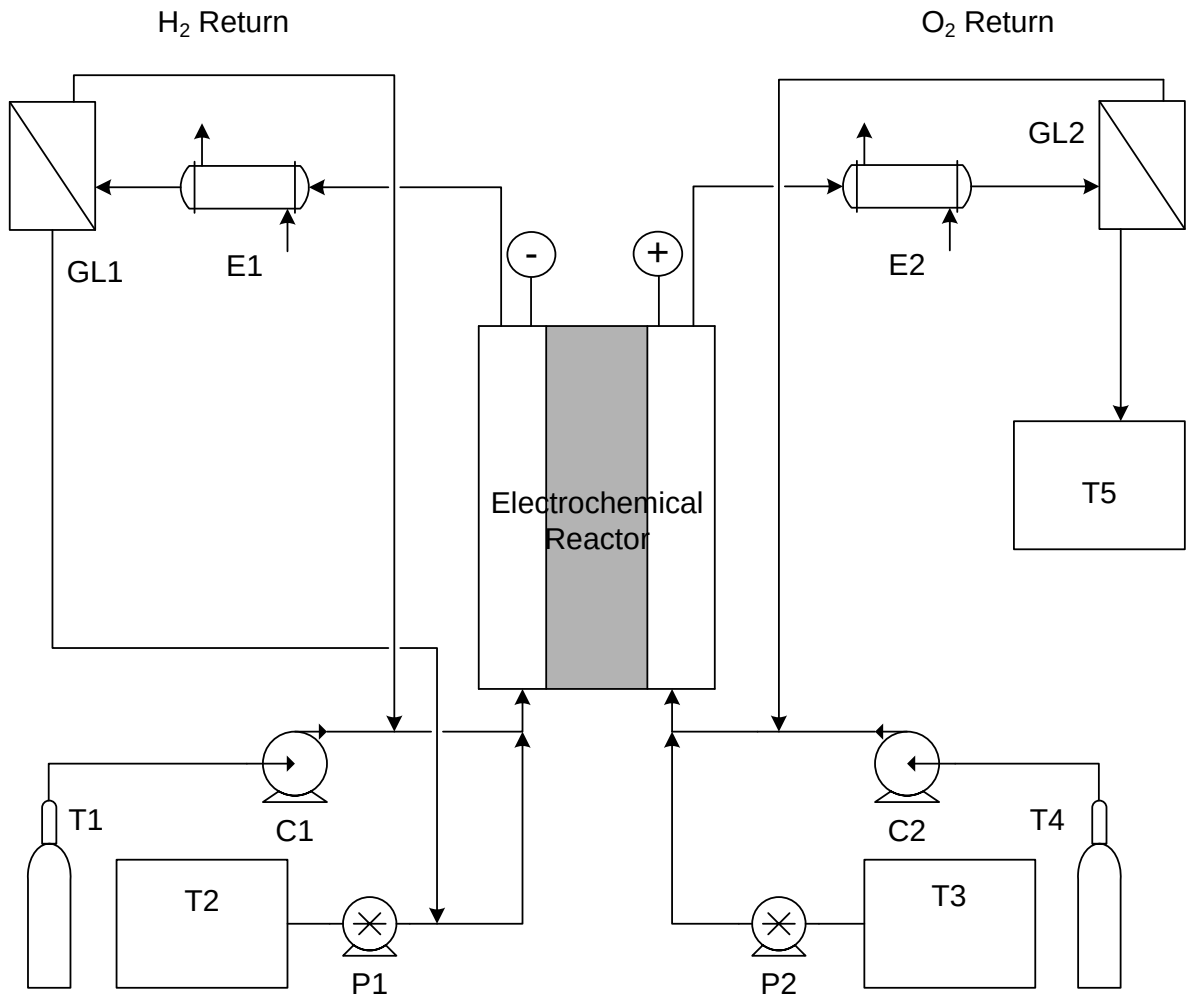

Figure 8.1 Conceptual flowsheet for fuel cell mode operation of H_2O_2 production process.

Table 8-4 H_2O_2 production process electrolysis mode operation component list

Component ID	Description
C1	Gas compressor
E1	Heat exchanger
GL1, GL2	Gas/Liquid separator
P1, P2	pump
T1, T2	Water supply tank
T4	Oxygen gas tank
T3	Product H_2O_2 storage tank

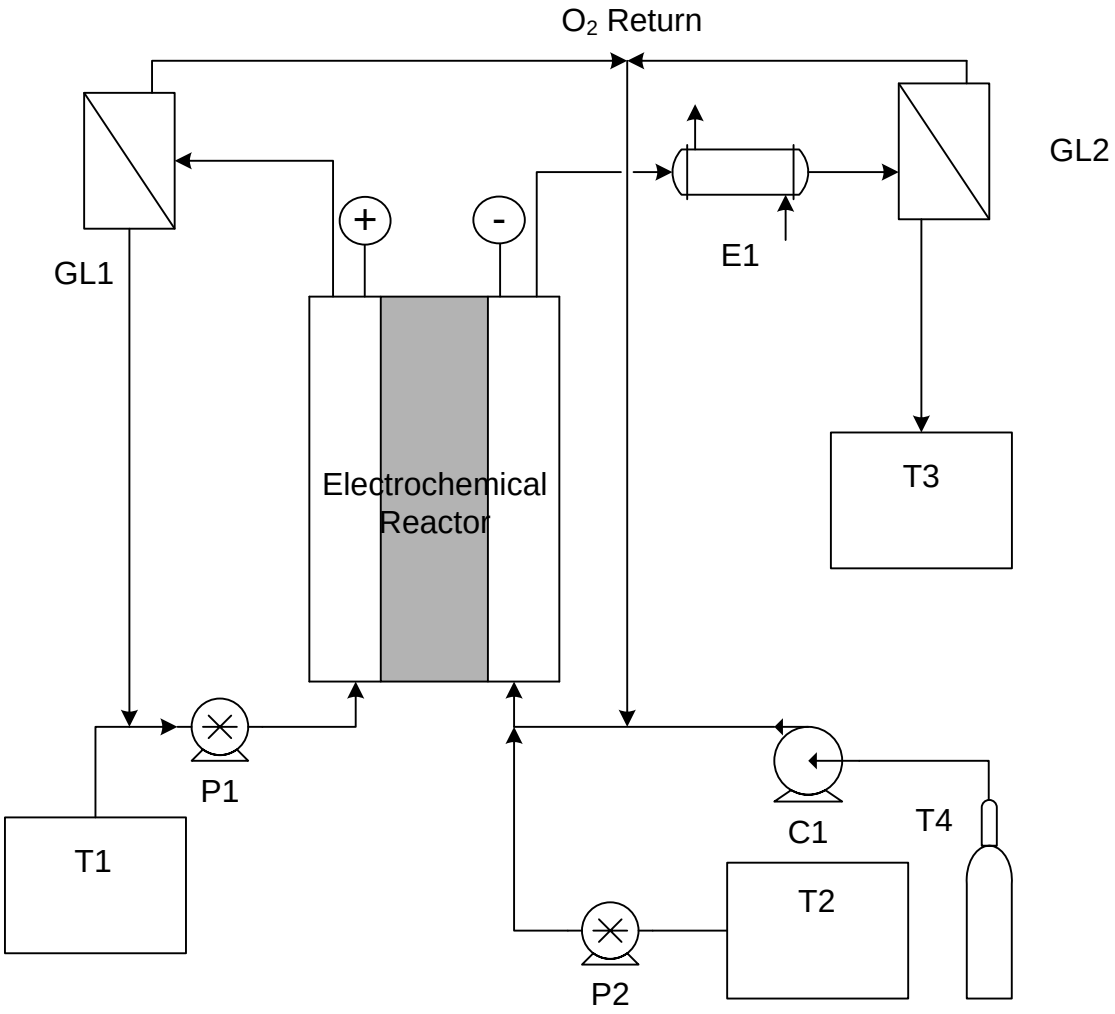

Figure 8.2 Flowsheet for electrolysis mode operation of H_2O_2 production process.

From Figures 8.1 and 8.2, for the most important component of the flowsheet, the electrochemical reactor, the total installed capital cost $C_{I,E}$, is the sum of the installed capital cost of the cells C_{IEC}, and the installed capital cost of the power supply system, C_{PS}, given as:

$$C_{I,E} = C_{IEC} + C_{PS} \qquad \text{(Eqn 8-5)}$$

The installed capital cost for electrochemical reactors, C_{IEC}, is given as [120]:

$$C_{IEC} = N_C \cdot G_C \cdot (A_C)^m \qquad \text{(Eqn 8-6)}$$

Where N_c is the number of cells, G_c is the cost constant expressed in \$ m^{-2}, A_c is the electrode area per cell (m^2), and m is the scale component (0.8-0.9). As slight differences exists for the

cell components used in fuel cell mode and electrolysis mode operation, Table 8-3 lists the cost estimate of the cell components used in both operation modes.

Table 8-5 Cost estimates of cell components for fuel cell mode and electrolysis mode operation. [120]

	Cost estimate per US $ m^{-2} superficial electrode area	
Cell component	**Fuel cell mode**	**Electrolysis mode**
Graphite anode	46	N/A
Gold plated anode/Nickel Mesh	N/A	6,200
Graphite cathode	46	46
Graphite water jacket plate (2x per cell)	92	92
Membrane Electrode Assembly	5,000	5,000
Current collector (gold plated steel)	100	100
Miscellaneous	1,000	1,000
Total	**6,284**	**12,438**

Note: The cost for Membrane Electrode Assembly includes cost for Nafion 115 PEM membrane, Toray carbon paper, and catalyst for both anode and cathode for an active area of 1 m^2.

The total uninstalled cost is US \$6,284 m^{-2} for fuel cell mode operation and US \$12,438 m^{-2} for electrolysis mode operation. A Lang factor of 3 is used to estimate the installed cost, US \$18,852 m^{-2} for fuel cell mode operation and US \$37,314 m^{-2} for electrolysis mode operation. In addition, it is assumed that the MEAs will be replaced twice a year; hence the cost constant, G_c, for a single cell of 1 m^2 active area, would be US \$23,852 m^{-2} for fuel cell mode operation, and US \$42,314 m^{-2} for electrolysis mode operation.

The number of required cells is related to the cathode area through Faraday's law:

$$N_C = \frac{zFP_r}{i \cdot CE \cdot A_C} \qquad \text{(Eqn 8-6)}$$

Where:

Z = number of electrons (2),

F = Faraday's constant (96486 kC $kmol^{-1}$),

Pr = H_2O_2 production rate (kmol s^{-1}),

i = superficial current density (kA m^{-2}),

CE = current efficiency,

For electrolysis mode operation, the installed capital cost of the power supply system, C_{PS}, is [120]:

$$C_{PS} = P_w\left(B' + \frac{C'}{V_t}\right), \text{ and} \qquad \text{(Eqn 8-7)}$$

$$P_w = N_C \cdot i \cdot A_C \cdot V_C, \text{ and } V_t = N_C \cdot V_C \qquad \text{(Eqn 8-8)}$$

where Pw is the total power consumption (kW), B' and C' are cost constants (100 and 20,000 \$ kW^{-1}, respectively), V_t is the total voltage (V), and V_c is the voltage per cell (V). For a superficial current density of 610 A m^{-2}, the cost of the power supply system is \$195,200 US.

The cost of dc electrical energy associated with the electrochemical reactor unit, C_{el} (US \$ hr^{-1}), is [120]:

$$C_{el} = \frac{C_{ac}P_w}{RE} \qquad \text{(Eqn 8-9)}$$

Where C_{ac} is the cost of ac electricity (\$0.03 US kWh^{-1}), and RE is the rectifier efficiency (0.96).

For the two operation modes, the installed capital and operating costs for the auxiliary equipments (including feed/storage tanks, gas/liquid separators, pumps and compressors, please see Figures 8.1 and 8.2) were estimated using their respective design equations and cost calculations found in Appendix C. A summary of the cost of auxiliary equipments used in both operation modes can be found in Table 8-4.

Table 8-6 Cost of auxiliary equipments for fuel cell mode and electrolysis mode operation in the H_2O_2 production process.

Equipment	**Uninstalled Cost (US $)**	**Installation Factor**	**Installed Capital Cost (US $)**	**Power (KW)**	**Cooling Water (m^3 hr^{-1})**	**Electrical Energy / Cooling Water Utility (US $ hr^{-1})**
Feed tanks	13,600	3	40,800			
Storage tank	13,600	3	40,800			
pump	4,400	5	22,000	0.1		0.01
Compressor	7,700	4.5	34,650	11.2		1.12
G/L separator	2,300	4	9,200			
Heat exchanger	16,200	3	48,600		48	1.44
Total	**57,800**		**196,050**			**2.57**

The maintenance and labor cost associated with the H_2O_2 production process, $C_{E,ML}$, is a function of the total applied current and the number of cells, N_c [121]:

$$C_{E.ML} = 0.2 \cdot N_C \cdot i \cdot A_C + 700 \cdot N_C \qquad \text{(Eqn 8-10)}$$

However, in most electrochemical plants this cost is typically 5-10% of the total capital cost [120]. For the present study, the maintenance and labor cost is chosen as 10% of the total installed capital cost (C_{IC}). Therefore,

$$C_{E,ML} = 0.1 \cdot C_{IC} \qquad \text{(Eqn 8-11)}$$

The total installed capital cost (C_{IC}) is therefore the sum of the installed capital cost of the electrochemical reactor (C_{IEC}), the installed cost of the power supply equipment (C_{PS}), and the installed capital cost of the auxiliary equipments (C_{IA}). In addition, this total cost is increased by 30% in order to cover any possible underestimation of the capital cost.

$$C_{IC} = 1.3 \cdot (C_{IEC} + C_{PS} + C_{IA}) \qquad \text{(Eqn 8-12)}$$

The total installed capital cost for the auxiliary process equipments, based on estimations from Appendix C, is $196,050 US. The total operating cost of the non-electrochemical equipments (i.e. utilities plus labor and maintenance) is ~ $2.57 US hr^{-1} (Table 8-4).

The net economic potential (NEP) and the yearly return on investment (ROI) are calculated as follows:

NEP ($ hr^{-1}) = GEP – Operating Costs (i.e., utilities + labor + maintenance), (Eqn 8-13)

$$\text{ROI (\% per year)} = \frac{\text{NEP x 8000}}{\text{Total Installed Capital Cost}} \times 100 \qquad \text{(Eqn 8-14)}$$

The dependence of NEP and ROI on the superficial current density is shown on Figure 8.3 (fuel cell mode operation) and Figure 8.4 (electrolysis mode operation). Typically processes are considered profitable and thus worthy of investment considerations if the ROI > 30% per year [120].

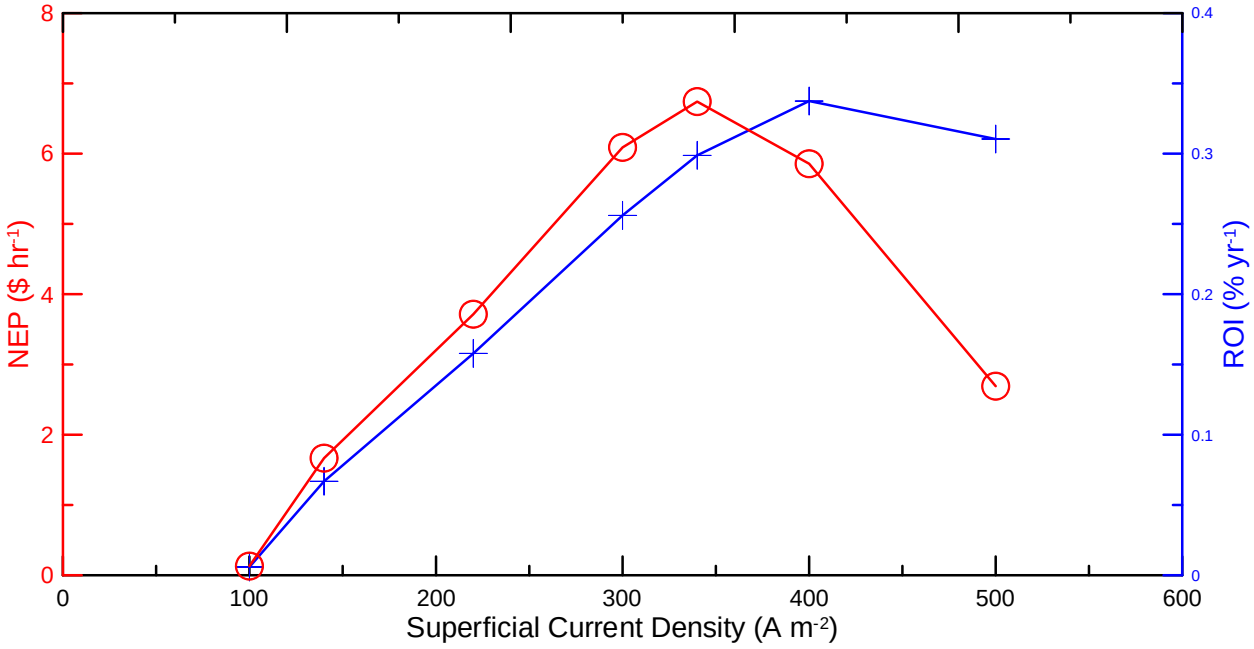

Figure 8.3 Net economic potential and return on investment versus superficial current density for H_2O_2 production in fuel cell mode operation.

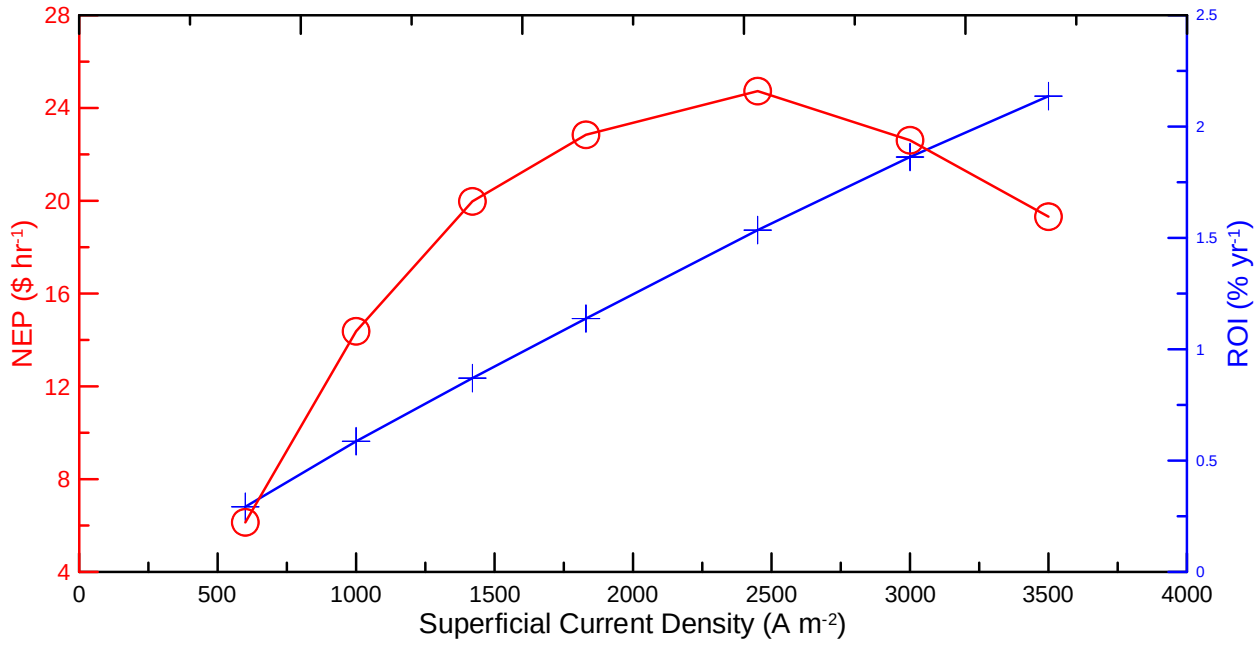

Figure 8.4 Net economic potential and return on investment versus superficial current density for H_2O_2 production in electrolysis mode operation.

For both modes of operation, the ROI is too low for reasonable investment considerations. However, as this is only a proof of concept research project, there are some important findings from this research undertaking.

The electrolysis mode operation has a much higher net economic potential vs. that of the fuel cell mode operation, mainly due to the higher cost of hazardous materials (H_2). The same holds true for return on investment.

For fuel cell mode operation, the highest ROI was $0.34\%_{peryear}$ *ca* 400 A m^{-2}, however, NEP had a maximum of 6.74 \$ hr^{-1} *ca* 340 A m^{-2} (Figure 8.3). This difference is mainly due to the reduced number of cells required (757 cells at 340 A m^{-2} vs. 582 cells at 400 A m^{-2}), which led to a reduction in total installed capital cost (from 18 million \$ yr^{-1} at 340 A m^{-2} to 13.9 million \$ yr^{-1} at 400 A m^{-2}).

For electrolysis mode operation, the maximum NEP was 24.7 \$ hr^{-1} *ca* 2450 A m^{-2}. However, there is no maximum ROI. Figure 8.4 did show that a decent return on investment can be obtained at superficial current densities above 3500 A m^{-2}.

Chapter 9 Conclusions and Recommendations

9.1 Conclusions

In this research project, a novel method for the electroreduction of oxygen to hydrogen peroxide was tested on two different cathode catalysts, operating in two different operation modes. To date no literature has reported this unique method of H_2O_2 production and capture from O_2 electroreduction. The two cathode catalysts investigated were the inorganic cobalt-carbon complex [28], and the organic riboflavin-anthraquinone complex [63]. The two operation modes tested were the fuel cell mode operation and the electrolysis mode operation.

Thus far there have only been a few publications on neutral two electron reduction of O_2 to H_2O_2 in a fuel cell environment, with the most notable research done by the Yamanaka group [1, 35-36]. However several key aspects of this study separate it from other reports:

- An inorganic and an organic catalyst were tested for H_2O_2 production in a fuel cell environment, the inorganic catalyst was tested in fuel cell mode operation, and both catalysts were tested in electrolysis mode operation
- No special catalyst for the anode is used. The anode used is platinum on carbon with typical fuel cell anode catalyst loadings
- Use of cathode carrier water to remove the product H_2O_2 generated at the cathode, thus preventing H_2O_2 corrosion at the electrode and membrane
- Long term recycle runs (72 hours) to test the durability of the novel catalysts, in both fuel cell mode operation and electrolysis mode operation

9.1.1 Fuel Cell Mode Operation with Inorganic Catalyst

This first demonstration of the continuous generation of H_2O_2 in a PEM fuel cell was conducted using a 49 cm^2 H_2/O_2 PEM fuel cell with a Co-C composite cathode catalyst, utilizing a continuous flow of water stream at the cathode side to remove the product H_2O_2. As this liquid stream creates a two-phase flow with the oxygen gas flow, possible cathode flooding may interfere with the oxygen gas mass transfer. However, in all experiments conducted, flooding did not play an important role in impeding H_2O_2 production.

Through a set of parametric experiments, the effect of the following parameters on H_2O_2 production was investigated: operating temperature, cathode catalyst loading, cathode teflon loading, and cathode carrier water flow rate. From these experiments the best fuel cell polarization performance and H_2O_2 production rate was achieved with a cathode catalyst loading of 3.6 $mg_{Co\text{-}C}$ cm^{-2} using a 10 wt% teflon content Toray carbon paper GDL and a cathode carrier water flow rate of 25 mL min^{-1}. A maximum H_2O_2 production rate of ~200 μmol hr^{-1} cm^{-2} was achieved at a cell operating temperature of 60°C with the fuel cell operated at 30 mA cm^{-2} with 30% current efficiency, at a corresponding cell voltage of 0.1 V.

In order to study the durability of the inorganic Co-C catalyst, long term (72 hours) experiments with complete recycle of the cathode carrier water containing the product H_2O_2 showed a maximum accumulated H_2O_2 concentrations of over 1400 ppm. Analysis of the cathode water samples showed insignificant amounts of cobalt and fluoride.

9.1.2 Electrolysis Mode Operation with Inorganic and Organic Catalyst

A modified PEM fuel cell capable of withstanding the harsh environment in electrolysis mode operation was used to test the inorganic and organic cathode catalyst in continuous generation of H_2O_2 in electrolysis mode operation. Just as in fuel cell mode operation, a continuous flow of water at the cathode side was used to remove the product H_2O_2. In addition to this cathode water stream mixed with oxygen gas, the anode also had a continuous water stream for water electrolysis with an external power supply. This is a special kind of water electrolysis since H_2O_2 instead of H_2 is produced at the cathode.

For the electrolysis mode operation, the effect of operating cell temperature and cathode carrier water flow rate on H_2O_2 production was investigated for both the inorganic and the organic cathode catalyst. The optimum operating temperature was 40°C compared to that of 60°C for the fuel cell mode operation. Overall both the inorganic Co-C and the organic RF-AQ catalyst in electrolysis mode had higher H_2O_2 production rates when compared to the inorganic Co-C catalyst operated in fuel cell mode. In addition, due to issues with the anode GDL support backing, alternative anode support backings were experimented with for the organic and inorganic cathode catalysts. It was found that the Ti-Pt||AQ-C with half-CCM MEA had the optimum H_2O_2 production at 480 μmol hr^{-1} cm^{-2} with a current density of 240 mA cm^{-2}, however the current efficiency was only 12%.

For the organic RF-AQ catalyst, long term (72 hours) experiments with complete recycle of the cathode carrier water containing the product H_2O_2 showed a maximum accumulated H_2O_2

concentration of over 3000 ppm. Analysis of the cathode water samples showed insignificant amounts of cobalt and fluoride.

9.2 Recommendations for Future Work

The aim of this research project initially was to investigate the proof of concept of continuous generation of H_2O_2 for a small water treatment system within the RES'EAU WaterNet program. However, further literature study revealed that this research can be applied to various other industries that could benefit from not using the traditional H_2O_2 supply chain. These industries include small wastewater treatment applications, cosmetics, and pharmaceuticals. Furthermore, these electrochemical approaches can be stacked together in order to increase H_2O_2 production, which would broaden the field of application to other industries.

Both modes of operation merit further studies as each show promising results. However, the nature of the reaction mechanism means they are on diverging paths and thus cannot be studied together. The following are some proposed directions of research for each mode of operation.

9.2.1 Fuel Cell Mode Operation

The inorganic Co-C catalyst underwent parametric studies to determine the optimum parameters in order to achieve maximum H_2O_2 production in a single cell environment. Further studies are needed if this method of operation is to be implemented for continuous H_2O_2 production:

- Decrease the operating temperature to study the effect of lower temperature on H_2O_2 production. Currently the optimum temperature is 60°C for fuel cell mode operation, if better production can be achieved with ambient temperature of 25°C, this would lower the cost of cooling down the product H_2O_2 stream.
- Study the effect of cathode gas pressure on H_2O_2 production. The reaction mechanism at the cathode involved three phases, thus effective O_2 mass transport and H^+ diffusion is crucial for the success of H_2O_2 production.
- Consider 3D catalyst layer design to allow for more reactive surface area, thus increasing H_2O_2 production.
- More investigations into power cogeneration with the implementation of platinum cathode catalyst with Co-C catalyst in a side-by-side configuration to produce power and H_2O_2.

9.2.2 Electrolysis Mode Operation

Electrolysis mode operation with either the inorganic Co-C catalyst or the organic RF-AQ catalyst produced more H_2O_2 versus the inorganic Co-C catalyst in fuel cell mode operation. In addition to this promising result, the electrolysis mode could be viewed as a more viable option, as it does not rely on hazardous H_2 transport, as well as easier integration with the existing power grid. However, there are still a number of areas recommended to be included in further studies:

- Additional temperature studies to include 25°C are also recommended.
- Fuel cell hardware redesign closer to those used in water electrolysis is recommended in order to overcome some of the issues faced in the current research.

- Gas pressure for both the anode and the cathode requires further investigation. As three phase reaction mechanism occurs on both electrodes, it is crucial that O_2 mass transport and H^+ diffusion on both sides of the membrane be properly maintained for effective H_2O_2 production.
- Current research showed that the RF-AQ catalyst performed better than the Co-C catalyst in electrolysis mode operation. However, a creative multi-zone catalyst layer integrating the organic RF-AQ catalyst with the Co-C catalyst could improve H_2O_2 production as well as current efficiency.
- Look at directing pure O_2 from the anode oxygen evolution reaction (OER) to the cathode for improved H_2O_2 production.

References

[1] I. Yamanaka, S. Tazawa, T. Murayama, T. Iwasaki, S. Takenaka, *ChemSusChem* **2010**, *3*, 59-62.

[2] P. M. L. J. Thenard, *Lu a l'Academie des Sciences* **1818**, 306-313.

[3] C. Samanta, *Applied Catalysis A: General* **2008**, *350*, 17.

[4] P. Tundo, P. Anastas, D. StC. Black, J. Breen, T. Collins, S. Memoli, J. Miyamoto, M. Ployakoff, W. Tumas, *Pure Appl. Chem.* **2000**, *72*, 1207-1228.

[5] U. S. Peroxide, in *http://www.h2o2.com/faqs/FaqDetail.aspx?fId=25*, **December 3, 2012**.

[6] U. o. York, in *http://www.essentialchemicalindustry.org/chemicals/hydrogen-peroxide.html*, **November 23, 2014**.

[7] C. W. Jones, *Applications of Hydrogen Peroxide and Derivatives*, The Royal Society of Chemistry, Cambridge, UK, **1999**.

[8] R. Gopal, US Patent 6712949 B2, **2004**

[9] P. C. Foller, R. T. Bombard, *J.Appl.Electrochem.* **1995**, *25*, 613-627.

[10] B. Keita, L. Nadjo, *J. electroanal. Chem.* **1983**, *145*, 431-437.

[11] C. L. Jenkins, US Patent US4800075A, **1987**

[12] M. Traube, *Ber. Kgl. Akad. Wiss. Berlin* **1887**, 1041.

[13] C. Oloman, *J. Electrochem. Soc.* **1979**, *126*, 8.

[14] C. Oloman, P. Watkinson, *J.Appl.Electrochem.* **1979**, *9*, 117-123.

[15] N. Guillet, L. Roue, S. Marcotte, D. Villers, J. P. Dodelet, N. Chhim, S. Trevin, *J.Appl.Electrochem.* **2006**, *36*, 863-870.

[16] N. Yamada, T. Yaguchi, H. Otsuka, M. Sudoh, *Journal of Electrochemical Society* **1999**, *146*, 2587-2591.

[17] K. Kinoshita, *Electrochemical Oxygen Technology*, John Wiley & Sons, Inc., **1992**.

[18] T. R. Ralph, M. P. Hogarth, *Platinum Metals Rev.* **2002**, *46*, 3-14.

[19] G. A. Kolyagin, V. L. Kornlenko, *Russian Journal of Applied Chemistry* **2003**, *76*, 6.

[20] G. A. Kolyagin, I. S. Vasil'eva, V. L. Kornlenko, *Russian Journal of Applied Chemistry* **2008**, *81*, 983-987.

[21] P. Tatapudi, J. M. Fenton, *J. Electrochem. Soc.* **1993**, *140*, 3.

[22] P. Tatapudi, J. M. Fenton, *J. Electrochem. Soc.* **1994**, *141*, 5.

[23] F. Jaouen, J. P. Dodelet, *Electrochim. Acta* **2007**, *52*, 5975-5984.

[24] J. P. Dodelet, *Oxygen Reduction in PEM Fuel Cell Conditions: Heat-Treated Non-Precious Metal-N4 Macrocycles and Beyond, in: N2-Macrocyclic Metal Complexes*, Srpinger, New York, **2006**.

[25] E. B. Easton, A. Bonakdarpour, R. Yang, D. A. Stevens, J. R. Dahn, *Journal of The Electrochemical Society* **2008**, *155*, B547-B557.

[26] M. Lefevre, E. Proietti, F. Jaouen, J. P. Dodelet, *Science* **2009**, *324*, 71-74.

[27] P. H. Matter, U. S. Ozkan, *Catalysis Letters* **2006**, *109*, 115-123.

[28] A. Bonakdarpour, D. Esau, H. Cheng, A. Wang, E. L. Gyenge, D. P. Wilkinson, *Electrochim.Acta* **2011**, *56*, 9074-9081.

[29] S. Marcotte, D. Villers, N. Guillet, L. Roue, J. P. Dodelet, *Electrochim. Acta* **2004**, *50*, 179-188.

[30] T. S. Olson, S. Pylypenko, J. E. Fulghum, P. Atanassov, *Journal of The Electrochemical Society* **2010**, *157*, B54-B63.

[31] R. Yang, K. Stevens, A. Bonakdarpour, J. R. Dahn, *Journal of The Electrochemical Society* **2007**, *154*, B893-B901.

[32] W. Zhang, A. U. Shaikh, E. Y. Tsui, T. M. Swager, *Chemistry of Materials* **2009**, *21*, 3234-3241.

[33] T. S. Olson, S. Pylypenko, P. Atanassov, *J. Phys. Chem. C* **2010**, *114*, 5049-5059.

[34] I. Yamanaka, S. Tazawa, T. Murayama, R. Ichihashi, N. Hanaizumi, *ChemSusChem* **2008**, *1*, 988-990.
[35] I. Yamanaka, T. Onizawa, S. Takenaka, K. Otsuka, *Angew. Chem. Int. Ed.* **2003**, *42*, 3653.
[36] I. Yamanaka, *Catal Surv Asia* **2008**, *12*, 78-87.
[37] I. Yamanaka, T. Hashimoto, R. Ichihashi, K. Otsuka, *Electrochimica Acta* **2008**, 4824-4832.
[38] I. Yamanaka, T. Murayama, *Angew. Chem. Int. Ed.* **2008**, 1900-1902.
[39] F. Alcaide, P. Cabot, E. Brillas, *Journal of Power Sources* **2006**, *153*, 47-60.
[40] T. van der Does, *Journal of Power Sources* **1996**, *61*, 49-51.
[41] J. J. Hwang, M. L. Zou, *Journal of Power Sources* **2010**, *195*, 2579-2585.
[42] K. Otsuka, K. Hosokawa, I. Yamanaka, Y. Wada, A. Morikawa, *Electrochim. Acta* **1989**, *34*, 1485-1488.
[43] X.-Z. Yuan, Z.-F. Ma, Q.-Z. Jiang, W.-S. Wu, *Electrochemistry Communications* **2001**, *3*, 599-602.
[44] A. Ilicic, D. P. Wilkinson, K. Faith, *Journal of The Electrochemical Society* **2010**, *157*, B529-B535.
[45] G. R. Agladze, P. Nikoleishvili, G. S. Tsurtsumia, V. Kveselava, G. Gorelishvili, R. Latsuzbaia, *Journal of The Electrochemical Society* **2010**, *157*, E140-E147.
[46] G. R. Agladze, P. Nikoleishvili, V. Kveselava, G. S. Tsurtsumia, G. Gorelishvili, D. Gogoli, I. Kakhniashvili, *Journal of Power Sources* **2012**, *218*, 46-51.
[47] I. Yamanaka, T. Hashimoto, K. Otsuka, *Chemistry Letters* **2002**, *31*, 852-853.
[48] E. Brillas, F. Alcaide, P. Cabot, *Electrochim. Acta* **2002**, *48*, 331-340.
[49] K. Otsuka, I. Yamanaka, *Electrochim. Acta* **1990**, *35*, 319-322.
[50] M. S. Hossain, D. Tryk, E. Yeager, *Electrochim. Acta* **1989**, *34*, 1733-1737.
[51] N. Aleksejeva, University of Tartu (Tartu, Estonia), **2010**.
[52] J. C. Forti, C. E. Venancio, M. R. V. Lanza, R. Bertazzoli, *J. Braz. Chem. Soc.* **2008**, *19*, 643-650.
[53] G. Jurmann, D. J. Schiffrin, K. Tammeveski, *Electrochim. Acta* **2007**, *53*, 390-399.
[54] A. Sarapuu, K. Helstein, D. J. Schiffrin, D. K. Tammeveski, *Electrochemcal and Solid-State Letters* **2005**, *8*, E30-E33.
[55] A. Sarapuu, University of Tartu (Tartu, Estonia), **2008**.
[56] B. Sljukic, C. E. Banks, R. G. Compton, *Journal of the Iranian Chemical Society* **2005**, *2*, 1-25.
[57] K. Tammeveski, K. Kontturi, R. J. Nichols, R. J. Potter, D. J. Schiffrin, *Journal of Electroanalytical Chemistry* **2001**, *515*, 101-112.
[58] J. Xu, W. Huang, R. L. McCreery, *Journal of Electroanalytical Chemistry* **1996**, *410*, 235-242.
[59] H. H. Yang, R. L. McCreery, *Journal of The Electrochemical Society* **2000**, *147*, 3420-3428.
[60] K. Vaik, A. Sarapuu, K. Tammeveski, F. Mirkhalaf, D. J. Schiffrin, *Journal of Electroanalytical Chemistry* **2004**, *564*, 159-166.
[61] P. Manisankar, A. M. Pushpalatha, S. Vasanthkumar, A. Gomathi, S. Viswanathan, *Journal of Electroanalytical Chemistry* **2004**, *571*, 43-50.
[62] P. Manisankar, A. Gomathi, *Journal of Power Sources* **2005**, *150*, 240-246.
[63] A. Wang, A. Bonakdarpour, D. P. Wilkinson, E. L. Gyenge, *Electrochimica Acta* **2012**, *66*, 222-229.
[64] P. Tissot, A. Huissoud, *Electrochim. Acta* **1996**, *41*, 2451-2456.
[65] S. Berchmans, R. Vijayavalli, *Langmuir* **1995**, *11*, 286-290.
[66] PEM, in *http://en.wikipedia.org/wiki/Proton_exchange_membrane_fuel_cell*, Wikipedia, **December 15, 2011**.
[67] J. H. Hirschenhofer, D. B. Stauffer, R. R. Engleman, M. G. LKlett, *Fuel Cell Handbook*, 4th ed. ed., U.S. Department of Energy, Morgantown, VA, **1998**.
[68] S. Q. Song, W. J. Zhou, W. Z. Li, G. Sun, Q. Xin, S. Kontou, P. Tsiakaras, *Ionics* **2004**, *10*, 458-462.
[69] J. Cruickshank, K. Scott, *Journal of Power Sources* **1998**, *70*, 40-47.
[70] K. N. Mahesh, Jawaharlal Nehru Technological University Hyderabad (Telangana, India), **2013**.

[71] R. S. Liu, L. Zhang, X. L. Sun, H. Liu, J. Zhang, *Electrochemical Technologies for Energy Storage and Conversion, Volume 1&2*, Wiley-VCH Verlag and Co., Weinheim, Germany, **2012**.
[72] J. B. Davison, J. M. Kacsir, P. J. Peerce-Landers, R. Jasinski, *J. Electrochem. Soc.* **1983**, *130*, 1497-1501.
[73] S. Wakita, US Patent 6159349, **2000**
[74] P. Drogui, S. Elmaleh, M. Rumeau, C. Bernard, A. Rambaud, *Journal of Applied Electrochemistry* **2001**, *31*, 877-882.
[75] E. L. Gyenge, C. Oloman, *Journal of Electrochemical Society* **2005**, *152*, D42-D53.
[76] E. L. Gyenge, C. Oloman, *Journal of Applied Electrochemistry* **2001**, *31*, 233-243.
[77] Y. Ando, T. Tanaka, *International Journal of Hydrogen Energy* **2004**, *29*, 1349-1354.
[78] E. L. Gyenge, C. Oloman, *Journal of Applied Electrochemistry* **2003**, *33*, 655-663.
[79] E. L. Gyenge, C. Oloman, *Journal of Applied Electrochemistry* **2003**, *33*, 665-674.
[80] A. Huissoud, P. Tissot, *Journal of Applied Electrochemistry* **1999**, *29*, 11-25.
[81] A. Huissoud, P. Tissot, *Journal of Applied Electrochemistry* **1998**, *28*, 653-657.
[82] M. Gao, F. Yang, X. Wang, G. Zhang, L. Liu, *J. Phys. Chem. C* **2007**, *111*, 17268-17274.
[83] M. Gao, F. Yang, G. Zhang, L. Liu, X. Wang, *Electrochim. Acta* **2009**, *54*, 2224-2228.
[84] E. Lobyntseva, T. Kallio, N. Alexeyeva, K. Tammeveski, K. Kontturi, *Electrochimica Acta* **2007**, *52*, 7262-7269.
[85] J. C. Forti, R. S. Rocha, M. R. V. Lanza, R. Bertazzoli, *Journal of Electroanalytical Chemistry* **2007**, *601*, 63-67.
[86] T. Wilson, J. Zhang, C. Oloman, D. D. M. Wayner, *Int. J. Electrochem. Sci.* **2006**, *1*, 99-109.
[87] ESCO, in *http://www.escouk.com/processes/advanced-oxidation-process/*, Conwy, UK, **October 9, 2010**.
[88] R. Andreozzi, V. Caprio, A. Insola, R. Marotta, *Catalysis Today* **1999**, *53*, 51-59.
[89] W. H. Glaze, J.-W. Kang, D. H. Chapin, *Ozone: Science and Engineering* **1987**, *9*, 335-352.
[90] R. Munter, *Proc. Estonian Acad. Sci. Chem.* **2001**, *50*, 59-80.
[91] W. H. Glaze, G. R. Peyton, *Environ. Sci. Technol.* **1988**, *22*, 761-767.
[92] D. R. Lide, *CRC Handbook of Chemistry and Physics*, **1996**.
[93] BI Pure Water, in *www.bipurewater.com*, **July 5 2010**.
[94] A. Clifford, D. Dong, E. Giziewicz, D. Rogers, in *Symposia on Electrochemical Engineering and Small Scale Electrolytic Processing* (Eds.: C. W. Walton, J. W. Van Zee, R. D. Varjian), Montreal, Quebec, Canada, **1990**, pp. 259-274.
[95] RES'EAU_WaterNet, in *http://www.reseauwaternet.ca/*, **September 5, 2016**.
[96] G. Imoberdorf, Vancouver, B.C., **2010**.
[97] M. Blanco, University of British Columbia (Vancouver), **2011**.
[98] H. K. Atiyeh, K. Karan, B. Peppley, A. Phoenix, E. Halliop, J. Pharoah, *Journal of Power Sources* **2007**, *170*, 111-121.
[99] W. Wagner, C. J. Hull, *Inorganic Titrimetric Analysis*, Marcel Dekker, New York, **1971**.
[100] N. V. Klassen, D. Marchington, H. C. E. McGowan, *Anal.Chem.* **1994**, *66*, 2921-2925.
[101] Z. H. Wang, C. Y. Wang, K. S. Chen, *Journal of Power Sources* **2001**, *94*, 40-50.
[102] J. J. Zhang, *PEM Fuel Cell Electrocatalysts and Catalyst Layers: Fundamentals and Applications*, Springer, **2008**.
[103] D. P. Wilkinson, J. J. Zhang, R. Hui, J. Fergus, X. Li, *Proton Exchange Membrane Fuel Cells: Materials Properties and Performance*, CRC Press, Boca Raton, Florida, **2010**.
[104] J. P. Owejan, T. A. Trabold, D. L. Jacobson, M. Arif, S. G. Kandlikar, *Int. J. Hydrogen Energy* **2007**, *32*, 4489-4502.
[105] F. Barbir, *PEM Fuel Cells: Theory and Practice*, Elsevier Academic Press, San Diego, **2005**.

[106] G. G. Park, Y. J. Sohn, T. H. Yang, Y. G. Yoon, W. Y. Lee, C. S. Kim, *Journal of Power Sources* **2004**, *131*, 182-187.
[107] F. Lufrano, E. Passalacqua, G. Squadrito, A. Patti, L. Giorgi, *Journal of Applied Electrochemistry* **1999**, *29*, 445-448.
[108] C. B. Roy, *Journal of Catalysis* **1968**, *12*, 129-133.
[109] G. o. B. C. Ministry of Environment, in *http://www.env.gov.bc.ca/wat/wq/BCguidelines/cobalt/cobalt_over.html*, **December 18, 2015**.
[110] J. H. Kim, H. J. Gibb, P. D. Howe, World Health Organization, **2006**, p. 15.
[111] G. o. B. C. Ministry of Environment, in *http://www.env.gov.bc.ca/wat/wq/BCguidelines/fluoride/fluoride.html*, **December 19, 2015**.
[112] J. Fawell, World Health Organization, **2004**, p. 7.
[113] W. Li, A. Bonakdarpour, D. P. Wilkinson, E. L. Gyenge, *ChemSusChem* **2013**, *6*, 2137-2143.
[114] J. L. Zhang, J. F. Wu, H. Zhang, J. J. Zhang, *PEM Fuel Cell Testing and Diagnosis*, Elsevier Science, **2013**.
[115] J. H. Nam, M. Kaviany, *International Journal of Heat and Mass Transfer* **2003**, *46*, 4595-4611.
[116] J. M. Song, H. Uchida, M. Watanabe, *Electrochemistry* **2005**, *73*, 189-193.
[117] N. Holmstrom, J. Ihonen, A. Lundblad, G. Lindbergh, *Fuel Cells* **2007**, *7*, 306-313.
[118] G. Y. Lin, T. V. Nguyen, *Journal of The Electrochemical Society* **2005**, *152*, A1942-A1948.
[119] M. Blanco, D. P. Wilkinson, *International Journal of Hydrogen Energy* **2014**, *39*, 16390-16404.
[120] C. Oloman, *Electrochemical Processing for the Pulp and Paper Industry*, The Electrochemical Consultancy, Romsey, UK, **1996**.
[121] R. D. La Roche, M. A. Stadtherr, R. C. alkire, *J Appl Electrochem* **1994**, *24*, 1206-1212.
[122] A. Wang, University of British Columbia (Vancouver), **2012**.
[123] *Perry's Chemical Engineer's Handbook*, 6th ed., McGraw Hill Inc., New York, **1984**.
[124] G. D. Uhlrich, *A guide to chemical engineering process design and economics*, John Wiley & Sons, New York, **1984**.
[125] K. D. Timmerhaus, T. M. Flynn, *Cryogenic Process Engineering*, Springer, **1989**.

Appendices

Appendix A Membrane Electrode Assembly Component Preparation Protocols

Appendix A.1 Cobalt-Carbon Composite Catalyst Preparation

The procedures outlined below are for preparing 4% Cobalt in carbon composite catalyst by weight [28].

1. Using the molecular weight of hydrate cobalt nitrate, $Co(NO_3)_2 \bullet 6H_2O$, weigh the appropriate amount of the salt with a weigh boat.
2. Place the salt in a beaker; add sufficient DI water in order to dissolve the salt (~ 5 mL).
3. Weigh the appropriate amount of XC-72 Vulcan carbon, add it to the salt solution, mix well, and then sonicate for 45 minutes to one hour, with intermittent manual mixing every 15 minutes.
4. Place the beaker on a hotplate (preset to 100°C), with constant stirring, allow the water in the solution to evaporate
5. When sufficient water has evaporated such that the solution has become a thick slurry, remove the beaker from the hotplate, cover it with aluminum foil (with holes on top), then dry it in an oven over night at 600°C.

6. Next day, transfer the dried solids to a clean ceramic boat, and place the boat in a tube furnace (preset to 800°C) for 2 hours, under flowing nitrogen gas.

7. Remove the catalyst mixture from the ceramic boat and transfer it to a small vial. The catalyst is now ready for ink preparation.

Appendix A.2 Anthraquinone-RiboFlavin Composite Catalyst Preparation

The anthraquinone-riboflavinyl composite catalyst was synthesized by Mr. Andrew Wang as part of his Masters project. The steps outlined below are taken from his Masters' thesis titled "Organic Redox Catalysts for Oxygen Electroreduction to Hydrogen Peroxide: An Application to Drinking Water Treatment" [122].

1. Measure four grams of anthraquinone-2-carboxylic acid (CAQ) in a round bottom flask, add 50 mL thionyl chloride ($SOCl_2$). Mix the solution well, heat and reflux the solution in a oil bath at 80°C for 3 hours. Remove excess $SOCl_2$ via distillation after the reflux.

2. Dissolve the yellow-green acyl chloride product in 50 mL pyridine at 0°C in an ice bath.

3. While stirring the pyridine solution, slowly add four grams of Riboflavin (RF). After the reaction, remove the excess pyridine via distillation at 100°C. Remove the side reaction product pyridinium chloride through DI water washing and vacuum filtration.

4. Heat hexane solution to 60°C, and then slowly add it to the solid product from step 5, while keeping the mixture at 60°C. Once all the solids have dissolved, remove the

mixture from heat and allow it to cool to room temperature slowly. Place the cooled product on a ice bath for about 10 minutes. Remove excess liquid via vacuum suction.

5. Place the dried RF-AQ product in the oven and dry it over night at 80°C.

6. The final RF-AQ product will have a yield of approximately 20%.

Appendix A.3 Catalyst Ink and Electrode Preparation

Appendix A.3.1 Cathode Catalyst Ink Mixture

The mixture composition for both inorganic and organic cathode catalyst ink mixtures are outlined in Table A-3-1. Same mixing protocol was followed for both the inorganic and the organic ink mixture. First the weighed catalyst is placed in a beaker, and then small amount of DI water is added to the catalyst, and mixed with a glass rod. Then appropriate amount of Teflon solution is added and mixed with the glass rod. Next appropriate amount of Ethanol is added and mixed with the glass rod. The solution mix is topped with appropriate amount of DI and stirred with the glass rod. Finally the beaker containing the mixture is covered with parafilm and placed in a sonicator for 1 hour to thoroughly mix the solution (stir with glass rod every 15 minutes).

Table A-3-1 Cathode Catalyst Ink Mixture Composition

	Inorganic	Organic
Catalyst	600 mg	10 mg
DI H_2O	30 mL	280 µL
Nafion	10 mL	100 µL
Ethanol	10 mL	70 µL

Appendix A.3.2 Anode Catalyst Ink Mixture

1) Choose an appropriate catalyst loading.

2) Calculate the mass of Pt/C powder mixture that should be used:

Notes for calculation

- *Catalyst loading symbolized by Φ_{Pt} (mg per geometric cm², actual loading can be calculated later, after catalyst is sprayed onto Toray paper)*

- *The catalyst is purchased as a dispersed deposit on Vulcan X carbon powder. Some common compositions of this powder based on mass are given: (20% Pt, 80% C; etek-inc.com ~$1500/100g), (40% Pt, 60% C) and(20% Pt, 20% Ru, 60% C). The following example uses the first composition.*

- *To account for losses (off-edge spraying, air-borne spray) while spraying the ink, the premixed Pt/C is added with an excess factor of 3 (may vary with preference, technique or procedures)*

$$m_{Pt+VulcanXC}(g) = 3\sigma_{Pt}A_{Geom}\left(\frac{1}{0.2}\right)$$

3) Choose an appropriate Nafion loading (~30% w/w is common). Sprayed Nafion provides bonding when pressing the MEA and increases the triple-phase boundary length.

4) Calculate the mass of Nafion solution required:

Notes for calculation

- *Nafion loading is symbolized as f_{Nafion} (fraction Nafion in Pt+VulcanXC+Nafion)*

- Nafion is available as a 5% w/w solution. Mass of solution expressed as m_{Naf_Sol}

$$m_{Naf\_Sol} = \frac{f_{Nafion} m_{Pt+VulcanXC}}{1 - f_{Nafion}} \left(\frac{1}{0.05} \right)$$

- The derivation can be realized by starting with:

$$m_{Nafion} = f_{Nafion} \left(m_{Pt+VulcanXC} + m_{Nafion} \right)$$

5) Clean an appropriate size beaker with isopropanol.

6) Weigh the calculated amount of premixed Pt/C powder in the beaker.

7) Add water (before adding isopropanol) to the weighed powder. The carbon powder will agglomerate over the water surface. Submerge as much of the carbon powder as possible by stirring.

8) Add isopropanol (after adding water) to completely solvate the carbon powder. Try to obtain reasonable dispersion by stirring. One can constantly adjust the amount of water and isopropanol added to find what works best. Generally, much less isopropanol is added than water. If the isopropanol is added before water, the carbon powder and isopropanol will combust together.

9) Add the calculated mass of Nafion solution (after adding water) with a micropipette. Stir the mixture.

10) Cover the mixing beaker with parafilm and sonicate the mixture for 30-60 min. Inspect and stir the mixture every 10-15 minutes. A homogenous dispersion is desired.

Appendix A.4 Gas Diffusion Electrode Preparation Protocol

The gas diffusion electrodes are prepared by combining the catalyst layer to the gas diffusion layer/substrate. The following is a protocol for depositing catalyst layer to the Toray paper GDL substrate using the air-powered hand spraying method.

1. Cut out a 15 cm x 15 cm piece of Toray paper. Weigh and record the Toray paper weight.
2. Turn on the hot plate, rotate the heater knob to 80°C on the display. Place a piece of aluminum plate on the hotplate. Place the Toray paper on the aluminum plate. Place the stainless steel plate with the 15 cm x 15 cm center cut out on top of the Toray paper. Allow the hotplate to reach the desired temperature.
3. Pour about half of the catalyst ink mixture into the canister on the spray gun. Use a piece of paper towel to test the pattern of the ink spray. Adjust the spray accordingly.
4. Position the spray gun (MasterCraft HVLP Air Gravity Spray Gun) at the top left corner of the steel plate, about five inches above the Toray paper surface. Start spraying, then move in a constant pace across the surface of the Toray paper, while keeping the height of the spray gun. Move in a back and forth motion until the entire surface of the Toray paper is covered with a thin layer of the catalyst ink mixture. Allow the catalyst ink to dry (about 1 minute).
5. Turn the aluminum plate ninety degrees, while keeping the Toray paper and steel plate in place. Repeat the same spray as in step 4. Again allow the catalyst ink to dry.
6. Repeat steps 4 and 5 until the desired catalyst loading is achieved. Keep the hotplate at 80°C for 30min. Then turn the heater off on the hotplate. Leave the finished GDE on the hotplate overnight in order to allow the GDE to completely dry.

7. Weigh the completed GDE. Determine the catalyst loading.

Appendix A.5 Anode Half-CCM Preparation Protocol

The anode Half-CCM is prepared in a similar manner to the anode gas diffusion electrode using Toray paper. Additional equipment used is a heated vacuum table. The following is the procedure for preparing a platinum Half-CCM with a 49 cm^2 active area:

1. Cut out a 10 cm x 10 cm piece of cleaned protonated Nafion membrane, place it between 2 Teflon sheets, then dry the Nafion membrane in the Dake Hotpress at 135℃ for 2 minutes. Leave the Nafion membrane under pressure to cool to room temperature. Pre-weigh the dried membrane.
2. Switch on the vacuum table, turn the temperature dial to 70℃, and press the dial to turn on the heater.
3. When the vacuum table reaches the desired temperature, place the dried membrane on the vacuum table. Place the orange rubber with center cut out on top of the membrane. Keep the membrane taught to create a vacuum seal between the membrane and the vacuum table.
4. Load the pre-cleaned spray gun (MasterCraft HVLP Air Gravity Spray Gun) with the pre-mixed platinum ink mixture from Appendix A-3, test the spray patter on a piece of paper towel.
5. Start at the top left corner of the membrane; spray a thin layer of ink on the membrane, utilizing a row-by-row, back and forth motion, while keeping the membrane from being oversaturated with liquid. Allow the first layer of ink to dry (about 1 minute).

6. Spray a second thin layer of ink on top of the first layer, with the same motion as the previous layer. Again allow the second layer to dry.
7. Repeat the spraying until the desired loading has been sprayed.
8. Leave the heater as well as the vacuum on for another 30 minutes.
9. Turn the heater off on the vacuum table, while leaving the vacuum on overnight to allow the catalyst layer to completely dry.
10. Remove the membrane from the vacuum table and weigh the membrane with the catalyst layer, determine the actual catalyst loading.

Appendix A.6 49 cm^2 Membrane Electrode Assembly Protocol

The procedures listed here are for fabricating membrane electrode assemblies (MEAs) with gas diffusion electrodes prepared in Appendix A-4. For MEAs assembled with half-CCMs (prepared in Appendix A-5), a similar procedure is followed. For simplicity, a footnote at the end of each step denotes whether it is for MEAs with GDE or MEAs with half-CCM.

1. Cut two pieces of Kapton polymide film and spread over the stainless steel frame by carefully removing the film from the plastic support. (GDE and half-CCM)

2. Place the stainless steel frame on the bench, with the glue side facing up. Lay the rule die cutter labeled "GDL" on the frame, ensuring the 2 holes on the corners match up for both the frame and the GDL cutter. Using a rubber mallet, hammer with medium force in a round pattern over the rule die on the GDL cutter, back and forth about 3-4 times. Slowly lift up the GDL cutter to ensure the center square hole is in place without ripping the Kapton film. Repeat this for the other stainless steel frame. (GDE and half-CCM)

3. Take the anode GDE previously prepared, and place it over a large piece of Kleenex paper, with the catalyst layer facing up. Lay the rule die cutter labeled "CCM" on the GDE, ensuring the center rule die covers all the catalyst area. Using a rubber mallet, gently tap around the center rule die few times. Carefully lift up the CCM cutter from the cut GDE. (GDE only)

4. Repeat step 3 for cathode GDE. (GDE and half-CCM)

5. Using a pair of steel scissors cut and clean a piece of titanium mesh (8 cm x 8 cm) and clean it with isopropanol under sonication for an hour. (half-CCM only)

6. Pre-heat the hot press to 135°C. (GDE only)

7. Place the cathode GDE (catalyst layer side up) on the clean surface of a Teflon plate. Cut a piece of the cleaned Nafion 112 film (9 cm x 9 cm) and carefully place it on the cathode GDE. Spread out the Nafion film with gloved fingers, and then place the anode GDE (catalyst layer side down) on top of the Nafion film, ensuring both electrode match up on either side of the Nafion film. Cover with another Teflon plate. Place the Teflon plates with the MEA inside in between 2 pieces of stainless steel plates. Move this sandwich to the hot press and press for 2 minutes and 30 seconds at 1100 psi. Remove the sandwich from the hot press and leave it under a stainless steel block for one hour. (GDE only)

8. For the GDE-MEAs, lay one of the stainless steel frame with Kapton film on the bench (with the glue side up). Remove the stainless steel/Teflon/MEA sandwich from the steel block, and carefully peel the MEA from the Teflon plate. Taking care not to rip the Nafion film. Place the MEA (with cathode side down) on the first Kapton film, centering

on the Kapton film opening. Next lay the other stainless steel frame with Kapton film on the first frame, maneuver the frames until the center opening of both Kapton film lines up. Then with a gloved hand, press the Kapton films together, starting at one corner of the electrode active area, and work in a round pattern outwards. (GDE only)

9. For the half-CCMs, no hot press is needed, so this step will describe the MEA assembly using half-CCM. Lay one of the stainless steel frame with Kapton film on the bench (with the glue side up), place the cathode GDE (catalyst layer side up) on the center opening of the Kapton film. Next lay the half-CCM (with the catalyst layer side up) carefully on the Kapton film, ensuring the areas of both electrodes match up. With a gloved finger, spread the Nafion film on the Kapton film. Place the cleaned titanium mesh on the other Kapton film, then combine the 2 Kapton films together, sandwiching the electrodes together (making sure the areas of either side match up before pressing the Kapton films together. (half-CCM only)

10. The assembled MEAs are now ready to be cut and placed inside the TP50 research fuel cell. (GDE and half-CCM)

Appendix A.7 5 cm^2 Membrane Electrode Assembly Protocol

The procedures listed here are for fabricating membrane electrode assemblies (MEAs) with gas diffusion electrodes prepared in Appendix A-4. These steps are similar to those for the 49 cm^2 MEA preparation; however, the cutting tool is specifically made for the 5 cm^2 Tandem Cell.

1. Cut two pieces of Kapton polymide film and spread over the stainless steel frame by carefully removing the film from the plastic support.

2. Place the stainless steel frame on the bench, with the glue side facing up. Lay the 5 cm^2 rule die cutter labeled "GDL" on the frame, ensuring the 2 holes on the corners match up for both the frame and the GDL cutter. Using a rubber mallet, hammer with medium force in a round pattern over the rule die on the GDL cutter, back and forth about 3-4 times. Slowly lift up the GDL cutter to ensure the center square hole is in place without ripping the Kapton film. Repeat this for the other stainless steel frame.

3. Take the anode GDE previously prepared, and place it over a large piece of Kleenex paper, with the catalyst layer facing up. Lay the 5 cm^2 rule die cutter labeled "CCM" on the GDE, ensuring the center rule die covers all the catalyst area. Using a rubber mallet, gently tap around the center rule die few times. Carefully lift up the CCM cutter from the cut GDE.

4. Repeat step 3 for cathode GDE.

5. Pre-heat the hot press to 135°C.

6. Place the cathode GDE (catalyst layer side up) on the clean surface of a Teflon plate. Cut a piece of the cleaned Nafion 112 film (7 cm x 7 cm) and carefully place it on the cathode GDE. Spread out the Nafion film with gloved fingers, and then place the anode GDE (catalyst layer side down) on top of the Nafion film, ensuring both electrode match up on either side of the Nafion film. Cover with another Teflon plate. Place the Teflon plates with the MEA inside in between 2 pieces of stainless steel plates. Move this sandwich to

the hot press and press for 2 minutes and 30 seconds at 1100 psi. Remove the sandwich from the hot press and leave it under a stainless steel block for one hour.

7. For the GDE-MEAs, lay one of the stainless steel frame with Kapton film on the bench (with the glue side up). Remove the stainless steel/Teflon/MEA sandwich from the steel block, and carefully peel the MEA from the Teflon plate. Taking care not to rip the Nafion film. Place the MEA (with cathode side down) on the first Kapton film, centering on the Kapton film opening. Next lay the other stainless steel frame with Kapton film on the first frame, maneuver the frames until the center opening of both Kapton film lines up. Then with a gloved hand, press the Kapton films together, starting at one corner of the electrode active area, and work in a round pattern outwards.

8. With the assembled MEA still inside the stainless steel frame, lay it on top of a piece of Kleenex paper, then place the 5 cm^2 cutting tool on top of the MEA. Using a rubber mallet, punch out the MEA along with the port holes for the Tandem Cell. The 5 cm^2 MEA are now ready to be placed inside the TP5 research fuel cell.

Appendix B Spectrophotometric Method for H_2O_2 Analysis

Solution A preparation:

500mL	Potassium Hydrogen Phthalate (KHP)	10g
	+ Distilled water (DI H_2O)	

Solution B Preparation:

500mL	KI	33g
	NaOH	1g
	Ammonium molybdate tetrahydrate (catalyst)	0.1g
	+ Distilled water (DI H_2O)	

Fresh stock solution prepared every 2 weeks.

Analysis:

Wavelength:	351nm
Zero:	DI water
Blank:	2.5mL of each solutions A and B
(~0.003 Abs)	Diluted with DI water to 10mL in volumetric flask
Sample:	2.5mL of each A and B
	0.5mL of sample (appropriate for $[H_2O_2]$ 1 to 10 ppm)
	Mix for 2 minutes to allow reaction

Calculations:

$$[\text{Peroxide}]: \quad \frac{(Abs_{sample} - Abs_{blank}) \times 10 \times D}{0.7776 \times S}$$

D = additional dilution (1 if none)

S = sample volume (0.5mL)

Appendix C Auxiliary Equipment Design and Cost Calculations for The H_2O_2 Production Process

For the in-situ H_2O_2 production process carried out in fuel cell mode operation and electrolysis mode operation, the auxiliary equipments used in each operation mode (Figures 8.1 and 8.2) are summarized in Table C-1.

Table C-1 List of auxiliary equipments used in fuel cell mode and electrolysis mode operation

Fuel cell mode operation	**Electrolysis mode operation**
Feed and storage tanks	Feed and storage tanks
pump	Pump
Compressor	Compressor
G/L separator	G/L separator
Heat exchanger	Heat exchanger

Cost projection values from Matche.com and design calculations from Perry's Handbook [123] were used to calculate the cost of the auxiliary equipment listed above.

A) Calculations for individual auxiliary equipment

1) Feed and Storage Tanks

Feed and storage tanks are designed to hold fluid volumes for the specified flow rates. For the H_2O_2 process, the feed tanks are used to store deionized water (dH_2O), and fed to the SPE cells at a combined flow rate of 0.18 m^3 hr^{-1} (200 cells @ 15 mL min^{-1} each). The cost for a 44 m^3 (approx. 10,000 gallons) glass lined carbon steel horizontal storage tank is $13,600 US [www.matche.com, 2014 price].

2) Pump

Two pumps are installed to feed the dH_2O to the system. For the current system the capital cost of the variable speed stainless steel injection pump with a feed rate of ~0.02 gpm is $4400 US [www.matche.com, 2014 price]. The capital and operating cost of a pump is a function of the required shaft power, Ws, given by the following equation [124]:

$$W_s = \frac{F_V \Delta P}{\varepsilon_P}, \text{ with } \varepsilon_P = 1 - F_V^{-0.27}, \text{ and } \Delta P = \rho g \Delta h \qquad \text{(Eqn C-1)}$$

Where F_v is the volumetric flow rate ($m^3\ s^{-1}$), ΔP is the pressure differential (kPa), and ε_p is the pump efficiency.

3) Compressor

For the electrolysis mode operation, a single compressor is used to compress oxygen supply to the cathode compartment. For the fuel cell mode operation, two compressors are used, one for hydrogen and one for oxygen. For the oxygen supply, oxygen gas is compressed from a pressure of near atmosphere (100 kPa abs.) to a pressure of 500 kPa abs. For a compression ratio > 4 the compressor has to be broken into stages to prevent overheating and minimize the shaft power to the compressors. For the present design a two stage compressor is employed with a compression ratio of 2.23 for each stage. This ratio is determined by the geometric progression in the three pressures of the two stages, i.e. the outlet pressure of the first stage is the geometric mean of the inlet pressure of the first stage (100 kPa abs.) and the outlet pressure of the second stage (500 kPa abs.).

The shaft power is calculated from the following equation [125]:

$$W_{s,c} = \left(\frac{m_v R T_{in}}{\varepsilon_C}\right)\left(\frac{r}{r-1}\right)\left[\left(\frac{P_{out}}{P_{in}}\right)^{\frac{r-1}{r}} - 1\right] \qquad \text{(Eqn C-2)}$$

Where m_v is the molar flow rate of oxygen (mol s^{-1}) including the oxygen recycle, R is the gas constant (8.314 J mol^{-1} K^{-1}), Tin is the inlet oxygen temperature to the compressor (K), r is the ratio of specific heats (C_p/C_v), P_{out}/P_{in} is the ratio of outlet to inlet pressure for the compressor and ε_c is the compressor efficiency.

For the present work, T_{in} is 298 K, r is 1.4 [92], the compression ratio is 2.23 and the compressor efficiency is assumed to be 80%. Thus the shaft power $W_{s,c}$ is calculated to be 5.58 KW (7.5 hp) for each stage, based on a oxygen molar flow rate of 2 mol s^{-1}. The cost for each stage of a two stage reciprocating compressor rated at 500 kPa abs. is $7700 US (www.matche.com, 2014 prices).

For hydrogen supply, the calculations followed the same route as the oxygen supply. Eqn C-2 is also used, with the specific heat of hydrogen being 1.405, the shaft power is calculated to be 5.59 KW (7.5 hp).

4) G/L separator

Both the electrolysis mode operation and the fuel cell mode operation will have two G/L separators, one each located at the outlet of the anode and the cathode. For electrolysis mode operation, the G/L separator at the anode is used to release O_2 from the liquid stream, while the G/L separator at the cathode is used to separate O_2 from the product liquid stream. For the fuel cell mode operation, the G/L separator at the anode is used to separate excess H_2 from

the liquid stream, while the G/L separator at the cathode separates O_2 from the product liquid stream.

The design diameter of separator s is based on the following equations [124]:

$$D = \left[\frac{4Q_G}{\pi U_{ave}} \right]^{\frac{1}{2}} \qquad \text{(Eqn C-2)}$$

$$U_{ave} = 0.06 \left[\frac{\rho_L - \rho_G}{\rho_G} \right]^{\frac{1}{2}} \qquad \text{(Eqn C-3)}$$

Where Q_G is the volumetric gas flow rate ($m^3\ hr^{-1}$) in the separator, U_{ave} is the gas velocity in the separator ($m\ s^{-1}$), ρ_L is the liquid density ($kg\ m^{-3}$), ρ_G is the gas density ($kg\ m^{-3}$).

Based on Eqns C-2 and C-3 the separator diameter is calculated to be 0.07 m. The cost of a stainless steel gas liquid separator with a 3" (0.07 m) diameter with 250 psi rating is $2300 US.

5) Heat Exchanger for Cathode stream

The product liquid stream exits the cathode with a temperature of 333 K for fuel cell mode operation and 313 K for electrolysis mode operation. To reduce the rate of peroxide decomposition, the product liquid stream is cooled to 283 K using a shell and tube, counter-current heat exchanger operated with chilled water of 276 K at the inlet and 282 K at the outlet. The design equations are:

$$Q_{HEX} = F_{m,c} C_{p,c} (T_{c,in,hex} - T_{c,out,hex}) = U \bullet A \bullet \Delta T_m = F_{m,w} C_{p,w} (T_{w,out,hex} - T_{w,in,hex}) \qquad \text{(Eqn C-4)}$$

Where Q_{HEX} is the heat transferred from the process stream to the cooling water [Watt], $F_{m,c}$ and $F_{m,w}$ are the flow rate of the cathode stream and the cooling water, respectively [$m^3\ s^{-1}$], $C_{p,c}$ and $C_{p,w}$ are the heat capacity of the liquid in the cathode stream and that of the cooling water [$kJ\ kg^{-1}$

K^{-1}]. U is the overall heat transfer coefficient (1.6 kW m^{-2} K^{-1} [123], and ΔT_m is the logarithmic temperature difference (K), expressed as:

$$\Delta T_m = \frac{(T_{c,in,hex} - T_{w,in,hex}) - (T_{c,out,hex} - T_{w,out,hex})}{\ln\left(\frac{T_{c,in,hex} - T_{w,in,hex}}{T_{c,out,hex} - T_{w,out,hex}}\right)} \qquad \text{(Eqn C-5)}$$

Based on the above 2 equations, the cost of a stainless steel shell and tube type heat exchanger with fixed bends with a heat exchanger area of 0.47 m^2 (~5.06 ft^2) and 300 psi rating is $16200 US [www.matche.com].

Appendix D Reaction Kinetics

The following simple reaction mechanism was considered for the in-situ electrosynthesis of hydrogen peroxide:

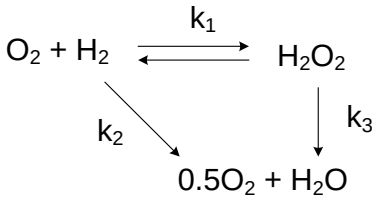

Figure D-1 Hydrogen peroxide electrosynthesis reaction mechanism

Appendix D-1 Fuel Cell mode Kinetics

For fuel cell mode operation, the 4 electron pathway is negligible since the 2 electron pathway is preferred due to the cobalt catalyst used. The material balance for H_2O_2 formation based on the above reaction mechanism can be written as:

$$\frac{dC_{H_2O_2}}{dt} = k_1 C_{H_2} C_{O_2} - k_3 C_{H_2O_2} \qquad \text{Eqn D-1}$$

At the same time, since the supply of both reactant gases are in excess, their concentration can be considered constant, hence Eqn D-1 can be re-written as:

$$\frac{dC_{H_2O_2}}{dt} = k_1' - k_3 C_{H_2O_2} \qquad \text{Eqn D-2}$$

Which can be solved analytically to give:

$$C_{H_2O_2} = \frac{k_1'}{k_3'}\left(1 - e^{-k_3' t}\right) \qquad \text{Eqn D-3}$$

Where k_1 is the rate constant for the H_2O_2 formation reaction, and k_3 is the rate constant for the H_2O_2 decomposition reaction. From experimental data obtained in previous sections of this chapter, the formation reaction constant, as well as the activation energy are listed below.

Table D-1 Fuel cell mode rate constants determined from experimental data.

	H_2O_2 formation	H_2O_2 decomposition
Ea (J mol^{-1})	18814	27474
A(s^{-1})	0.0805	2489
K (s^{-1})	9e-5	0.122

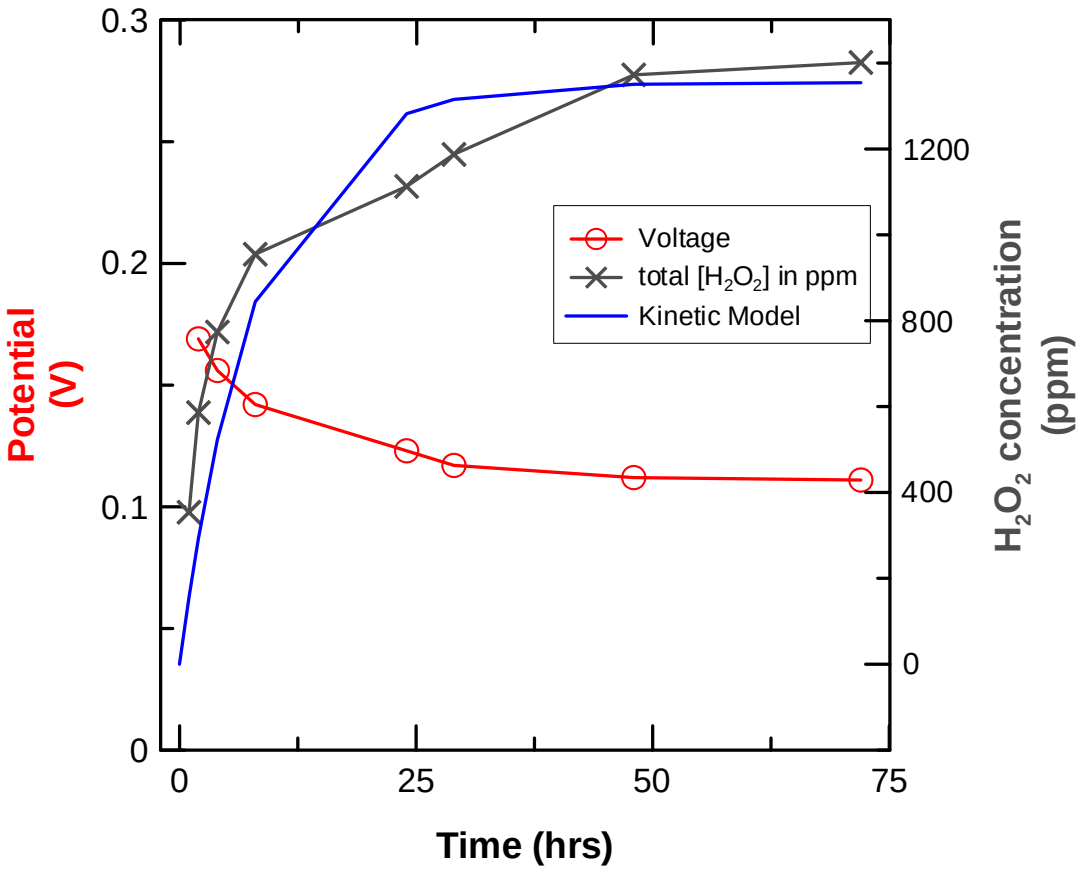

Figure D-2 Fuel cell mode kinetic model based on rate constants determined with experimental data. Note figure is in addition to Figure 5.9, where the black and red lines are experimental data.

Appendix D-2 Electrolysis mode Kinetics

For electrolysis mode operation, the 4 electron pathway is negligible since the 2 electron pathway is preferred due to the cathode catalyst used. The material balance for H_2O_2 formation based on the above reaction mechanism can be written as:

$$\frac{dC_{H_2O_2}}{dt} = k_1 C_{O_2} - k_3 C_{H_2O_2} \qquad \text{Eqn D-4}$$

At the same time, since the supply of the oxygen reactant gas is in excess, its concentration can be considered constant, hence Eqn D-4 can be re-written as:

$$\frac{dC_{H_2O_2}}{dt} = k_1' - k_3 C_{H_2O_2} \qquad \text{Eqn D-5}$$

Which can be solved analytically to give:

$$C_{H_2O_2} = \frac{k_1'}{k_3'}\left(1 - e^{-k_3' t}\right) \qquad \text{Eqn D-6}$$

Where k_1 is the rate constant for the H_2O_2 formation reaction, and k_3 is the rate constant for the H_2O_2 decomposition reaction. From experimental data obtained in previous sections of this chapter, the formation reaction constant, as well as the activation energy are listed below.

Table D-2 Electrolysis mode rate constants determined from experimental data.

	H_2O_2 formation	H_2O_2 decomposition
Ea (J mol^{-1})	9882	26644
A(s^{-1})	0.0017	1828
K (s^{-1})	4.8e-5	0.121

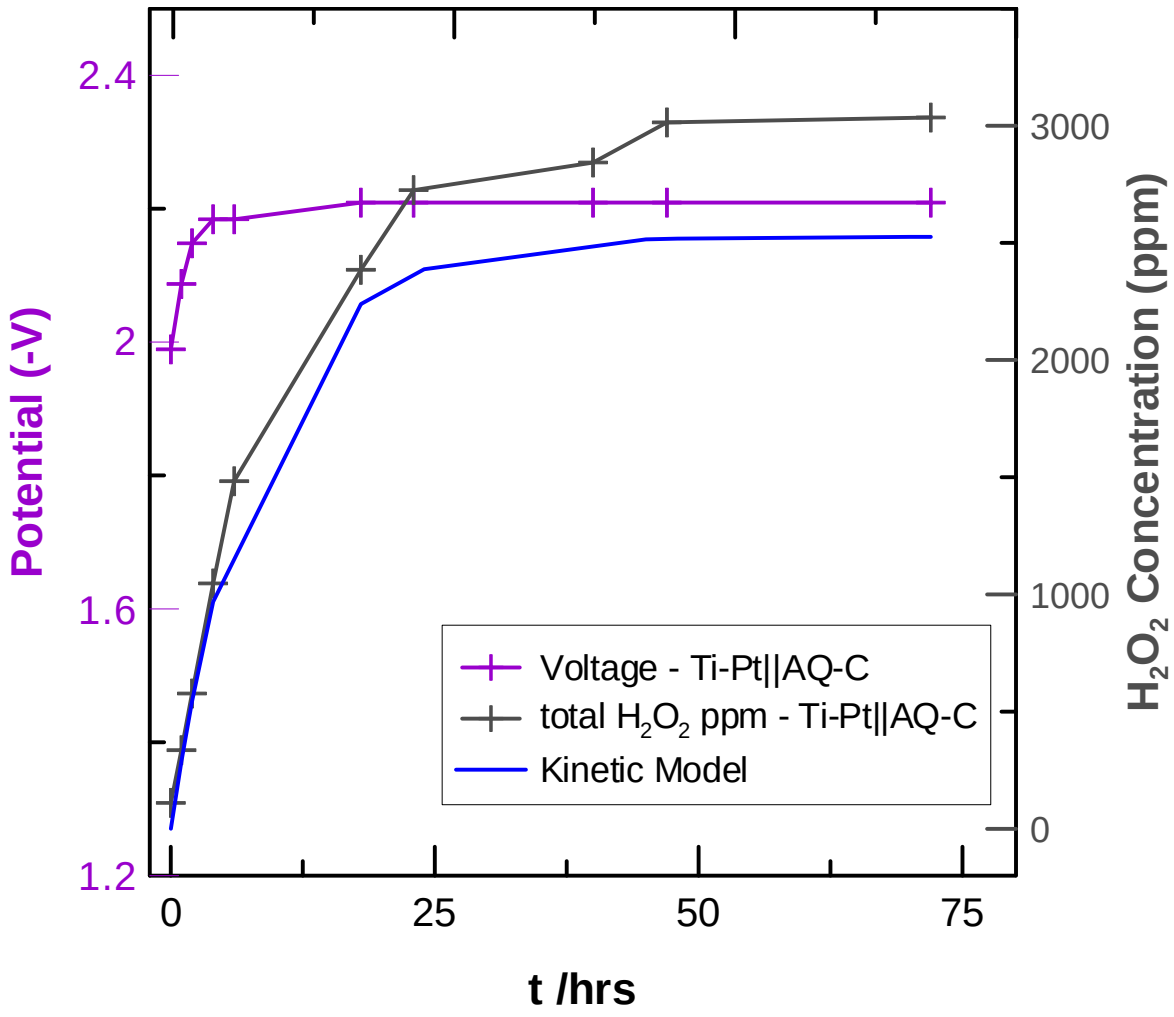

Figure D-3 Fuel cell mode kinetic model based on rate constants determined with experimental data. Note figure is in addition to Figure 7.7, where the black and purple lines are experimental data.

From the graphs it can be safe to assume that the initial assumption of hydrogen peroxide formation follows a first order reaction mechanism does indeed hold true. While this is a simplistic approach to the reaction mechanism, lacking consideration of many important factors that needs to be considered in a thorough kinetic study. The result of this simple kinetic test showed that the data collected here in this project are indeed valid and provides a basis for further study of this project.